CHARLES J. MERRIAM
WILLIAM A. MARSHALL
JEROME B. KLOSE
NORMAN M. SHAPIRO
BASIL P. MANN
CLYDE V. ERWIN, JR.
ALVIN D. SHULMAN
EDWARD M. O'TOOLE
ALLEN H. GERSTEIN
OWEN J. MURRAY
DONALD E. EGAN
NATE F. SCARPELLI

LAW OFFICES
MERRIAM, MARSHALL, SHAPIRO & KLOSE
THIRTY WEST MONROE STREET
CHICAGO, ILLINOIS 60603

TELEPHONE
FINANCIAL 6-5750

December 16, 1966

Mrs. Helen K. Thomas
Official Court Reporter
United States District Court
Room 2328 A
219 South Dearborn Street
Chicago, Illinois

Re: University of Illinois Foundation
v. Blonder-Tongue Laboratories, Inc.
v. JFD Electronics Corporation
Civil Action No. 66 C 567

Dear Mrs. Thomas:

Enclosed are Exhibits B-45 and B-46 which were introduced during the deposition of Dr. Paul E. Mayes taken before Miss Lucile E. Moore on December 14, 1966.

I have had copies of these exhibits made and I am forwarding them directly to counsel for JFD and Blonder-Tongue.

Sincerely yours,

Original Signed by
BASIL P. MANN

Basil P. Mann

BPM/mto
cc: Richard S. Phillips, Esq.
W/Enclosures
Myron C. Cass, Esq.
W/Enclosures

B45a

½ λ LP ANTENNA

B65a 6/15/59

PATTERN MODEL

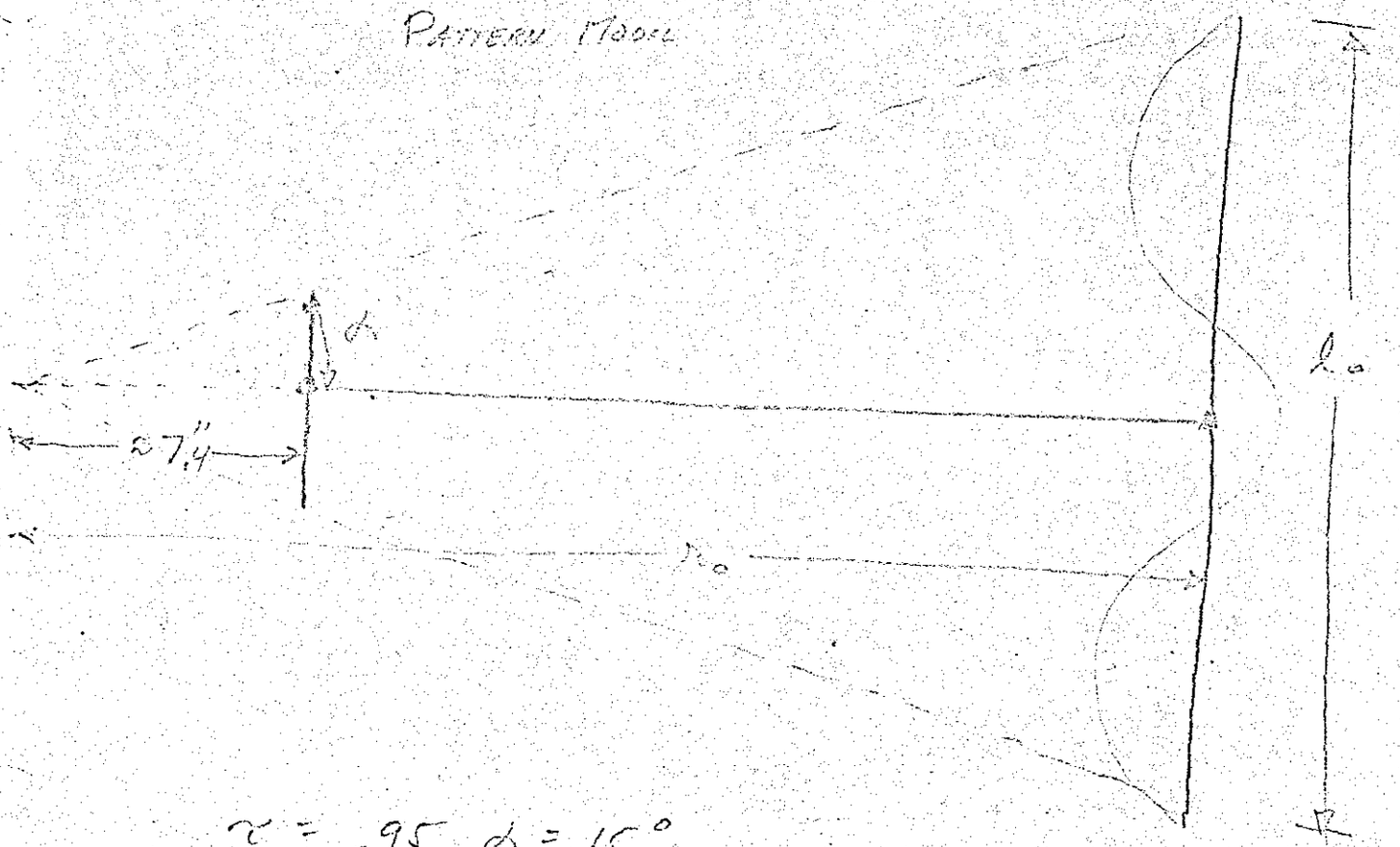

$r = .95$ $\alpha = 15°$

$l_o = 11.8"$

$R_o = 22"$

total no. of ~~elements~~ = 20

smallest element is approx. 24" from the virtual apex

this element is fed ~~from~~ across the gap

around

Cut frequency - 1500 mcs and higher

smallest element ½ @ 1500 mcs

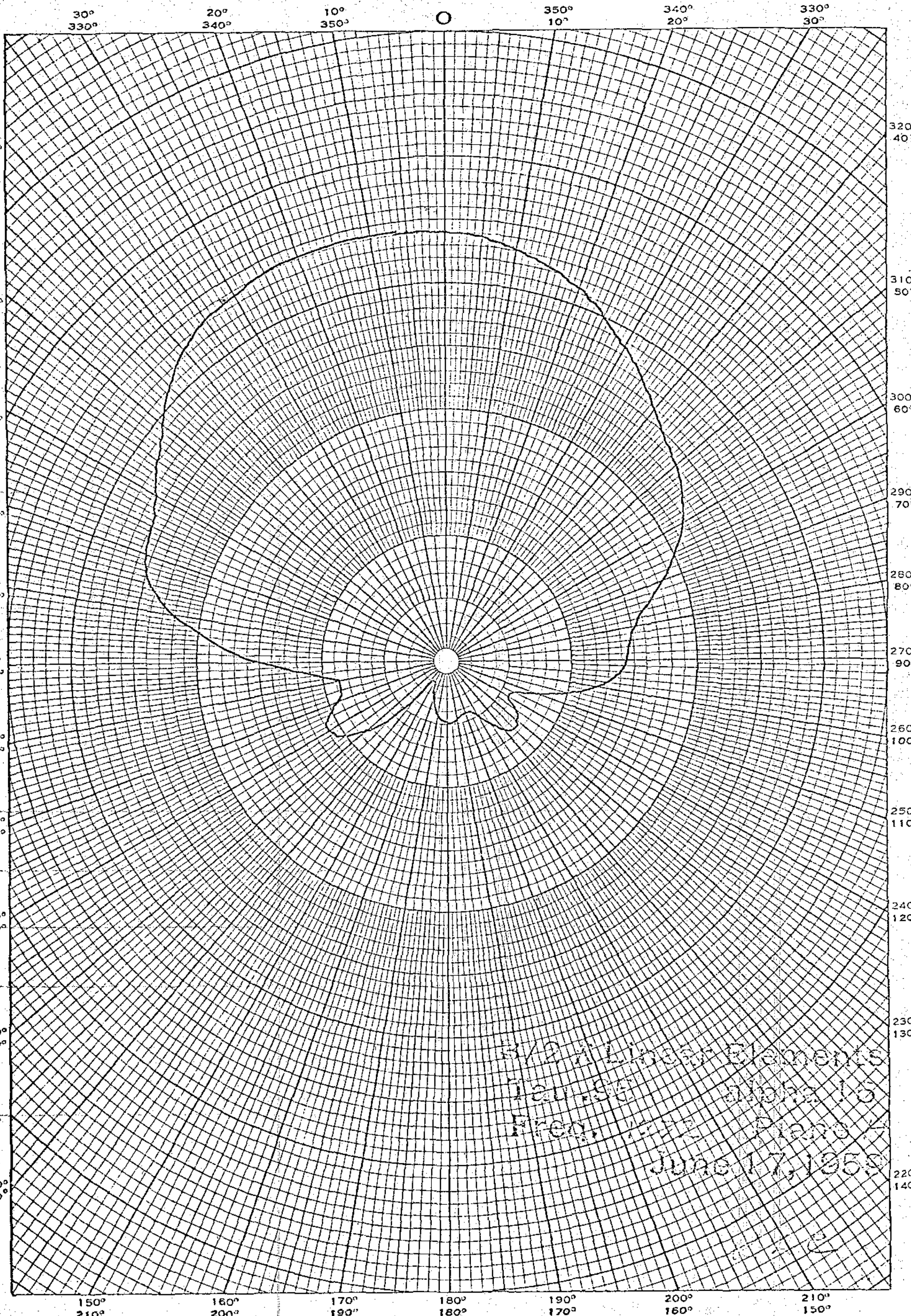

A00427

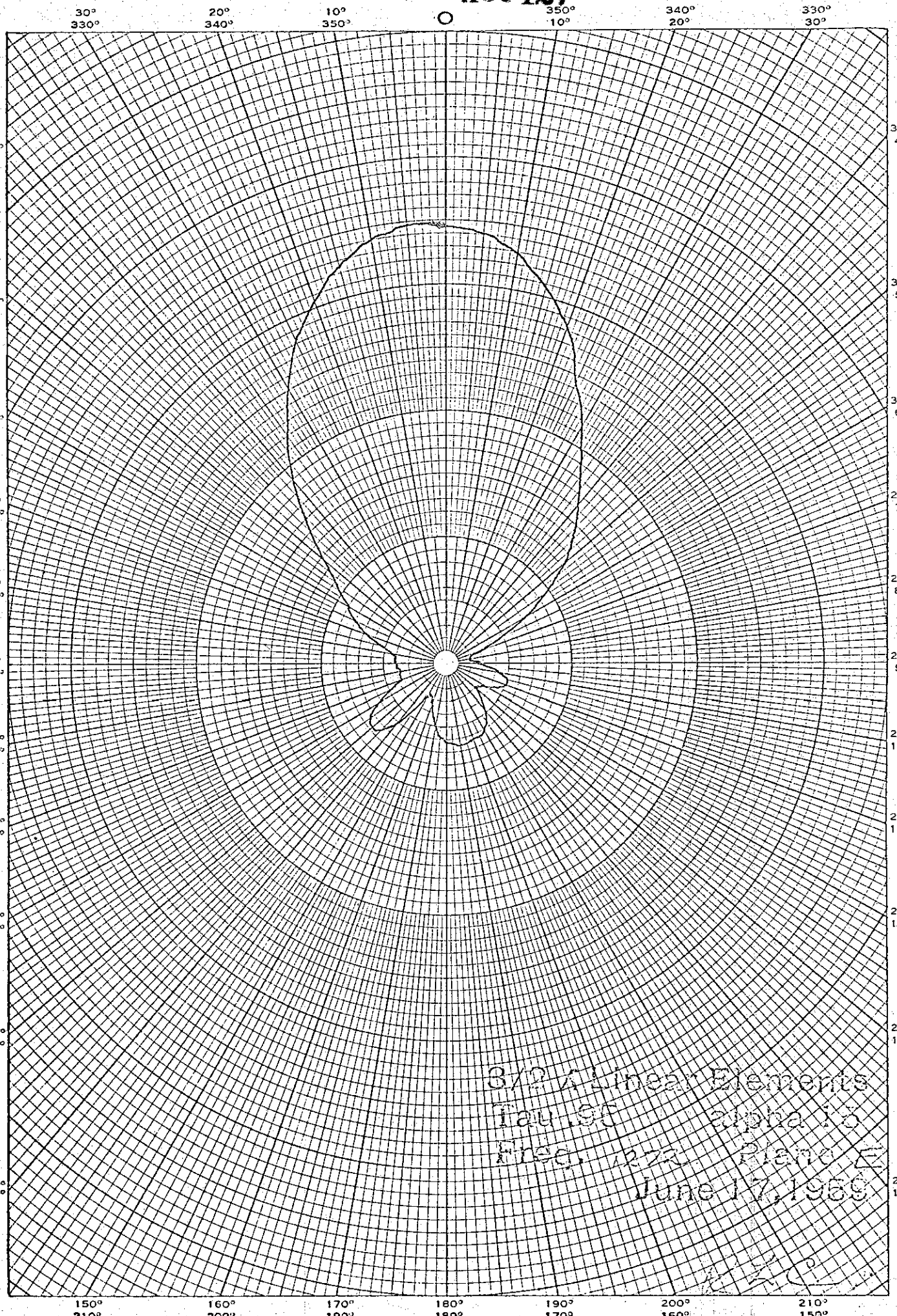

EUGENE DIETZGEN CO.
PRINTED IN U. S. A.

NO. 340-P DIETZGEN GRAPH PAPER
POLAR CO-ORDINATE

A00428

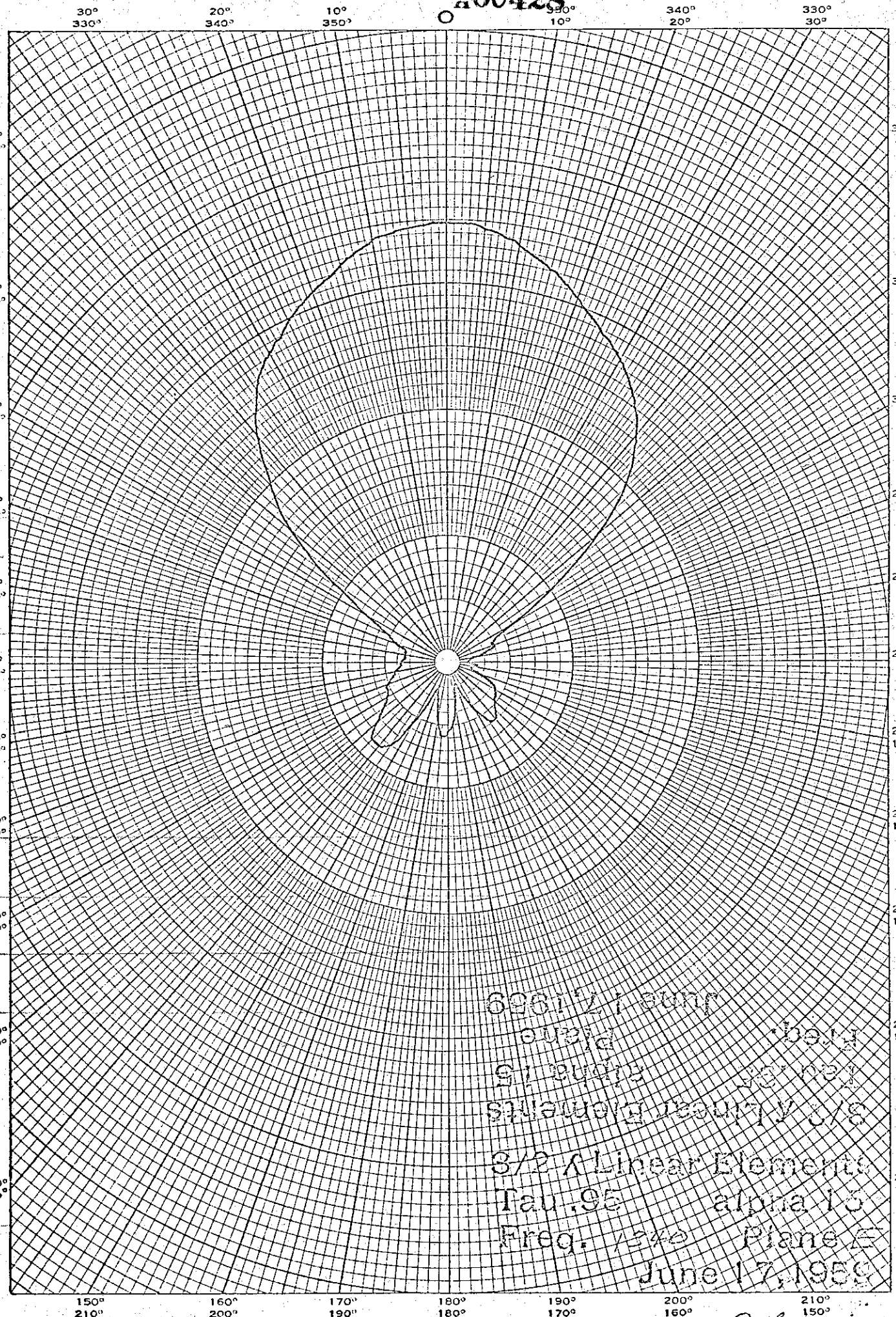

EUGENE DIETZGEN CO.
PRINTED IN U. S. A.

NO. 340-P DIETZGEN GRAPH PAPER
POLAR CO-ORDINATE

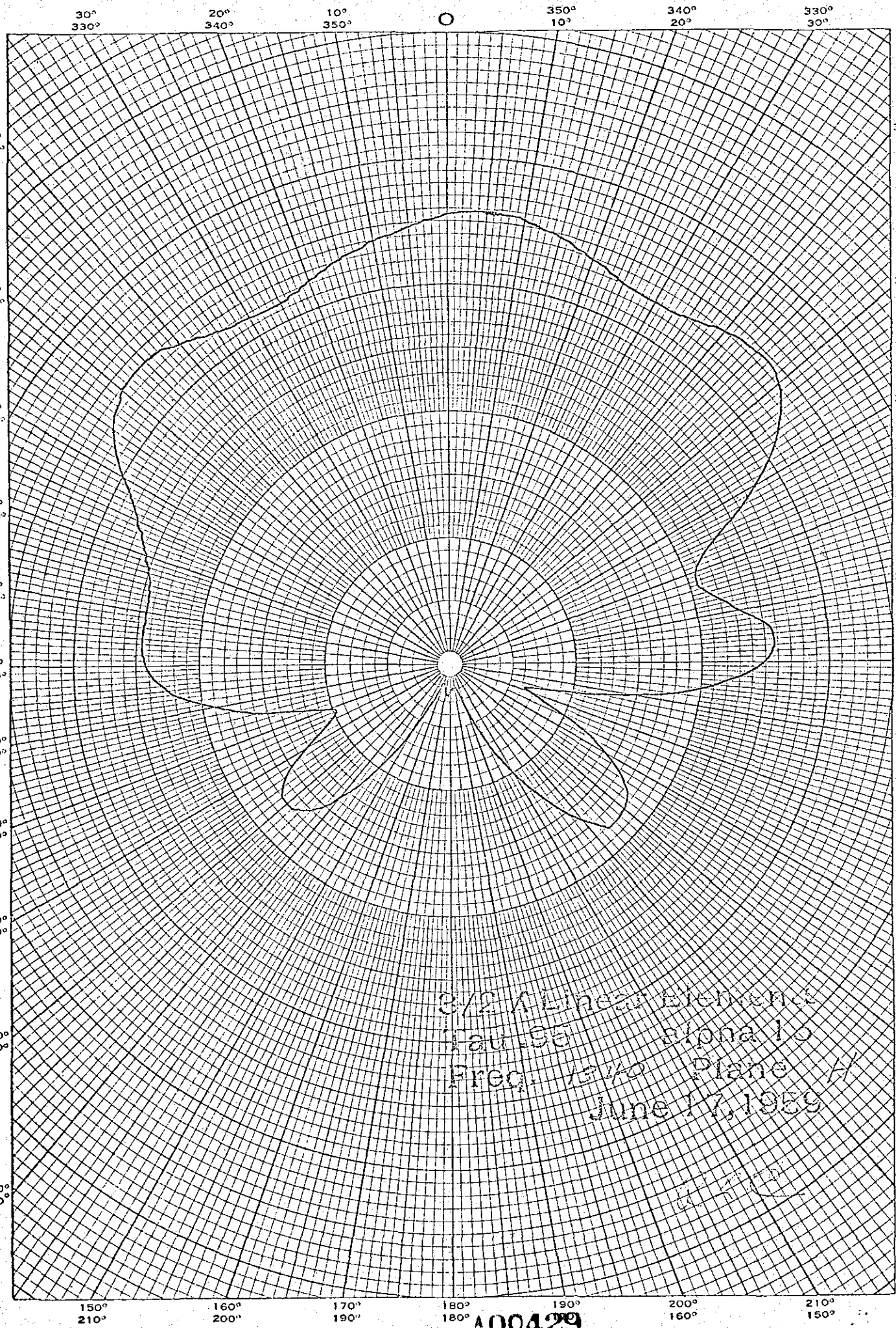

EUGENE DIETZGEN CO.
PRINTED IN U.S.A.

NO. 340-P DIETZGEN GRAPH PAPER
POLAR CO-ORDINATE

A00429

$\frac{3}{2}\lambda$ thin linear element

$\psi = 0$

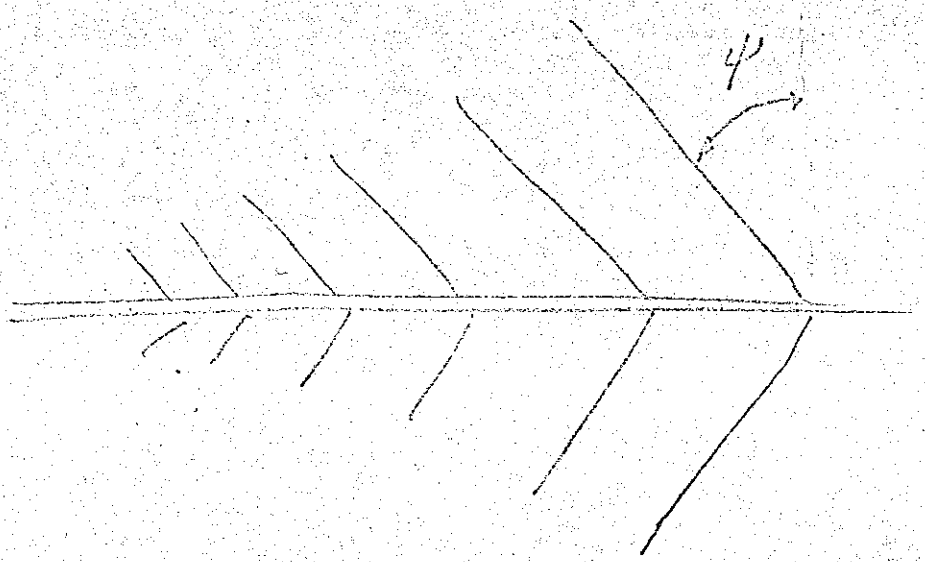

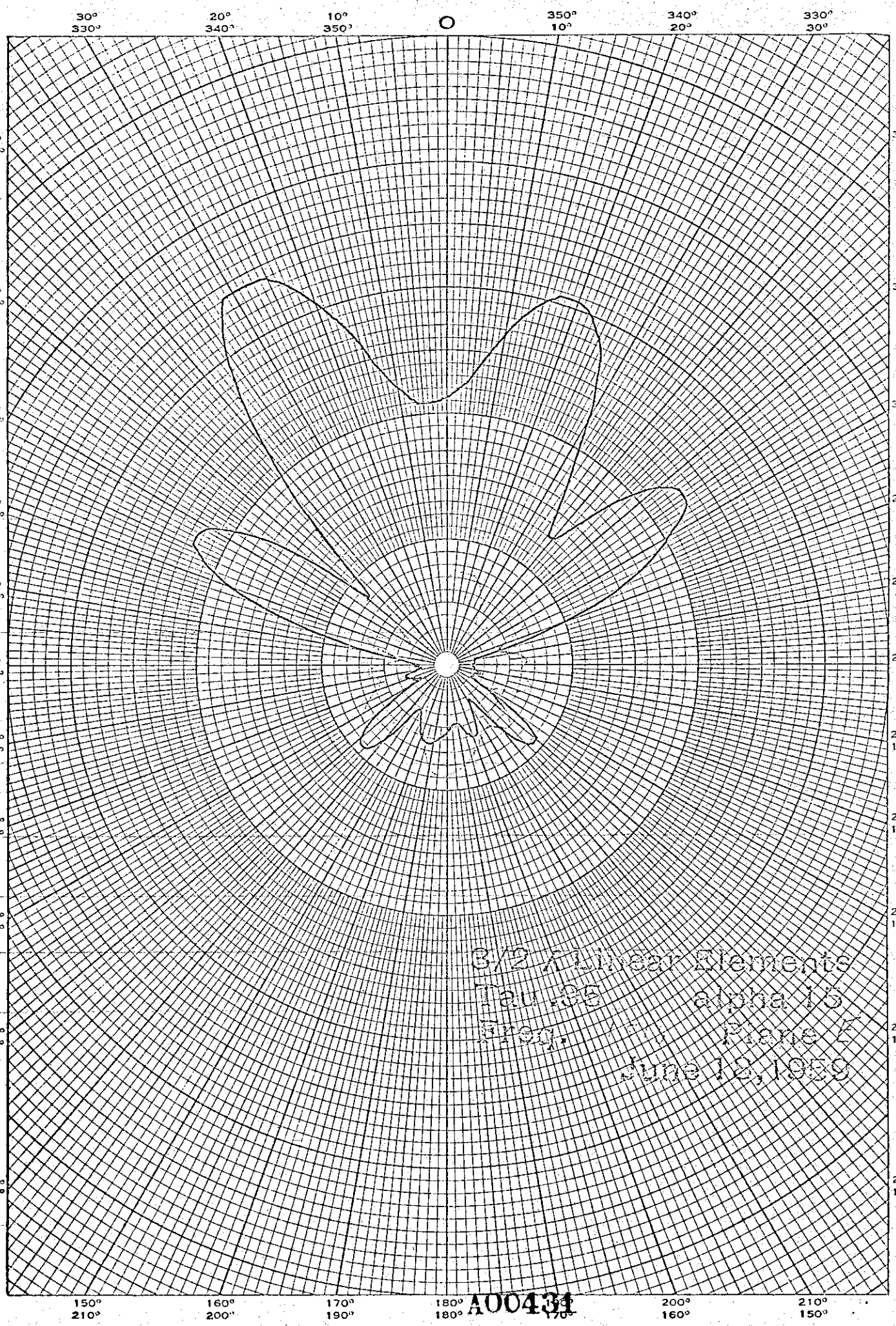

EUGENE DIETZGEN CO.
PRINTED IN U.S.A.

NO. 340-P DIETZGEN GRAPH PAPER
POLAR CO-ORDINATE

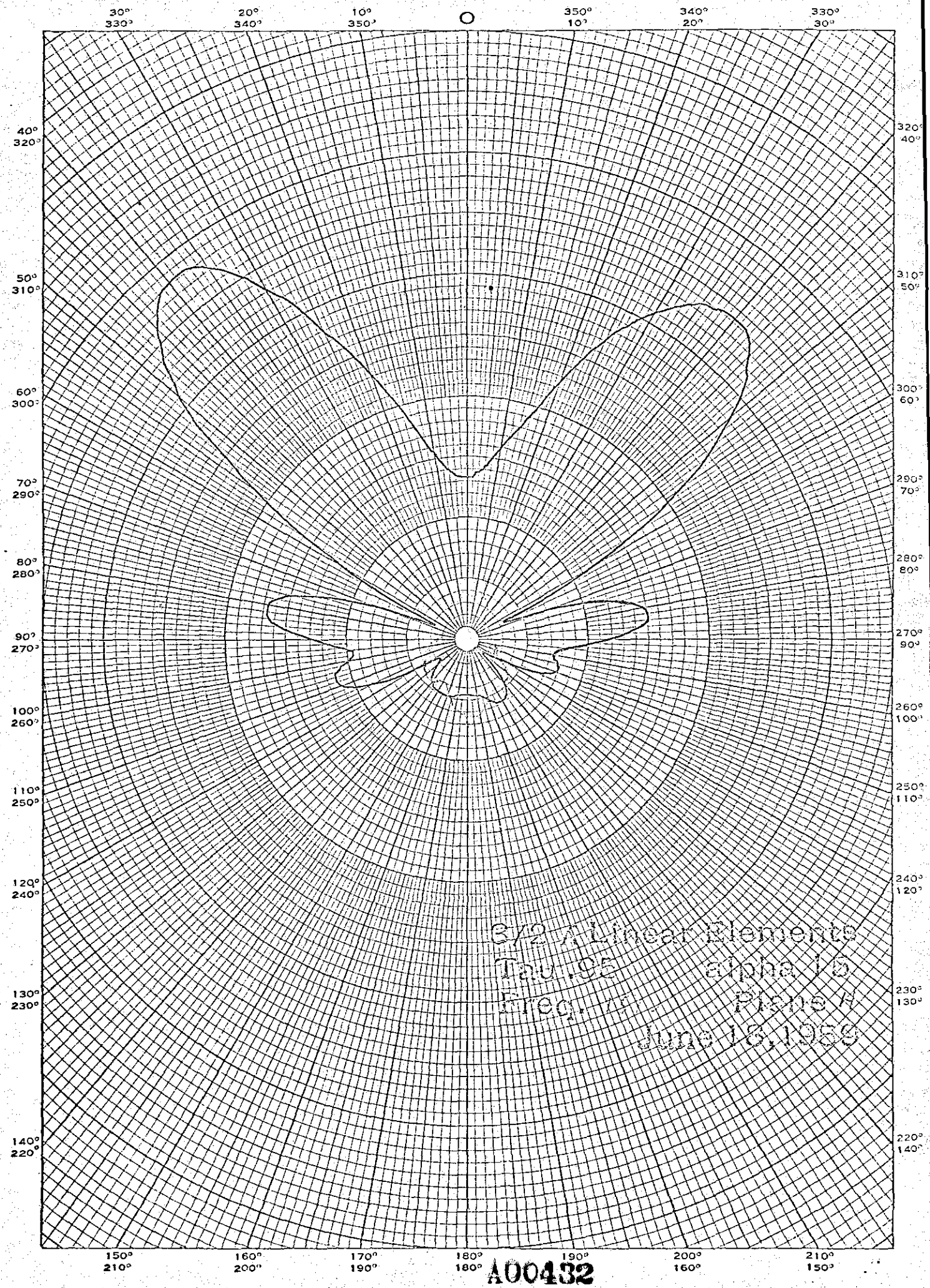

EUGENE DIETZGEN CO.
PRINTED IN U.S.A.

NO. 340-P DIETZGEN GRAPH PAPER
POLAR CO-ORDINATE

A00432

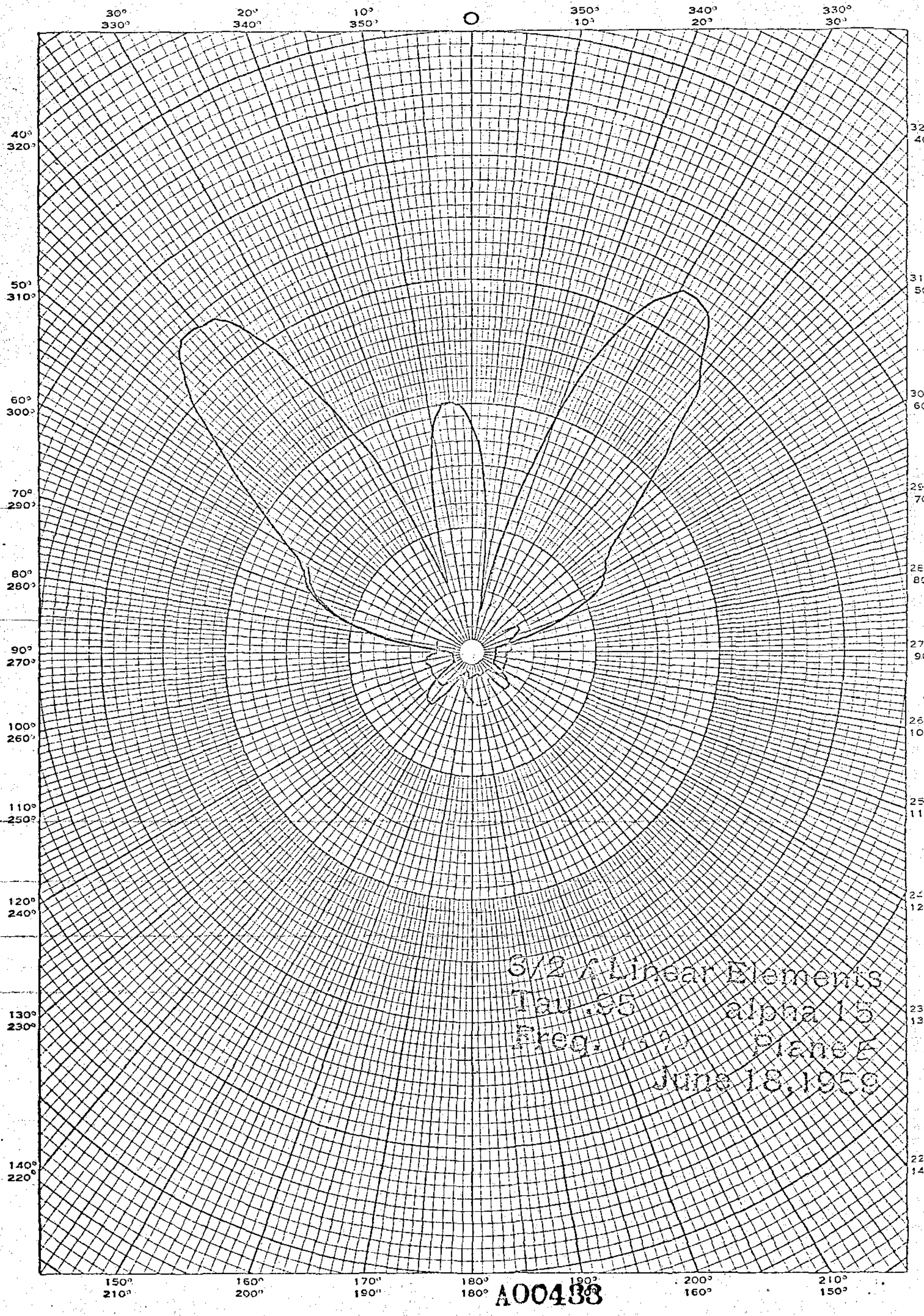

A00433

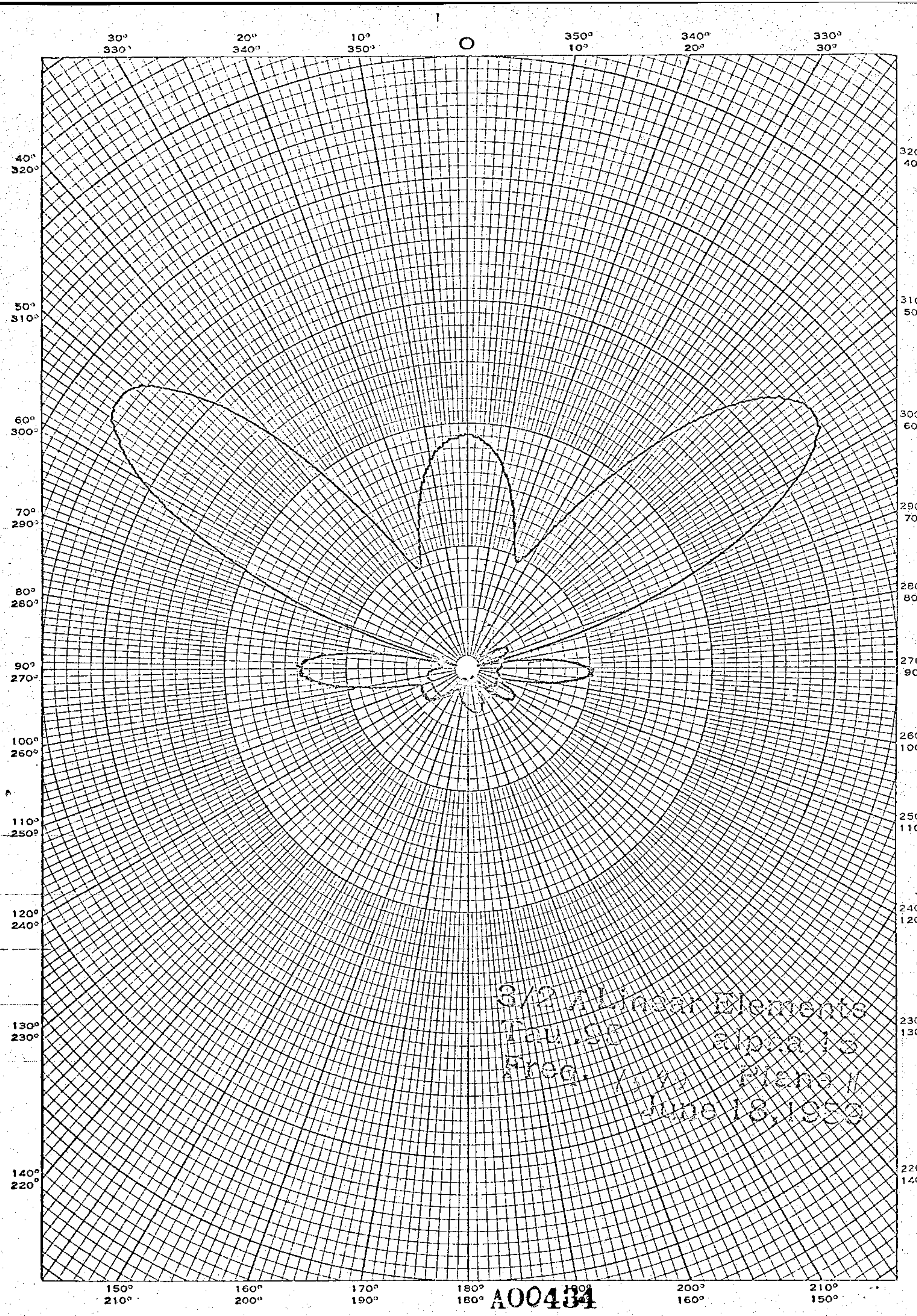

A00434

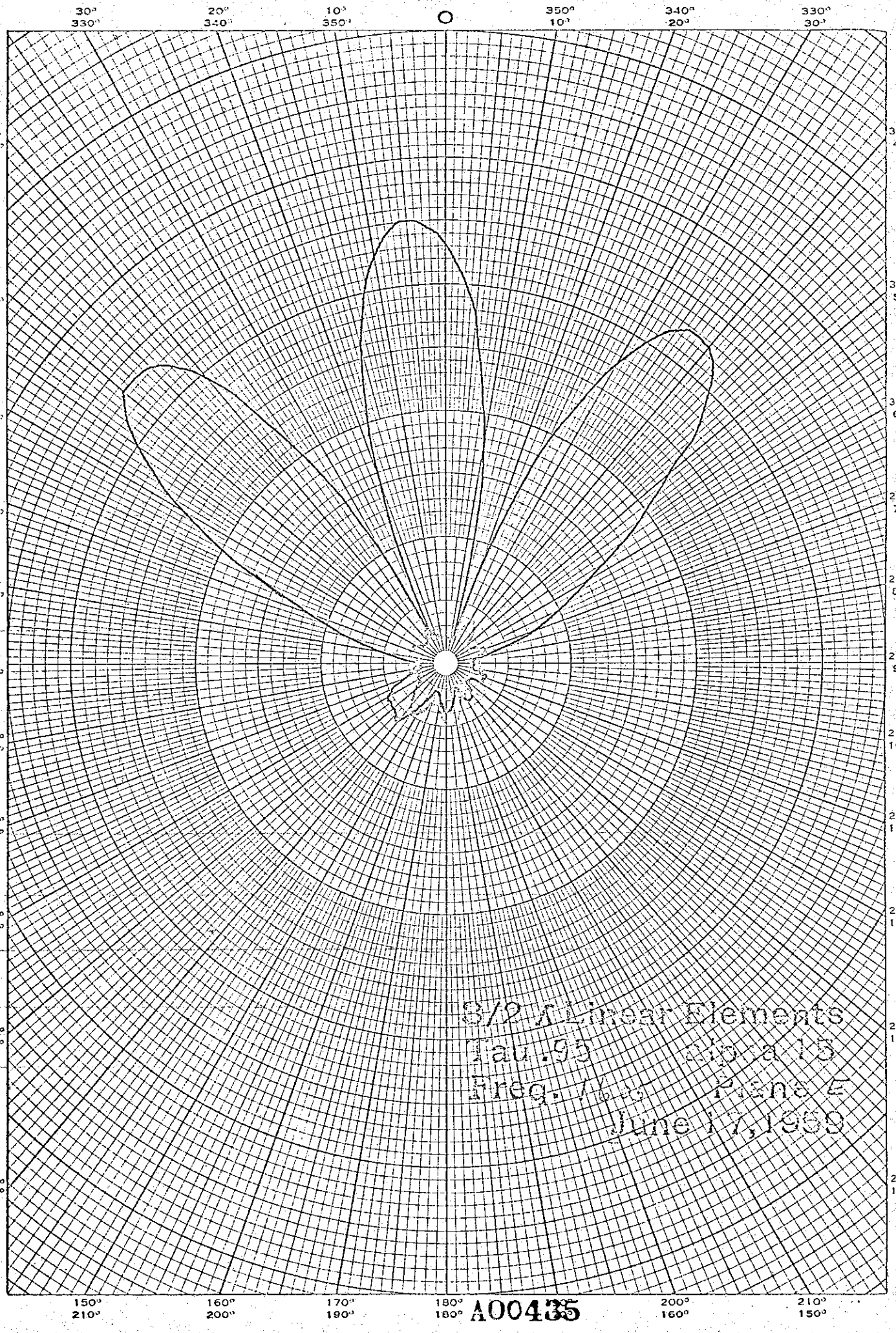

EUGENE DIETZGEN CO.
PRINTED IN U.S.A.

NO. 340-P DIETZGEN GRAPH PAPER
POLAR CO-ORDINATE

A00435

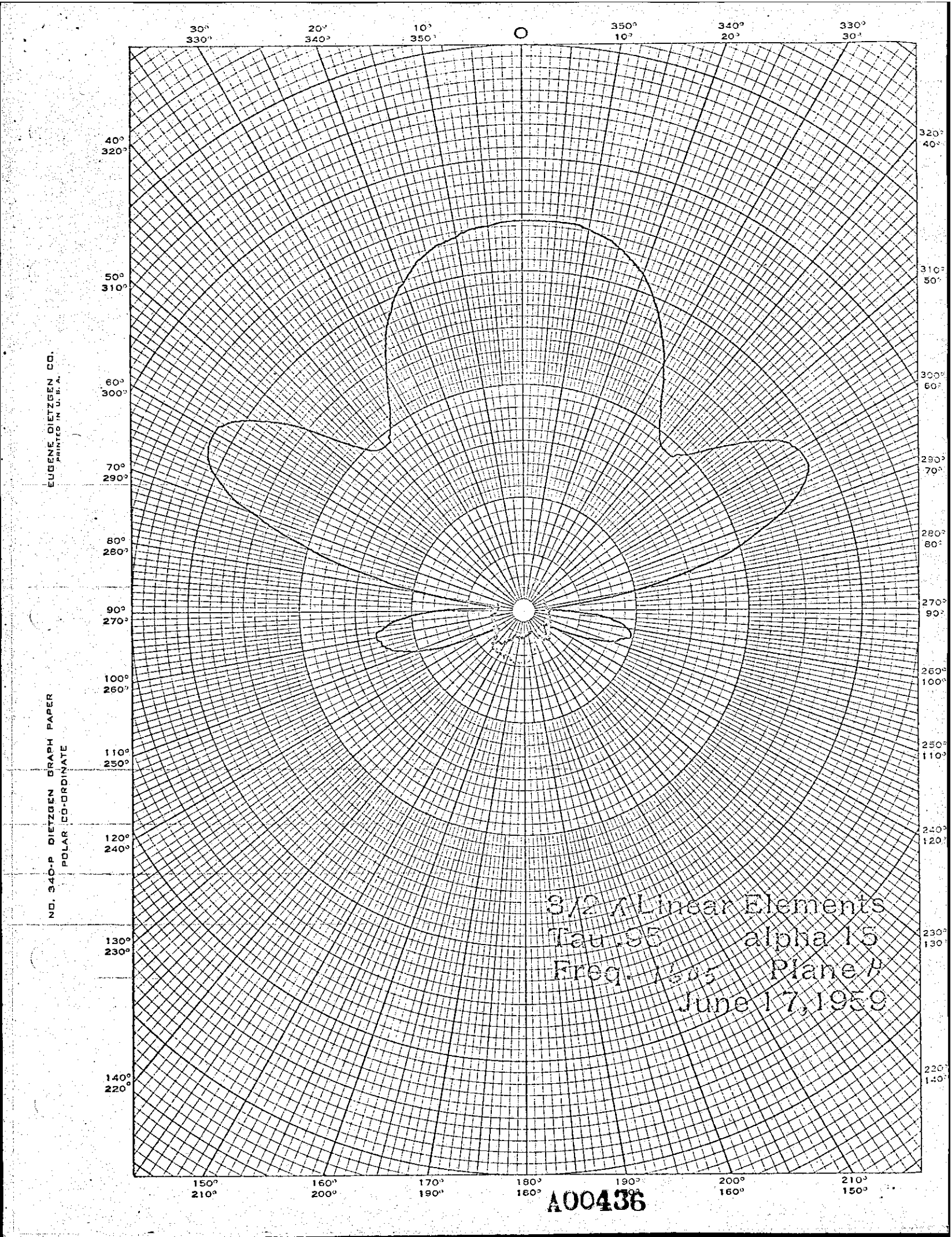
30° 330°
20° 340°
10° 350°
0
350° 10°
340° 20°
330° 30°
40° 320°
50° 310°
60° 300°
70° 290°
80° 280°
90° 270°
100° 260°
110° 250°
120° 240°
130° 230°
140° 220°
320° 40°
310° 50°
300° 60°
290° 70°
280° 80°
270° 90°
260° 100°
250° 110°
240° 120°
230° 130°
220° 140°
150° 210°
160° 200°
170° 190°
180° 180°
190° 170°
200° 160°
210° 150°
EUGENE DIETZGEN CO.
PRINTED IN U.S.A.
NO. 340-P DIETZGEN GRAPH PAPER
POLAR CO-ORDINATE
3/2 λ Linear Elements
Elev. 35° alpha 1.5
Freq. 1285 Plane φ
June 17, 1959

A00436

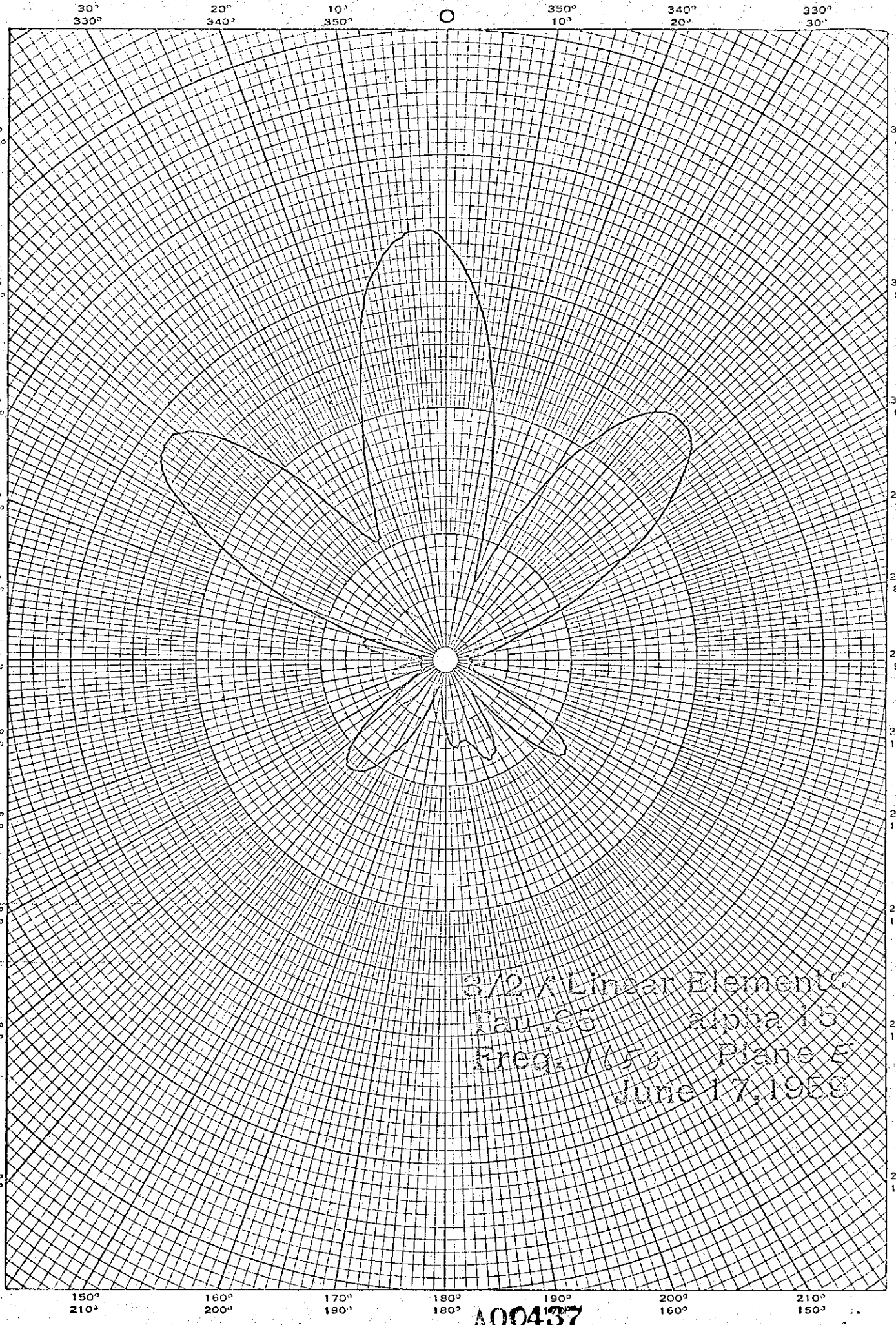

EUGENE DIETZGEN CO.
PRINTED IN U.S.A.

NO. 340-P DIETZGEN GRAPH PAPER
POLAR CO-ORDINATE

A00437

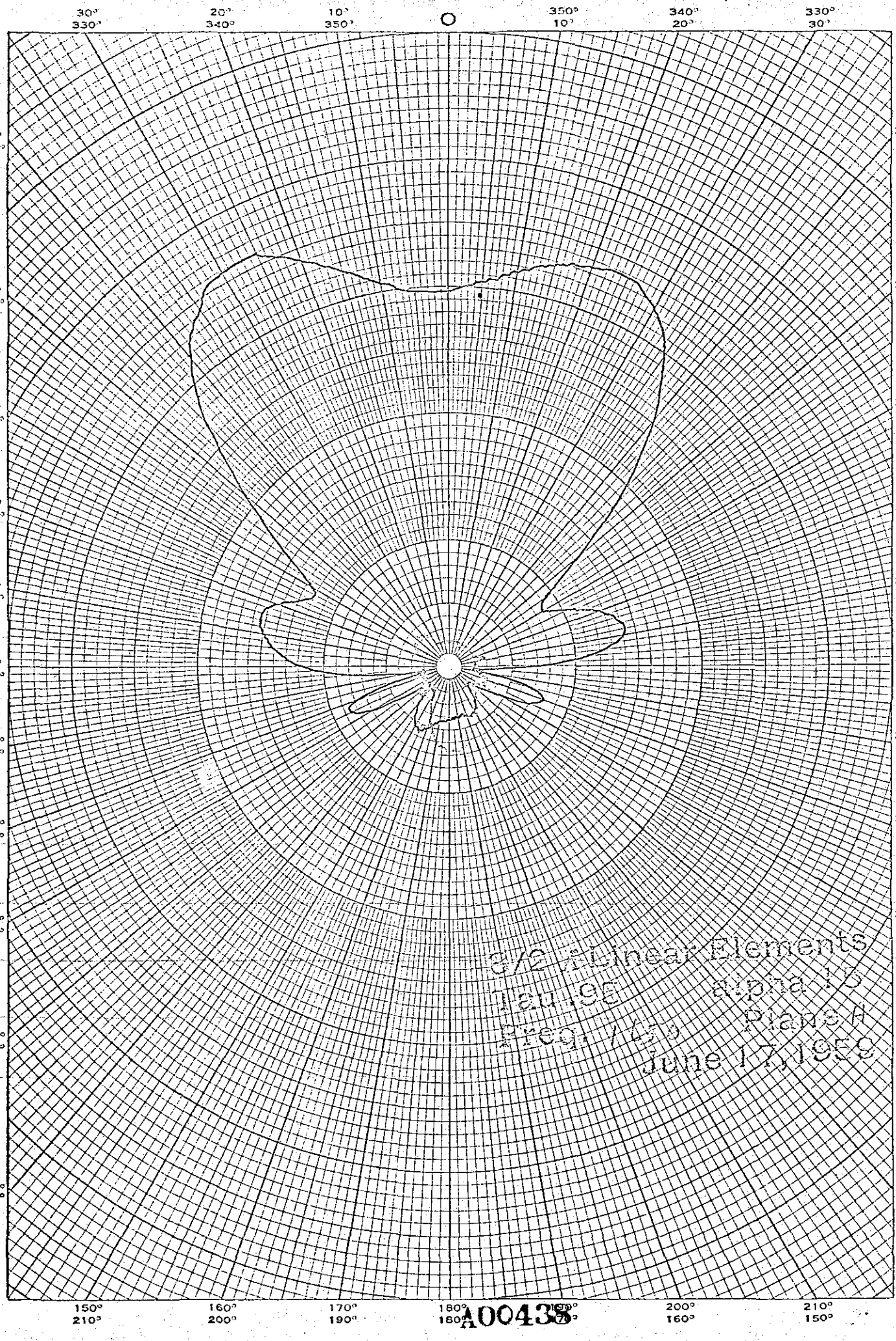

EUGENE DIETZGEN CO.
PRINTED IN U.S.A.

NO. 340-P DIETZGEN GRAPH PAPER
POLAR CO-ORDINATE

A00438

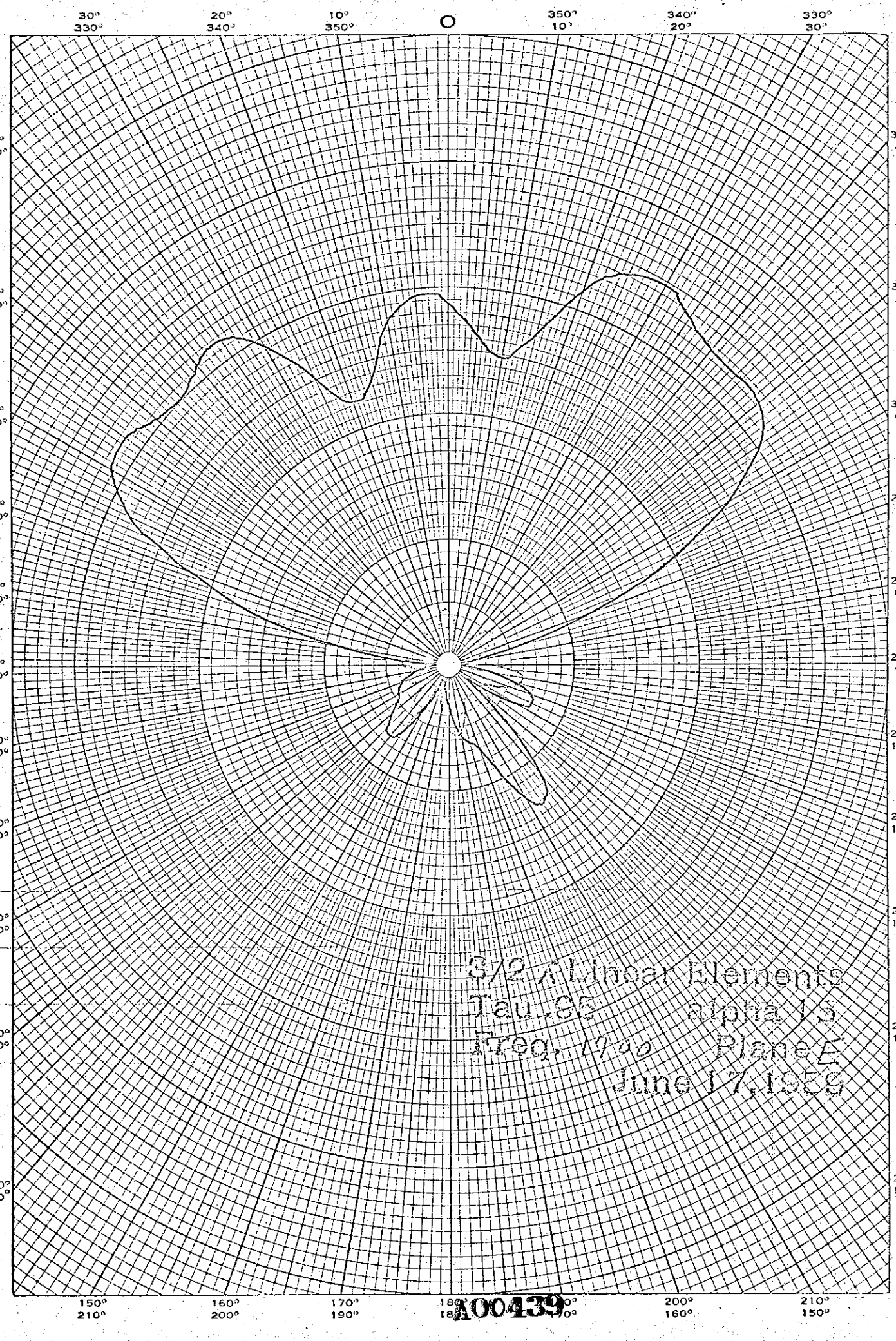

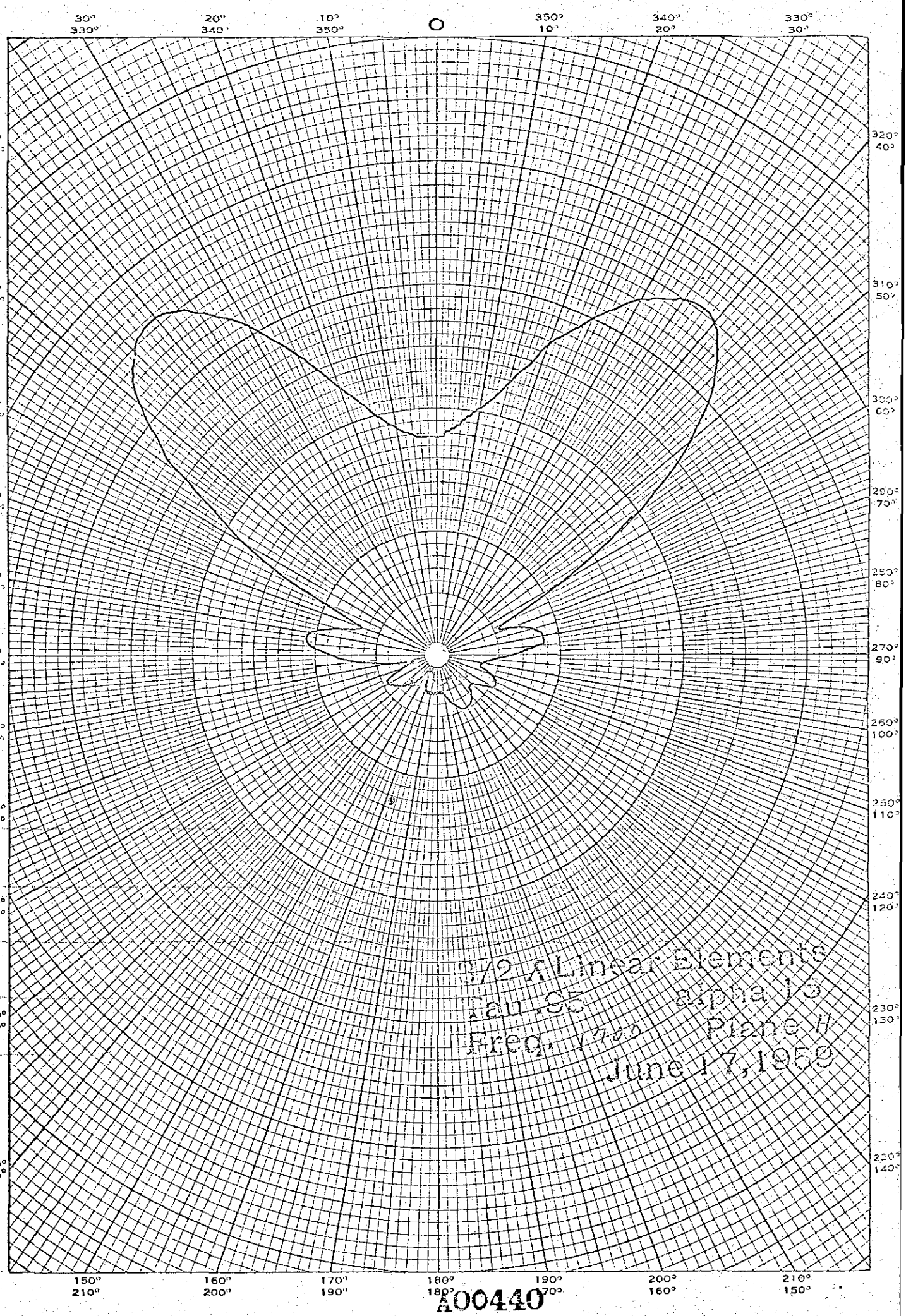

EUGENE DIETZGEN CO.
PRINTED IN U.S.A.

NO. 340-P DIETZGEN GRAPH PAPER
POLAR CO-ORDINATE

A00440

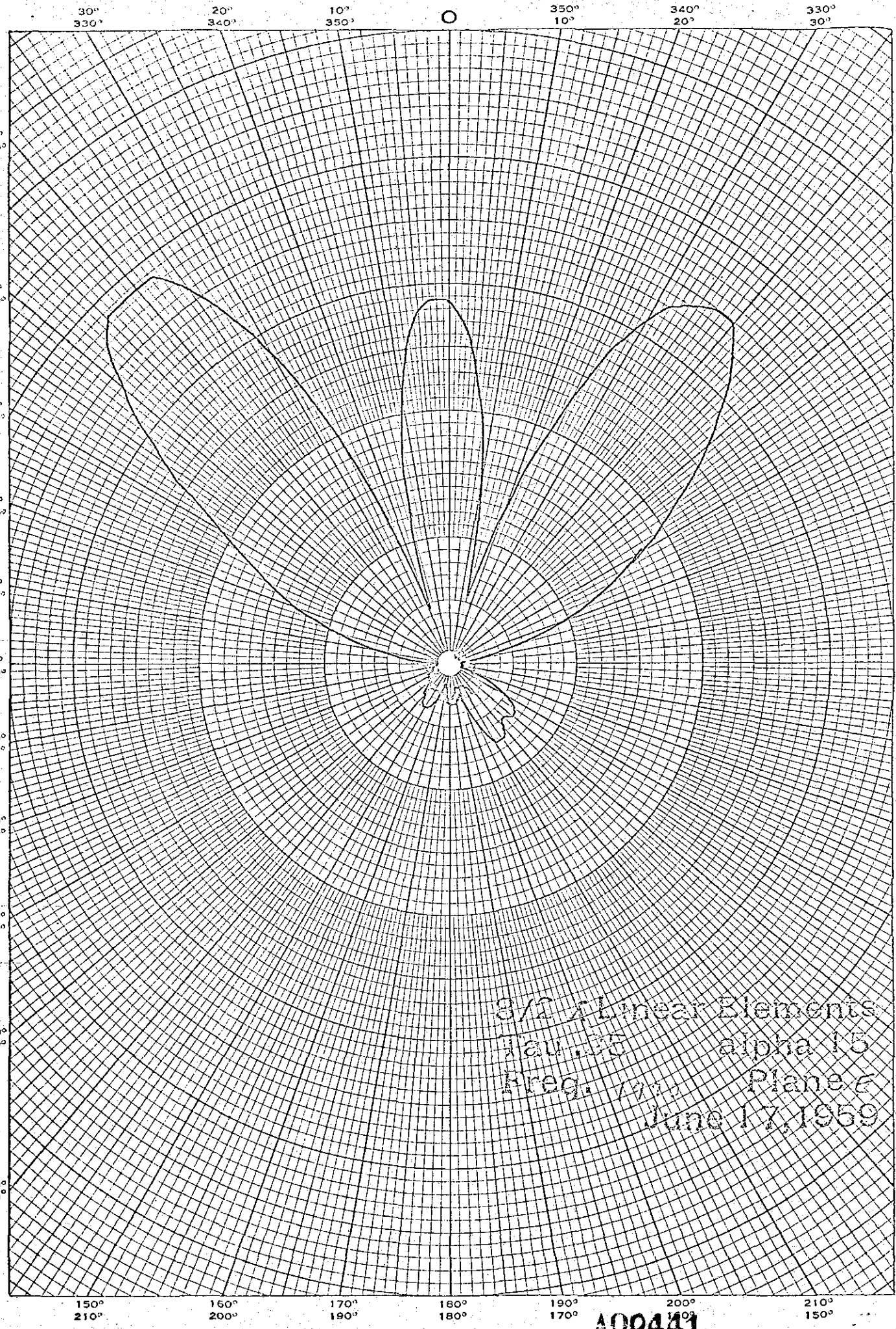

EUGENE DIETZGEN CO.
PRINTED IN U. S. A.

NO. 340-P DIETZGEN GRAPH PAPER
POLAR CO-ORDINATE

A00441

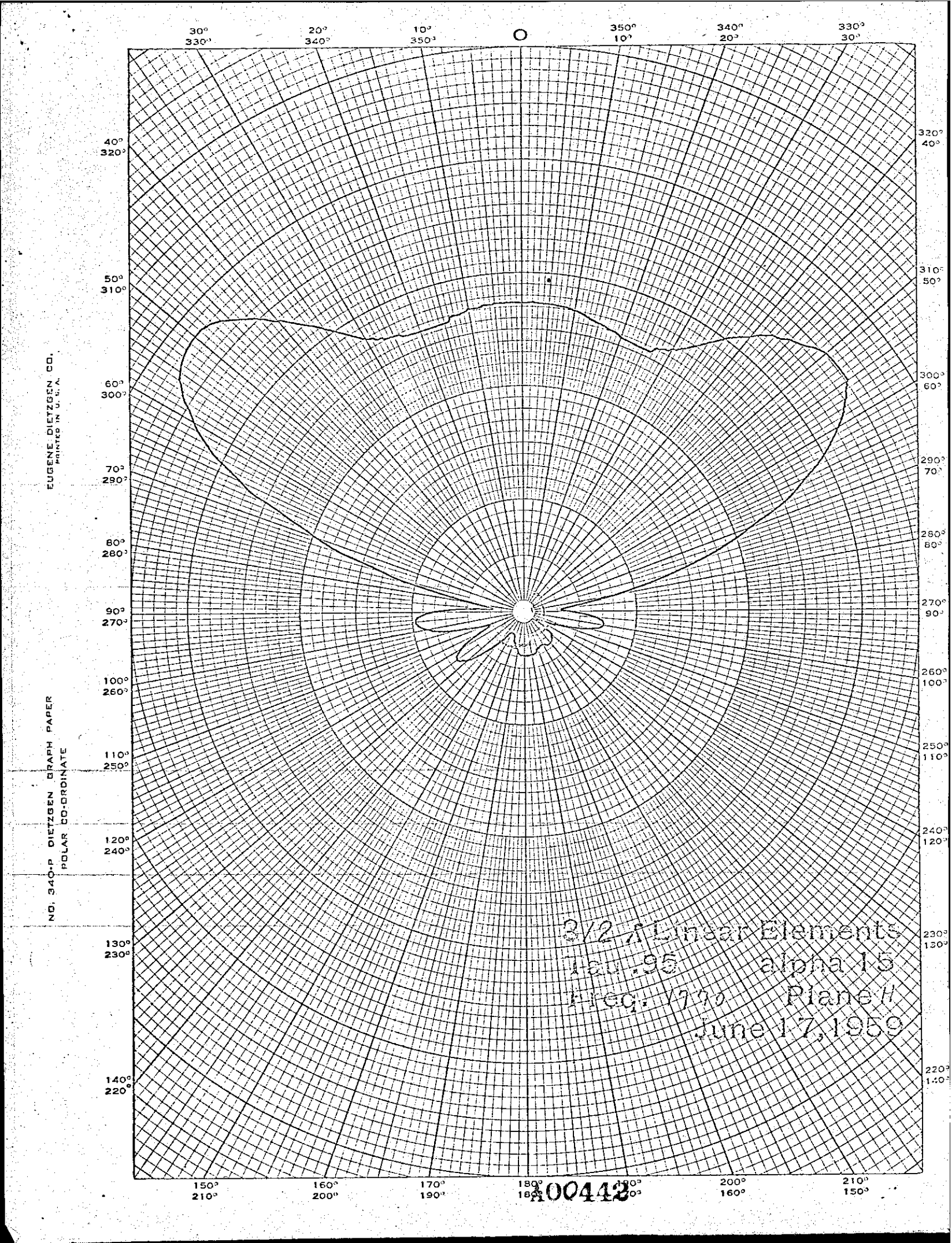

EUGENE DIETZGEN CO.
PRINTED IN U. S. A.

NO. 340-P DIETZGEN GRAPH PAPER
POLAR CO-ORDINATE

A00442

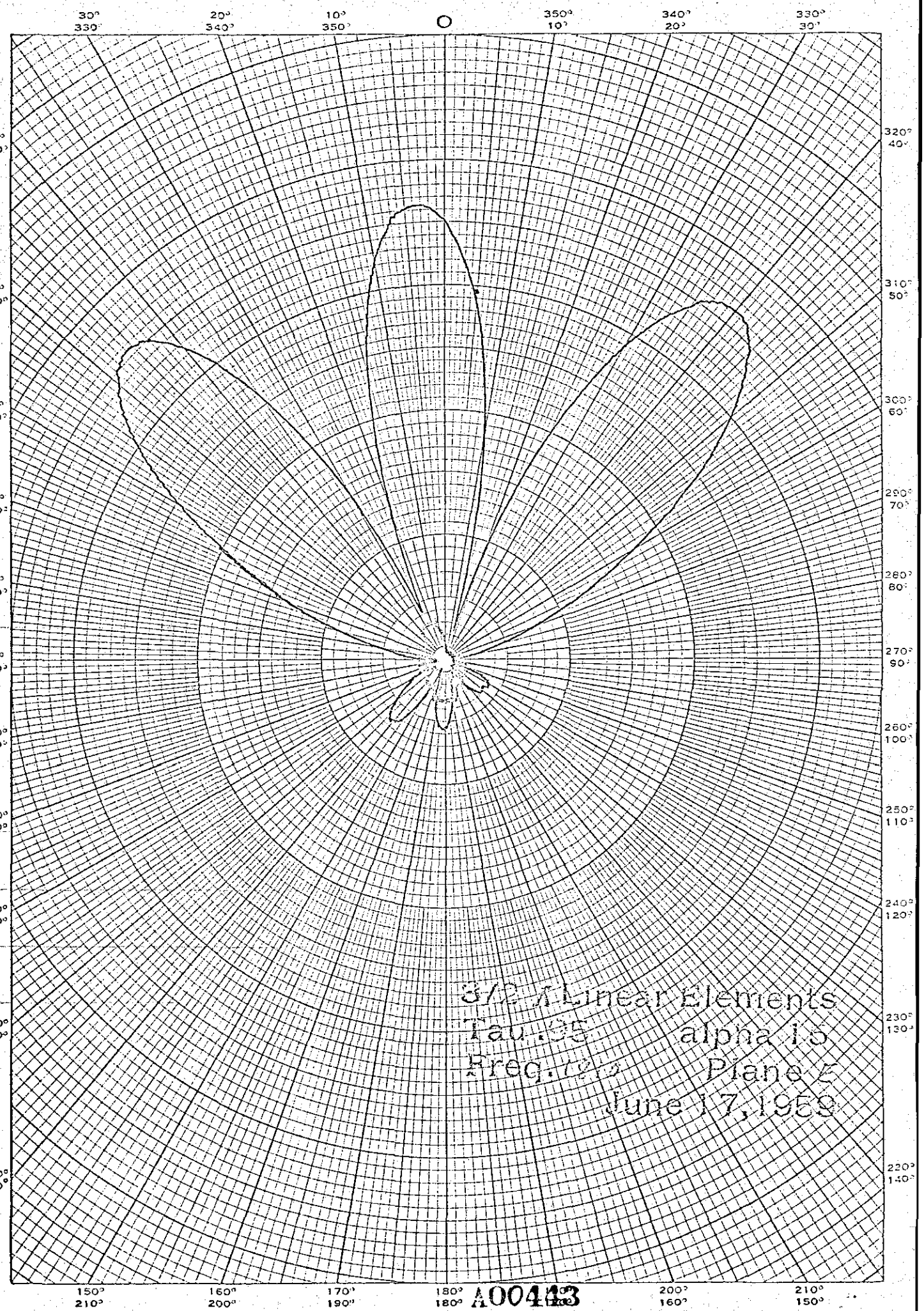

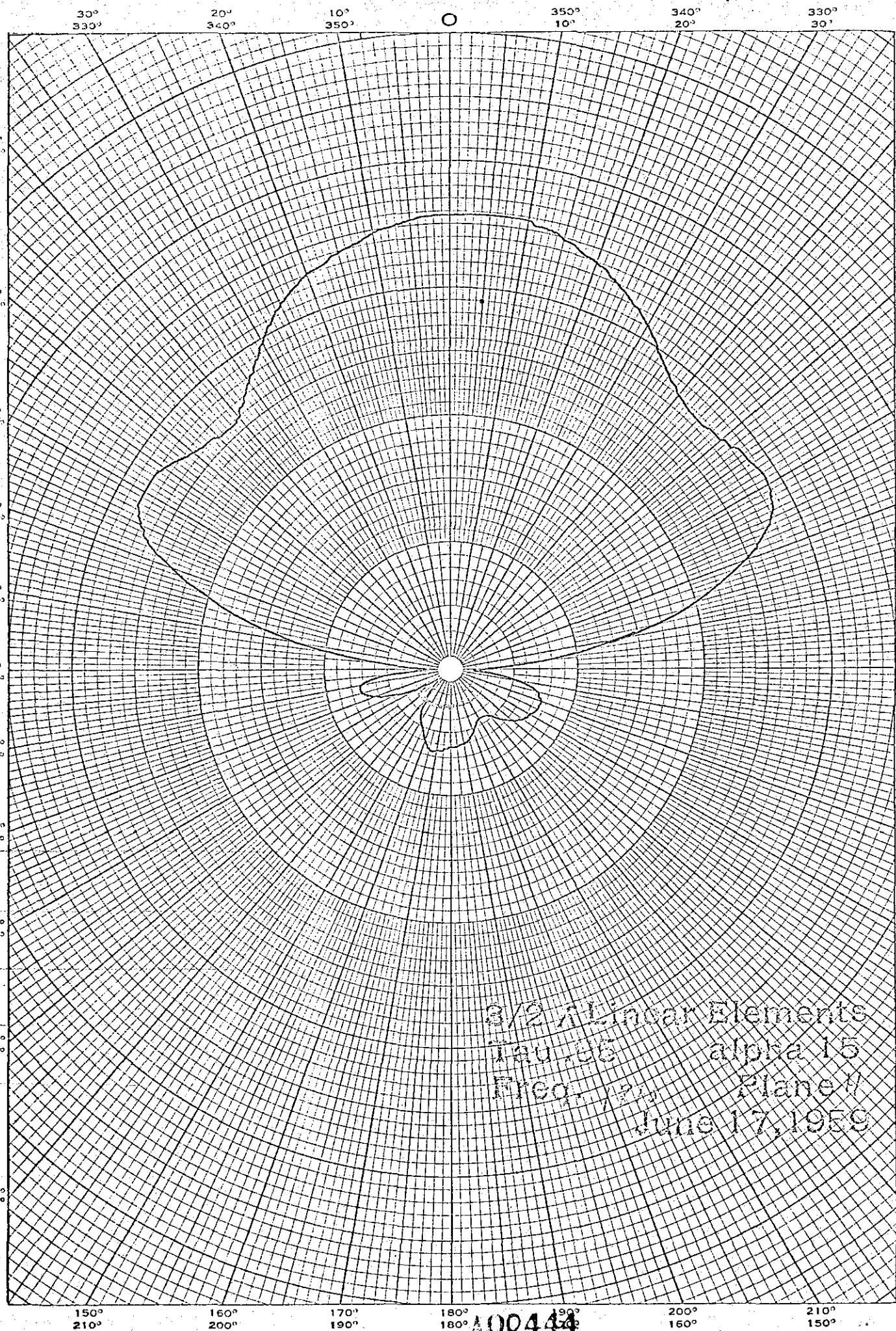
3/2 λ Linear Elements
alpha 15
Plane H
June 17, 1958

$\psi = 32.5°$

A00445

1515 E

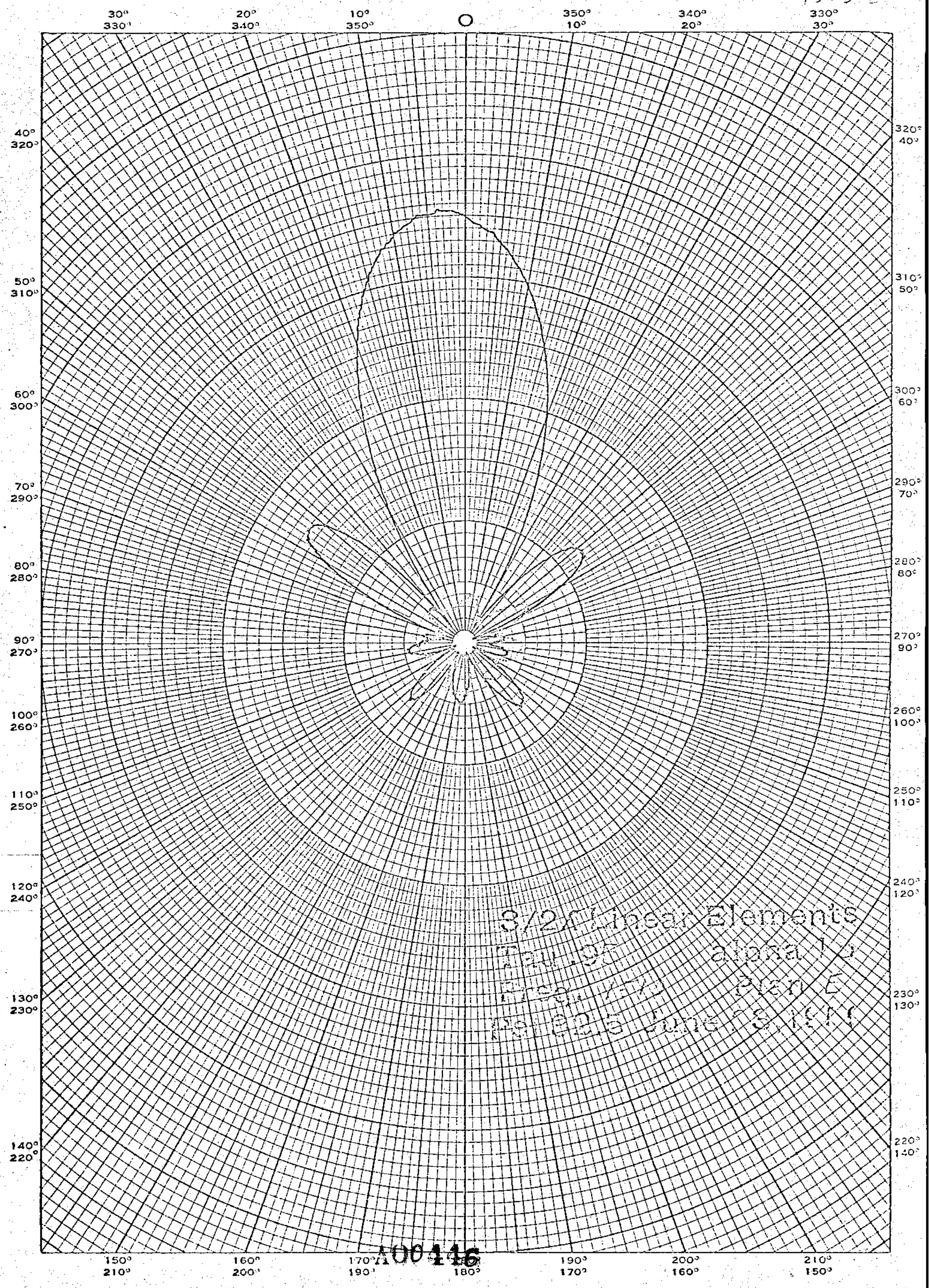

A00116

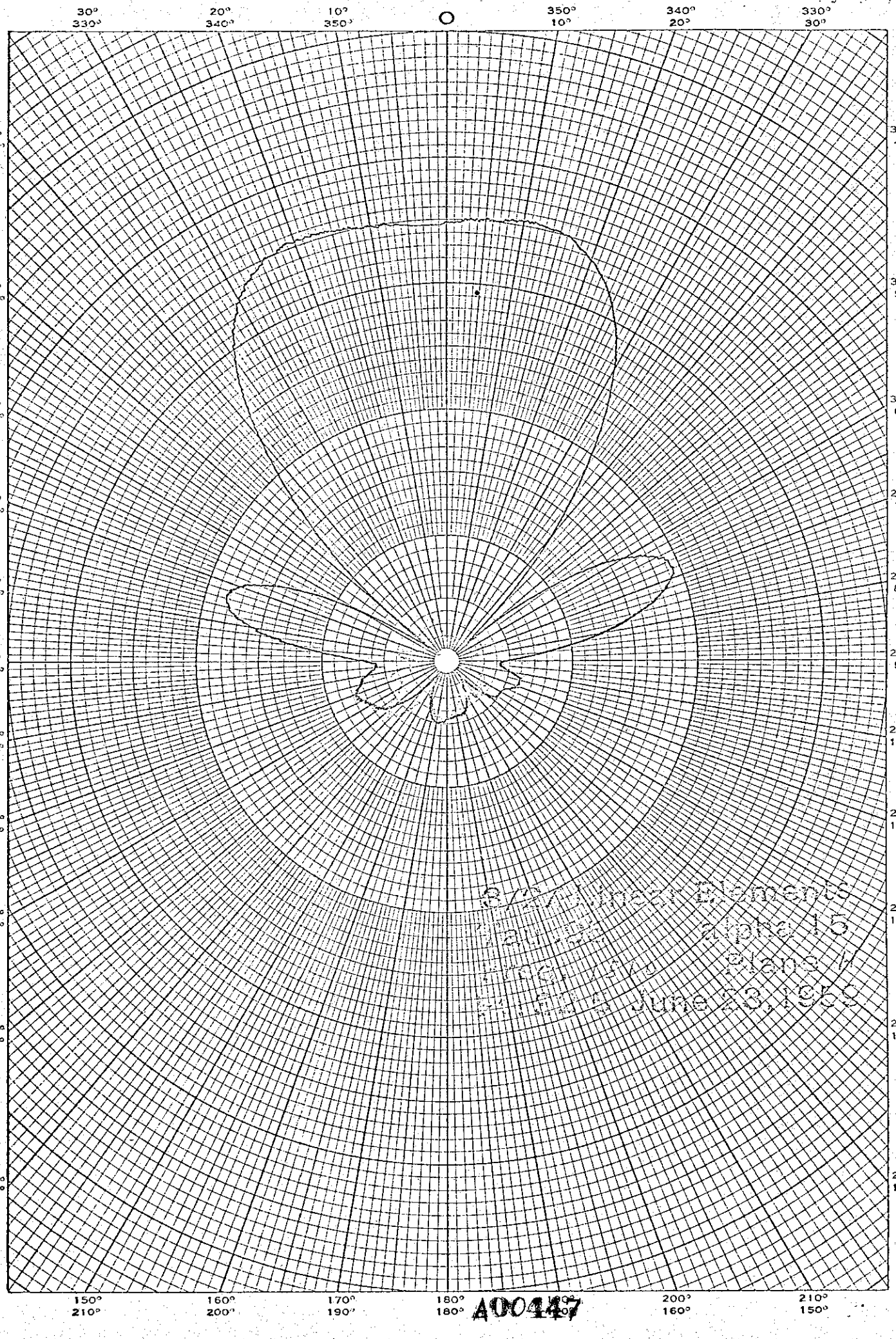

EUGENE DIETZGEN CO.
PRINTED IN U.S.A.

NO. 340-P DIETZGEN GRAPH PAPER
POLAR CO-ORDINATE

A00147

U of I. Foundation Project

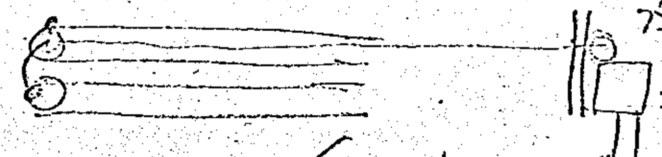

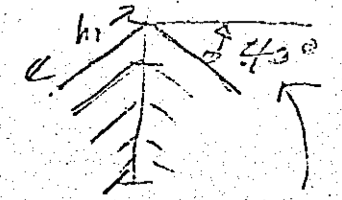

TV-6 (VHF only) Bent Element

$\tau = 0.9$ $\alpha = 17.5°$ $\sigma = 0.085$
$3\sigma = 0.255$

$h/\lambda_{max} = 0.4$ $\frac{3}{1.2\lambda}$ in 3 inch 40°

$N = 7$ 1.4 Bdwdth

diameter	h	d	R_n	D_n
.050	h_1 = 56"	d_1 = 19.05"	17.75"	8.30
.045	h_2 = 50.4"	d_2 = 17.15"	15.96	6.51
.040	h_3 = 45.4"	d_3 = 15.4"	14.39	4.99
.0365	h_4 = 40.8"	d_4 = 13.9"	12.92	3.47
.033	h_5 = 36.8"	d_5 = 12.5"	11.67	2.22
.029	h_6 = 33.1"	d_6 = 11.2"	10.50	1.05
.027	h_7 = 29.8"		9.45"	0
	292.3	L = 89.2"	92.64	
	584.6			

8.3
+2.8
11.1

$h/a = 224$ feeder D = .174

$Z_a = 380$

$\sigma' = .0896$

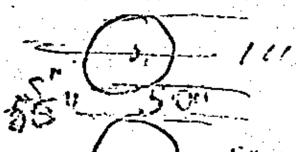

$R_0 = 65$ $\frac{1}{8\sigma' \frac{Z_a}{R_0}} = \frac{65}{8(.0896)(380)} = .238$ $.238^2 = .0569$

$.238 + \sqrt{1.0569}$
$= .238 + 1.028$
1.266

$\frac{Z_0}{R_0} = 1.266$

$Z_0 = 1.266\,(65)$
$= 82.5$

75 — 300
Balun — transformer $= 1.266$

$\cosh \frac{82.5}{120} = \frac{s}{d} = 1.2466$

$s = .217$

A00424

KB ed 47

perfec

assault on

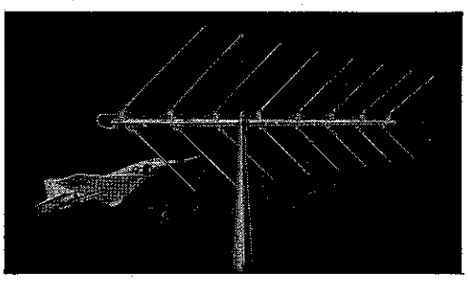

Back in 1962, we invented a new kind of TV antenna.

UNITED STATES DISTRICT COURT
NORTHERN DISTRICT OF ILLINOIS
BEFORE JUDGE HOFFMAN

DEFENDANT EX. NO._____
DOROTHY L. BRACKENBURY
OFFICIAL COURT REPORTER

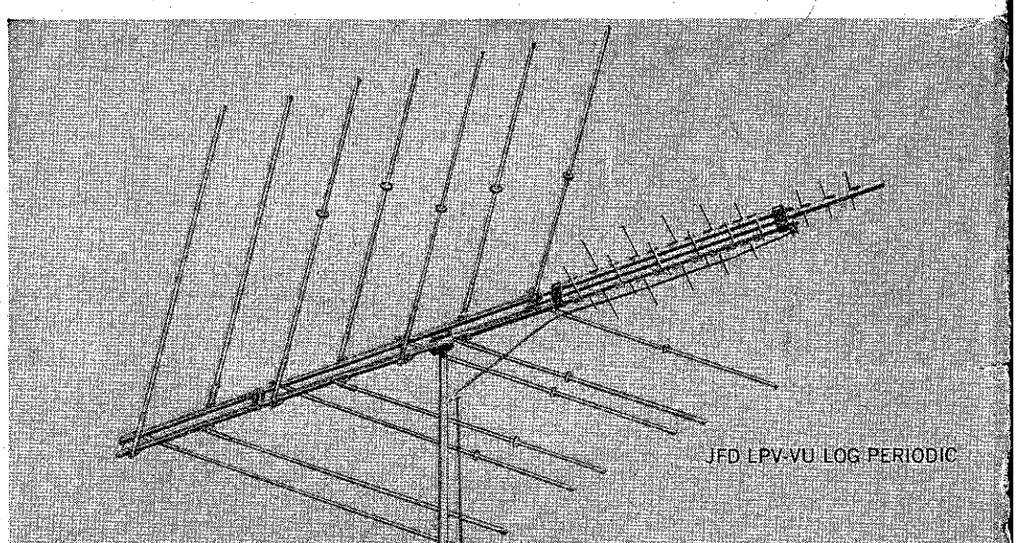

Licensed under one or more of U.S. patents 2,958,081; 2,985,879; 3,011,168; 3,108,280; 3,150,376; 3,210,767, RE. 25,740 and additional patents pending in U.S.A. and Canada. Produced by JFD Electronics Co. under exclusive license from the University of Illinois Foundation.

ANDREWS ELECTRONICS
1500 W. Burbank Boulevard
Burbank, California

DEAN'S ELECTRONICS
2310 Long Beach Boulevard
Long Beach, California

GROSSMAN & REYNOLDS
1800 West Valley Boulevard
Alhambra, California

MARCUS ELECTRONICS
5751 W. Pico Boulevard
Los Angeles, California

MARTIN DISTRIBUTING COMPANY
2509 East Florence Avenue
Huntington Park, California

HURLEY ELECTRONICS
2101 N. Fairview, Santa Ana, 638-7220
In: Inglewood, 679-2276 Ontario, YU 6-6638; San Bernardino, TU 5-0721; Long Beach, HE 6-8268; Oxnard, HU 3-0133; Oceanside, SA 2-7694.

PAPEL BROTHERS
4652 E. Third Street
Los Angeles, California

RABER WHOLESALE ELECTRONICS
265 So. Laurel St., Ventura
116 No. Nopal St., Santa Barbara

RADIO PRODUCTS SALES
1501 So. Hill Street
Los Angeles, California

WESTERN RADIO & T.V.
1415 India Street
San Diego, California

VALLEY RADIO SUPPLY
1134 33rd Street
Bakersfield, California

electronic service dealer

the official publication of the california state electronics association

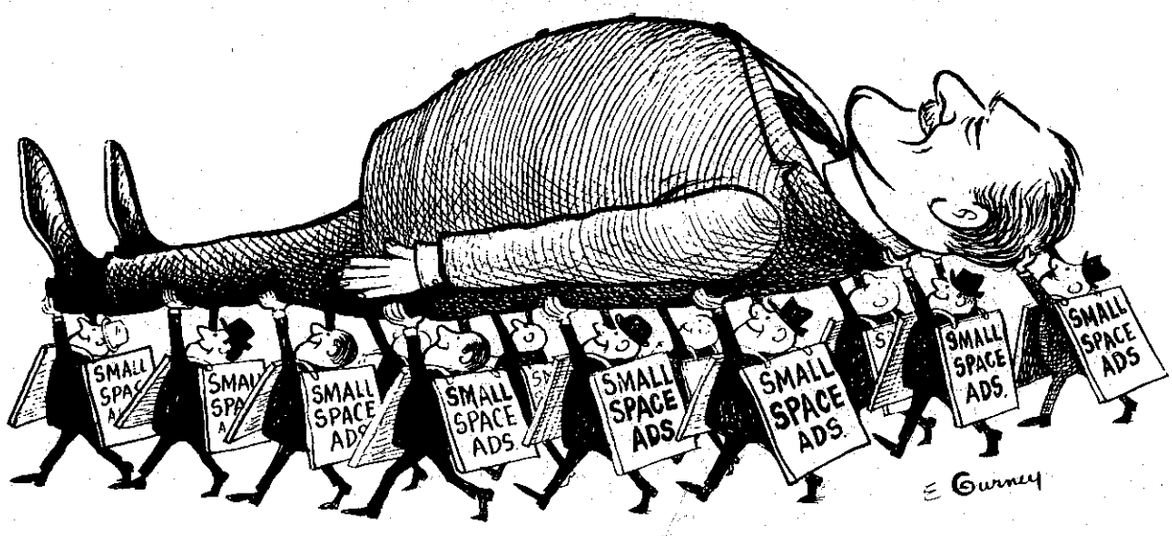

How to Make Your SMALL ADS WORK

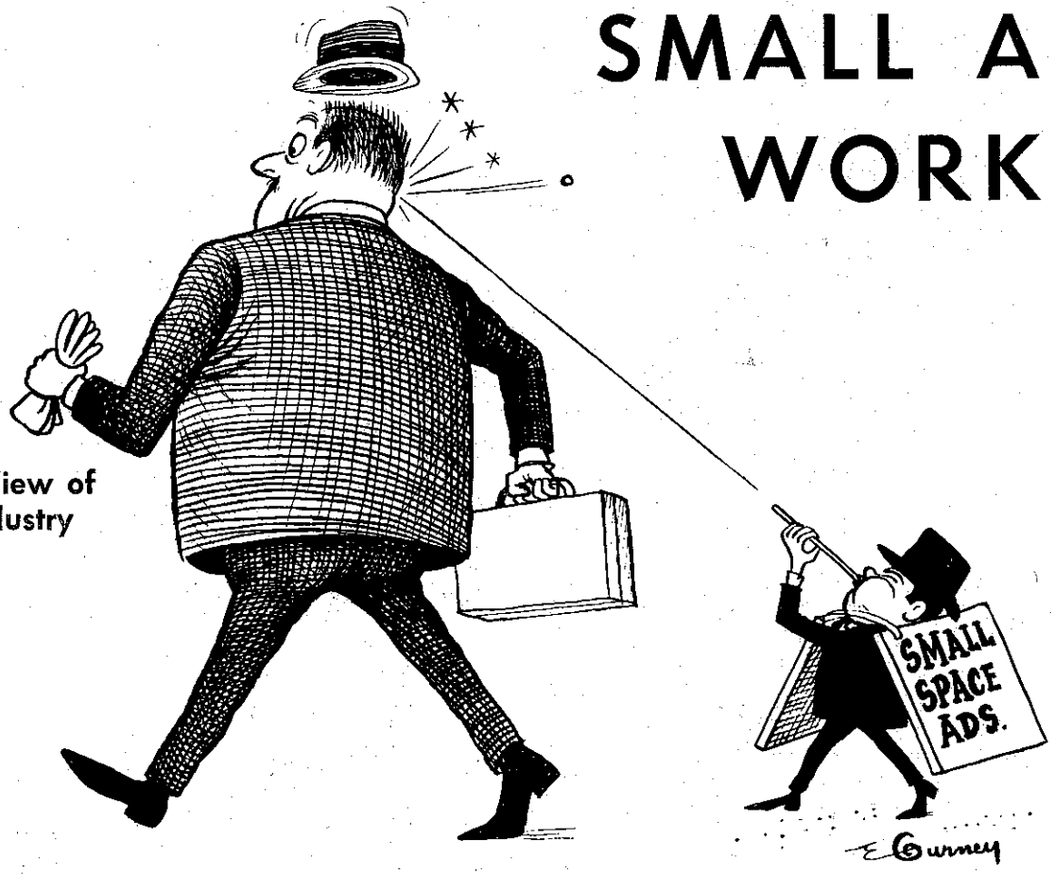

Also In This Issue:
A Broadcaster's View of
The Television Industry

tion: PERFECTION CONQUERED

We did not improve on an old antenna. We started from scratch to design a new one. *Really new.*

It wasn't easy. And it wasn't cheap. But it worked like mad.

We called it the LPV Log Periodic. Its performance caught our competitors with their charts down. But it wasn't long before they came up with LPV copies in every way—except in performance.

Meanwhile back at the JFD labs in Champaign, Illinois, our scientists and engineers continued their "assault on perfection." In 1963, they again shattered antenna precedent by coming up with the *first* combination VHF/UHF/FM log periodic antenna, the LPV-VU. Instead of three different antennas, installers now needed only *one* LPV-VU and *one* downlead.

Our competitors scoffed at the idea. They said it couldn't be done. Until the "eye-popping" results started to roll in. Then there was a mad scramble for the LPV-VU bandwagon.

These "me-too" antennas looked like the LPV-VU Log Periodic. Sounded like it, too. But their charms were skin-deep.

Only the JFD LPV-VU delivered deluxe 82-channel log periodic performance. Because only the JFD LPV-VU followed the genuine patented log periodic concept of the University of Illinois Antenna Research Laboratories. Thanks to the protection of eleven different LPV-VU U.S. patents issued and pending—more than those of any other antenna.

You would think by now our Research and Development people in Champaign would leave well enough alone. But no. These "Young Turks" have gone and done it again. This time it's a new all-band log periodic design—the LPV-CL Color Laser. (Must be that "assault on perfection" bug they've still got up their polinear recorder.)

Why did we call it the Color Laser?

Well, engineers tell us that laser light beams with their tremendous bandwidth capacity are the communications carrier of the future. And we believe that our new VHF/UHF/FM Color Laser with its extreme bandwidth, among other unique characteristics, is the antenna of the future—only it's available to you *now*. How does the Color Laser deliver unsurpassed natural color, black and white across 82 channels, and FM, too?

Three reasons: (1) *Patented *VHF "cap-electronic" Log Periodic V Design,* (2) *a new broad band UHF "zoned" trapezoid driver,* (3) *a new disc-on-rod UHF director system.* And there are patents issued and pending on all three.

We've also spun off the LPV "cap-electronic" Log Periodic section of the Color Laser. It forms the heart of a great new VHF antenna series we've named the LPV-TV.

This "assault on perfection" of ours involved a complete new mechanical design, as well. Results: "fast-lok" element brackets, "hot" twin booms (no lossy harnesses or transformers), new super-strength double U-bolt profiles, high reliability cylindrical capacitors, plus our electrically conductive gold alodized aluminum.

If you're the breed of professional contract installer or self-servicing appliance dealer who *never* settles for less than the best, we have a suggestion. Use a JFD LPV-CL Color Laser or LPV-TV Color Log Periodic on your next installation. See what it feels like to install the *best* of all in performance and customer satisfaction.

You will also see why our research and development people have now changed their watchword from "assault on perfection" to "perfection *conquered*".

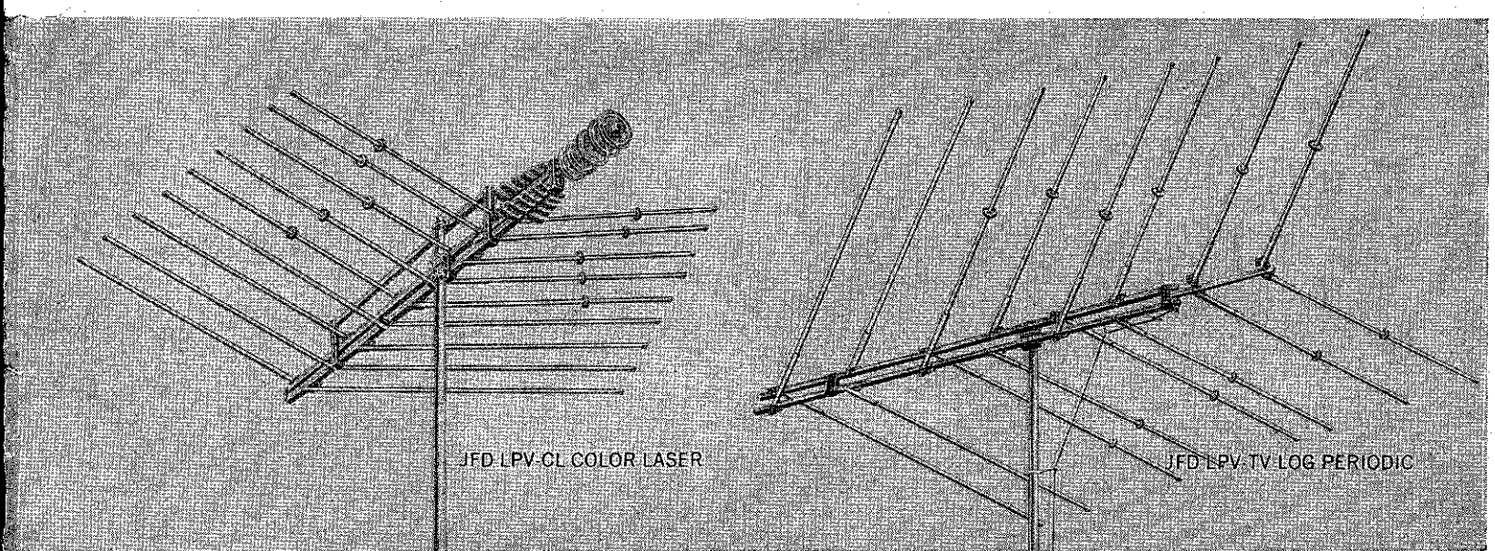

Licensed under one or more of U.S. Patents 2,955,287 and 3,015,821 and additional patents pending.

JFD®

JFD ELECTRONICS CO.
15th Avenue at 62nd Street, Brooklyn, N.Y. 11219
JFD International, 64-14 Woodside Ave., Woodside, N.Y. 11377 JFD Canada, Ltd., Canada
JFD de Venezuela, S.A., Avenida Los Haticos 125-97, Maracaibo, Venezuela

CASS ALTSHULER
801 Seventh Avenue
Oakland, California

DUNLAP ELECTRONICS
1800 - 18th Street
Sacramento, California 95809
Also in: Chico, Vallejo, Modesto, Fresno, Walnut Creek, Bakersfield, Marysville, Stockton, Merced, Redding and Reno, Nevada

QUEMENT ELECTRONICS
1000 South Bascom Avenue
San Jose, California

REDWOOD ELECTRONICS SUPPLY COMPANY
711 Summer Street
Eureka, California

WHOLESALE RADIO & ELECTRIC SUPPLY COMPANY
1348 El Camino Real
San Carlos, California

WHOLESALE RADIO & ELECTRIC SUPPLY COMPANY
1116 Folsom Street
San Francisco, California 94103
Also in Petaluma

LETTERS

Dear Sir:

In the October issue of ESD you had in your feature issue a report on service pricing.

I would like ver ymuch to obtain some copies of this article. If you are able to send me some reprints of this article they would be used by our men to give to their customers. Your assistance would be greatly apreciated.

Wimpy Jones
Radio Service, Sacramento

Ed: We are trying to work out an idea to reproduce the article and send supplies to all distributors to give to their customers. As yet it is not worked out but, if you wish, you have our permission to reprint the article and use it as you see fit.

Dear Sir:

Would like to procure a copy of ESD for October if posible. Would you please send me a copy of this or advise me as to cost of same and I will glady send along my remittance. Also your subscription rate.

Edward Hocking
Buena Park, Calif.

Dear Mr. Martin:

Thank you for all the personal endeavor that must have gone into compiling the ESD report on Service Pricing. Personally, I wish it could be made available to all registered service shops, on one page, that could be displayed for customers to see. I would eliminate many beefs and then all shops would have a standard foundation for setting their prices. We certainly don't advocate the same price but this is the first real guide to pricing practices we have ever seen.

Warren's Stereo-vision
Corona Del Mar, Calif.

A TELEGRAM:

Congratulations your August ESD editorial also Winston Salem Session. Will send copy of our survey later.

John Keppinger Gross Point Magnavox
Detroit, Michigan

Dear Sir:

We wish to thank the Electronic Service Dealer for the editorial leadership in bringing about this vital need to upgrade the industry. Reports on items in the Electronic Service Dealer have a permanent place on the agenda of our monthly meetings.

William E. Phillips, President
Coachella Valley Electronics Association
Palm Desert, California

Editor's Note:

These are just a few of the stacks of letters we have received concerning our current editorial policy to review and report pricing practices throughout California. We sincerely hope we have been a factor in a re-evaluation of the pricing structure and that the Industry as a whole will benefit. We believe that this is the only way in which the industry can take its place as a profession, to attract new people, and to be financially sound.

Dear Don:

I want you to know how much I enjoy reading Electronic Service Dealer from cover to cover and consider it the best service publication in the country. Particularly enjoy your "Service Pricing" articles which I wish could be read by every service dealer.

Sincerely,
John P. Graham, Ed. ARTSD News

X Bid 48

UNITED STATES DISTRICT COURT
NORTHERN DISTRICT OF ILLINOIS
BEFORE JUDGE HOFFMAN

DEFENDANT EX. NO. _____

DOROTHY L. BRACKENBURY
OFFICIAL COURT REPORTER

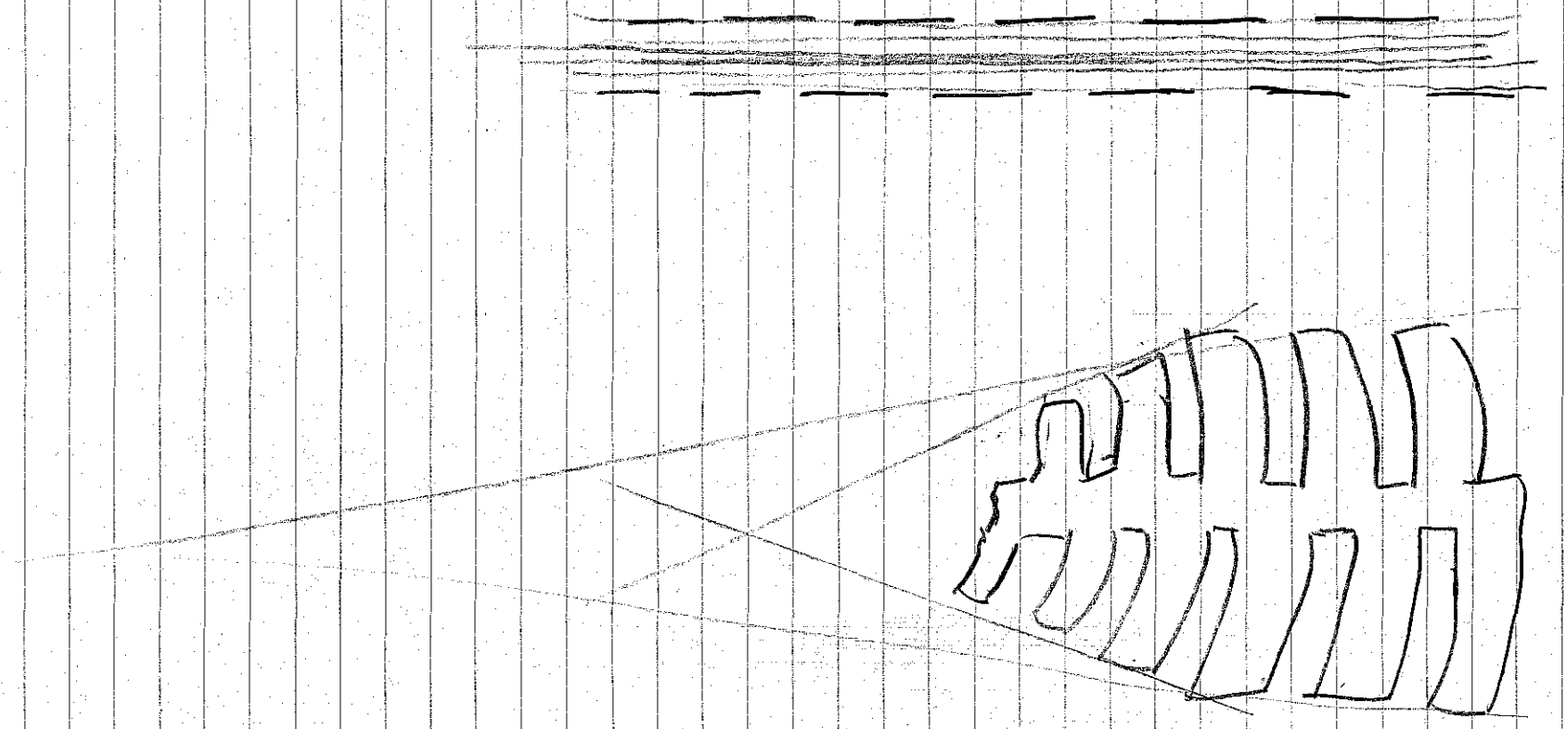

Feb. 26, 1963 R. H. DU HAMEL ET AL 3,079,602

LOGARITHMICALLY PERIODIC ROD ANTENNA

Filed March 14, 1958 9 Sheets-Sheet 1

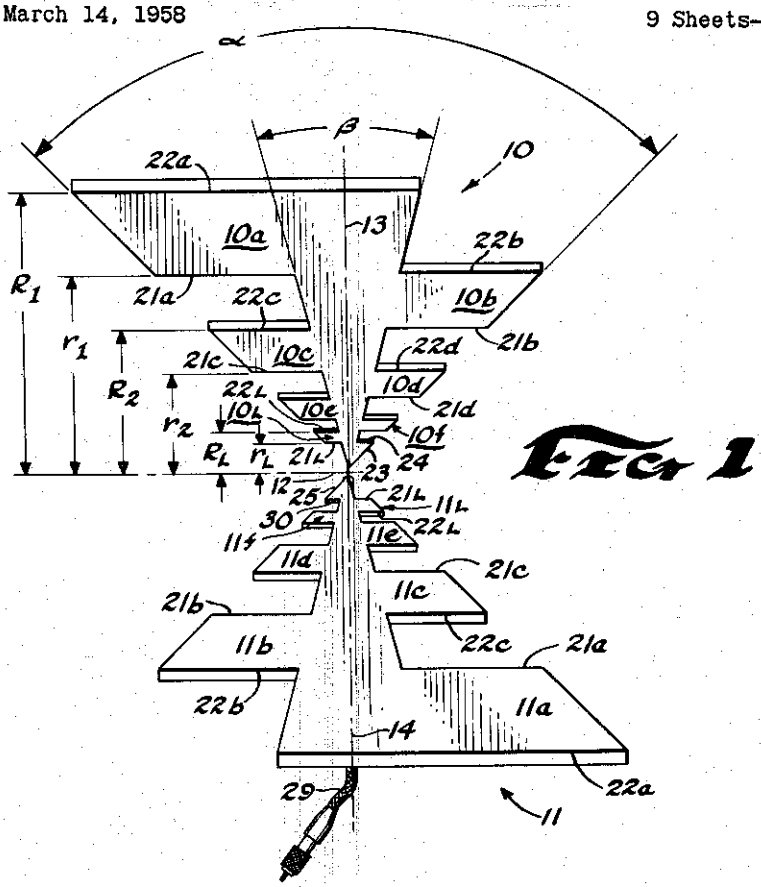

FIG 1

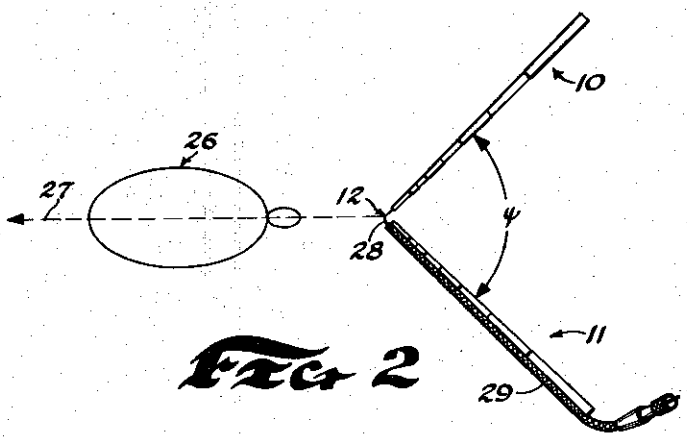

FIG 2

INVENTORS
RAYMOND H. DUHAMEL
FRED R. ORE
BY Woodyard & Goldman
ATTORNEYS

Feb. 26, 1963 R. H. DU HAMEL ET AL 3,079,602

LOGARITHMICALLY PERIODIC ROD ANTENNA

Filed March 14, 1958 9 Sheets-Sheet 2

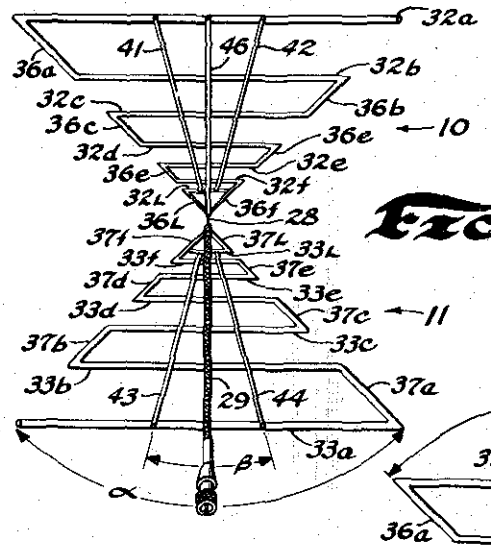

Fig 3

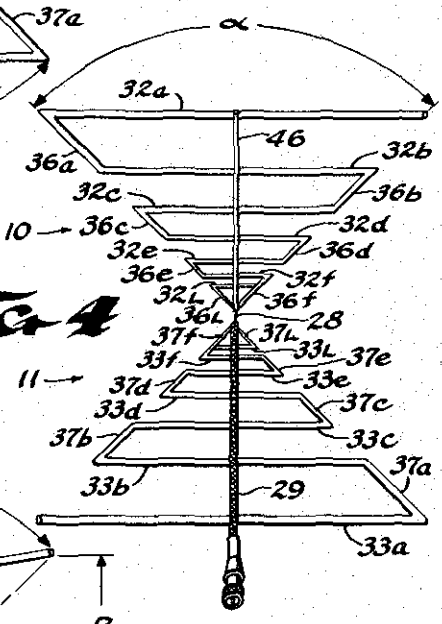

Fig 4

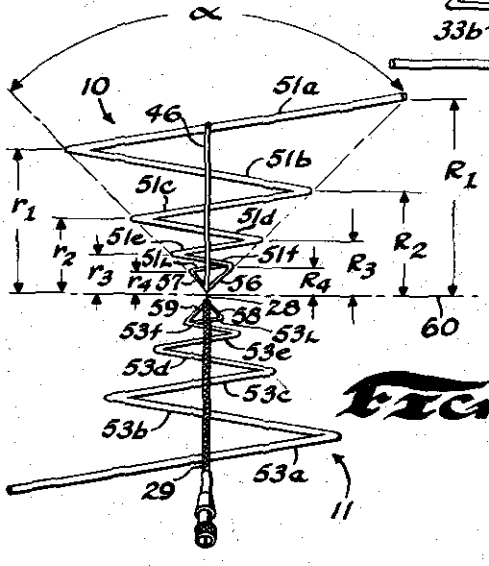

Fig 5

INVENTORS
RAYMOND H. DUHAMEL
FRED R. ORE
BY Moody and Goldman
ATTORNEYS

Feb. 26, 1963 R. H. DU HAMEL ET AL 3,079,602

LOGARITHMICALLY PERIODIC ROD ANTENNA

Filed March 14, 1958 9 Sheets-Sheet 3

FIG 6(A)

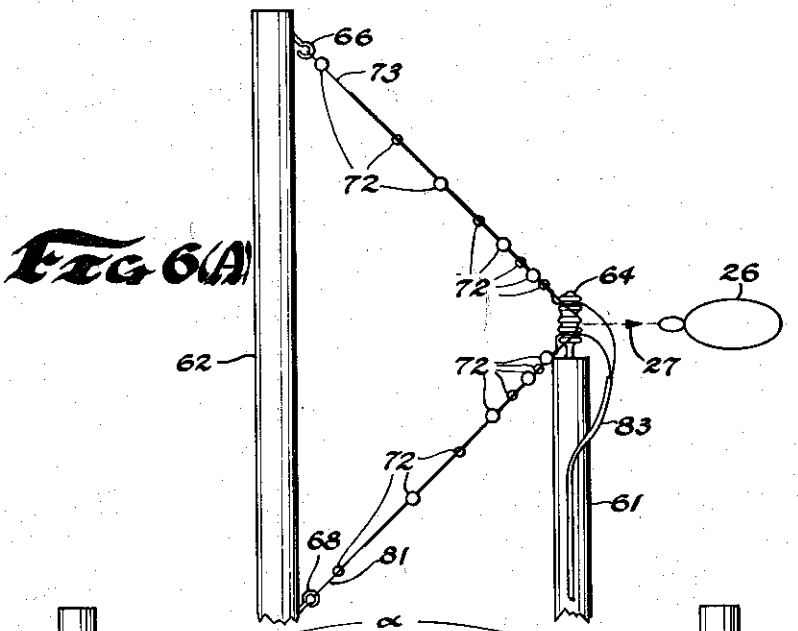

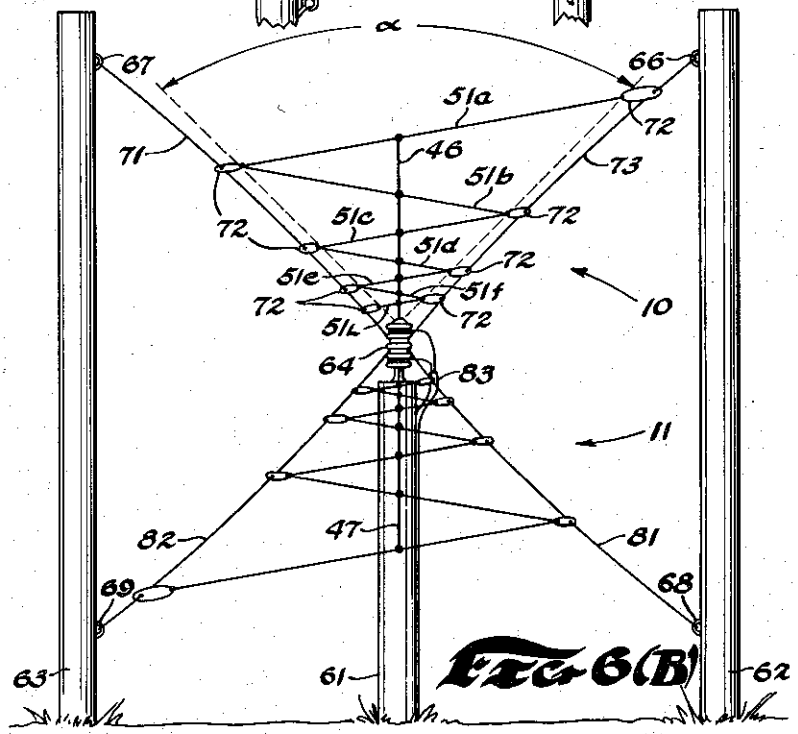

FIG 6(B)

INVENTORS
RAYMOND H. DUHAMEL
FRED R. ORE
BY Moody and Goldman
ATTORNEYS

Feb. 26, 1963 R. H. DU HAMEL ET AL 3,079,602

LOGARITHMICALLY PERIODIC ROD ANTENNA

Filed March 14, 1958 9 Sheets-Sheet 4

Fig. 7

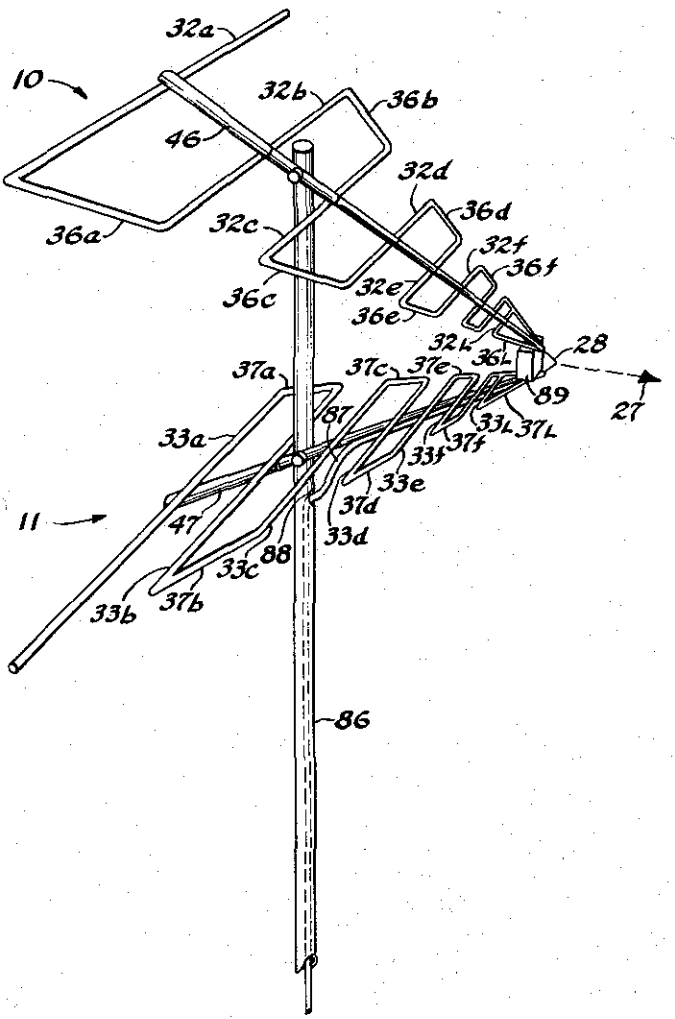

INVENTOR.
RAYMOND H. DUHAMEL
FRED R. ORE
BY
Moody and Goldman
ATTORNEYS

Feb. 26, 1963 R. H. DU HAMEL ET AL 3,079,602

LOGARITHMICALLY PERIODIC ROD ANTENNA

Filed March 14, 1958 9 Sheets-Sheet 5

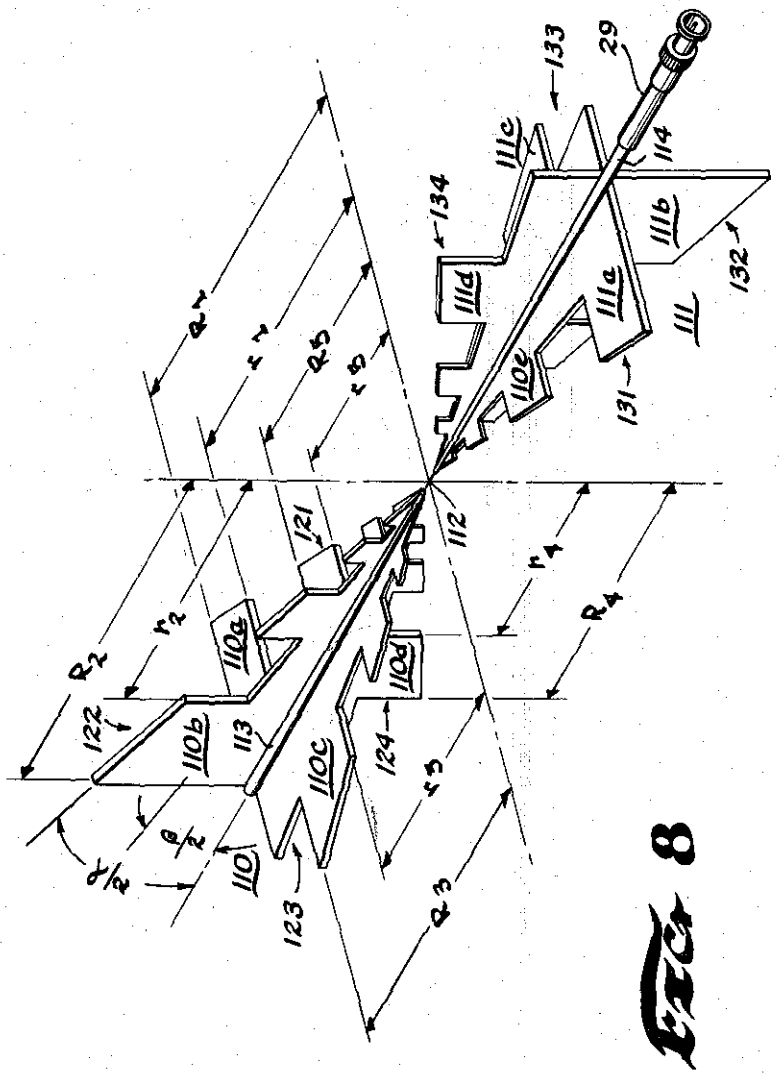

FIG 8

INVENTORS
RAYMOND H. DUHAMEL
FRED R. ORE
BY Moody and Goldman
ATTORNEYS

Feb. 26, 1963 R. H. DU HAMEL ET AL 3,079,602

LOGARITHMICALLY PERIODIC ROD ANTENNA

Filed March 14, 1958 9 Sheets-Sheet 6

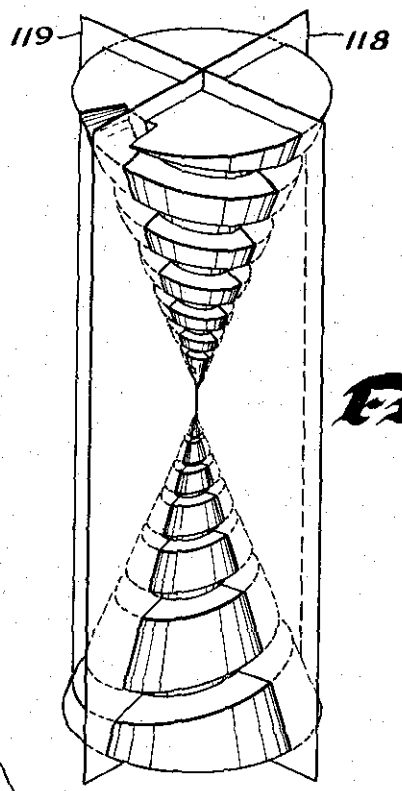

FIG 9

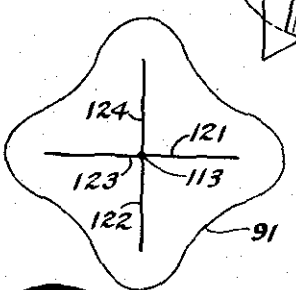

FIG 10(A)

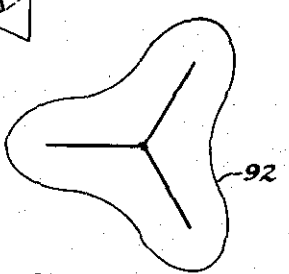

FIG 10(B)

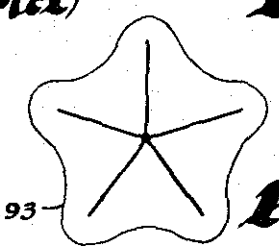

FIG 10(C)

INVENTORS
RAYMOND H. DUHAMEL
FRED R. ORE
BY Moody and Goldman
ATTORNEYS

Feb. 26, 1963 R. H. DU HAMEL ET AL 3,079,602

LOGARITHMICALLY PERIODIC ROD ANTENNA

Filed March 14, 1958 9 Sheets-Sheet 7

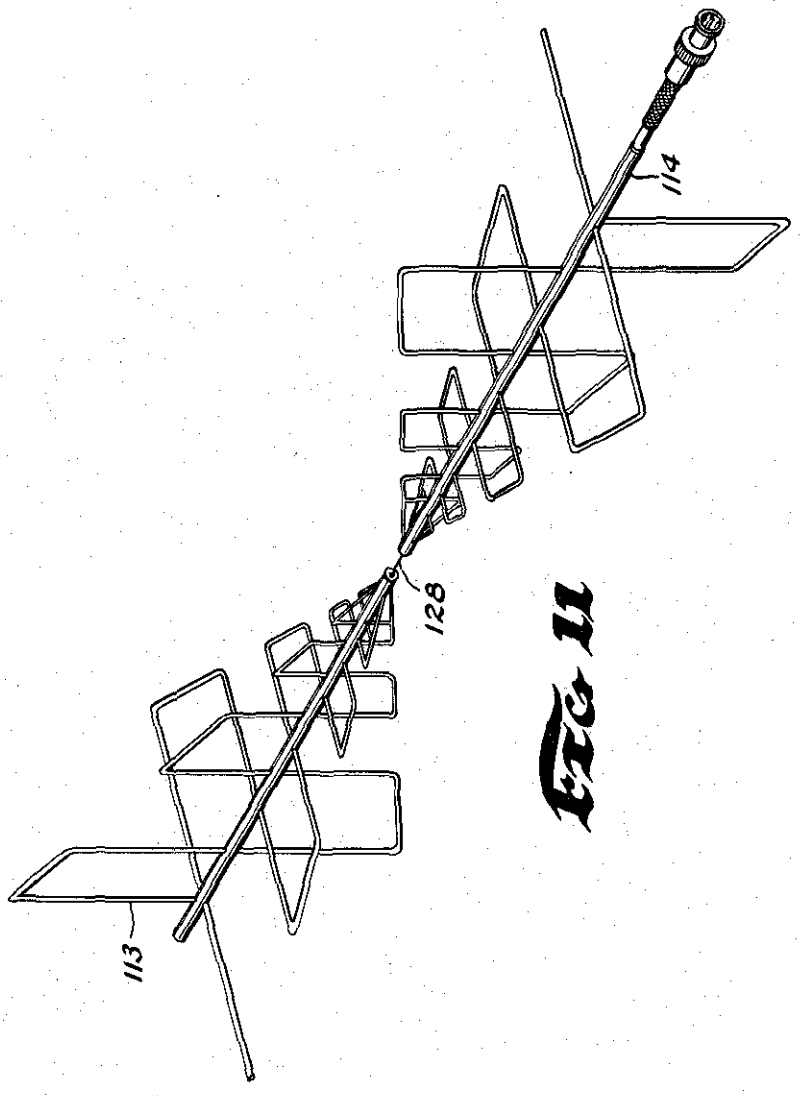

Fig. 11

INVENTORS
RAYMOND H. DUHAMEL
FRED R. ORE
BY Moody and Goldman
ATTORNEYS

Feb. 26, 1963 R. H. DU HAMEL ET AL 3,079,602

LOGARITHMICALLY PERIODIC ROD ANTENNA

Filed March 14, 1958 9 Sheets-Sheet 8

FIG 12

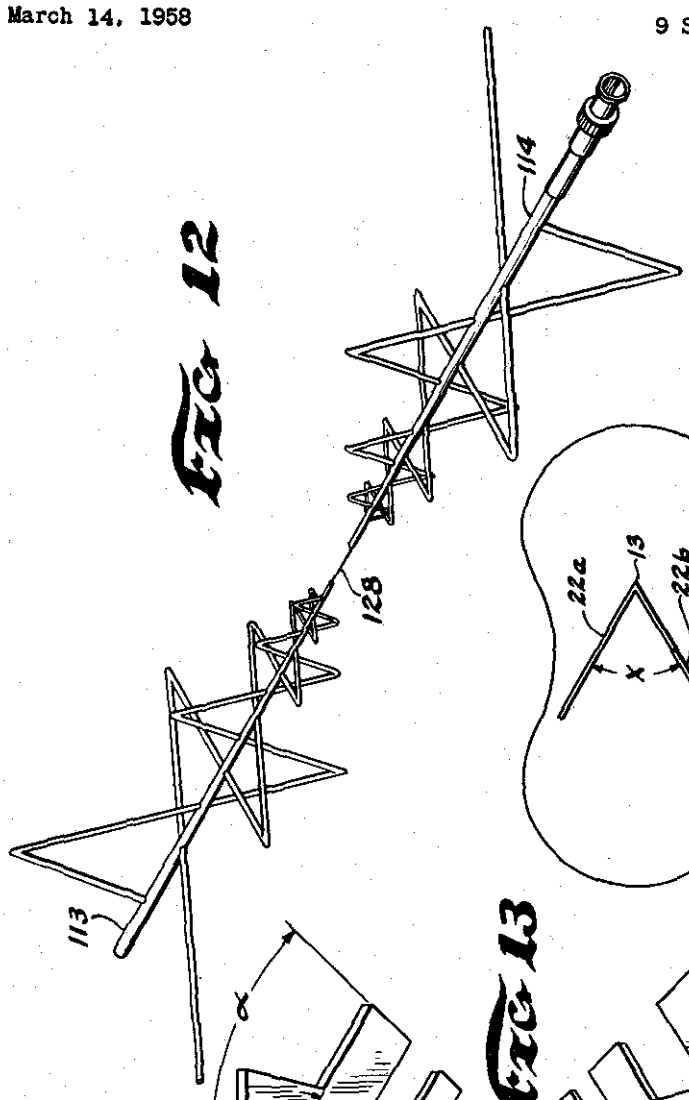

FIG 16

FIG 13

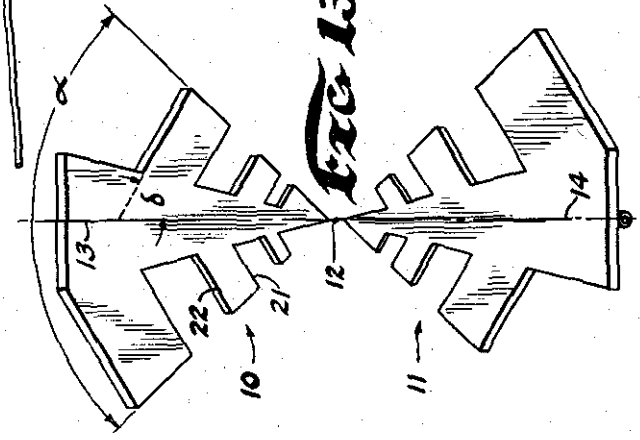

INVENTORS
RAYMOND H. DUHAMEL
FRED R. ORE
BY Moody and Goldman
ATTORNEYS

Feb. 26, 1963 R. H. DU HAMEL ET AL 3,079,602

LOGARITHMICALLY PERIODIC ROD ANTENNA

Filed March 14, 1958 9 Sheets-Sheet 9

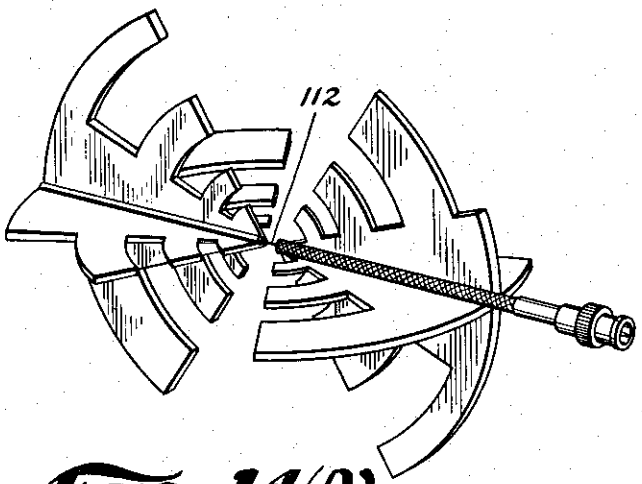

FIG. 14(A)

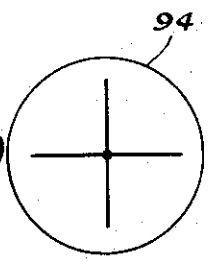

FIG. 14(B)

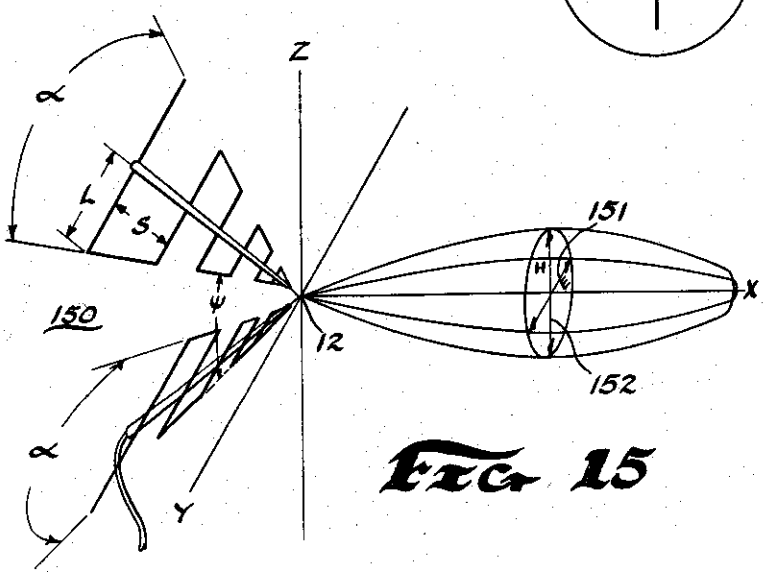

FIG. 15

INVENTORS
RAYMOND H. DUHAMEL
FRED R. ORE
BY Moody and Goldman
ATTORNEYS

United States Patent Office 3,079,602 Patented Feb. 26, 1963

3,079,602

LOGARITHMICALLY PERIODIC ROD ANTENNA

Raymond H. Du Hamel and Fred R. Ore, Cedar Rapids, Iowa, assignors to Collins Radio Company, Cedar Rapids, Iowa., a corporation of Iowa

Filed Mar. 14, 1958, Ser. No. 721,408
14 Claims. (Cl. 343—908)

This invention relates to antennas of a type that can be described as logarithmically periodic, since their structure is repetitive in a logarithmic manner. Such antennas are particularly useful because they are capable of maintaining substantially-fixed radiation patterns and input impedances over a very broad frequency range, which may be greater than ten-to-one.

The general subject of such antennas is treated in a paper by R. H. DuHamel and D. E. Isbell, titled "Broadband Logarithmically Periodic Antenna Structures" and is found in the 1957 I.R.E. National Convention Record, Part I, of the group on Antennas and Propagation, Microwave Theory and Techniques. This article is only concerned with planar logarithmically periodic antennas which comply with the complementary principle when they are infinitely extended. The complementary principle requires that the same form be obtained when the antenna structure is interchanged with the planar space surrounding it. That is, the complementary principle requires that when an antenna and its complement are added together a complete infinite screen is obtained. In many situations, if an antenna has a complementary shape, it may be rotated by 90° about its center, and it will fill the area previously existing between its elements. If an antenna is identical to its principle it has a constant impedance of 60π ohms which is independent of frequency. This is explained in an article by V. H. Rumsey titled "Frequency Independent Antenna" found in the same I.R.E. records as the first-mentioned article. It was previously believed that the complementary principle must be adhered to in order to obtain a constant antenna input impedance independent of frequency.

The present invention deviates from the complementary principle in several ways and yet is able to maintain a radiation pattern and input impedance that are very nearly independent of frequency over a very broad range. For example, antenna structures made according to this invention need not lie in a single plane, which is a requirement of the complementary principle. Furthermore, when a form of the invention is made to lie in a single plane, it need not satisfy the complementary principle. The invention teaches how a logarithmically periodic antenna structure can be made entirely with a straight-lined configuration.

The invention provides a structure that is logarithmically periodic from a given vertex point. As a consequence, similar portions of the antenna repeat with a geometric-progression relationship as a function of their distance from the vertex. Transverse construction lines in the invention can be made linear to permit substantial structural simplifications, particularly for large sized antennas to extend their range to relatively low frequencies.

Some of the objects of this invention are the following:

To provide an antenna which maintains the same radiation pattern throughout an extremely large operating frequency range;

To provide an antenna which maintains a very-nearly constant input impedance over an extremely large frequency range;

To provide a logarithmically periodic antenna with a radiation pattern that can be made omnidirectional;

To provide a logarithmically periodic antenna with a radiation pattern that is controllably asymmetric;

To provide logarithmically periodic antennas having structural simplicity, while permitting frequency independence of radiation pattern and input frequency over extremely broad frequency ranges; and

To provide a logarithmically periodic antenna which can be entirely made of straight-lined structure, capable of easy fabrication from wire or rods.

Further objects, features and advantages of the invention will become apparent to a person skilled in the art upon further study of the specification and accompanying drawings, in which:

FIGURE 1 illustrates an elevational view of one form of the invention;

FIGURE 2 shows a side view and radiation pattern;

FIGURES 3, 4, 5, 6(A), 6(B) and 7 represent other forms of the invention;

FIGURE 8 is a perspective of a three-dimensional form of the invention;

FIGURE 9 illustrates a conical development of the three-dimensional form in FIGURE 8;

FIGURES 10(A), (B) and (C) show end views of various forms of the invention with their radiation patterns;

FIGURES 11 and 12 show perspectives of other three-dimensional forms of the invention;

FIGURE 13 provides a modification of the invention;

FIGURES 14(A) and (B) respectively illustrate a rounded-tooth three-dimensional form, and its end view and radiation pattern;

FIGURE 15 represents a radiation pattern; and

FIGURE 16 shows an end view of a center-line folded antenna.

Now referring to detailed forms of the invention, FIGURE 1 is first considered. It shows a back-elevational view of an antenna made from a pair of metal sheets having a thickness that tapers toward a terminal point **12**. FIGURE 2 shows a side view of the same antenna and orients the position of point **12**, which is a reference point for the system but has no structural existence. The antenna includes half-portions **10** and **11** which are generally triangular in shape and have respective vertexes adjacent to point **12**. Each half-portion **10** or **11** encompasses an angle α which is bisected by a center line **13** or **14**, respectively, passing down their center. However, it is to be noted that neither half-portion **10** nor **11** is symmetrical about its center line.

Each half-portion **10** or **11** has transverse teeth extending on opposite sides of an inner triangular-shaped segment that is defined by an angle β. Angle β is symmetrically placed within angle α.

The two planes of half-portions **10** and **11** are oriented apart by an angle ψ, which can vary from 180° to 0°. increasing angle ψ beyond 180° causes it to repeat.

A plurality of teeth **10***a*, **10***b* through **10**L are formed on half-portion **10**; and a similar plurality of teeth **11***a*, **11***b* through **11**L are formed on half-portion **11**. In FIGURE 1, each of the teeth is trapezoidal in form when its transverse parallel sides are extended to meet center-line **13** or **14**; and the parallel sides are perpendicular to their center-line. The teeth vary in size and spacing in a logarithmically periodic manner from terminal point **12**. Thus, each tooth has parallel sides **21** and **22** with outer side **22** being the more distant of the two from point **12**. Each tooth is bounded on its remaining two sides by lines defining angles α and β.

The location and size of the set of teeth of half-portion **10** on the left side of its center line **13** will first be defined. The location and size of the remaining teeth of the antenna can then be defined in terms of this set of teeth. The distances along center line **13** between point **12** and the outer sides **22** of alternate teeth **10***a*, **10***c* through **10**L

are represented by distances R_1, R_2 through R_L. Any two consecutive values of R are R_N and R_{N+1}, with the latter being the smaller distance. Similarly, r_1, r_2 through r_L represent distances of the inner sides of the same teeth from point 12; and of any consecutive pair of r are r_N and r_{N+1}, with the latter being the smaller distance. They are defined by the following expression:

$$\tau=\frac{R_{N+1}}{R_N}=\frac{r_{N+1}}{r_N} \quad (1)$$

where τ is a constant less than one, which is fixed for a given antenna design.

Expression 1 positions the teeth with respect to each other along the center-line but does not specify the width of the teeth. The width of any tooth of the set is the difference between R_n and r_n, which are related by the following expression:

$$\sigma=\frac{r_N}{R_N} \quad (2)$$

where σ is constant for a given antenna design.

Consequently, expression 2 completes the general definition of the set of teeth on the left side of center-line 13 in FIGURE 1.

The remaining teeth of antenna half-portion 10 can then be defined, because the teeth on the right-hand side of center-line 13 have their sides 22 and 21 aligned with the defined sides 21 and 22 respectively of the left-hand side, with the teeth on the right-hand side aligning with spaces between teeth on the left-hand side.

Furthermore, the teeth on the opposite antenna half-portion 11 are also thereby defined, because half-portions 10 and 11 are identically shaped. Thus, in FIGURE 1 the teeth on the right-hand side of portion 11 correspond to the teeth on the left-hand side of portion 10. Likewise, the teeth on the left-hand side of portion 11 correspond to the teeth on the right-hand side of portion 10.

Although the half-portions 10 and 11 are constructed in the same manner, they are positioned unsymmetrically with respect to each other in the sense that one is not the image of the other. This prevents the same antenna response from being obtained by positioning a single half-portion over a ground-plane that bisects angle ψ.

Expressions 1 and 2 determine a geometric-ratio sequence for tooth sizing and for tooth spacing. However, they permit different geometric-sequencies having the same geometric-ratio to define distances to inner and outer sides of a tooth, respectively. A particularly useful special case occurs when the teeth are similarly proportioned on opposite sides; and this is obtained when

$$\sigma=\sqrt{\tau} \quad (3)$$

When angle ψ is less than 180°, an asymmetrical radiation pattern 26 shown in FIGURE 2 is obtained, with the major lobe pointing in the direction of arrow 27. The primary polarization of the radiation is parallel to teeth sides 21 and 22. A secondary transverse polarization is also obtained, which is small and can be controlled. The radiation pattern is discussed below in more detail.

Theoretically, an infinite bandwidth from zero to infinite cycles-per-second can be obtained for the antenna by making each half-portion infinitely long, wherein the teeth become infinitely small as vertex 12 is approached and infinitely large in the opposite direction. In practice, finite dimensions are mandatory, and a finite number of teeth must be used. Thus, the bandwidth is then no longer infinite, but nevertheless, extremely large bandwidths can still be obtained. The number of teeth used in the given antenna is therefore somewhat arbitrary, although generally speaking more than two teeth must be used to obtain a structure which is logarithmically periodic. In each case, there is a practical limit to the size of the largest tooth, and the smallest tooth also has its limit. Thus, in antenna half-portion 10 in FIGURE 1, tooth 10L is the smallest, and tooth 10*a* is the largest. Accordingly, the small triangular part 23 of half-portion 10 near vertex 12 has no teeth, due to the practical difficulties in making very small teeth. However, the outer side 24 of triangular portion 23 performs like the outer side 22 of a tooth, and it acts electrically like the smallest tooth of the antenna.

Half-portion 11 similarly has a small triangular portion 25 with an outer side 30 that corresponds to triangular part 23 and its outer side 24, respectively.

Structurally, the size of the largest and smallest teeth determine the lowest and highest frequency limits, respectively, of the range.

The high-frequency limit of the frequency independent range is reached when the length of smallest side 24 or 25 from the center-line to its α-boundary becomes about one-tenth of a wavelength of the radiated frequency.

On the other hand, the low frequency limit of the range is determined when the length of the largest side 22*a*, measured from center-line 13 to its α-boundary, is approximately one-quarter wavelength.

Although the frequency limits are determined by the sizes of the largest and smallest teeth in the structure, it is by no means to be implied that radiation occurs only from these teeth at the respective frequency limits. Rather, radiation at all times occurs from several of the teeth in varying degrees in a complex manner.

Ideally, the sheets of metal from which each of the antenna half-portions 10 and 11 is made have tapered thickness as explained above. In practice, however, it has been found that stepped thickness can be used to the same effect, and further that uniform thickness can be used without substantially inhibiting the operation of the antenna for very large bandwidths of the order of five-to-one.

The antenna of FIGURE 1 can be fed by means of either a balanced or an unbalanced line, but special precautions must be taken to prevent the line from interfering with the radiation pattern. An unbalanced line, coaxial cable 29, is used in FIGURES 1 and 2. In order to prevent it from interfering with the radiation pattern, it is brought along the solid triangular portion within angle β, with the outer conductor making contact therewith, and it terminates at the apex of half-portion 11. Its inner conductor 28 extends from the end of coaxial line 29 across the space between the apexes of the half-portions, and connects to the apex of half-portion 10. Outer conductor 29 is not at ground potential along half-portion 11 but varies in a manner that automatically transduces the unbalanced-line impedance to a balanced impedance connection for the antenna without unbalancing the antenna pattern. The near-zone electro-magnetic fields associated with the antenna decrease rapidly as extremity 22*a* is approached. Therefore, the presence of coaxial line 29 has little effect on the field and hence on the balance of the antenna structure. This effectively produces a very-wide-band balanced feed for the antenna.

Also, a balanced line can be connected to the antenna by being brought toward the antenna in FIGURE 2 along the direction of arrow 27, with opposite sides of the line being connected to the apexes of the respective half-portions. If the transmission line is brought from the side of the antenna that is perpendicular to the paper at point 27 in FIGURE 2, it interferes with the radiation pattern to some degree, which in many cases makes such type of connection undesirable.

Although each half-portion 10 and 11 is in a respective plane in FIGURES 1 and 2, each can also be folded about its center-line 13 and 14. FIGURE 16 shows an end view of such antenna where Ψ is 180° and x is the fold angle between the radical members of half-portion 10 having respective end teeth 22*a* and 22*b*. The figure-eight type radiation pattern 15 of this antenna is made more omnidirectional as angle x is made smaller. Optimum omnidirectionality is obtained with x between 120° and 130°. As angle x is made smaller the antenna be-

comes more frequency-sensitive and its bandwidth decreases.

We have also discovered structural modifications of the antenna given in FIGURES 1 and 2, which greatly facilitate the use of the invention. FIGURES 3 through 7 illustrate such modifications, and teach how the invention can be constructed from conducting rods or wire, while still maintaining the required operating characteristics of the invention. With regard to FIGURE 3, rods are used to provide an outline of the configuration given in FIGURE 1. Although the antenna of FIGURE 1 does not have an identical complementary structure, it still provides a clear distinction between the teeth and spaces between the teeth. The structure of FIGURE 3 is hence even farther from the complementary principle, since the internal portion of any tooth defined by rods or wire is also a space. Nevertheless, we have experimentally determined that the structure of FIGURE 3 operates in substantially the same manner as the structure of FIGURE 1.

FIGURE 3 also includes two half-portions **10** and **11**. Half-portion **10** includes a plurality of transverse rods **32***a*, **32***b* through **32**L. Similarly, half-portion **11** comprises transverse rods **33***a*, **33***b* through **33**L. The rods of half-portion **10** are positioned with respect to the center of the antenna in the same manner as tooth sides **21** and **22** were located in FIGURE 1, that is, by means of expressions 1 and 2 above. Rod sections **36***a*, **36***b* through **36**L are placed on the boundary of the teeth of portion **10**, as defined by angle α. Similarly, the teeth in portion **11** have lateral bounds provided by rod sections **37***a*, **37***b* through **37**L, which likewise are aligned along angle α. A pair of rods **41** and **42** are fixed to portion **10** along the sides of angle β; and rods **43** and **44** are similarly positioned in portion **11**. A centrally positioned rod **46** is also provided along half-portion **10**, while coaxial cable **29** is brought centrally along half-portion **11** with its outer conductor connected to respective transverse rods **33**. Its inner conductor **28** exits from the coaxial line at the apex of portion **11** and connects to the apex of portion **10**.

The antenna system of FIGURE 4 is similar to that shown in FIGURE 3 and like portions carry like reference numbers. However, in effect, angle β is made zero in FIGURE 4 by not providing rods **41**, **42**, **43** and **44**.

FIGURE 5 shows a modification of the antenna of FIGURE 4, wherein the trapezoidal teeth elements of FIGURE 4 are modified into triangular shapes. Thus, in FIGURE 5 the two antenna portions **10** and **11** are again confined within an angle α; and like FIGURE 4, there is also provided a center rod **46** in portion **10** of FIGURE 5 and coaxial cable **29** along portion **11**. In effect, items **46** and **29** are bisectors of angle α.

Thus, in FIGURE 5, portion **10** is composed of transverse rods **51***a*, **51***b* through **51**L. Similarly, portion **11** comprises transverse rods **53***a*, **53***b* through **53**L. The rods connected at their ends to form transverse triangular teeth. The outer apex of each triangular tooth lies on a defining line of angle α.

If the antenna of FIGURE 5 were superimposedl on a corresponding antenna of the type in FIGURE 1, the apexes of the triangular teeth of FIGURE 5 would be located on the lateral sides of corresponding trapezoidal teeth.

The positioning of the transverse rods in FIGURE 5 is preferably determined by means of expressions 1 and 2 given above. However, the terms of the expressions are preferably defined in FIGURE 5 with respect to the apex points of the transverse teeth. This is done with respect to antenna half-portion **10** by designating its apexes on the right-hand side in FIGURE 5 by means of R and by designating its apexes on the left-hand side by *r*. The dimensions R and *r* are measured from a transverse line **60** that passes through terminal point **12** and is transverse to center-line members **46** and **29**. The end of each rod **51***a* and **53***a* farthest from point **12** is considered an apex, and each has a distance R_1 from line **60**.

With this definition of the positions of the elements in FIGURE 5, it will be found that their points of intersection with center-line members **46** and **29** also satisfy expressions 1 and 2 above, with expression 3 being a specific case. Also, it will be noted that alternate elements in FIGURE 5 are parallel to each other; for example, elements **51***a* and **51***c* are parallel, **51***b* and **51***d* are parallel, and so forth.

In FIGURE 5, the apex part of portion **10** is defined by rods **56**, **57** and **51**L. Likewise, in portion **11** the apex triangle is defined by rods **58**, **59** and **53**L.

FIGURE 2 may also represent a side view of any FIGURES 3, 4 and 5, wherein their two half-portions are separated by an angle Ψ which may vary from 0° to 180°.

The basic triangular-toothed configuration of FIGURE 5 leads to the greatest structural simplification in some cases over other forms of the invention, while maintaining the desired operating conditions. Thus, the configuration of FIGURE 5, as also do FIGURES 3 and 4, permits wire structures for very large antennas capable of having extreme broadbandedness which extends into the lower frequencies. In order to lower the low frequency limit of the antenna range, it is necessary to increase the size of the larger elements of the antenna. Since the width of the largest transverse element approximates one-half wavelength of the lowest frequency, it can be realized that at very low frequencies the transverse elements can become rather large.

FIGURES 6(A) and (B) illustrate how the antenna configuration given in FIGURE 5 can be constructed of wire. It is constructed using three poles **61**, **62** and **63** firmly supported uprightly from the ground. Again the antenna comprises the two half-portions **10** and **11**. A plural waisted insulator **64** is provided at the top of a pole **61** and is situated at the apex of the antenna. The poles are preferably wood so as not to interfere with the radiation. A pair of hooks **66** and **67** are respectively fastened in horizontal alignment to poles **62** and **63** near their top. Similarly, a second pair of hooks **68** and **69** are fastened with horizontal alignment to the lower portions of poles **62** and **63**. A taunt line **71** is connected between hook **67** and the upper-middle waist of insulator **64**. Line **71** consists of metal wire segments mechanically coupled but electrically separated by insulators **72**. Similarly, another line segment **73** is connected between the upper-middle waist of insulator **64** and hook **66**. Line **73** is likewise comprised of wire segments similarly coupled by insulators **72**. Lines **71** and **73** are structural only and are interrupted electrically by the insulator to prevent them from having an antenna function. A dielectric type of structural line could preferably be used for lines **71** and **72** without insulators; however, no dielectric material is known which is properly stable under tension. The insulators **72** along lines **71** and **73** are positioned to support the apexes of the triangular teeth.

Transverse wires **51***a* through **51**L are positioned between the supporting lines **71** and **73** with an angle α in the manner defined for FIGURE 5. Insulators **72** connect to the apex of each transverse tooth along lines defining α.

In a like manner, the lower half-portion **11** of the antenna is strung between a pair of structural lines **81** and **82**, which correspond respectively to lines **71** and **73**. Thus, lines **81** and **82** are strung between the lower-middle waist of insulator **64** and hooks **68** and **69**, respectively. A central wire **46** connects the elements of section **10** along the bisector of angle α. Similarly, a central wire **47** connects the transverse elements of antenna portion **11** to bisect its angle α. Central lines **46** and **47** connect to the upper and lower waists of insulator **64**.

A balanced transmission line **83** is brought along pole **61**. It fans away from the antenna and then is brought directly toward its apex, where the opposite sides of the

line respectively connect to the ends of leads **46** and **47**. The directivity of the antenna system of FIGURES 6(A) and (B) is the direction of arrow **27** in FIGURE 6(A) and provides pattern **26** in that figure.

Where it is desired to make the antenna of FIGURE 6 have a symmetrical figure-eight pattern, angle ψ should be 180°, and the entire antenna may be supported between two parallel upright poles in a manner which is obvious in view of the description of the antenna in FIGURE 6. A coaxial feed line is then preferably used, as given in the prior figures.

FIGURE 7 illustrates a rotatable single-mast mounting of the form of the invention shown in FIGURE 4, and like reference numbers are used for like components. The antenna system of FIGURE 7, for example, can be a radio-ham antenna which is preferably extremely broadband to receive many of the ham bands. Unlike other ham antennas, the one in FIGURE 7 does not require any tuning for the various bands, and furthermore it maintains a directivity which is constant for all bands within its range. Thus, if the antenna is designed for a fifteen-to-one range, it can provide a horizontally polarized transmission at various points in the spectrum between two and thirty megacycles. In FIGURE 7, the opposite halves of the antenna, **10** and **11**, are supported on rotatable mast **86**. The central members **46** and **47** of antenna portions **10** and **11** are step-tapered in cross-section, *in order to* enhance broadbandedness. The taper is largest at elements **32***a* and **33***a* and narrows to a point adjacent to the antenna apex. Also, in order to enhance broadbandedness the largest diameter rods are **32***a* and **33***a*, with the diameters of the rods decreasing as their positions approach the antenna apex.

Mast **86** can be made of conducting material, and when it is made of conducting material it should be connected to supports **46** and **47** at points midway between any two adjacent rods **32** or **33**, respectively. It has been found *experimentally that a metal mast does* not interfere with the radiation pattern when it is connected to such midpoints, because it appears that voltage-null points exist along rods **46** and **47** at the points midway between adjacent transverse rods.

A coaxial transmission line **87** passes upwardly through mast **86**, which is hollow, and passes outwardly through a hole **88** in the mast and has its outer conductor connected along central member **47** until it terminates at the apex of the antenna as taught with FIGURE 4. Thus, its center conductor **28** extends outwardly and connects to the end of central member **46**. A dielectric block **89** connects the apex ends of half-portions **10** and **11** to provide mechanical rigidity only.

It has been found that the center-line conducting member **46** and **29** in FIGURES 4 and 5, and **46** and **47** in FIGURE 6 can be removed with some deterioration of broadbandedness but with substantial broadbandedness remaining. Then, balanced transmission lines are preferable, although a coaxial cable connected along the periphery of the teeth of one side to the apex could also be used to feed the antenna.

FIGURE 8 illustrates an omnidirectional form of the invention. With an oversimplification of statement which will be realized shortly, FIGURE 8 comprises two antennas of the type shown in FIGURE 1 positioned in space quadrature. The oversimplification referred to is that such two antennas do not have corresponding teeth. That is, the quadrature plane antennas have their teeth differently placed. A picturesque manner of describing the positioning of the teeth of each antenna half-portion **110** and **111** in FIGURE 8 is to say that the teeth of each provide a spiral staircase leading to the antenna terminal **112**. The spiral effect is shown in FIGURE 9, which shows a logarithmic or equiangular spiral developed on a cone. Thus, one would have an antenna of the type in FIGURE 8 by passing two transverse planes **118** and **119** along the axis of the cones in FIGURE 9.

While theoretically the spiralling can extend to infinity, in practice, it must be finitely terminated. Thus in FIGURES 8 and 9, termination is defined by planes transversely intersecting the center-line of the half-portions **110** and **111** at points equally distant from terminal point **112**.

FIGURE 10(A) shows an end view of the antenna of FIGURE 8, which provides an omnidirectional-type radiation pattern **91**.

Half-portion **110** includes four radial members **121**, **122**, **123** and **124** shown in FIGURE 10(A), which are fastened together along the center-line of **113—114** that passes through both half-portions. In the same sense, there are two radial members on the opposite sides of center line **13** in FIGURE 1 to define half-portion **10**. The same situation is found in each half-portion in each of FIGURES 1–9. A radial member thus is confined within an angle

$$\frac{\alpha}{2}$$

from the center line of a half-portion. Similarly, half-portion **111** includes four radial members **131**, **132**, **133** and **134**. Each radial member is included within an angle

$$\frac{\alpha}{2}$$

from the antenna center line, as shown in FIGURE 8. In obtaining the spiral-staircase effect, the outer edge of any two adjacent spiral-related teeth, not being cut off by the bounding planes, such as **110***c* and **110***d*, have their respective outer sides defined by the expression:

$$\tau^{1/4}=\frac{R_{N+1}}{R_N}=\frac{r_{N+1}}{r_N} \tag{4}$$

Hence, distances R_N and R_{N+1} in expression 4 from a transverse plane passing through a point **112** are given by R_3 and R_4 for teeth **110***c* and **110***d*. Similarly, r_N and r_{N+1} are taken from the inner sides of consecutive spiral teeth to satisfy expression 4. Also, the center-line distance r_N and R_N of the inner and outer sides of any tooth from point **112** will also have the fixed ratio given in expression 2 above, and the special case of expression 3 can like wise be satisfied.

Antenna portion **111** is formed in the same manner as portion **110** except that the spiralling goes in reversed directions for the respective half-portions **110** and **111** looking from terminal point **112**. Nevertheless, portion **111** is twisted 180° with respect to portion **110** about their center-line. Thus, tooth **110***b* corresponds to **111***b*, tooth **110***c* corresponds to tooth **111***c*, etc., with corresponding teeth being on opposite sides of the common center-line.

Due to the 180° reversal about the center-line of antenna half-portions **110** and **111** with respect to each other, the two half-portions are not antenna images of one another. Accordingly, one half-portion cannot be provided over a transverse ground-plane through point **112** to obtain the same omnidirectional-type response which is obtained with the two half-portions disposed as shown.

Although there are four radial members used in each half-portion of FIGURE 8, actually any number greater than two can be used, and the same rules apply for proportioning adjacent teeth in the spiral-staircase manner. The dimensions of an antenna having m number of radial members per half-portion can be found as follows:

$$\tau^{\frac{1}{m}}=\frac{R_{N+1}}{R_N}=\frac{r_{N+1}}{r_N} \tag{5}$$

Where three radial members are used in each half-portion, *an end view is shown in* FIGURE 10(B). *Extending the* rationale to five radial members per half-portion, an end view is given by FIGURE 10(C). This can be extended to any number m of radial members with the ultimate

limit being the spiral-grooved cones of FIGURE 9 as the number m approaches infinity.

The omnidirectional-type patterns such as patterns **91**, **92** and **93** in FIGURES 10(A), (B) and (C) are slightly distorted according to the number of radial members used per antenna portion. However, this deviation from a perfect omnidirectionality is generally small and not objectionable in practice, while at times has definite advantages.

FIGURE 11 is basically the same as FIGURE 8 except that it is made of wire network which simplifies construction in many cases. Thus, the individual radial sections of FIGURE 11 are outlined by wire to form the toothed-configuration of FIGURE 8. The transverse rods in FIGURE 11 do not intersect the coaxial cable **114**, but merely fasten to its outer conductor. In practice, the rods are continuous and coaxial line **114** and center-rod **113** lie in a corner of their cross-over planes. The center-conductor **128** connects to the apex end of rod **113**, which can be a solid conducting rod.

The antenna network of FIGURE 12 is a triangular-toothed version of the form in FIGURE 11 and has similarities to FIGURE 5. Accordingly, the variation from 11 and 12 is similar to the variations from FIGURES 4 to 5.

In regard to the three-dimensional structures given in FIGURES 8 through 12, it was stated above that opposite half-portions are not images. However, when the entire antenna assembly having both halves is erected over a ground plane, the image of the entire antenna is view in the ground plane and this does not interfere with the radiation pattern.

FIGURE 14(A) illustrates a rounded-tooth version of the form of the invention given in FIGURE 8. FIGURE 14(A) differs from FIGURE 8 in that in FIGURE 14(A) the edge of each tooth is a segment of a circle about terminal point **112**. Thus, dimensions R_N and r_N in FIGURE 14(A) are taken from point **112** of the antenna to any point along a respective tooth edge. An improvement in the omnidirectionality of the radiation pattern was found in the rounded-toothed version of FIGURE 14(A) over the previously straight-toothed version of FIGURES 8, 11 and 12. Thus, the circular radiation pattern **94** shown in FIGURE 14(B) is obtained about an end view of the antenna given in FIGURE 13(A).

FIGURE 13 illustrates a modified version of FIGURE 1. Unlike FIGURE 1, where all the teeth have their inner and outer edges perpendicular to center-lines **13** and **14**, the teeth in FIGURE 14 have their outer and inner sides **22** and **21** intersect center-lines **14** and **13** at an angle δ. The points of intersection of the tooth edges with the center line are determined in the same manner as was given for FIGURE 1. That is, the points of intersection are determined by expressions 1 and 2 above. Otherwise the antenna in FIGURE 14 is the same as that shown in FIGURE 1, and a corresponding radiation pattern is obtained. The angle δ may be proportioned as desired, but better performance is taken if the teeth drop toward terminal point **12**.

FIGURE 15 illustrates the forward radiation lobe of the antenna. There will also be a backward lobe, not shown here. The backward lobe is equal to the forward lobe only when angle ψ is 180°. As ψ decreases, the backward lobe decreases, and accordingly the front-to-back intensity ratio increases. Thus, by making ψ small, the back lobe is made minor in comparison to the forward lobe, and can be made to have an intensity of twenty or thirty decibels below that of the forward lobe.

Antenna **150** in FIGURE 15 is illustrated with respect to x, y and z coordinate axes. These axes intersect at the apex terminal point **12** of antenna **150**. Thus, axis x aligns centrally with the entire antenna structure to bisect angle ψ. Axis y is parallel to the transverse rods of the antenna, which is of the type shown in FIGURE 4. The radiation E-vector is parallel to the y axis. Accordingly the xy plane will be called the E-plane. Furthermore, the radiation H-vector is parallel to the z axis, and the xz plane is called the H-plane.

When angle ψ is decreased from 180° toward zero with all other parameters remaining constant, the beam-width **151** of the E-plane pattern remains substantially fixed. However, the beam-width **152** of the H-plane pattern increases in beam-width. Furthermore, the front-to-back ratio increases. The H-plane variation is a first order effect with variataion of ψ.

When angle α is decreased with all other parameters remaining constant including angle ψ, there is a small second-order decrease in E-plane beam-width **151**. However, there is a first-order decrease in H-plane beam-width **152**. Nevertheless, there is a practical limit to decreasing angle α without increasing τ. The limit can be specified approximately by referring to a parameter ϵ which relates tooth width S to tooth length L, shown in FIGURE 15, according to the following expression:

$$\epsilon = \frac{S}{L} \tag{6}$$

It has been found desirable to maintain ϵ equal to or less than 0.6.

If the tooth-spacing ratio τ of expression 1 above is increased while all other parameters remain fixed, the number of teeth, of course, increases for a given sized antenna. As a consequence, both beam-widths **151** and **152** in the E and H-planes, respectively, decrease in a small corresponding amount, which is a second-order effect.

Although this invention has been described with respect to particular embodiments thereof, it is not to be so limited as changes and modifications may be made therein which are within the full intended scope of the invention as defined by the appended claims.

We claim:

1. A straight-toothed logarithmically periodic antenna comprising two half-portions, each comprising two opposite radial members connected along the central part of their half-portion, the two half-portions bounding a solid angle ψ and being generally triangular in shape and having adjacent apexes, each of said radial members being bounded by an apex angle

$$\frac{\alpha}{2}$$

from a line along the central part of either half-portion, first and second center-conducting members respectively extending from the apexes to the ends of the respective half-portions along their central parts, each half-portion having a plurality of rods cross-connected to its center-conducting member and terminated by the bounds of its angle

$$\frac{\alpha}{2}$$

connecting means provided at the ends of said transverse rods along the outer boundaries of each angle

$$\frac{\alpha}{2}$$

of each radial member, respective teeth closed by said connecting means, the connecting means on opposite radial members of each half-portion being staggered with respect to each other, the distances along a radial from the apex of said transverse rods of each radial member being a geometric sequence, and a transmission line having opposite sides connected to the respective apexes of said two half-portions.

2. An antenna as defined in claim 1 in which the diameters of said rods are proportioned to their distance from their apex.

3. An antenna as defined in claim 1 in which alternate rods of each half-portion are parallel.

4. An antenna as defined in claim 1 in which both

antenna half-portions and their radial members lie in the same plane.

5. An antenna as defined in claim 1 in which a plurality of rod portions comprise said connecting means, with said rod portions of each radial member being aligned.

6. A triangular-toothed logarithmically periodic antenna comprising opposite antenna half-portions, each half-portion being in a respective plane and having a generally-triangular shape, said half-portions having adjacent apexes and being bounded by a respective apex plane-angle α, the respective planes being oriented by a solid-angle ψ, a respective conducting center-member provided with each half-portion and positioned along the bisector of its angle α, a plurality of rods connected across said center-member of each half-portion, adjacent rods connected at their ends along the boundaries of angle α and there terminated, alternate rods being parallel, the distances from the apex of each half-portion to the opposite ends of each of its rods having a geometric-sequence ratio σ.

7. A three-dimensional straight-toothed logarithmically periodic antenna comprising two opposite half-portions which are aligned along the same center-line, each half-portion triangularly tapering to an apex, with the apexes of both half-portions being closely adjacent, a transmission-line having opposite sides connected to the respective apexes, each half-portion having more than two radial-toothed members symmetrically connected along said center-line, the teeth of each member extending outwardly from the center-line of its half-portion, each radial member having an apex angle

$$\frac{\alpha}{2}$$

with respect to its center-line, the teeth of said radial members of each half-section aligned along a conical logarithmic spiral beginning at the respective apex of each half section.

8. A three-dimensional periodic antenna as defined in claim 7 in which the thickness of the radial sections increases linearly from the apex of each antenna half-portion.

9. A three-dimensional periodic antenna as defined in claim 7 in which said teeth are formed of rods located along the periphery of said teeth, a respective center rod positioned along the center-line of each of said half-portions and connected to transverse ones of the rods forming said teeth.

10. A three-dimensional logarithmically periodic antenna comprising a pair of half-portions aligned along a common center-line, each half-portion formed in the same manner as the other but one rotated 180° about the center-line with respect to the other, each half-portion having an apex, with the apexes being closely adjacent, a respective center member of each half-portion passing along its center-line, more than two radial members provided in each half-portion and being symmetrically disposed around their center-line, each radial member having a triangular shape and a common apex, each radial member bounded by an apex angle of

$$\frac{\alpha}{2}$$

measured from the center-line, a transmission-line having opposite sides connected respectively to the apexes of said antenna half-portions, each radial member comprising a plurality of triangular teeth positioned transversely from said center-line, each of said teeth having its outer side bounded by angle

$$\frac{\alpha}{2}$$

the teeth of the radial members of any one half-portion arranged along a conical logarithmic spiral from the apex of the half-portion.

11. A triangular-toothed three-dimensional antenna as defined in claim 10 in which each of said antenna half-portions is formed from wire aligned with the periphery of said teeth, a central wire being provided along the center-line of each of said half-portions and connecting to the wires forming its teeth that cross said center-line.

12. An antenna as defined in claim 11 in which four radial members are provided for each antenna half-portion.

13. A three-dimensional rounded-toothed logarithmically periodic antenna comprising two half-portions symmetrically aligned about a center-line passing through said antenna, with each half-portion having an apex, and said apexes being closely adjacent although separated from one another, a transmission line having opposite sides connected to the respective apexes, a plurality of more than two radial members comprising each half-section, each radial member being generally triangular in shape and having an apex at the apex of its antenna half-portion, with each radial member having an apex angle of

$$\frac{\alpha}{2}$$

a plurality of teeth formed in each radial member, with each tooth having inner and outer sides which are circular about its apex as a center, the teeth of each half-portion arranged to form a conical logarithmic spiral from its apex, the distances of adjacent sides of adjacent spiral teeth having a fixed ratio τ, the opposite antenna half-portions being formed in the same manner but being rotated 180° with respect to each other about the center-line.

14. A curved-tooth three-dimensional antenna as defined in claim 13 in which each half-portion includes four symmetrically placed radial members.

References Cited in the file of this patent

UNITED STATES PATENTS

2,480,154	Masters	Aug. 30, 1949
2,656,463	Woodward	Oct. 20, 1953
2,712,602	Hallen	July 5, 1955
2,737,656	Cumming	Mar. 6, 1956
2,780,808	Middlemark	Feb. 5, 1957

OTHER REFERENCES

"Broadband Logarithmically Periodic Antenna Structures," by DuHamel and Isbell, 1957 IRE National Convention Record, Part I, pages 118–128, March 18, 1957.

"Frequency Independent Antennas," by Rumsey IRE Convention Record, Part I, pages 118–128, March 18, 1957.

"Logarithmically Periodic Antenna Designs," by DuHamel & Ore 1958 IRE National Convention Record, Part I, (March 1958), page 140.

Book, Very High Frequency Techniques, complied by Radio Research Laboratory of Harvard U., McGraw-Hill, 1947, vol. 1, pages 2 and 3 relied upon.

AN ANALYSIS OF THE LOG-PERIODIC DIPOLE ANTENNA*

Robert Carrel
University of Illinois
Urbana, Illinois

1. INTRODUCTION

The log-periodic dipole is a linearly polarized frequency independent antenna of moderate gain. By frequency independent, we mean that the observable characteristics of the antenna such as the pattern and input impedance vary negligibly over a band of frequencies within the design limits of the antenna, and this band may be madearbitrarily wide merely by properly extending the geometry of the antenna structure. The band limits of a given design are determined by non-electrical restrictions: size governs the low frequency limit and precision of construction governs the high frequency limit.

This paper presents a mathematical analysis of the log-periodic dipole antenna which leads to a simplified picture of the mechanism of radiation from these types of structures. Graphs and nomograms which enable one to design a log-periodic dipole antenna over a range of the parameters that control the input impedance, bandwidth, gain, and antenna size are also presented.

2. DESCRIPTION OF THE LOG-PERIODIC DIPOLE ANTENNA

The LPD antenna, shown in Figure 1, consists of a plurality of parallel, linear dipoles arranged side by side in a plane. The lengths of the dipole elements and the spacing between elements form a geometric progression. The common ratio τ is defined in the figure. The spacing factor σ is defined as the distance in wave lengths between a half-wave dipole and its next smaller

---

* Presented at the 10th Annual Symposium on the USAF Antenna Research and Development Program, 4 October 1960

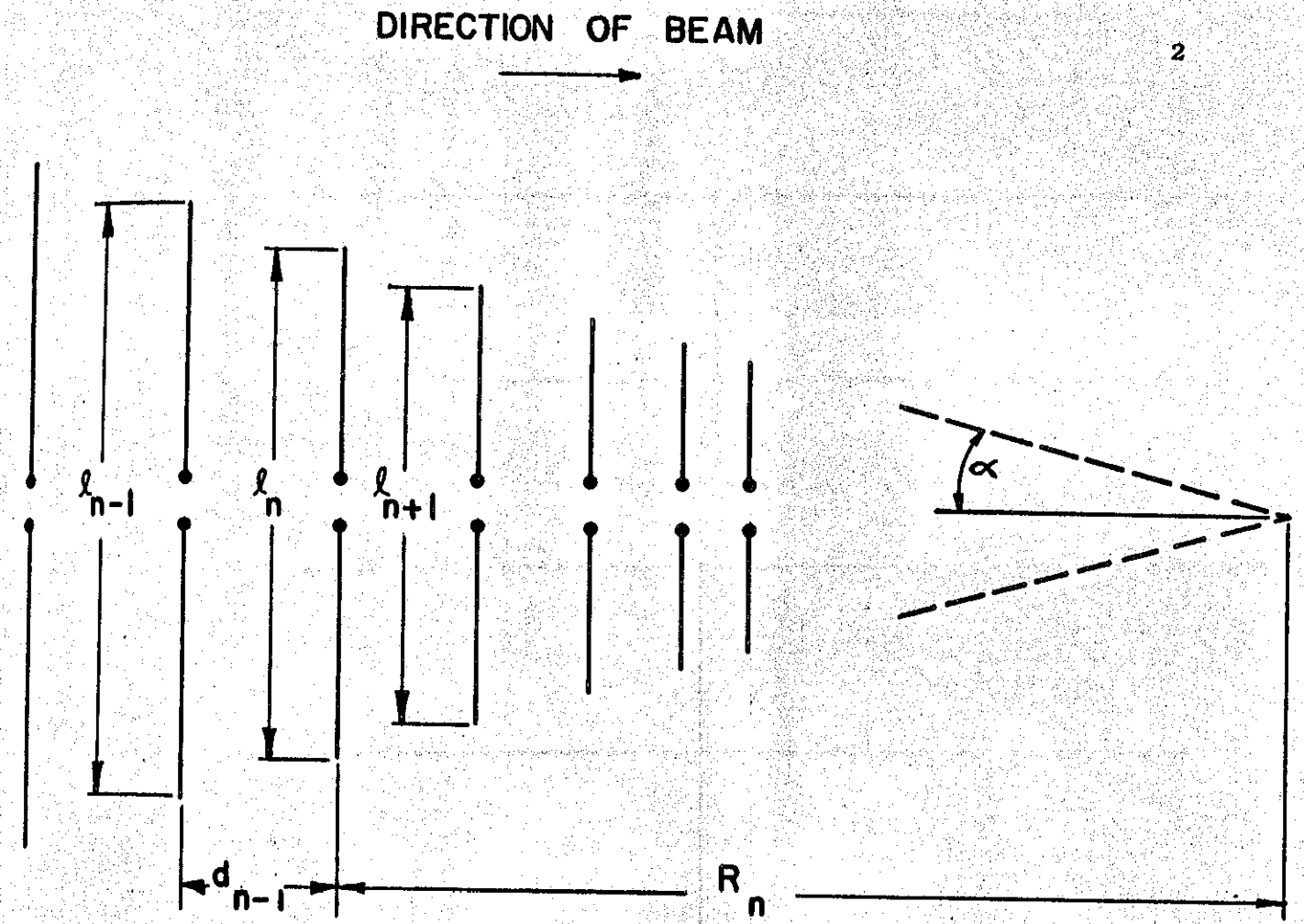

$$\frac{R_n}{R_{n-1}} = \frac{\ell_n}{\ell_{n-1}} = \tau \qquad \frac{d_n}{2\ell_n} = \sigma$$

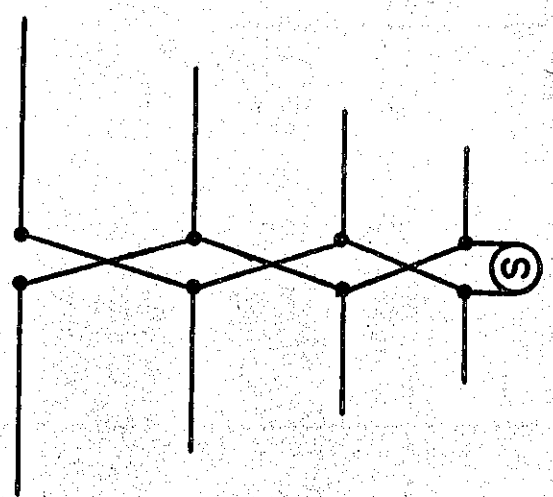

METHOD OF FEEDING

Figure 1. The log-periodic dipole antenna

neighbor. σ is related to τ and α by $\sigma = 1/4(1-\tau)\cot\alpha$. The elements are energized from a balanced, constant impedance feeder, adjacent elements being connected to the feeder in an alternating fashion. The antenna may be fed by a balanced line connected to the small element end. Alternatively, a coaxial line running through one of the feeders from back to front may be used, the center conductor being connected to the other feeder as shown in Figure 2. In the latter method, the antenna becomes its own balun. Radiation is end-fire in the direction of the shorter elements. When the operating frequency is within the design limits, the feeder currents behind the longest element are negligible; hence, the termination has little effect.

3. FORMULATION OF THE PROBLEM

The LPD antenna was invented by Isbell[1] at the University of Illinois in 1958. At that time he speculated that since the LPD is made of conventional dipole elements, it may be amenable to analysis in terms of the known properties of dipoles. This paper presents the first mathematical analysis of the log-periodic dipole antenna.

The approach is taken that the antenna may be divided into two parts for the purpose of simplifying the analysis. Determining the unknown fields of the dipole elements constitutes the exterior part of the problem. In this part we are primarily interested in the far field radiation pattern produced by the currents on the elements. The unknown voltages and currents along the feeder constitute the interior problem. Since the transverse dimensions of the feeder are small compared to wave length, its principal function is to guide and distribute the energy to the radiating elements. The feeder furnishes us with the circuit properties of the antenna: impedance, voltage, and current. Thus, circuit theory techniques can be used in the treatment of the feeder.

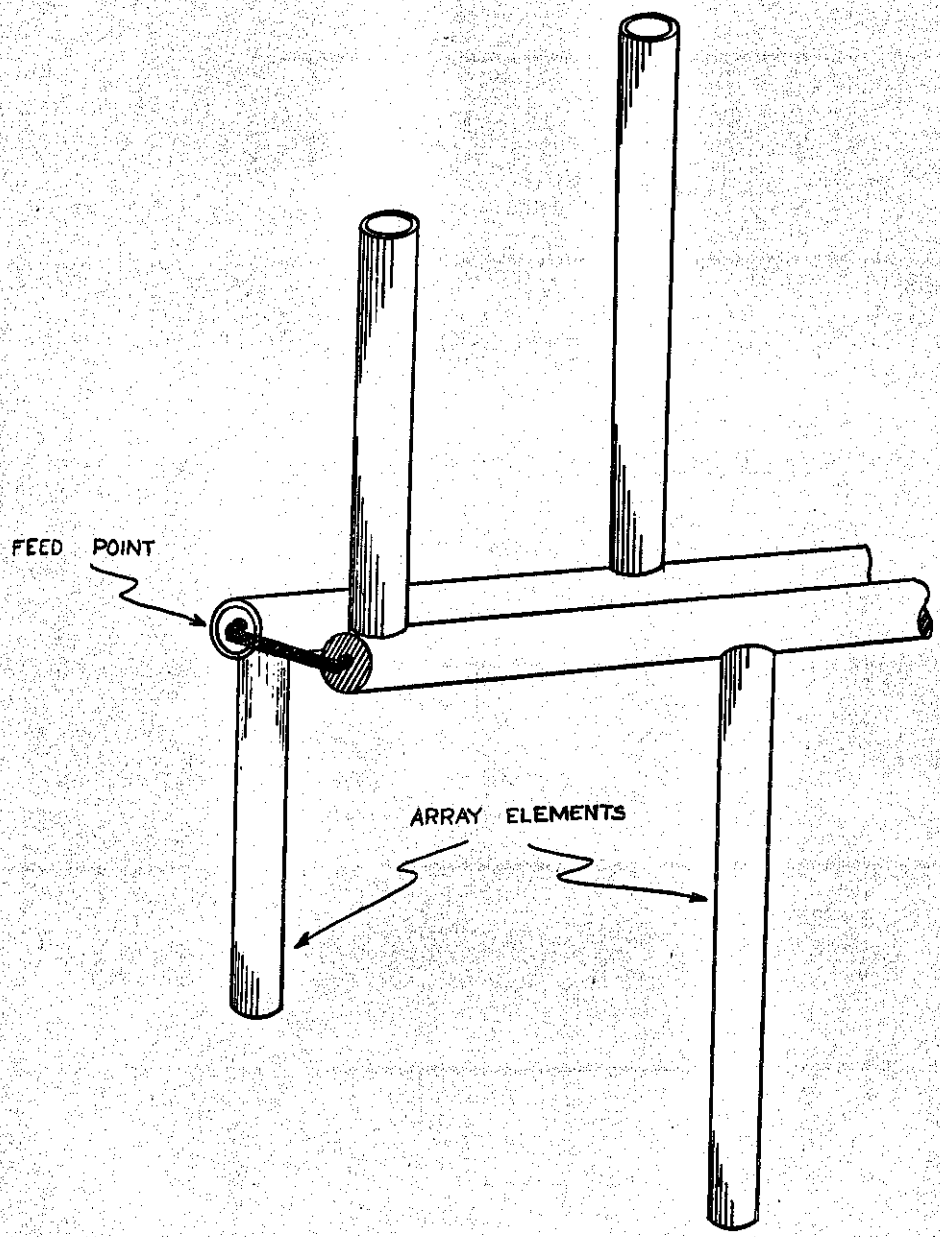

FIGURE 2 CONNECTION OF ELEMENTS TO BALANCED FEEDER

4. THE INTERIOR PROBLEM

Insofar as the interior problem is concerned, the connection of the dipole elements with the feeder is equivalent to the parallel connection of two N terminal-pair circuits. One circuit consists of the feeder with alternating, properly-spaced taps which represent the terminals to which the elements are eventually attached. The feeder circuit is shown schematically in Figure 3b. Note the inclusion of a terminating impedance Z_{T-1}. Z_T is arbitrary and can be varied to test for end effect. The parameters which describe this circuit are: Z_o, the feeder characteristic impedance; β_o the feeder propagation constant; σ, τ, and d_1 which determine the spacing; and N.

Consider the admittance matrix of the feeder circuit $\bar{Y}_L$ and its inverse $\bar{Z}_L = \bar{Y}_L^{-1}$.

$$\bar{Y}_L = \begin{bmatrix} y_{11} & y_{12} & 0 & 0 & \cdots & 0 \\ y_{21} & y_{22} & y_{23} & 0 & \cdots & 0 \\ 0 & y_{32} & y_{33} & y_{34} & 0 & \cdots & 0 \\ & & & \cdots & & & \\ & & & \cdots & & & \\ 0 & \cdots & & & 0 & y_{NN-1} & y_N \end{bmatrix} \qquad (1)$$

$\bar{Y}_L$ is given in more detail in Appendix A. It becomes evident why all the elements off the diagonal by two or more are zero when we consider that y_{ij} is the current in terminal i due to a unit voltage at j, all terminal-pairs other than j being shorted. The short circuit restricts current flow to sections of line

adjacent to the terminals to which the voltage is applied. The y_{ij}'s are trigonometric functions. Note the convention for the direction of current and voltage at the terminal-pairs.

The fields of the dipole elements determine the driving point impedances of the elements which shunt the feeder. The circuit properties of the elements are described by an N terminal pair circuit as shown in Figure 3a. Let $\bar{Y}_A$ be the element admittance matrix with $\bar{Z}_A = \bar{Y}_A^{-1}$.

$$\bar{Y}_A = \begin{bmatrix} y_{11} & y_{12} & y_{13} & \cdots \\ \cdots & \cdots & \cdots & \cdots \\ \cdots & \cdots & \cdots & \cdots \\ \cdots & \cdots & \cdots & y_{NN} \end{bmatrix} \tag{2}$$

The y_{ij}'s represent the element to element coupling, the range of which extends throughout the antenna. The y's are complex functions of τ, σ, h_1, and a/h, the radius to height ratio of the dipole elements. The method used to determine the y's depends on an assumption of the form of the current on a dipole. See Appendix B.

The following relations obtain:

$$\bar{I}_L = \bar{Y}_L \bar{V}_L , \tag{3}$$

where $\bar{I}_L$ and $\bar{V}_L$ are column vectors which represent the N driving currents and response voltages respectively of the feeder circuit. Also,

$$\bar{I}_A = \bar{Y}_A \bar{V}_A , \tag{4}$$

where $\bar{I}_A$ and $\bar{V}_A$ are column vectors which represent the N driving currents and response voltages of the element circuit. If the corresponding terminals of

the feeder and element circuits are connected in parallel, a new circuit is obtained as shown in Figure 3c. The response voltage vector is equal to either $\bar{V}_A$ or $\bar{V}_L$ since they are equivalent. The driving current vector of the new circuit is now the sum of $\bar{I}_A$ and $\bar{I}_L$ due to conservation of current at a node. If equations (3) and (4) are added,

$$\bar{I} = \bar{I}_A + \bar{I}_L = \bar{Y}_A \bar{V}_A + \bar{Y}_L \bar{V}_L . \tag{5}$$

$\bar{V}_L$ is set equal to $\bar{V}_A$ and factored,

$$\bar{I} = (\bar{Y}_A + \bar{Y}_L)\bar{V}_A . \tag{6}$$

We are interested in $\bar{I}_A$, the base current to the antenna terminals. Therefore,

$$\bar{I} = (\bar{Y}_A + \bar{Y}_L)\bar{Z}_A \bar{I}_A \tag{7}$$

or

$$\bar{I} = (\bar{U} + \bar{Y}_L \bar{Z}_A)\bar{I}_A \tag{8}$$

where $\bar{U}$ is the unit matrix. The elements of $\bar{I}$ represent the input currents to the new circuit of Figure 3b. However, in the actual antenna all these currents are zero except the current at the feed point which is the driving current of the antenna. We may set the driving current equal to one ampere. Therefore,

$$\bar{I} = \begin{bmatrix} 0 \\ 0 \\ \cdot \\ \cdot \\ \cdot \\ 0 \\ 1 \end{bmatrix} \tag{9}$$

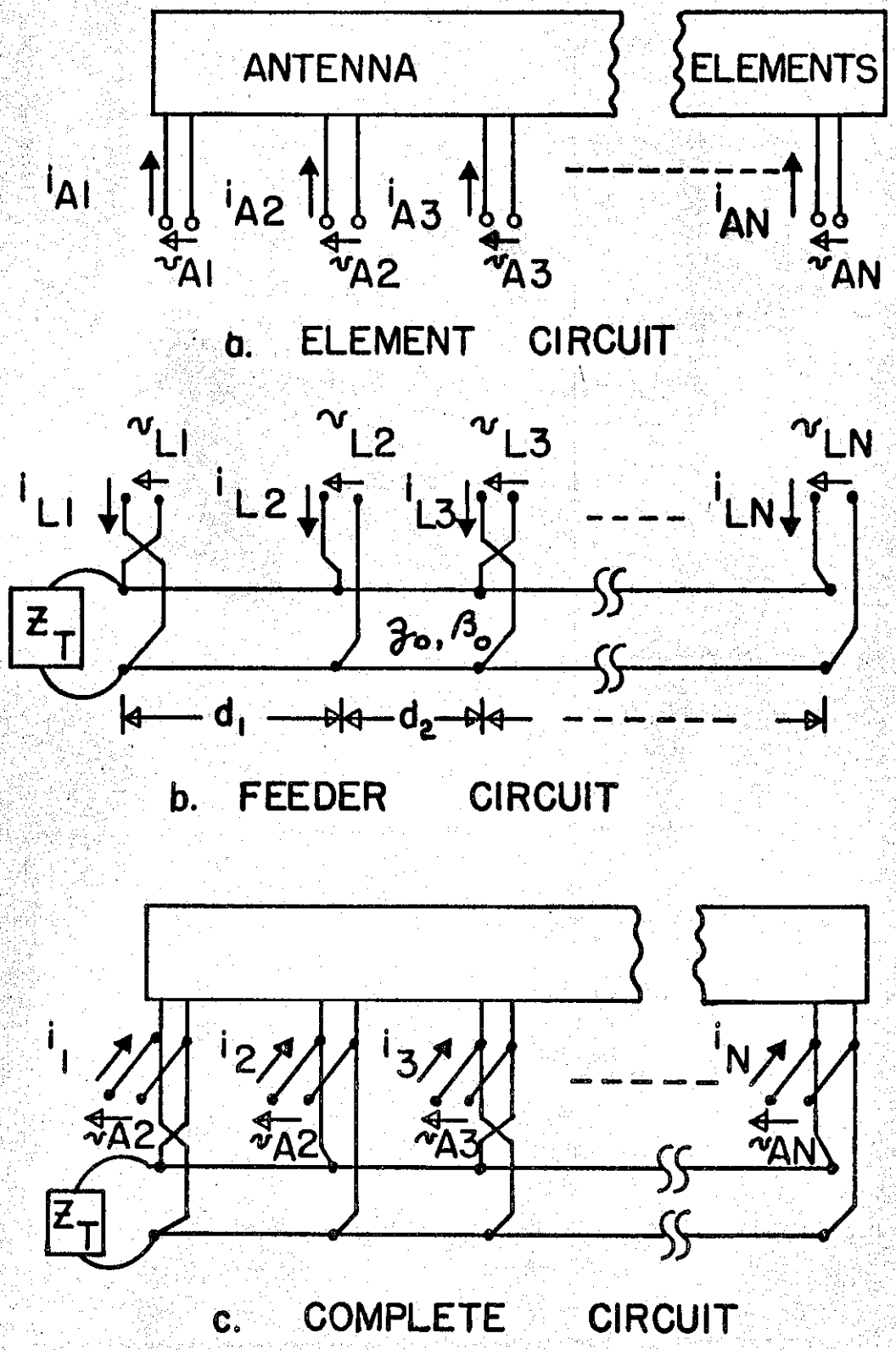

Figure 3. Schematic circuits for the LPD interior problem

Equation (8) must be solved for $\bar{I}_A$. This can be done by inverting the matrix $\bar{T}$,

$$\bar{T} = \bar{U} + \bar{Y}_L \bar{Z}_A, \tag{10}$$

or by solving directly the set of simultaneous equations posed by (8). The latter is easier to do in terms of computer time and accuracy due to the simplicity of $\bar{I}$. Once $\bar{I}_A$ is determined, $\bar{V}_A$ can be found by

$$\bar{V}_A = \bar{Z}_A \bar{I}_A \tag{11}$$

Note that the N^{th} element of $\bar{V}_A$ is the voltage across the smallest dipole; it is also the input impedance of the entire antenna since we assumed one ampere of input current.

5. THE EXTERIOR PROBLEM

The far field radiation pattern can be calculated once the element base currents $\bar{I}_A$ are known, using ordinary array theory. The magnitude of the H-plane pattern is given by

$$\left| P_H(\varphi) \right| = \left| \sum_{n=1}^{N} \frac{i_{An}(1-\cos \beta h_n)}{\sin \beta h_n} \exp\left(-j\beta \left| x_n \right| \cos \varphi\right) \right| \tag{12}$$

The magnitude of the E-plane pattern is given by

$$\left| P_E(\theta,\varphi) \right| = \left| \sin\theta \sum_{n=1}^{N} \frac{i_{An}[\cos(\beta h_n \cos\theta) - \cos \beta h_n]}{\sin\beta h_n} \exp(-j\beta \left| x_n \right| \sin\theta \cos\varphi) \right| \tag{13}$$

The coordinate system used is shown in Figure 4. x_n is the distance from the origin to the n^{th} element.

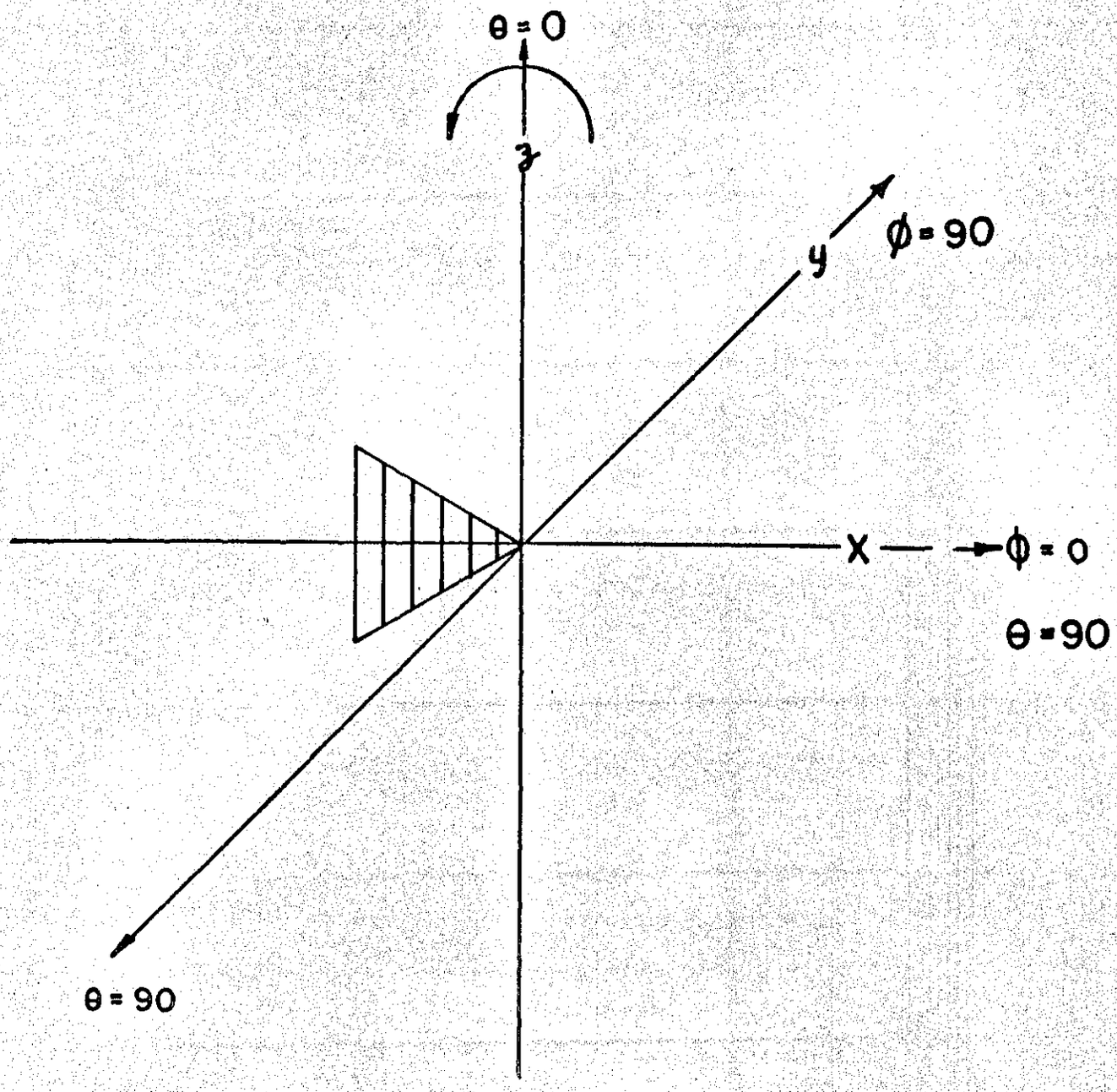

Figure 4. LPD pattern coordinate system

6. THE COMPUTER SOLUTION

The above formulas were programed in complex number arithmetic for use of the ILLIAC, a high speed digital computer operated by the University of Illinois Graduate College. Because of the large amount of intermediate results which must be stored in the fast access electrostatic memory (capacity 1024 forty bit words), the program was split into six different parts, each stored on the slow access magnetic drum (capacity 16,384 forty bit words). They are:

1. Input: The descriptive parameters of the antenna are read into ILLIAC.
2. Computation of $\overline{Z}_A$
3. Computation of $\overline{Y}_L$
4. Matrix multiplication of $\overline{Y}_L$ Z_A and solution of $\overline{I} = \overline{T}\,\overline{I}_A$.
5. Output $\overline{I}_A$, multiply $\overline{Z}_A\,\overline{I}_A = \overline{V}_A$ and output $\overline{V}_A$
6. Pattern calculation and scope display of patterns.

A control program calls each section into play as needed.

The input and basic output of the computer is by perforated paper tape which is translated by a teletypewriter. The patterns are calculated point by point and are plotted by the ILLIAC on a scope to which is attached an automatic 35 mm. camera. The camera takes a picture of the completed pattern and advances the film into position for a new exposure. The details of the programing are not of general interest and will be omitted.

7. RESULTS OF COMPUTATIONS AND MEASUREMENTS

A. Patterns

An example of the computed patterns is shown in Figure 5. f_j denotes the frequency,

$$f_j = f_1 \tau^{1-j} \tag{14}$$

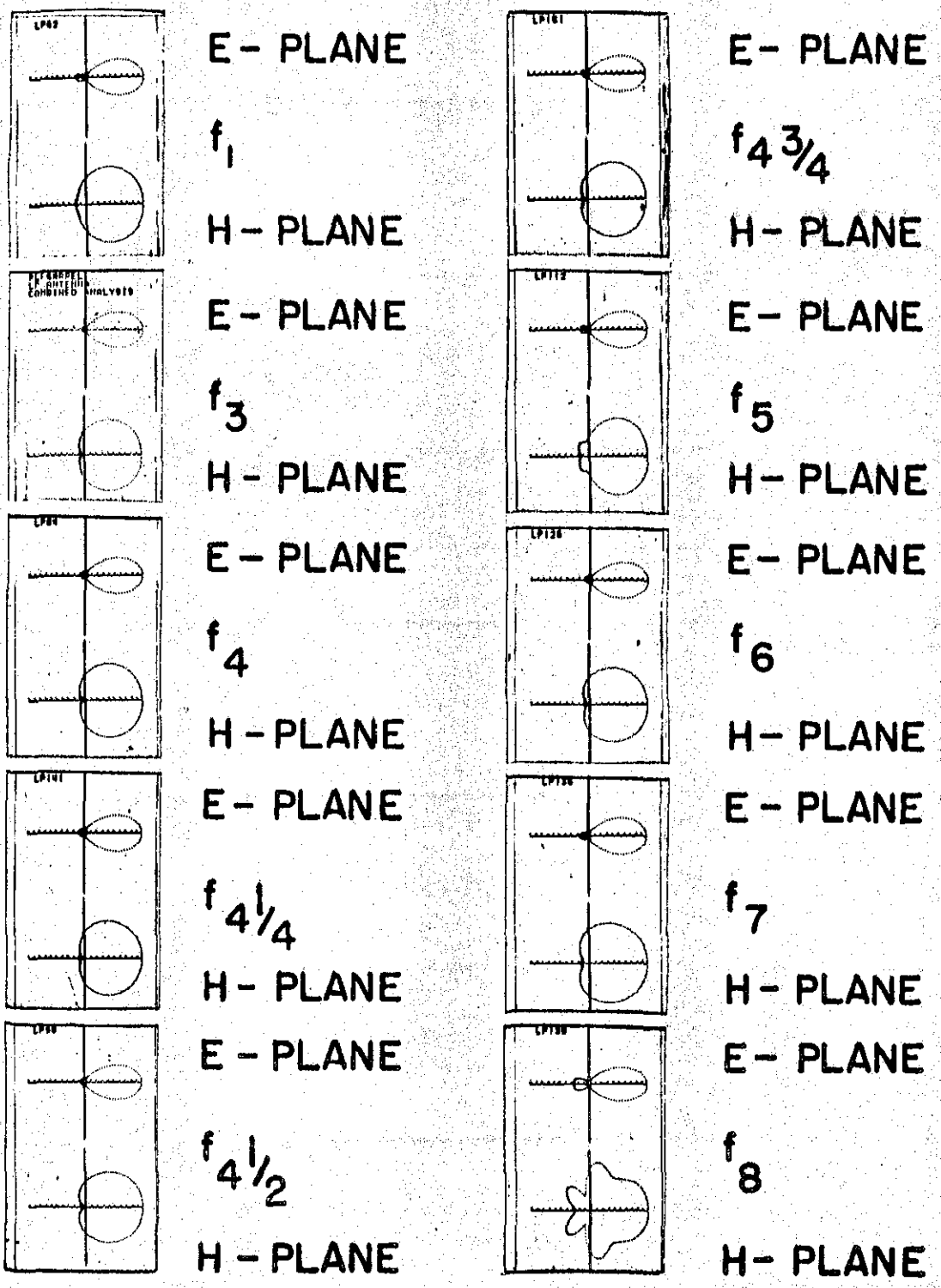

Figure 5. Computed patterns $\tau = .888$ $\alpha = 17.5^{o}$
$z_o = 100\Omega$, Z_T = short circuit at $\frac{d_1}{\tau}$ from biggest element

where f_1 is the frequency at which dipole number one is a half-wavelength long.

Frequency independent behavior is observed over the design range of the antenna. Several of these patterns are compared to the measured patterns in Figure 6. In every case, the measured patterns exhibited smaller H-plane beam width and larger E-plane beam width than the calculated patterns. Pattern break-up is observed at f_8, the high frequency limit. Other patterns show that the directivity depends only slightly on the feeder impedance; increasing feeder impedance somewhat decreases the gain. Figure 7 shown that the gain can be increased by increasing the radius to height ratio of the elements. This is due to a widening of the "active region" by the greater bandwidth of the individual elements. At present, data is being collected to extend the directivity data over the range of the variables τ and α.

B. Input Impedance

A typical locus of calculated input impedance versus frequency on a Smith chart is shown in Figure 8. The points cluster around a mean resistance level R_o. To determine R_o, one draws a circle around the cluster. Its intersection with the resistance axis determines the minimum and maximum swing of resistance. R_o is then given by

$$R_o = \sqrt{R_{max} R_{min}} \tag{15}$$

The standing wave ratio with respect to R_o is given by

$$SWR = \sqrt{\frac{R_{max}}{R_{min}}} \tag{16}$$

A plot of R_o and SWR as a function of feeder characteristic impedance is given in Figure 9. Several measured points are also shown. The mean resistance level

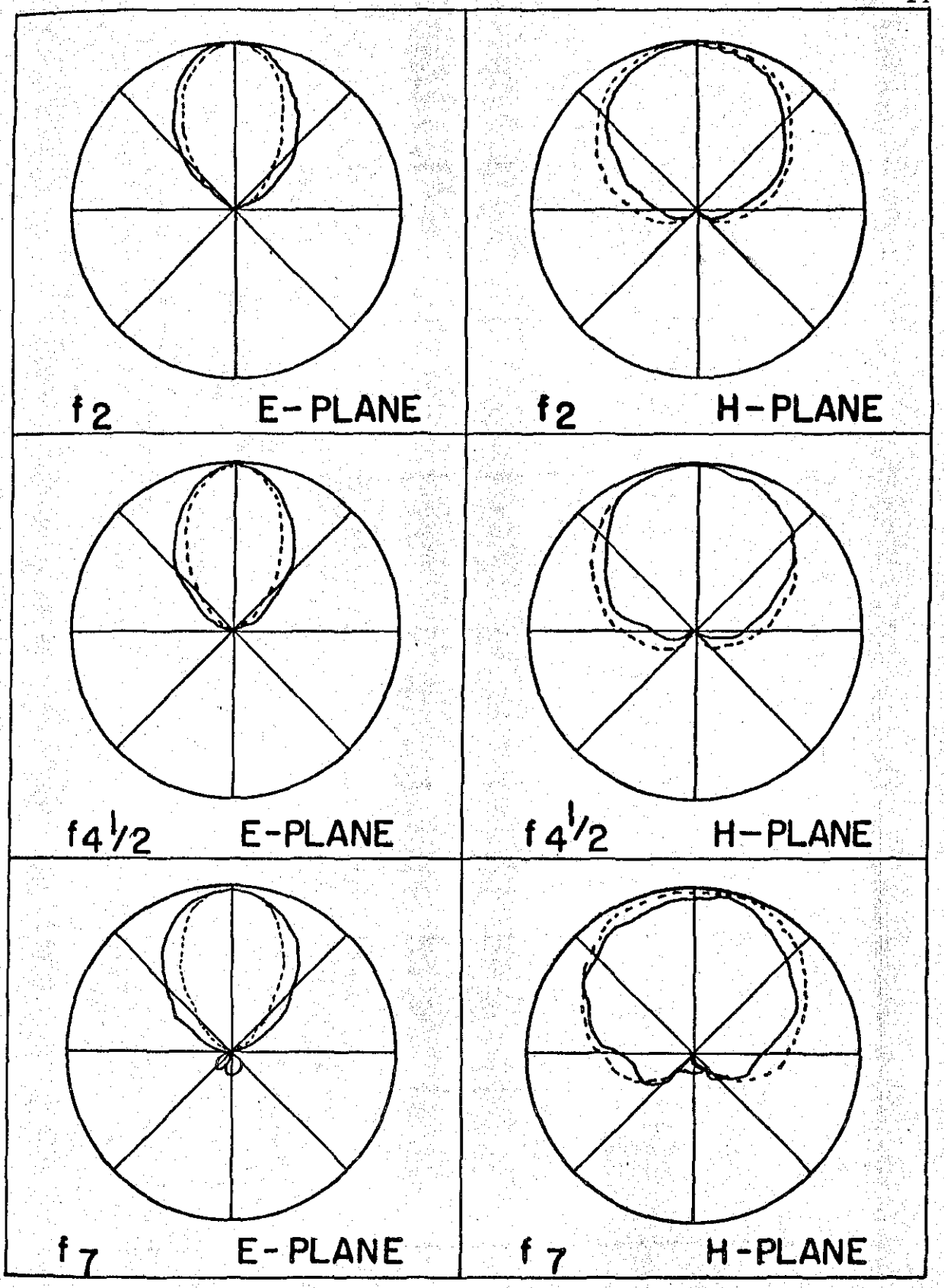

——— measured
------ computed

Figure 6. Radiation Patterns
$\tau = .888$, $a = 17.5$ $N = 8$

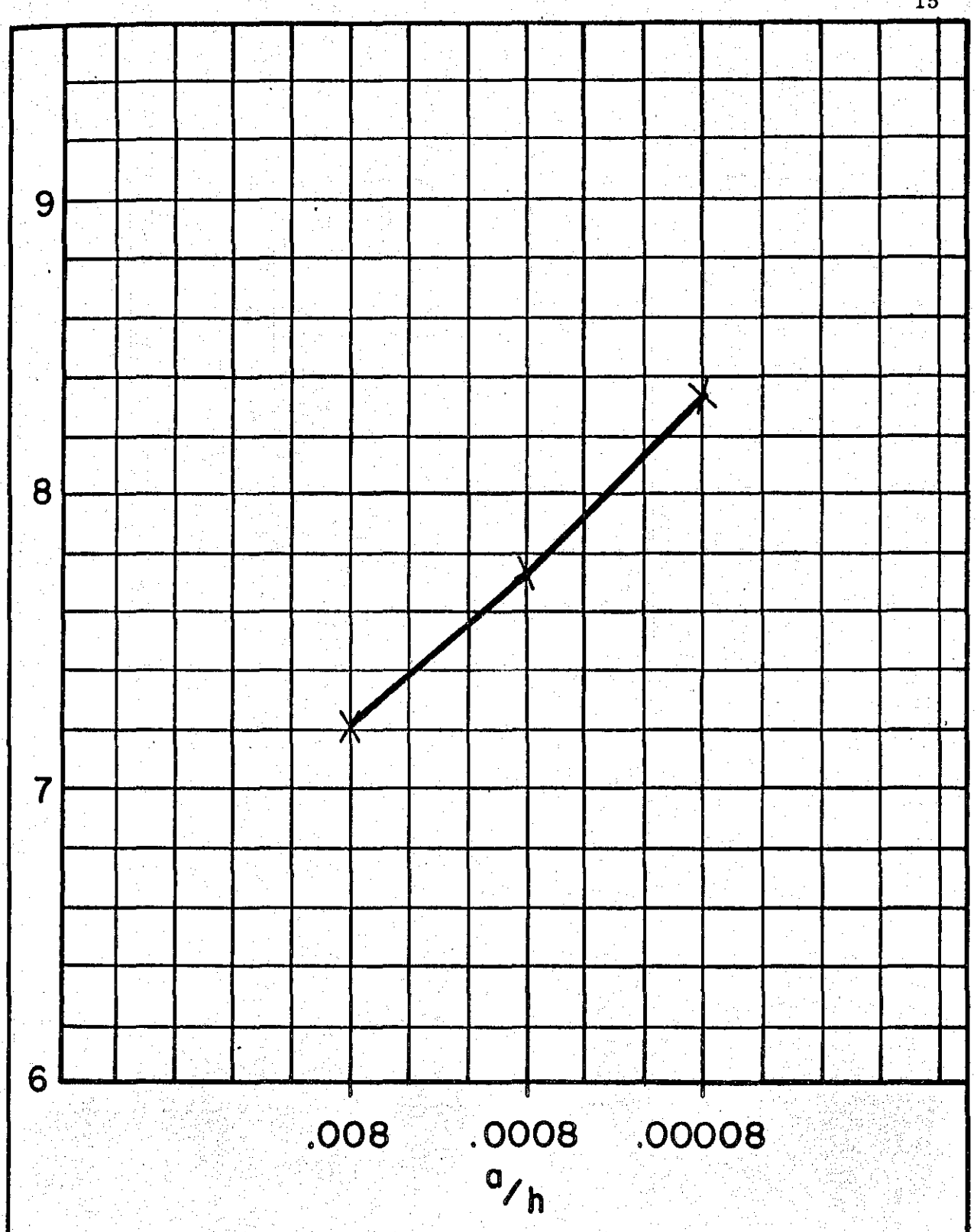

Figure 7. Computed directivity vs. radius to height ratio
$\tau = .888$ $\alpha = 17.5^{o}$ $N = 8$ at frequency f_4

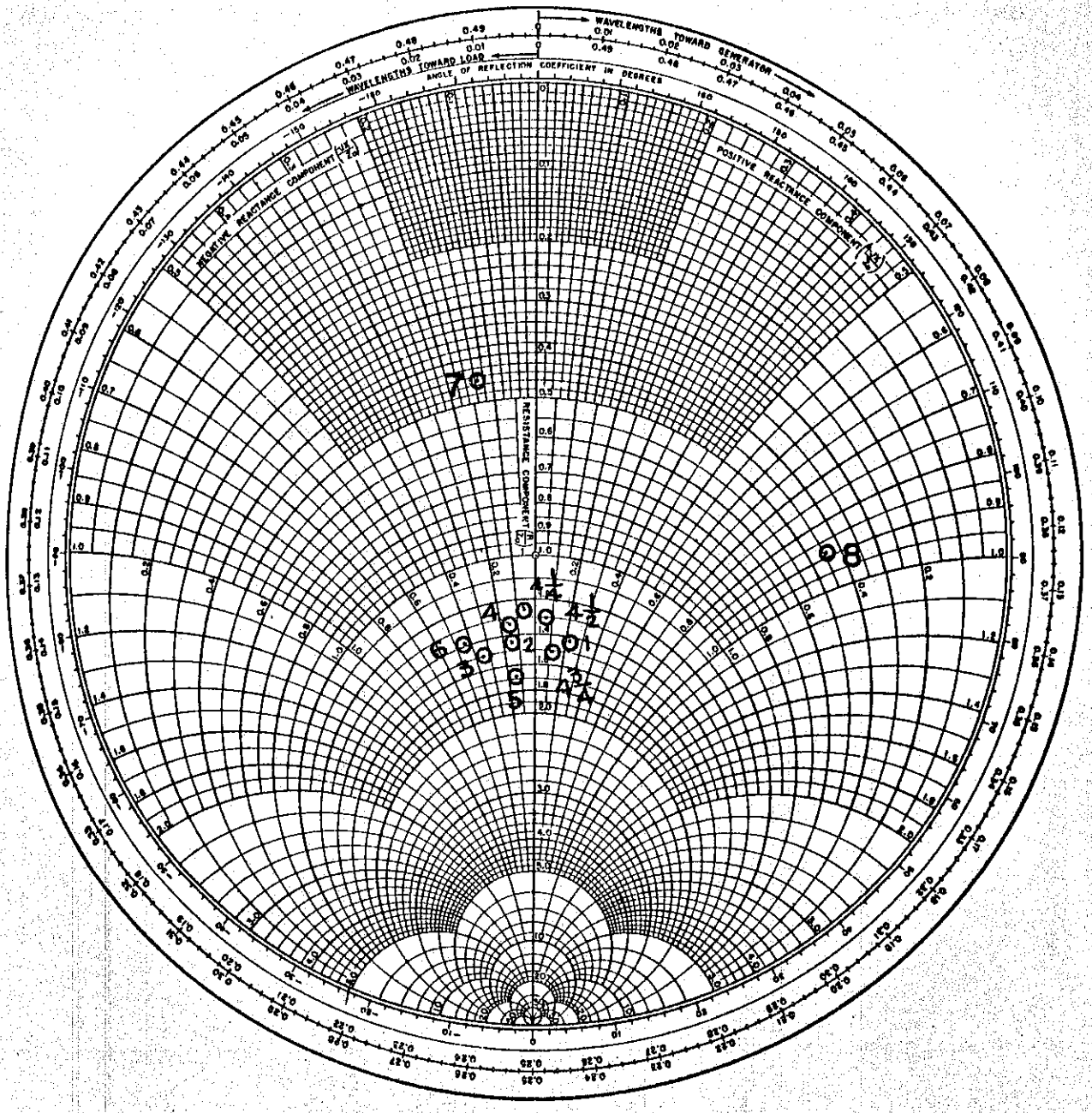

Figure 8. Computed input impedance vs. frequency

$\tau = .888 \quad \alpha = 17.5^{o} \quad N = 8 \quad z_{o} = 100\Omega \quad Z_{T} = 100\Omega$

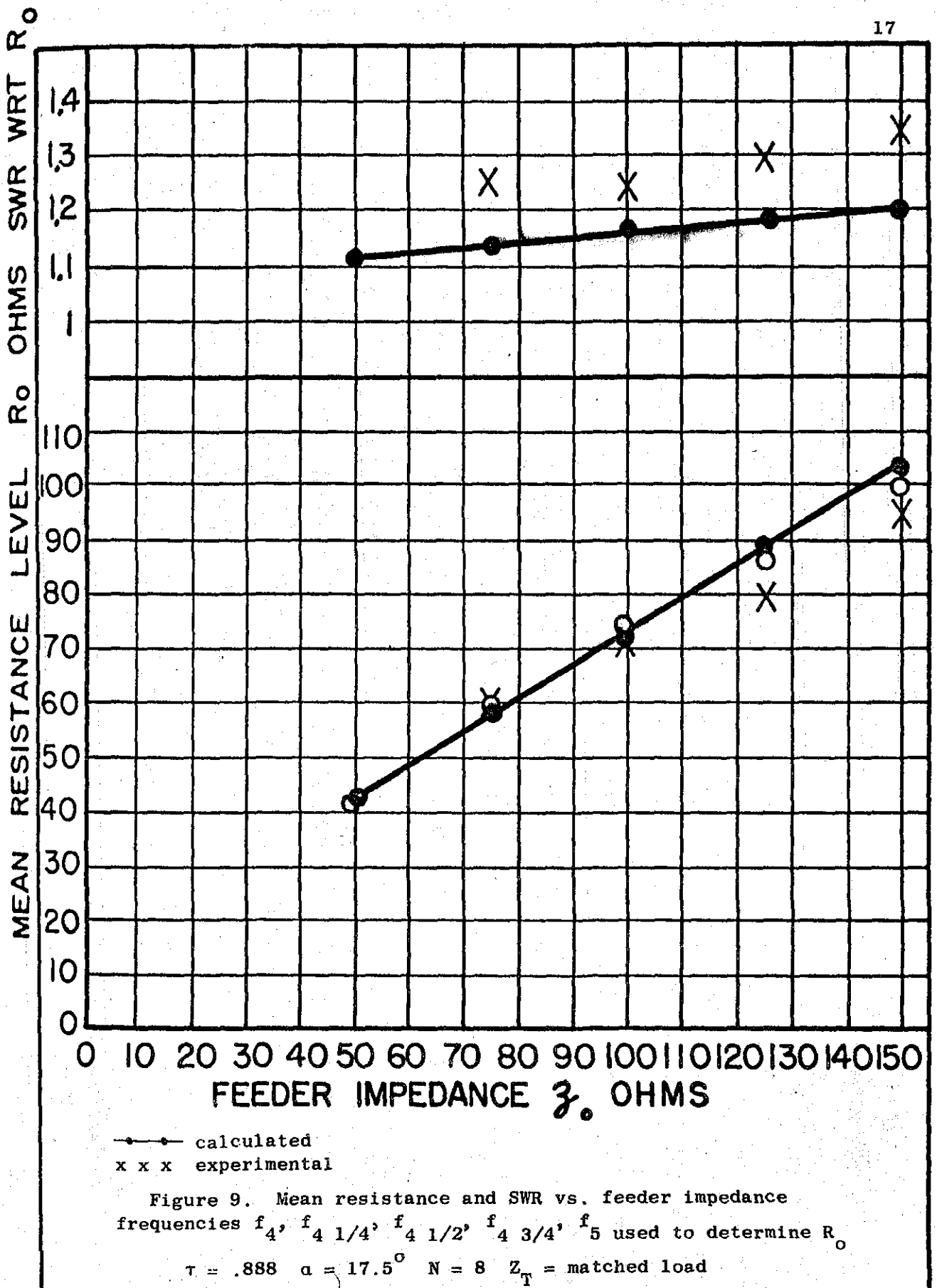

Figure 9. Mean resistance and SWR vs. feeder impedance frequencies f_4, $f_{4\ 1/4}$, $f_{4\ 1/2}$, $f_{4\ 3/4}$, f_5 used to determine R_o

$\tau = .888$ $\alpha = 17.5^o$ $N = 8$ Z_T = matched load

is almost linearly related to the feeder impedance, a fact which is useful in the design of these antennas for particular applications. The trend for various values of τ and α is being established. Some calculated results are shown in Figure 10. These values agree with those published by Isbell[1], in which R_o decreases with increasing τ and increasing α.

C. The Transmission Wave

The mechanism of the transfer of energy from the feeder to the radiated field leads one to consider two types of waves on the structure, as first pointed out by Bell, Elfving, and Franks[2]. One wave travels along the feeder in the direction of the larger elements. This is called the transmission wave. The other wave travels from the active region to and beyond the tip of the antenna. This wave is called the radiation wave because it manifests itself in the radiated field.

As the energy is launched from the feed point onto the small element end of the antenna, a TEM type wave is set up, supported by the feeders and the small elements which load the feeder log-periodically. This transmission line mode is evidenced by the voltages $\bar{V}_L^+$ along the feeder. ($\bar{V}_L^+$ is the true transmission line voltage. $\bar{V}_L$ differs from $\bar{V}_L^+$ by an additional 180^o phase in every other element due to the alternating feeder connection). A plot of the measured magnitude of the feeder voltage is shown as a function of normalized distance from the apex in Figure 11. The calculated voltage $\bar{V}_L^+$ at the location of each element is also plotted. The results are in good agreement. The plot shows a steadily decaying voltage away from the feed point to the short circuit which terminats the feeder beyond the largest element. The phase measurements are yet to be completed. The calculated phase variation is

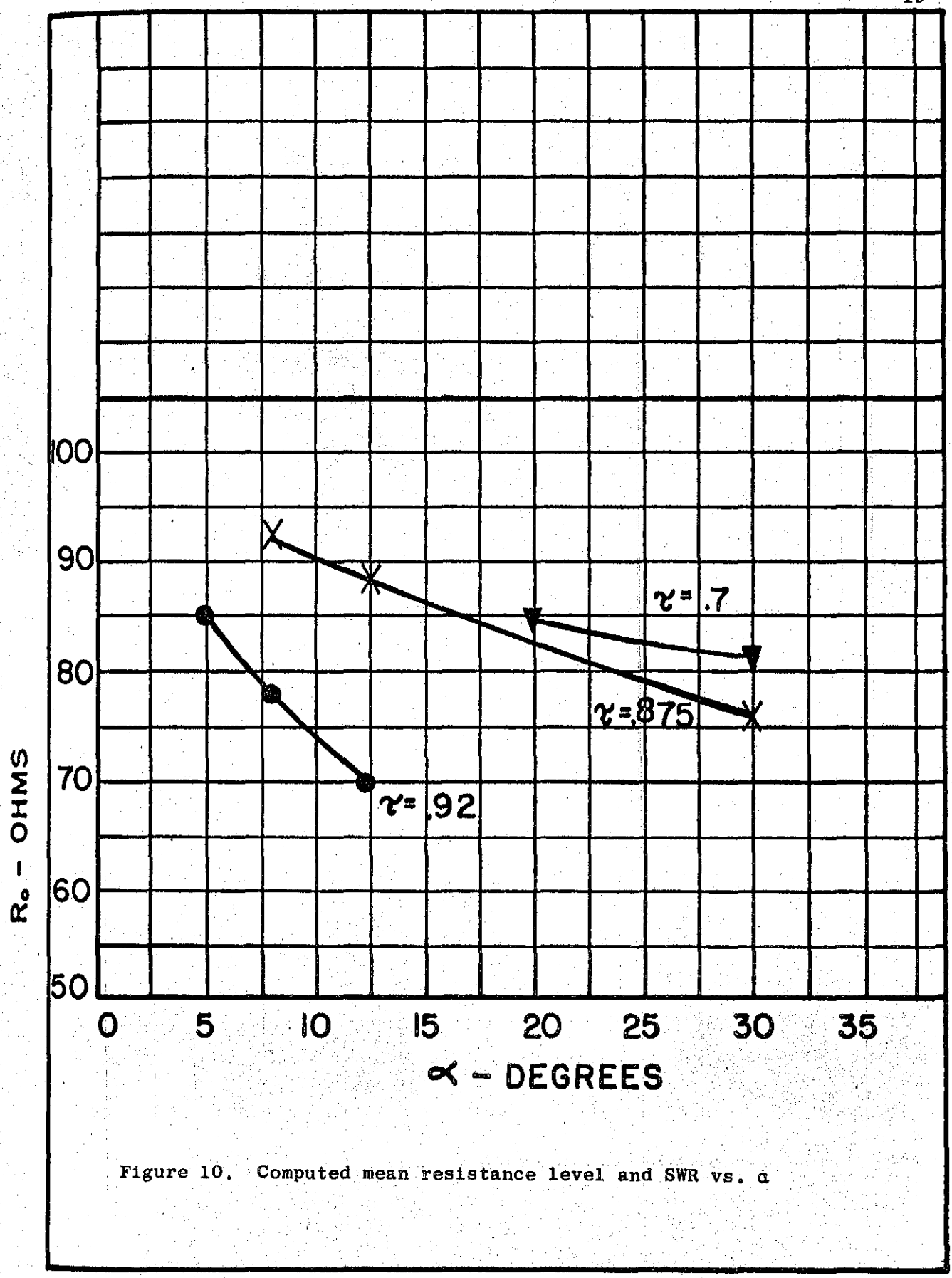

Figure 10. Computed mean resistance level and SWR vs. α

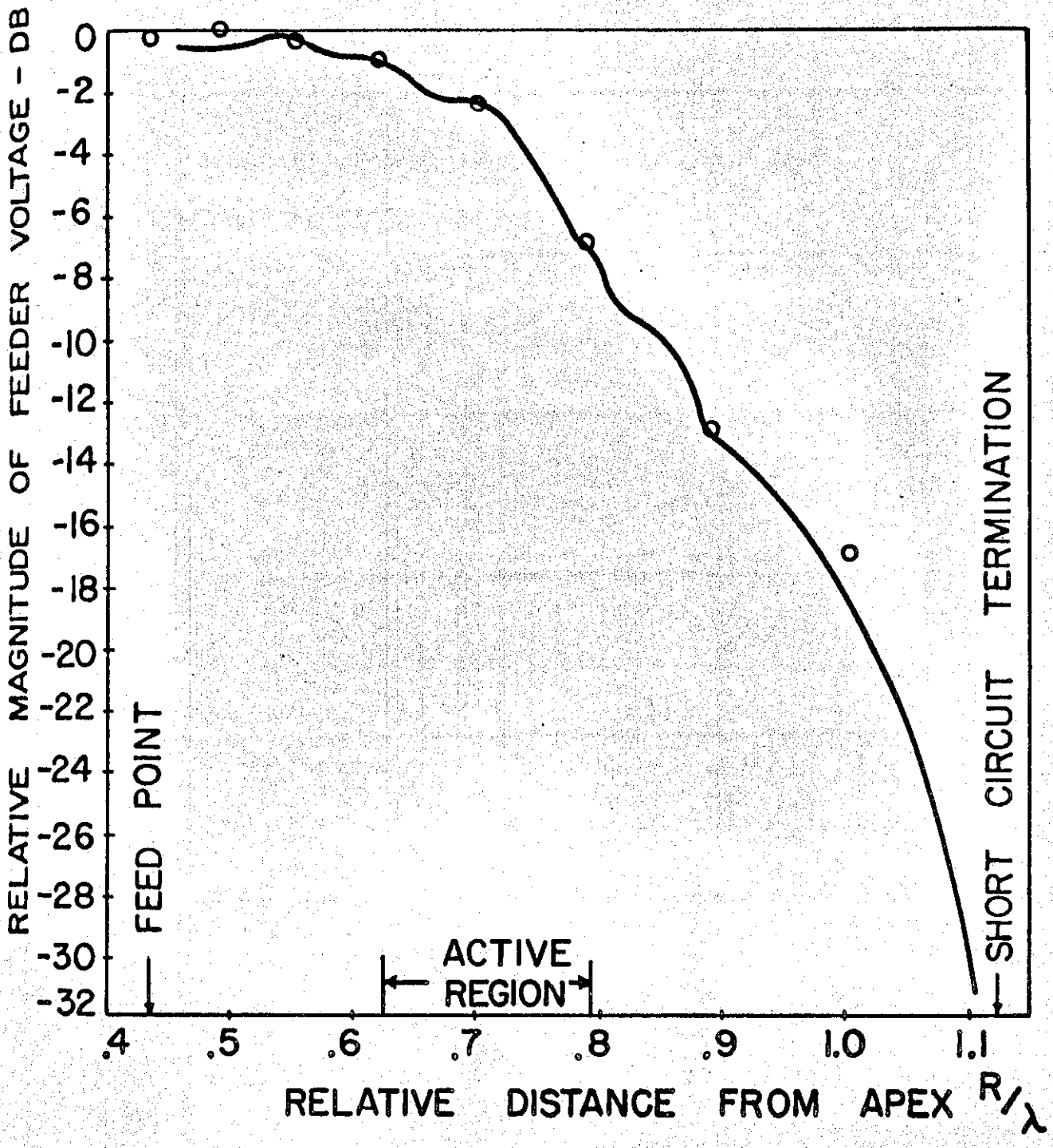

Figure 11. Relative magnitude of feeder voltage vs. R/λ at f_3 $\tau = .888$ $\alpha = 17.5^{\circ}$ $N = 8$

shown in Figure 12, yielding a phase change linear with distance. The slope of this curve is related to the relative apparent velocity of propagation δ.

$$\delta = \frac{v_a}{v_c}, \tag{17}$$

where v_a is the apparent phase velocity of the transmission wave and v_c is the velocity of light in the medium. δ is a function of the feeder impedance as shown in Figure 13. The slow wave nature of the transmission wave has been verified on a different type of LP structure by Bell, Elfving, and Franks[2].

D. The Radiation Wave

The element base currents $\bar{I}_A$ in the region of half-wavelength elements (the "active region") provide a connection between the transmission wave and the radiation wave. The driving point impedance of the elements in the active region become predominately real as shown in Figure 14. Thus energy is efficiently coupled from the feeder to the radiating elements in the active region. The element base currents in the active region rise to a peak somewhat ahead of the resonant element, and then drop off rapidly as shown in Figure 15. The phase change from element to element in the active region is also shown in Figure 15. The slope of the curve implies a slow wave traveling in the end fire direction with $\delta = .378$. Since the element currents are directly related to the radiated wave, it can be concluded that the transfer of energy from the transmission wave to the radiated wave has been accomplished.

8. DESIGN PROCEDURE

For most applications one is usually interested in designing an antenna which exhibits maximum gain over a given frequency band compatible with limitations on the boom length (the length of the feeder from smallest to largest

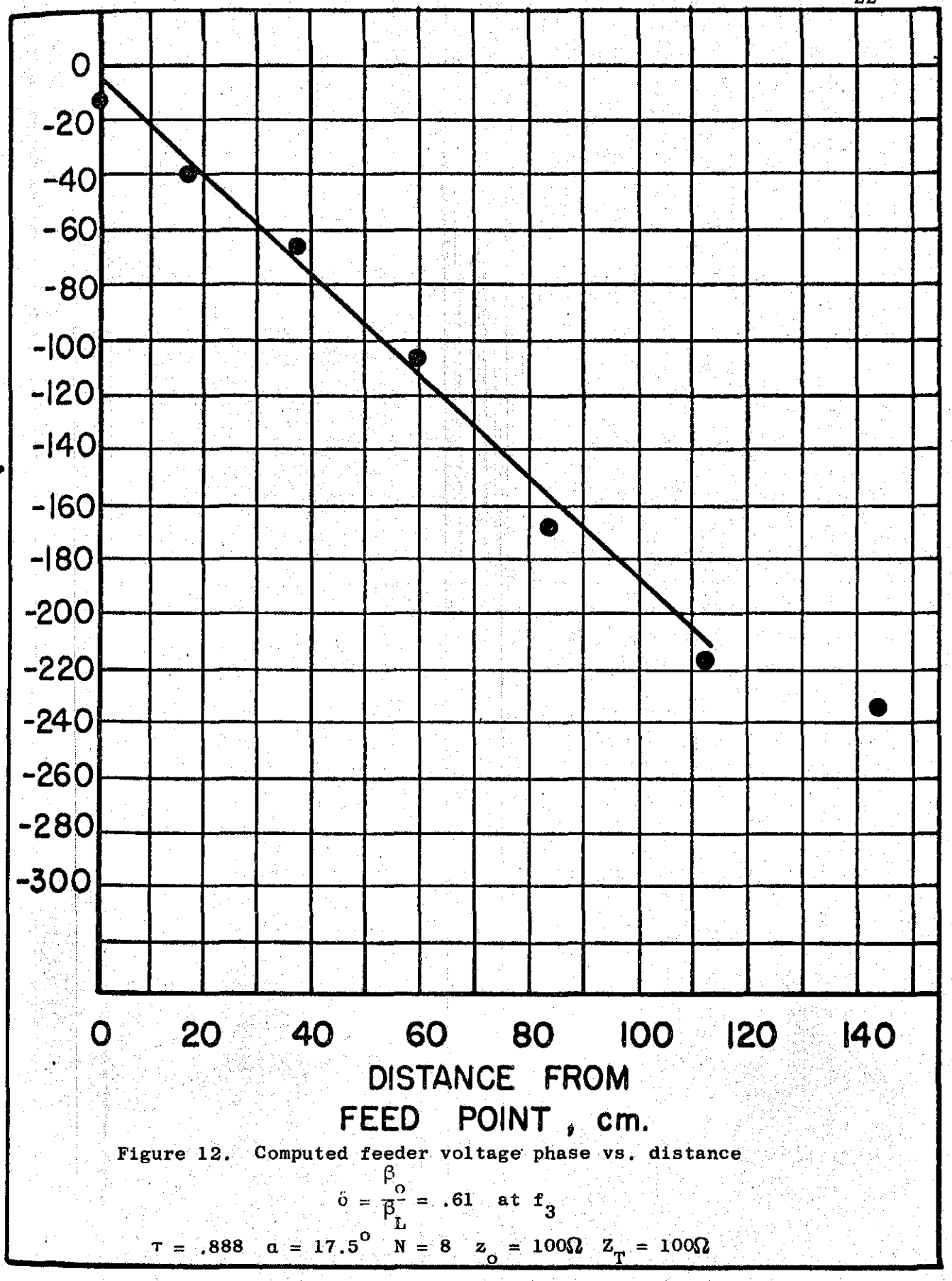

Figure 12. Computed feeder voltage phase vs. distance

$$\delta = \frac{\beta_o}{\beta_L} = .61 \quad \text{at } f_3$$

$\tau = .888$ $\alpha = 17.5^o$ $N = 8$ $z_o = 100\Omega$ $Z_T = 100\Omega$

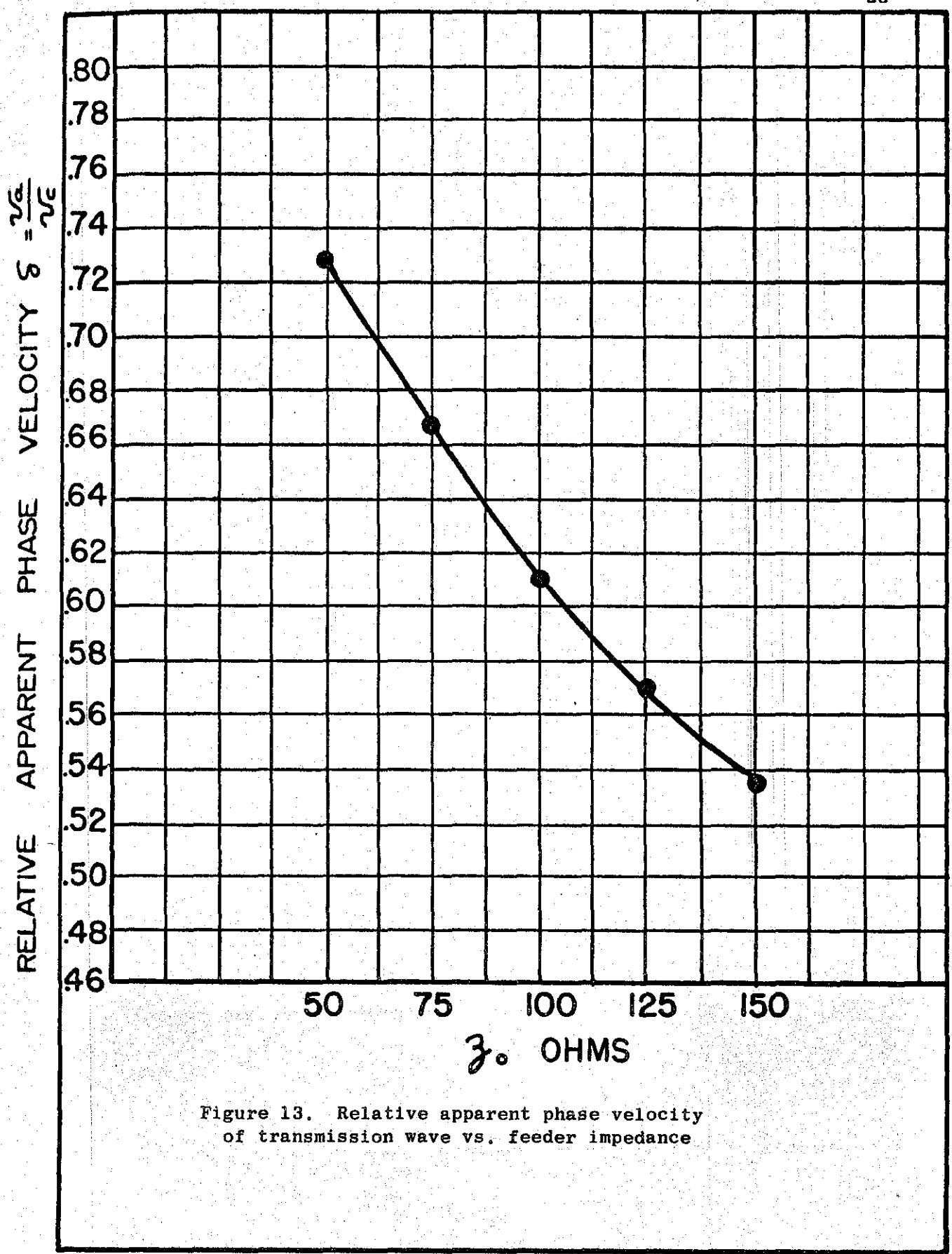

Figure 13. Relative apparent phase velocity of transmission wave vs. feeder impedance

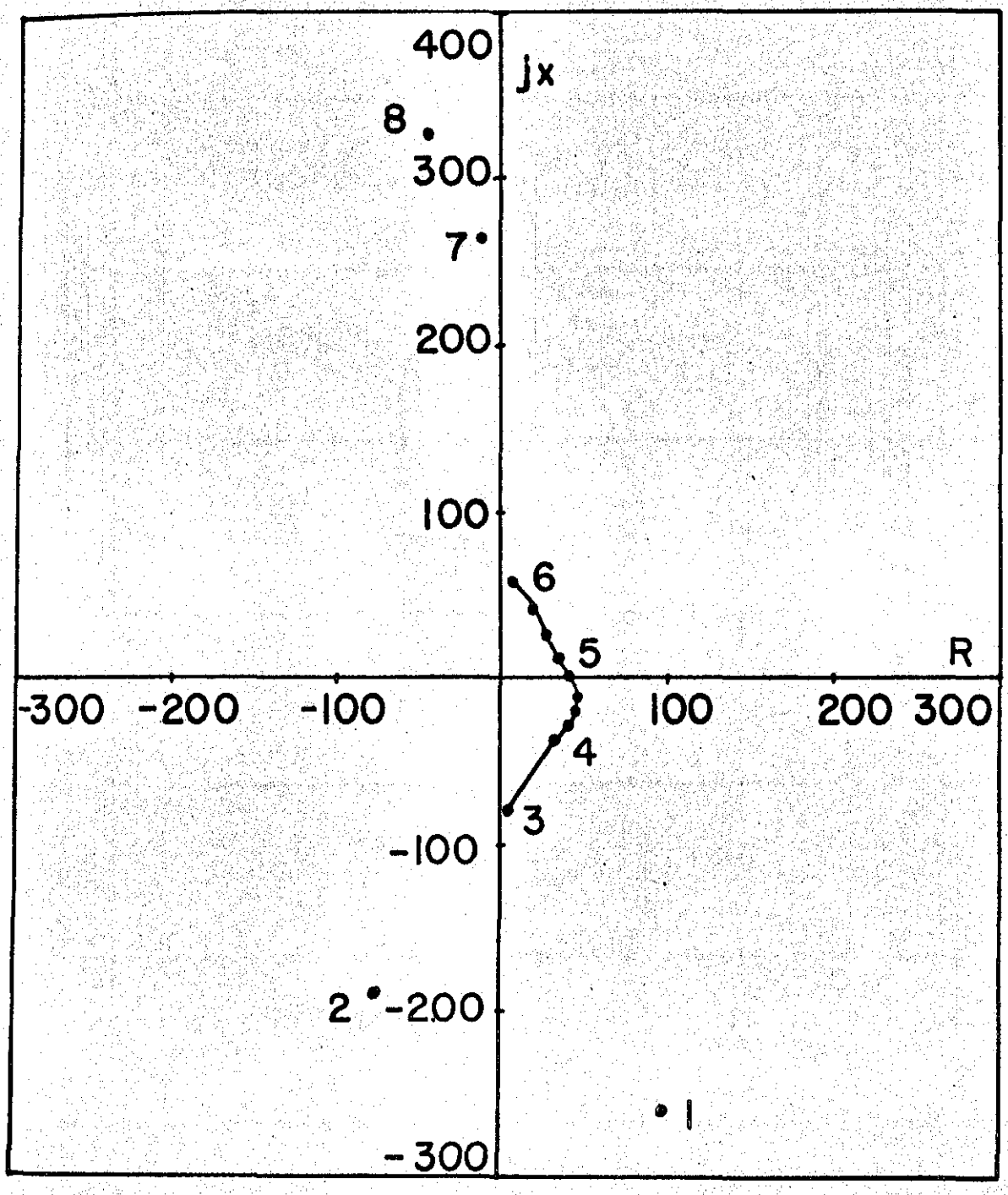

Figure 14. Computed driving point impedance of element number 5 vs. frequency f_n numbers are shown

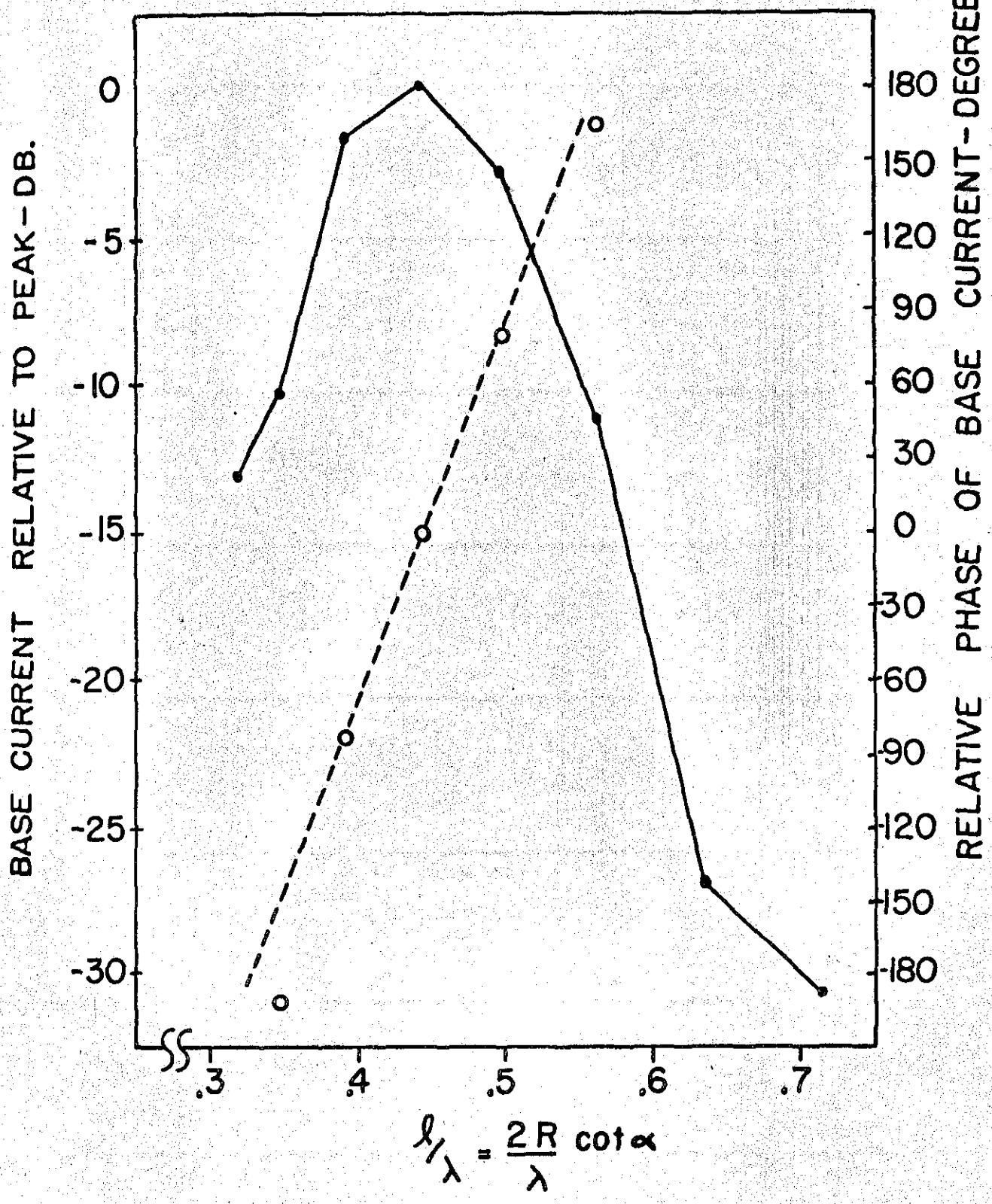

Figure 15. Calculated magnitude and phase of base current vs. relative element length at f_4. $\tau = .888$ $\alpha = 17.5^{\circ}$ $N = 8$

element) and the input impedance. Other limiting factors may be the number of elements and the weight, which in turn could depend on the a/h ratio. We must assume that the boom length is great enough to support a well formed active region over the frequency band. This will be discussed in more detail later. Assuming that the boom length criterion is met, the gain of an LPD is determined primarily by τ and α. Examining the work of Isbell[1]. (and extensions of this work to be published by the author), we can make a preliminary choice of τ and α. The spacing ratio σ is then determined through the formula

$$\sigma = \frac{1}{4} (1 - \tau) \cot \alpha \qquad (18)$$

a nomogram of which is shown in Figure 16. Preliminary results of extending gain vs. τ and α curves indicate that σ is in the range from 0.1 to 0.15 for maximum gain, although satisfactory performance is observed from 0.05 to 0.22. τ should be greater than 0.75 for end-fire frequency independent patterns.

The bandwidth B and α determine the boom length relative to the low frequency wavelength through the formula

$$\frac{L}{\lambda_{max}} = \frac{1}{2} \left(0.47 - \frac{0.38}{B}\right) \cot \alpha \qquad (19)$$

where B is the bandwidth ratio. A nomograph of Equation 19 is shown in Figure 17. Equation 19 is a semi-empirical formula, based on an antenna whose active region must contain an element 0.47 λ_{max} long at the low frequency band limit and an element 0.38 λ_{min} long at the high frequency band limit. This formula applies to mid-range values of τ. For τ greater than 0.90 the active region must contain an element shorter than 0.38 λ_{min} at the high frequency band limit. L/λ_{max} must be at least 0.5 for satisfactory operation,

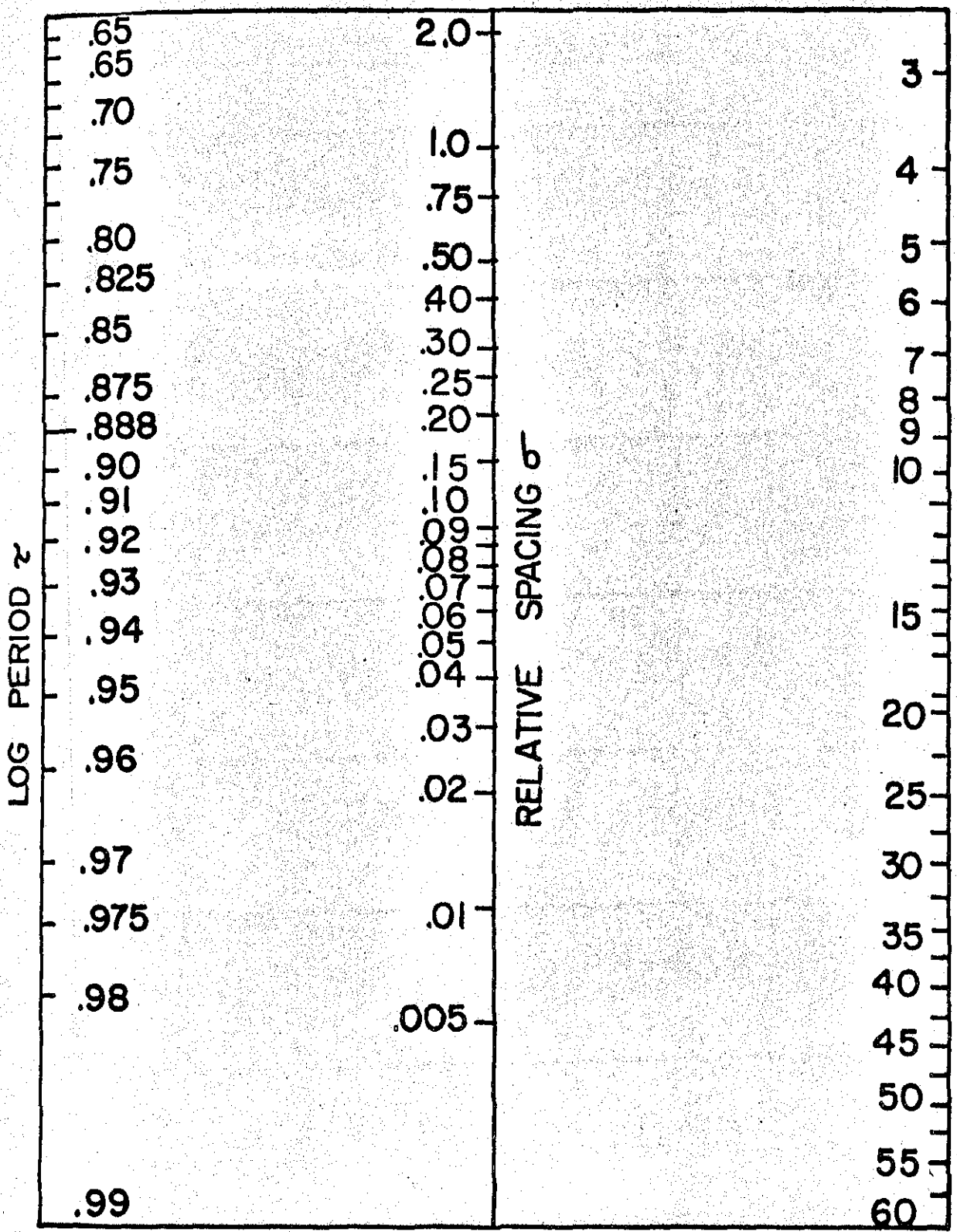

Figure 16. Nomograph of
$\sigma = 1/4\ (1-\tau)\cot\ \alpha$

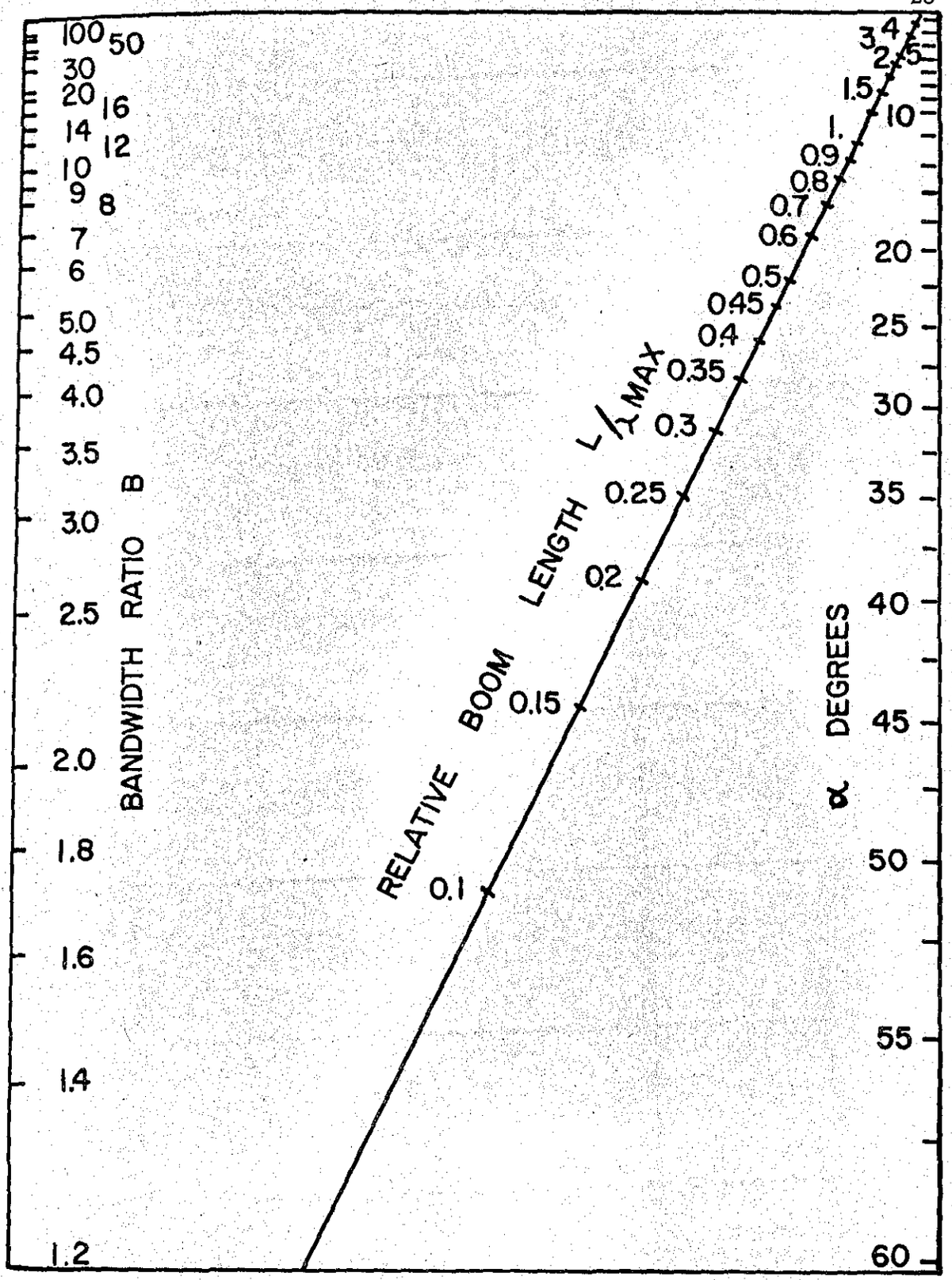

Figure 17. Nomograph of

$$L/\lambda_{max} = \tfrac{1}{2}(0.47 - \frac{0.38}{B}) \cot \alpha$$

so a readjustment of τ and α may be necessary. Once τ and α have been settled, the number of elements can be determined from the formula

$$N = 1 + \frac{\log 1.237\ B}{\log \frac{1}{\tau}} \tag{20}$$

which is based on the same assumptions about the active region as formula 19. A nomograph of equation 20 is shown in Figure 18.

An approximate formula for the mean resistance level R_o has been found which agrees within $\pm$ 5% of the measured and computed results to date. Its derivation is based on the assumption that the small elements add a constant capacity per unit length to the feeder in the transmission wave region of the antenna. Once σ and a/h is determined, the formula can be used to determine the feeder characteristic impedance Z_o which will yield a given R_o.

$$Z_o = R_o \left(\frac{1 + \sqrt{1 + 64\sigma'^2 Z_a^2}}{8 \sigma' Z_a} \right) \tag{21}$$

where

$$\sigma' = \frac{\sigma}{\sqrt{\tau}} \tag{22}$$

is a mean spacing factor and

$$Z_a = 120 \left(\ln \frac{h}{a} - 2.25 \right) \tag{23}$$

is an average characteristic impedance of a short dipole as a function of the dipole "thickness" ratio a/h. The derivation of Equation 21 is given in Appendix C. Values of R_o according to Equation 21 are plotted as small circles in Figure 9.

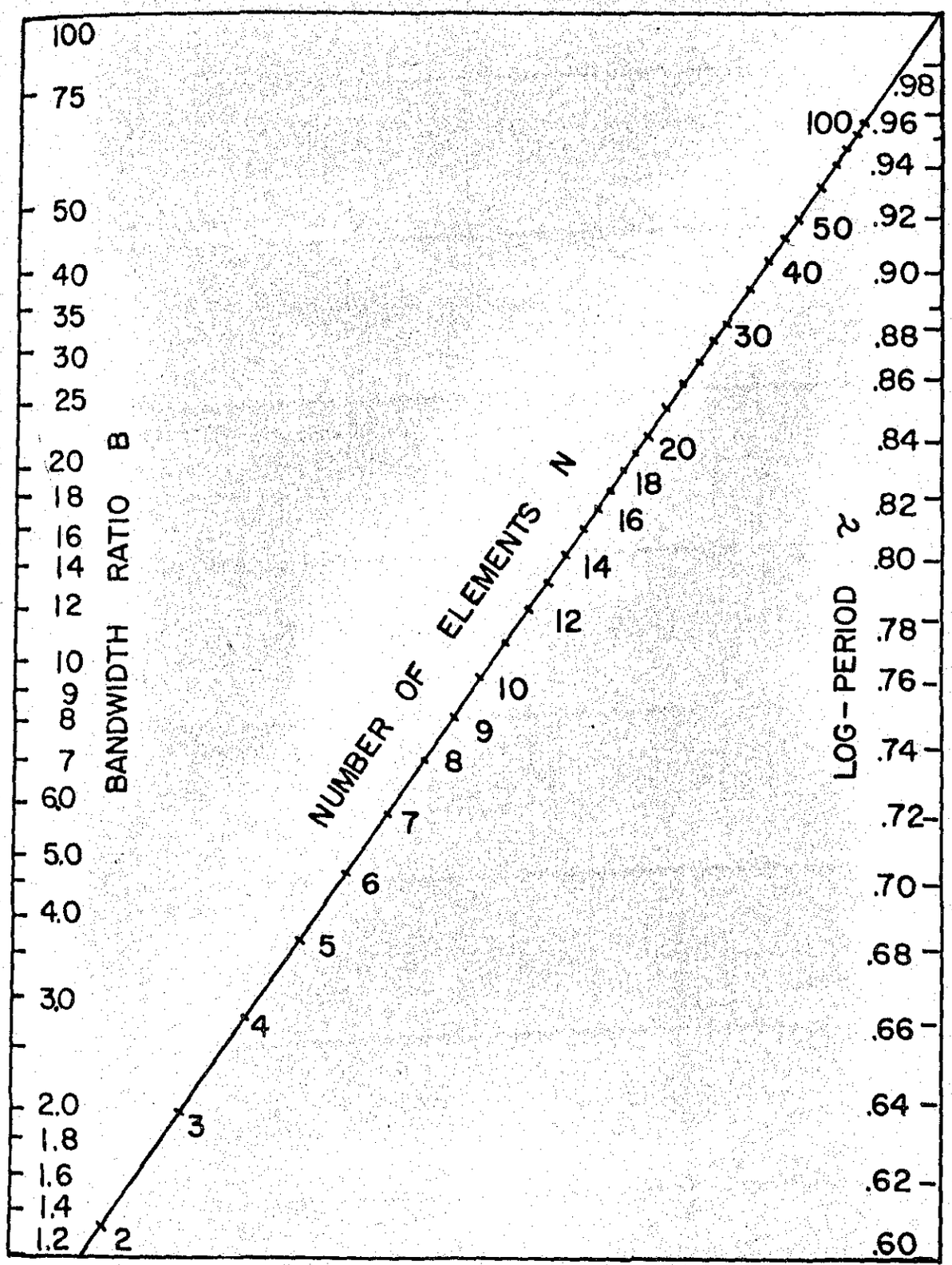

Figure 18. Nomograph of

$$N = 1 + \frac{\log 1.237B}{\log 1/\tau}$$

Thus we have the formulas needed to design a log periodic dipole antenna. The nomographs are particularly useful, since they allow one to work out many preliminary designs without resorting to calculations. In the future a study will be made which will hopefully lead to a simple formula for the standing wave ratio with respect to R_o as a function of antenna parameters.

APPENDIX A. ELEMENTS OF $\bar{Y}_L$

The admittance matrix for one section of transmission line of length d, propagation constant β, and characteristic admittance Y_o is

$$\bar{Y} = \begin{bmatrix} -jY_o \cot \beta d & +jY_o \csc \beta d \\ +jY_o \csc \beta d & -jY_o \cot \beta d \end{bmatrix} \qquad (24)$$

If a series of these sections are connected in cascade along with the terminating admittance Y_T, as shown in Figure 3b, the following matrix results.

$\bar{Y}_L =$

$$\begin{bmatrix} (Y_T - jY_o \cot \beta d_1) & -jY_o \csc \beta d_1 & 0 & \cdots & 0 \\ -jY_o \csc \beta d_1 & -jY_o(\cot \beta d_1 + \cot \beta d_2) & -jY_o \csc \beta d_2 & \cdots & 0 \\ 0 & -jY_o \csc \beta d_2 & -jY_o(\cot \beta d_2 + \cot \beta d_3) & \cdots & 0 \\ \cdots & \cdots & \cdots & \cdots & \cdots \\ \cdots & \cdots & \cdots & \cdots & \cdots \\ 0 & 0 & 0 & \cdots & -jY_o \csc \beta d_{N-1} \end{bmatrix} \qquad (25)$$

Y_T, the terminating admittance, has been added in y_{11}.

$\bar{Y}_L$ is the admittance matrix of the complete N terminal-pair feeder circuit as shown in Figure 3b.

APPENDIX B. ELEMENTS OF $\tilde{Z}_A$

The self and mutual impedances are calculated according to the formulas of Brown and Cox[3] as reported by King[4]. The following approximations are made:

1. The elements are infinitesimally thin in the calculation of mutual impedances. This means that the current at a cross section of the actual dipole has been replaced by an average current concentrated at the center of the cross-section.

2. A sinusoidal current distribution is assumed over the length of the dipole. This is a valid assumption as long as the dipole is reasonably less than a full-wavelength long, the accuracy being greatest for half-wave and shorter dipoles. We can ensure accuracy by always operating the computer model antenna at frequencies for which no full wave dipole exists on the structure.

3. The mutual term involves only the two elements considered; i.e., the intervening effects of neighboring elements are neglected.

4. The self impedances are calculated from the same formulas as the mutuals; the spacing is set equal to the thickness of the dipole.

After rearranging the formulas of King[4] we obtain the complex conjugate of Z_{12}

$$I^*_{12} = \frac{60}{\cos z_2 - \cos z_1}\left[e^{jz_1}(Ku_o - Ku_1 - Ky_1) + e^{-jz_1}(Kv_o - Kv_1 - Kw_1) \right.$$

$$\left. + e^{jz_2}(Ku'_o - Ku_1 - Kw_1) + e^{-jz_2}(Kv'_o - Kv_1 - Ky_1) + 2Kz(\cos z_1 + \cos z_2) \right] \quad (26)$$

where $Kx = Ci\ x + j\ Si\ x$,

Ci x and Si x are the cosine integral and sine integral functions. Also,

$$u_o = \beta \left[\sqrt{d^2 + (h_1 + h_2)^2} - (h_1 + h_2) \right]$$

$$v_o = \beta \left[\sqrt{d^2 + (h_1 + h_2)^2} + (h_1 + h_2) \right]$$

$$u'_o = \beta \left[\sqrt{d^2 + (h_1 - h_2)^2} - (h_1 - h_2) \right]$$

$$v'_o = \beta \left[\sqrt{d^2 + (h_1 - h_2)^2} + (h_1 - h_2) \right]$$

$$u_1 = \beta \left[\sqrt{d_1^2 + h_1^2} - h_1 \right]$$

$$v_1 = \beta \left[\sqrt{d^2 + h_1^2} + h_1 \right]$$

$$y_1 = \beta \left[\sqrt{d^2 + h_2^2} - h_2 \right]$$

$$w_1 = \beta \left[\sqrt{d^2 + h_2^2} + h_2 \right]$$

$$z_1 = \beta (h_1 + h_2)$$

$$z_2 = \beta (h_1 - h_2)$$

$$z = \beta d \qquad (27)$$

where β is the free space propagation constant, d is the separation of the two dipoles, and h_1 and h_2 are the half lengths of dipoles one and two, respectively.

APPENDIX C. APPROXIMATE FORMULA FOR R_o

It is an established fact that the standing wave ratio with respect to R_o of a well made LPD is small, usually less than 1.4:1. The small standing wave ratio is observed no matter how severe the front truncation, as long as a well-formed active region remains on the antenna. These two facts suggest that the observed R_o is actually the characteristic impedance of a transmission line made up of the feeder and the small elements, and that the active region is a good match to this transmission line.

If we consider the capacitive loading of the small elements, we note that the capacity is proportional to the length of the elements and that the spacing d_j of element j is proportional to the length of element j. As an approximation, then, the capacity per unit length is constant. Thus we add to the nominal capacity per unit length of unloaded feeder a term which represents the capacitive loading of the small elements. Consider the approximate formula for the input impedance of a dipole antenna,

$$Z = - j Z_a \cot \beta h . \tag{28}$$

Z_a is an average characteristic impedance of the dipole.

$$Z_a = 120 \left(\ln \frac{h}{a} - 2.25\right) \tag{29}$$

This is Jordan's[5] modification of a formula from Siegel and Labus[6]. If the dipole is small, β is the free space propagation constant. We may also replace the cotangent function by its small argument approximation,

$$Z \approx - j \frac{Z_a}{\beta h} \tag{30}$$

Therefore the capacity of the n-th dipole is given by

$$C_n = \frac{h_n}{cZ_a} \quad , \tag{31}$$

where c is the velocity of light in vacuo. If we use the mean spacing at dipole n,

$$d_{mean} = \sqrt{d_n d_{n-1}} = \frac{d_n}{\sqrt{\tau}} \quad , \tag{32}$$

the average capacity per unit length is given by

$$\Delta C = \frac{C_n}{length} = \frac{h_n \sqrt{\tau}}{c d_n Z_a} \quad . \tag{33}$$

But h_n/d_n is related to the spacing factor σ by

$$\sigma = \frac{1}{4} \frac{d_n}{h_n} \quad , \tag{34}$$

hence

$$\Delta C = \frac{\sqrt{\tau}}{4cZ_a} \quad . \tag{35}$$

Since

$$Z_o = \sqrt{\frac{L_o}{C_o}} \quad \text{and} \quad c = \frac{1}{\sqrt{L_o C_o}} \quad ,$$

$$R_o = \sqrt{\frac{L_o}{C_o + \Delta C}} = \sqrt{\frac{L_o}{C_o}} \left(\sqrt{\frac{1}{1 + \frac{\sqrt{\tau}}{4C_o c Z_a}}} \right) \quad . \tag{36}$$

or

$$R_o = \frac{\mathcal{Z}_o}{\sqrt{m}} \tag{37}$$

where

$$m = 1 + \frac{\mathcal{Z}_o}{Z_a} \frac{\sqrt{\tau}}{4\sigma} \quad . \tag{38}$$

The new propagation constant β_L is given by

$$\beta_L = \beta_o \sqrt{m} \tag{39}$$

thus we have a formula for the mean resistance level R_o and the propagation constant in terms of the spacing parameter σ, τ and the a/h ratio.

Inverting the formula to find the feeder impedance $\mathcal{Z}_o$ in terms of R_o, we find

$$\mathcal{Z}_o = \frac{R_o}{8\sigma' Z_a} \left(1 + \sqrt{1 + 64\, \sigma'^2 z_a^2}\right) \quad , \tag{40}$$

where

$$\sigma' = \frac{\sigma}{\sqrt{\tau}} \quad .$$

REFERENCES

1. D.E. Isbell, "Log Periodic Dipole Arrays," IRE Trans. on Antennas and Propagation, Vol. AP-8, pp 260-267, May, 1960 also University of Illinois Antenna Lab. Technical Report No. 39, June 10, 1959.

2. R.L. Bell, C.T. Elfving, R.E. Franks, "Near Field Measurements on a Logarithmically Periodic Antenna," Electronic Defense Laboratories Technical Memorandum No. EDL-M231, December 23, 1959.

3. C.R. Cox, "Mutual Impedance between Vertical Antennas of Unequal Heights," Proc. IRE, Vol. 35, pp 1367-1370, November 1947.

4. H.E. King, "Mutual Impedance of Unequal Length Antennas in Echelon," IRE Trans. on Antennas and Propagation, Vol. AP-5, pp 306-313, July 1957.

5. E.C. Jordan, "Electromagnetic Waves and Radiating Systems," Prentice-Hall Inc., New York, pp 464, 1950.

6. E. Siegel and J. Labus, "Apparent Resistance of Antennas," Hochf. und Elek., Vol. 43, p 166, 1934.

ACKNOWLEDGMENT

This work was sponsored by Wright Air Development Division under Contract AF33(616)-6079. The author gratefully acknowledges the direction and assistance given by Professors P. E. Mayes and G. A. Deschamps.

XB
55 Ld

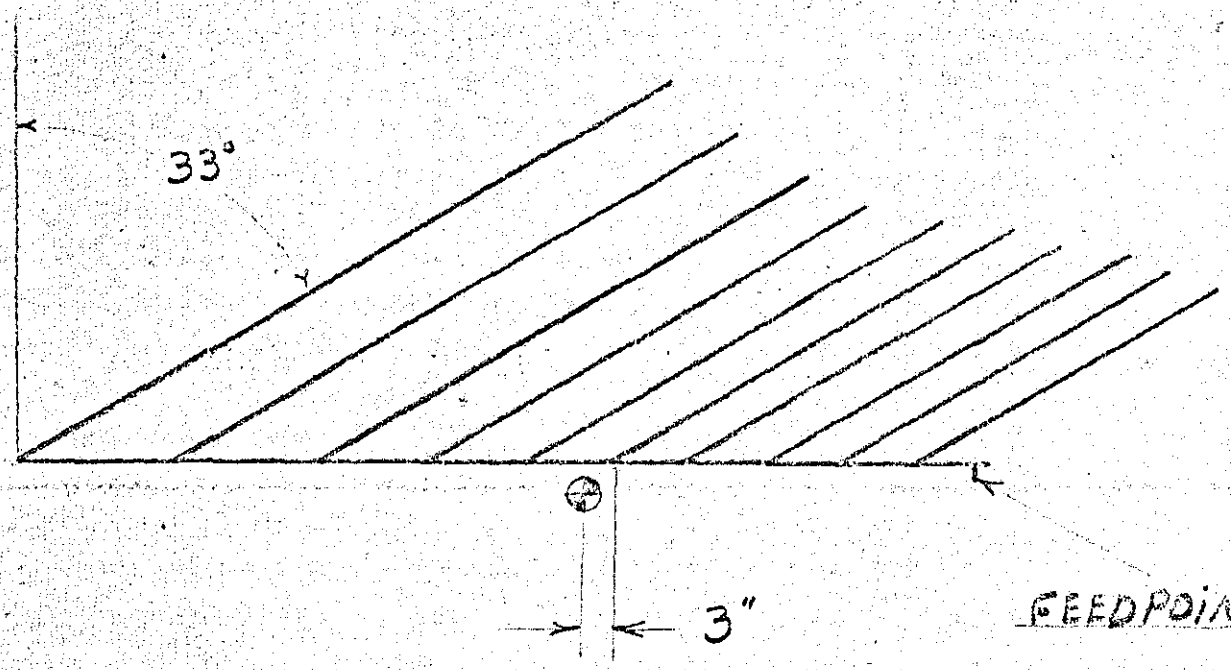

DIMENSIONS			
ELEMENT LENGTH		SPACINGS	
h_1	54.6	d_1	13.0
h_2	50.75	d_2	12.25
h_3	47.5	d_3	11.5
h_4	44.25	d_4	10.5
h_5	41.25	d_5	10.0
h_6	38.5	d_6	9.25
h_7	36.0	d_7	8.6
h_8	33.5	d_8	8.0
h_9	31.9	d_9	7.5
h_{10}	29.4	d_{10}	2.0

UNITED STATES DISTRICT COURT
NORTHERN DISTRICT OF ILLINOIS
BEFORE JUDGE HOFFMAN

DEFENDANT EX. NO. _____

DOROTHY L. BRACKENBURY
OFFICIAL COURT REPORTER

TEMPORARY SKETCH

BLONDER TONGUE

MODEL 220/6-12-10 VHF

DATE 8-20 | APPROVED

DRAWN RSA | SCALE —

JFD ELECTRONICS CORP.
ANTENNA LABORATORY

A00415

MATERIAL NOTES Twin-Boom const.
3/4" sq. 2 1/2" apart

XB
55 vd

UNITED STATES DISTRICT COURT
NORTHERN DISTRICT OF ILLINOIS
BEFORE JUDGE HOFFMAN

DEFENDANT EX. NO._____

DOROTHY L. BRACKENBURY
OFFICIAL COURT REPORTER

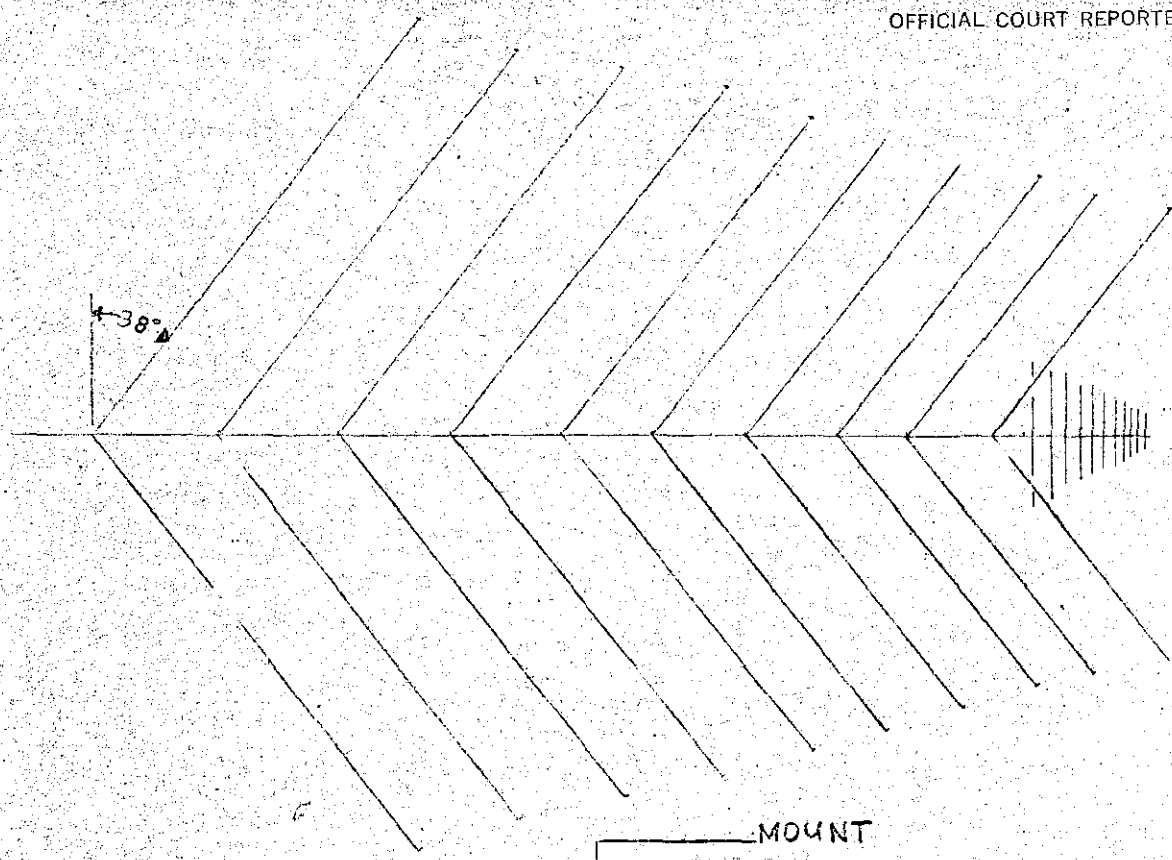

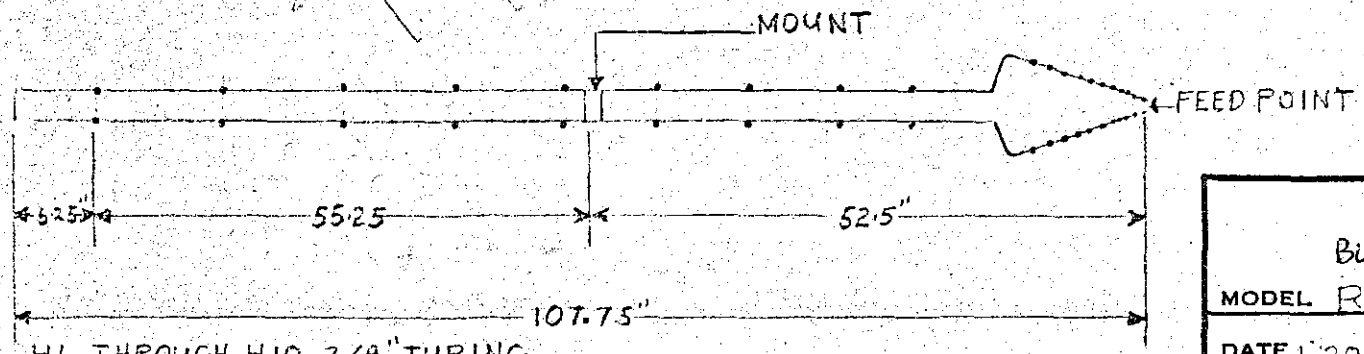

H1 THROUGH H10 3/8" TUBING
H11 THROUGH H21 WIRE FORM

A00418

DIMENSIONS			
ELEMENT LENGTH		SPACINGS	
H1	54.75	D1	13.00
H2	51.00	D2	12.25
H3	47.50	D3	11.40
H4	44.25	D4	10.60
H5	41.30	D5	10.00
H6	38.50	D6	9.25
H7	36.00	D7	8.75
H8	33.50	D8	8.10
H9	31.25	D9	7.40
H10	29.20	D10	3.00
H11	7.00	D11	1.80
H12	6.50	D12	1.70
H13	5.75	D13	1.50
H14	5.25	D14	1.30
H15	4.60	D15	1.20
H16	4.10	D16	1.10
H17	3.75	D17	1.00
H18	3.40	D18	0.90
H19	3.00	D19	0.80
H20	2.80	D20	0.70
H21	2.50		

TEMPORARY SKETCH

BLONDER-TONGUE (VHF-UHF)
MODEL RANGER / 10

DATE 1-20-66 APPROVED

DRAWN R.P SCALE ~ 1:20

MATERIAL NOTES 1 INCH TWIN BOOM
15.5-INCH SHORTING STUB

JFD ELECTRONICS CORP.
ANTENNA LABORATORY

OGILVIE PRESS, INC., BROOKLYN 17, N. Y. ULTRAVEL NO. 490M

X13
55-cd

UNITED STATES DISTRICT COURT
NORTHERN DISTRICT OF ILLINOIS
BEFORE JUDGE HOFFMAN

DEFENDANT EX. NO. _____

DOROTHY L. BRACKENBURY
OFFICIAL COURT REPORTER

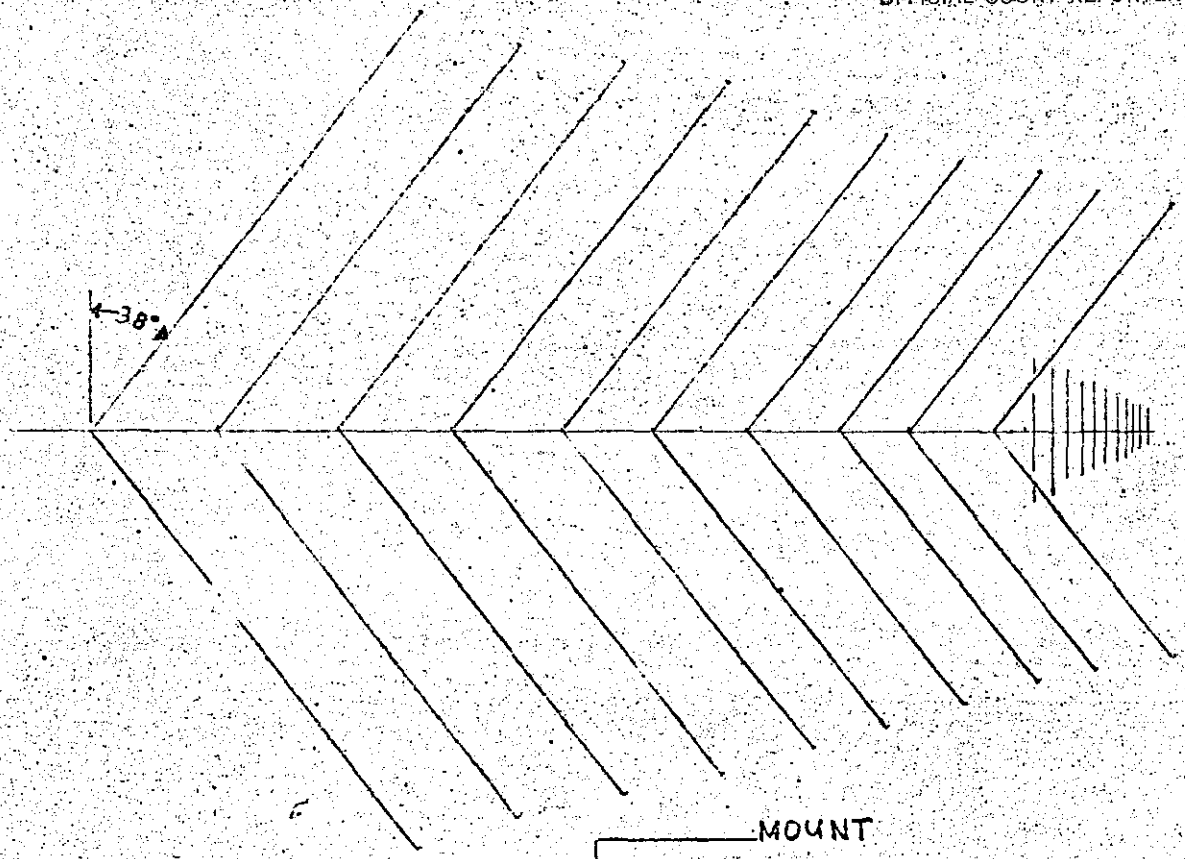

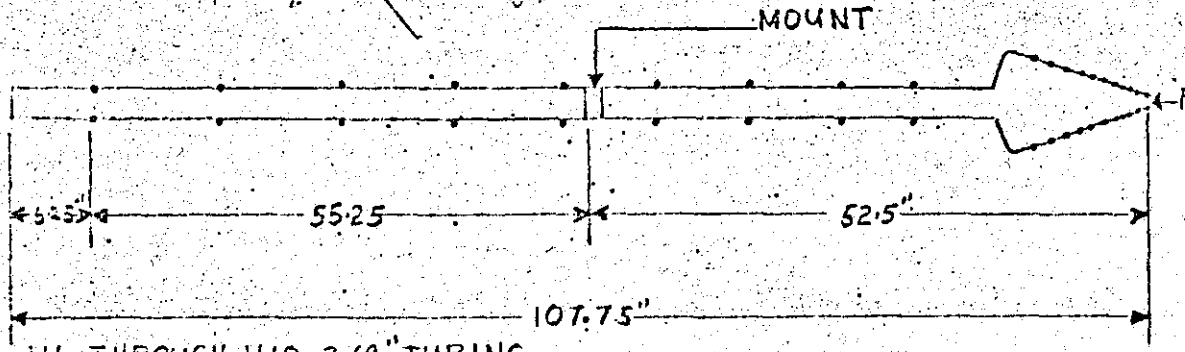

H1 THROUGH H10 3/8" TUBING
H11 THROUGH H21 WIRE FORM

A00421

DIMENSIONS					
ELEMENT LENGTH		τ	SPACINGS		
H1	54.75	.930	D1	13.00	.943
H2	51.00	.930	D2	12.25	.930
H3	47.50	.930	D3	11.40	.930
H4	44.25	.932	D4	10.60	.943
H5	41.30	.933	D5	10.00	.925
H6	38.50	.935	D6	9.25	.948
H7	36.00	.930	D7	8.75	.928
H8	33.50	.933	D8	8.10	.914
H9	31.25	.933	D9	7.40	
H10	29.20		D10	3.00	
H11	7.00	.929	D11	1.80	.945
H12	6.50	.884	D12	1.70	.882
H13	5.75	.913	D13	1.50	.866
H14	5.25	.877	D14	1.30	.923
H15	4.60	.890	D15	1.20	.918
H16	4.10	.915	D16	1.10	.905
H17	3.75	.907	D17	1.00	.900
H18	3.40	.884	D18	0.90	.889
H19	3.00	.934	D19	0.80	.875
H20	2.80	.893	D20	0.70	
H21	2.50				

MATERIAL NOTES: 1 INCH TWIN BOOM

15.5-INCH SHORTING STUB

TEMPORARY SKETCH

BLONDER-TONGUE

MODEL RANGER/10 (VHF-UHF)

DATE 1-20-69 APPROVED

DRAWN R.P SCALE ~ 1:20

JFD ELECTRONICS CORP.
ANTENNA LABORATORY

A00416

UNITED STATES DISTRICT COURT
NORTHERN DISTRICT OF ILLINOIS
BEFORE JUDGE HOFFMAN

DEFENDANT EX. NO. _____

DOROTHY L. BRACKENBURY
OFFICIAL COURT REPORTER

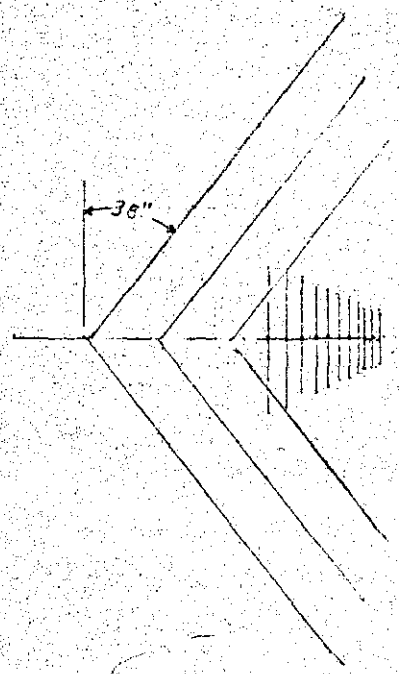

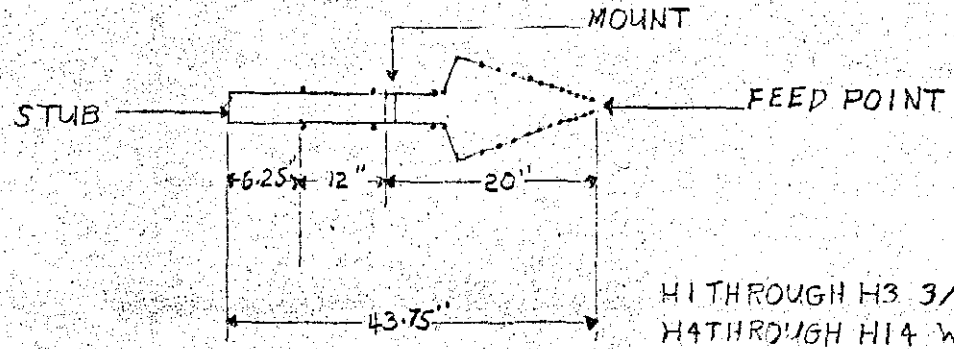

A00416

H1 THROUGH H3 3/8" TUBING
H4 THROUGH H14 WIRE FORM

DIMENSIONS			
	ELEMENT LENGTH		SPACINGS
H1	54.56	D1	8.75
H2	42.75	D2	7.00
H3	33.25	D3	3.00
H4	7.75	D4	1.80
H5	6.90	D5	1.70
H6	6.25	D6	1.50
H7	5.55	D7	1.30
H8	5.00	D8	1.20
H9	4.50	D9	1.10
H10	4.20	D10	1.00
H11	3.69	D11	0.90
H12	3.30	D12	0.80
H13	3.20	D13	0.70
H14	2.90		

MATERIAL NOTES	1-INCH TWIN BOOM 15.5-INCH SHORTING STUB

TEMPORARY SKETCH

BLONDER – TONGUE

MODEL RANGER/3 (VHF-UHF)

DATE 1-20-66 APPROVED LCA

DRAWN R.P. SCALE ~ 1:20

JFD ELECTRONICS CORP.
ANTENNA LABORATORY

OGILVIE PRESS, INC., BROOKLYN 17, N. Y. ULTRAVEL NO. 480M

UNITED STATES DISTRICT COURT
NORTHERN DISTRICT OF ILLINOIS
BEFORE JUDGE HOFFMAN

DEFENDANT EX. NO. _____
DOROTHY L. BRACKENBURY
OFFICIAL COURT REPORTER

VHF

UHF

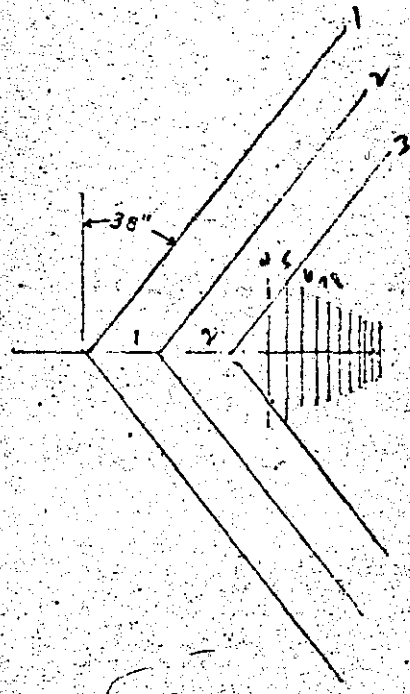

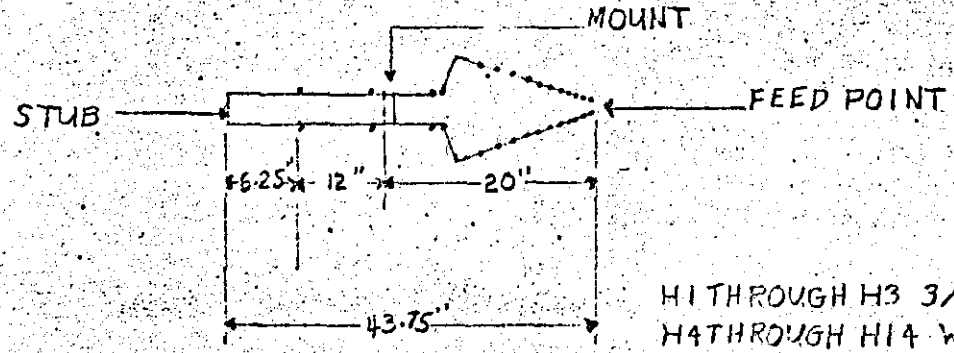

H1 THROUGH H3 3/8" TUBING
H4 THROUGH H14 WIRE FORM

A00419

MATERIAL NOTES 1-INCH TWIN BOOM
15.5-INCH SHORTING STUB

DIMENSIONS

	ELEMENT LENGTH	τ		SPACINGS	τ
H1	54.56	.783	D1	8.75	.800
H2	42.75	.778	D2	7.00	.778
H3	33.25		D3	3.00	
H4	7.75		D4	1.80	.945
H5	6.90	.76	D5	1.70	.882
H6	6.25	.906	D6	1.50	.866
H7	5.55	.889	D7	1.30	.923
H8	5.00	.90	D8	1.20	.918
H9	4.50	.90	D9	1.10	.908
H10	4.20	.935	D10	1.00	.900
H11	3.69	.894	D11	0.90	.889
H12	3.30	.970	D12	0.80	.875
H13	3.20	.906	D13	0.70	
H14	2.90				

TEMPORARY SKETCH
BLENDER – TONGUE
MODEL RANGER/3 (VHF-UHF)
DATE 1-20-66 APPROVED LEA
DRAWN R.P. SCALE ~ 1:20

JFD ELECTRONICS CORP.
ANTENNA LABORATORY

UNITED STATES DISTRICT COURT
NORTHERN DISTRICT OF ILLINOIS
BEFORE JUDGE HOFFMAN

DEFENDANT EX. NO. _____
DOROTHY L. BRACKENBURY
OFFICIAL COURT REPORTER

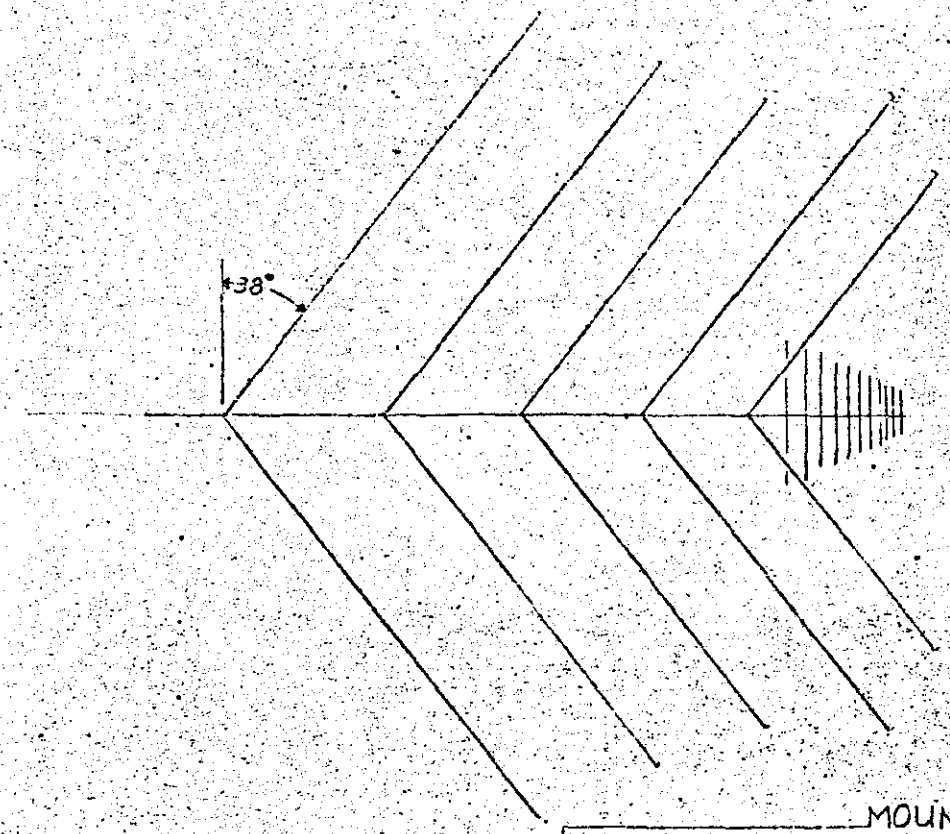

H1 THROUGH H5 3/8" TUBING
H6 THROUGH H16 WIRE FORM

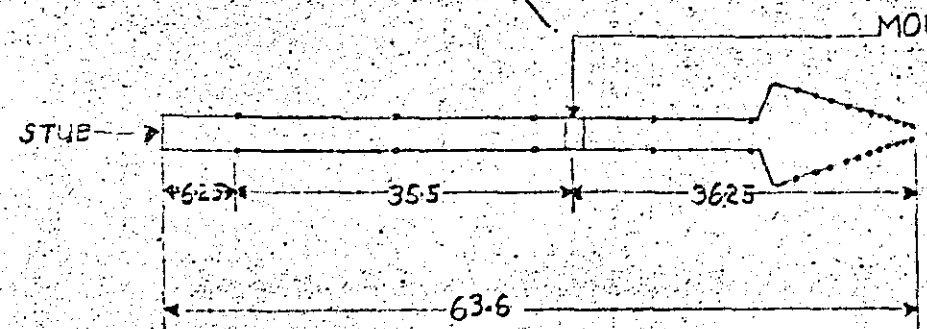

A00420

DIMENSIONS					
ELEMENT	LENGTH	τ	SPACINGS		
H1	52.50	.876	D1	16.45	.879
H2	46.00	.875	D2	14.45	.865
H3	40.25	.869	D3	12.50	.88
H4	35.00	.878	D4	11.00	
H5	30.75		D5	3.00	
H6	7.00	.938	D6	1.80	.945
H7	6.50	.985	D7	1.70	.887
H8	5.75	.913	D8	1.50	.866
H9	5.25	.876	D9	1.30	.933
H10	4.60	.892	D10	1.20	.918
H11	4.10	.914	D11	1.10	.908
H12	3.75	.908	D12	1.00	.900
H13	3.40	.883	D13	0.90	.889
H14	3.00	.933	D14	0.80	.875
H15	2.80	.893	D15	0.70	
H16	2.50				

MATERIAL NOTES
1 INCH TWIN BOOM
15.5-1 INCH SHORTING STUB

TEMPORARY SKETCH

MODEL BLONDER-TONGUE RANGER / 5 (VHF-UHF)

DATE 1-20-66 APPROVED LEJ

DRAWN R.P SCALE ~ 1:20

JFD ELECTRONICS CORP.
ANTENNA LABORATORY

OGILVIE PRESS, INC., BROOKLYN 17, N. Y. ULTRAVEL NO. 4B0N

UNITED STATES DISTRICT COURT
NORTHERN DISTRICT OF ILLINOIS
BEFORE JUDGE HOFFMAN

DEFENDANT EX. NO._____

DOROTHY L. BRACKENBURY
OFFICIAL COURT REPORTER

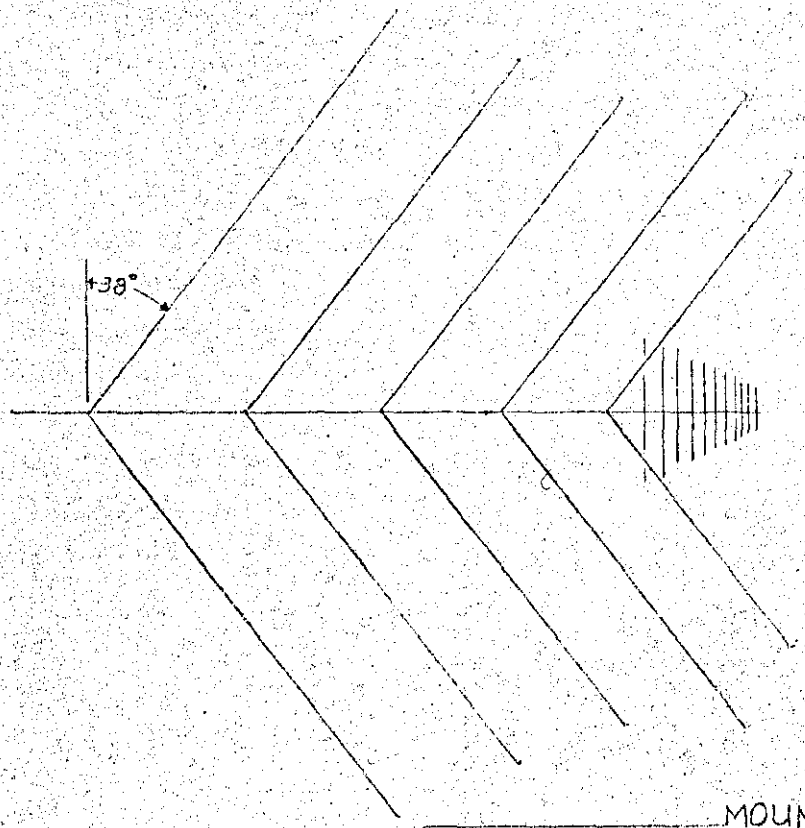

H1 THROUGH H5 3/8" TUBING
H6 THROUGH H16 WIRE FORM

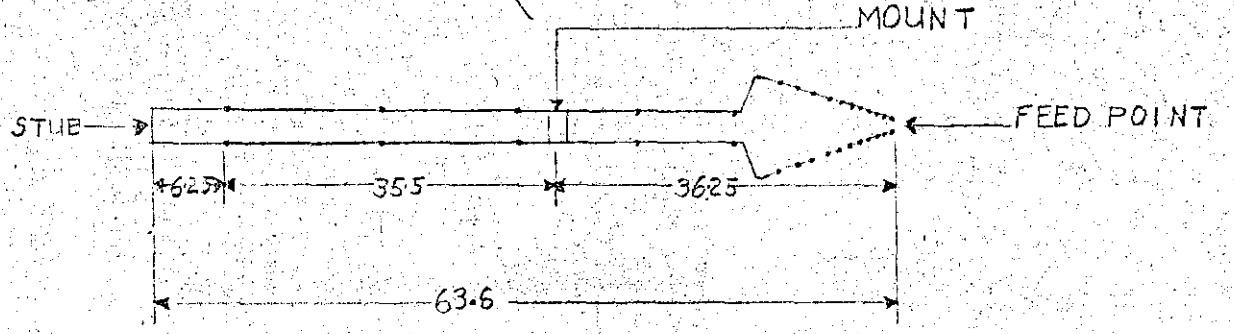

DIMENSIONS			
ELEMENT LENGTH		SPACINGS	
H1	52.50	D1	16.45
H2	46.00	D2	14.45
H3	40.25	D3	12.50
H4	35.00	D4	11.00
H5	30.75	D5	3.00
H6	7.00	D6	1.80
H7	6.50	D7	1.70
H8	5.75	D8	1.50
H9	5.25	D9	1.30
H10	4.60	D10	1.20
H11	4.10	D11	1.10
H12	3.75	D12	1.00
H13	3.40	D13	0.90
H14	3.00	D14	0.80
H15	2.80	D15	0.70
H16	2.50		

A00417

MATERIAL NOTES 1 INCH TWIN BOOM
15.5-INCH SHORTING STUB

TEMPORARY SKETCH

BLONDER-TONGUE
MODEL RANGER / 5 (VHF-UHF)

DATE 1-20-66 APPROVED LCJ

DRAWN R.D SCALE ~1:20

JFD ELECTRONICS CORP.
ANTENNA LABORATORY

OGILVIE PRESS, INC., BROOKLYN 12, N. Y. ULTRAVEL NO. 490M

ANTENNA LABORATORY

Report No. 66-11

WAVE PROPAGATION ON SMOOTH AND PERIODIC STRUCTURES AND APPLICATIONS TO ANTENNA DESIGN

NASA Grant No. NGR 14-005-043

Prepared by

ANTENNA LABORATORY
ELECTRICAL ENGINEERING DEPARTMENT
UNIVERSITY OF ILLINOIS
URBANA, ILLINOIS

P. E. MAYES, Editor

For

GODDARD SPACE FLIGHT CENTER
GREENBELT, MARYLAND

DEPARTMENT OF ELECTRICAL ENGINEERING
ENGINEERING EXPERIMENT STATION
UNIVERSITY OF ILLINOIS
URBANA, ILLINOIS

Antenna Laboratory Report No. 66-11

Wave Propagation on Smooth and Periodic Structures and Applications to Antenna Design

NASA Grant No. NGR 14-005-043

Prepared by

Antenna Laboratory
Electrical Engineering Department
University of Illinois
Urbana, Illinois

P. E. Mayes, Editor

for

Goddard Space Flight Center
Greenbelt, Maryland

PREFACE

In January, 1964 an Applications Forum on Antenna Research was held at the University of Illinois. A group of seven speakers from other university and industrial laboratories and five professors from the University of Illinois Antenna Laboratory presented four days of comprehensive lectures on four phases of modern antenna research. One of the principal topics was that of frequency independent antennas.

Recent research had indicated that dispersion data for periodic structures can be very useful in the analysis and design of frequency independent antennas. An introductory paper on the relationship between the near- and far-field behavior of various types of waves was scheduled for early presentation in the Forum program and the relationships established therein were used in the discussion of frequency independent antennas by several succeeding speakers. It became apparent in the discussion periods which followed these papers that most of the Forum participants had limited background in methods of calculating, measuring and presenting dispersion data for various waveguiding structures and relationship to radiation characteristics of the structures. At the request of several of the attendees, an impromptu informal evening session was scheduled to explore these background topics in greater detail. Almost half of the 70 Forum participants came to the special session and a lively discussion continued late into the evening.

It was felt by several of the Forum speakers and participants that the events described above indicated a basic deficiency in the background of many engineers presently involved in antenna research and development. The need for further information and study in this area was expressed by some who have been in the antenna field for many years. As an outgrowth of these discussions the NASA Grant No. NGR 14-005-043 was awarded to the University of Illinois Antenna Laboratory for the preparation of this survey report. It was originally intended only to collect and review presently available data in the area of dispersion characteristics of both smooth and periodic structures which may be applicable to antenna design. However, in an effort to better connect the simple examples to the present use in research, some additional computations and derivations

were undertaken which have both expanded and delayed the report. Unfortunately, the task of connecting classical and recent problems proved to be too great to complete within the scope of the grant. Thus, although several new results were obtained which are presented herein, there are still questions which remain at least partially unanswered. Nevertheless, it is hoped that this report will prove useful as an introduction to the wave analysis of antennas and will help practicing engineers to better understand the current literature in this area.

ACKNOWLEDGMENT

V. H. Rumsey and R. H. DuHamel merit special credit as the pioneers in frequency independent antenna research. The results of co-workers in the Antenna Laboratory, particularly Professors Deschamps, Mittra, Dyson and Klock and students Isbell, Carrel, Patton, Greiser, Hudock, Stephenson, Jones, Ingerson, Mikenas, Kuo and Yaminy is also gratefully acknowledged. The work described here has been supported by the U. S. Air Force, U. S. Navy Electronics Laboratory, U. S. Navy Bureau of Ships, and the National Aeronautics and Space Administration. Preparation of this special survey report was made possible by NASA Grant No. NGR 14-005-043. Part III is largely the work of K. E. Jones. J. W. Greiser and V. Mikenas contributed sections of Parts II and IV and P. G. Ingerson supplied several calculated dispersion plots for Part II.

TABLE OF CONTENTS

LIST OF ILLUSTRATIONS

List of Illustrations continued -

List of Illustrations continued -

PART I

RELATION OF ANTENNA PATTERNS TO DISPERSION DIAGRAMS

1.1 Introduction

In numerous antenna applications values of gain and/or directivity are required which cannot be achieved conveniently through the use of a single, simple, radiating element, such as a dipole. In these instances, it is customary engineering practice to employ a number of simple elements in an antenna array. Those elements which are connected to a transmission line are called "driven elements." Additional elements may also be employed to increase the gain, even though not connected to the transmission line. These latter elements are commonly called "parasites." Various combinations of driven and parasitic elements may be used, depending upon the application. When several of the elements are driven, the problems associated with the design of a feeder network become more involved.

The analysis of the directional characteristics of an antenna array depends primarily upon the determination of the relative phase and amplitude of the currents in the various elements. The problem of determining these excitation coefficients theoretically is complicated by the coupling between each element of the array and every other element of the array. Because of this, the theoretical analysis of antenna arrays has been largely limited to arrays of few elements. However, in some cases primarily involving linear arrays, it is possible to employ a traveling wave concept, both in the determination of the array excitation and for the computation of the radiation patterns. This approach is very useful when the number of elements in the array is more than a few. The present investigation will deal with this approach to antenna array analysis.

When several elements in a linear array are driven by successive connection to the same feeder, the traveling wave concept can be applied in both parts of the analysis problem, that is, to the determination of the excitation coefficients as well as the directional characteristics of the array. In Part I we shall direct our attention primarily to the problem of the radiation patterns, and consider the calculation of array excitation in Part II. In Part III, the relationship between periodic and log-periodic structures is considered with emphasis on open structures. Several applications to antenna design are discussed in Part IV.

Therefore, for the present we shall assume that the pertinent characteristics of the dominant traveling wave on the antenna array have already been determined and we shall consider at this time the determination of the directional characteristics. Each traveling wave on the array is characterized by a (complex) propagation constant, $\gamma = \alpha + j\beta$. In most instances the array will behave like a dispersive medium whereby the phase constant β will not be a linear function of frequency. Plots of β versus radian frequency ω (or free-space wave number $k = \frac{\omega}{c}$ where c is intrinsic phase velocity of free-space) are then needed for each wave. The dispersion curves for periodic structures are often called Brillouin diagrams. Frequency bands where γ is complex are of great interest in antenna applications of periodic structures. Hence, for antenna work plots of α versus k should be added to the conventional k-β diagram. When several traveling waves exist simultaneously, the complex coefficients giving relative amplitude and phase of these several waves are also needed. However, as we shall later show, the analysis in terms of a single wave is many times sufficient.

1.2 Basic Electromagnetic Field Equations

The electromagnetic field produced in a homogeneous medium of infinite extent by an arbitrary distribution of electric and/or magnetic currents is obtained by solving the inhomogeneous Maxwell's equations.

$$\text{curl } \underset{\sim}{E} = - \mathcal{Z} \underset{\sim}{H} - \underset{\sim}{\mathcal{K}} \tag{1}$$

$$\text{curl } \underset{\sim}{H} = \mathcal{Y} E + \mathcal{J} \tag{2}$$

where $\underset{\sim}{E}$ and $\underset{\sim}{H}$ are complex fields representing the electric and magnetic vectors, respectively; $\mathcal{J}$ and $\underset{\sim}{\mathcal{K}}$ are complex vector functions describing the density of "idealized" electric and magnetic current distributions in the homogeneous space; and $\mathcal{Y}$ and $\mathcal{Z}$ are complex numbers which describe the medium in the sinusoidal steady-state theory.

$$\mathcal{Y} = \sigma + j\omega\epsilon \tag{3}$$

$$\mathcal{Z} = \tau + j\omega\mu \tag{4}$$

where σ, τ, ϵ and μ are the electric conductivity, the magnetic conductivity, the capacitivity and the inductivity of the medium, respectively, and ω is the radian frequency of all harmonic oscillations in the system.

The solution of Equations (1) and (2) which is subject to a "radiation condition" at great distances from a source distribution of finite dimensions is usually expressed in terms of a pair of vector potential functions $\underset{\sim}{A}$ and $\underset{\sim}{F}$.

$$\underset{\sim}{A} = \frac{1}{4\pi} \int_{V_{\mathcal{J}}} \mathcal{J}\ (\underset{\sim}{r}') \ \frac{e^{-\gamma\ |\underset{\sim}{r}-\underset{\sim}{r}'|}}{|r-r'|}\ dv \tag{5}$$

$$\underset{\sim}{F} = -\ \frac{1}{4\pi} \int_{V_{\mathcal{K}}} \mathcal{K}\ (\underset{\sim}{r}') \ \frac{e^{-\gamma\ |\underset{\sim}{r}-\underset{\sim}{r}'|}}{|\underset{\sim}{r}-\underset{\sim}{r}'|}\ dv \tag{6}$$

where $\underset{\sim}{r}$ and $\underset{\sim}{r}'$ are position vectors from the origin of a coordinate system to an observation point P and a source point P', respectively, as shown in Figure 1. Note that $|\underset{\sim}{r} - \underset{\sim}{r}'|$, which denotes the magnitude of the difference vector, is the distance from the source point P' to the observation point P. The parameter γ in the exponent is the intrinsic propagation constant of the medium.

$$\gamma = \sqrt{\mathcal{Z}\ \mathcal{Y}} \tag{7}$$

In most cases the medium is assumed to be free-space and

$$\gamma = j\omega \sqrt{\mu_o \epsilon_o} \qquad = j\ k \tag{8}$$

The integrals (5) and (6) are evaluated over the source regions, $V_{\mathcal{J}}$ denoting the volume occupied by electric currents and $V_{\mathcal{K}}$ that occupied by magnetic currents. Once the vector potentials $\underset{\sim}{A}$ and $\underset{\sim}{F}$ are found, the electric and magnetic vectors are calculated from

$$\underset{\sim}{E} = \frac{1}{\mathcal{Y}} (\text{curl curl } \underset{\sim}{A} - \mathcal{J}) + \text{curl } \underset{\sim}{F} \tag{9}$$

$$\underset{\sim}{H} = \text{curl } \underset{\sim}{A} - \frac{1}{\mathcal{Z}} \ (\text{curl curl } \underset{\sim}{F} + \mathcal{K}) \tag{10}$$

The derivation of these solutions of Maxwell's equations can be found in several texts[1,2] on electromagnetic theory and therefore, will not be discussed further here.

1.3 The Far-Zone Approximations (the Distant Field)

The radiation pattern of a transmitting antenna represents the directional distribution of power at large distances away from the antenna. That is, the minimum distance from any source point to an observation point for radiation

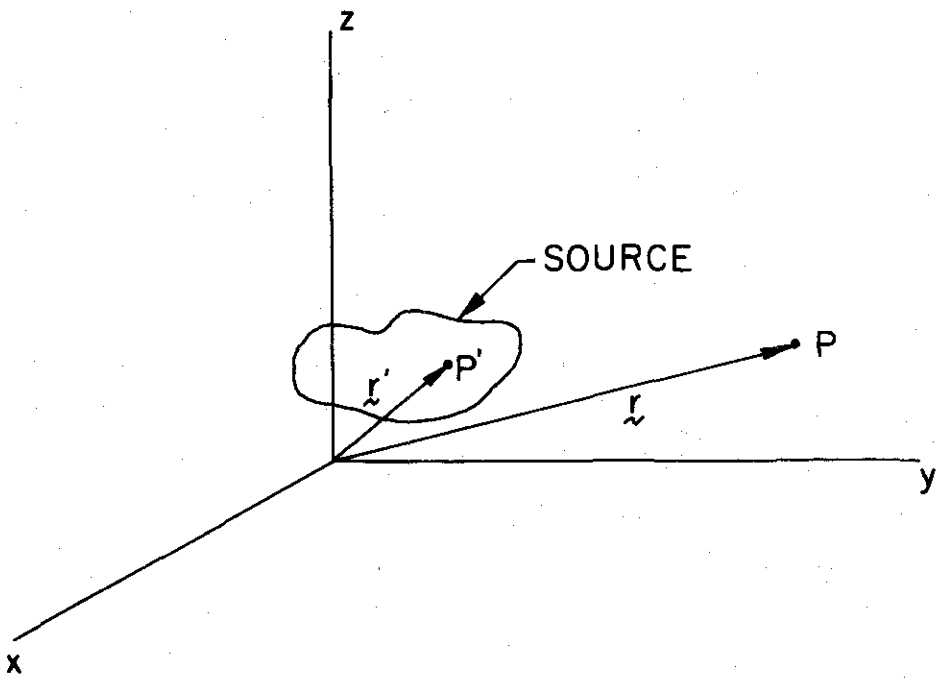

Figure 1. Coordinate system used to locate observation and source points in problem of calculating field due to a given source.

pattern measurements is much greater than the largest dimension of the antenna and also much greater than the wavelength. In this case it is possible to greatly simplify the formulas for calculation of the field.

Consider the evaluation of the integral (5) for the vector potential $\underset{\sim}{A}$ due to an electric current source $\mathcal{J}$. Using cartesian coordinates

$$\underset{\sim}{A}(x,y,z) = \frac{1}{4\pi} \iiint_{\text{source}} \mathcal{J}(x',y',z') \frac{e^{-jkr_{pp'}}}{r_{pp'}} \, dx' \, dy' \, dz' \tag{11}$$

where

$$r_{pp'} = [(x-x')^2 + (y-y')^2 + (z-z')^2]^{1/2} = |\underset{\sim}{r}-\underset{\sim}{r}'|$$

x',y',z' denotes point of integration (source point)

x,y,z denotes point of observation

Let r be the distance from the origin of the coordinate system to the point of observation, and let r' be the distance to the source point as shown in Figure 2. If the origin is placed in the vicinity of the source, then for observation points such that $r \gg r'$, we can replace $r_{pp'}$ by r in the denominator of the superposition integral (11). This is too gross an approximation in the phase factor, however. When $r \gg r'$, $\overline{PP'}$ and $\overline{OP}$ are nearly parallel, whence the difference in their lengths is simply the projection of $\overline{OP'}$ on $\overline{OP}$. Let $\hat{\underset{\sim}{r}}$ be a unit vector in the direction from the origin O to the observation point P and r' be a position vector from the origin O to the source point P'. Then

$$r_{pp'} = r - \hat{\underset{\sim}{r}} \cdot \underset{\sim}{r}' \tag{12}$$

The vector potential in the distant field is approximately given by

$$\underset{\sim}{A}(x,y,z) \sim \frac{e^{-jkr}}{4\pi r} \iiint_{\text{source}} \mathcal{J}(x',y',z') \, e^{jk(\hat{\underset{\sim}{r}} \cdot \underset{\sim}{r}')} \, dx' \, dy' \, dz' \tag{13}$$

Radiation patterns are conventionally measured as functions of the spherical coordinates θ,ϕ (defined in Figure 3) with the radial variable r held constant. Hence, it is convenient to express the vector potential in terms of the spherical coordinates. Hence, we introduce the spherical coordinates to locate the observation points while retaining the cartesian variables for source points to simplify the integration along linear paths. This

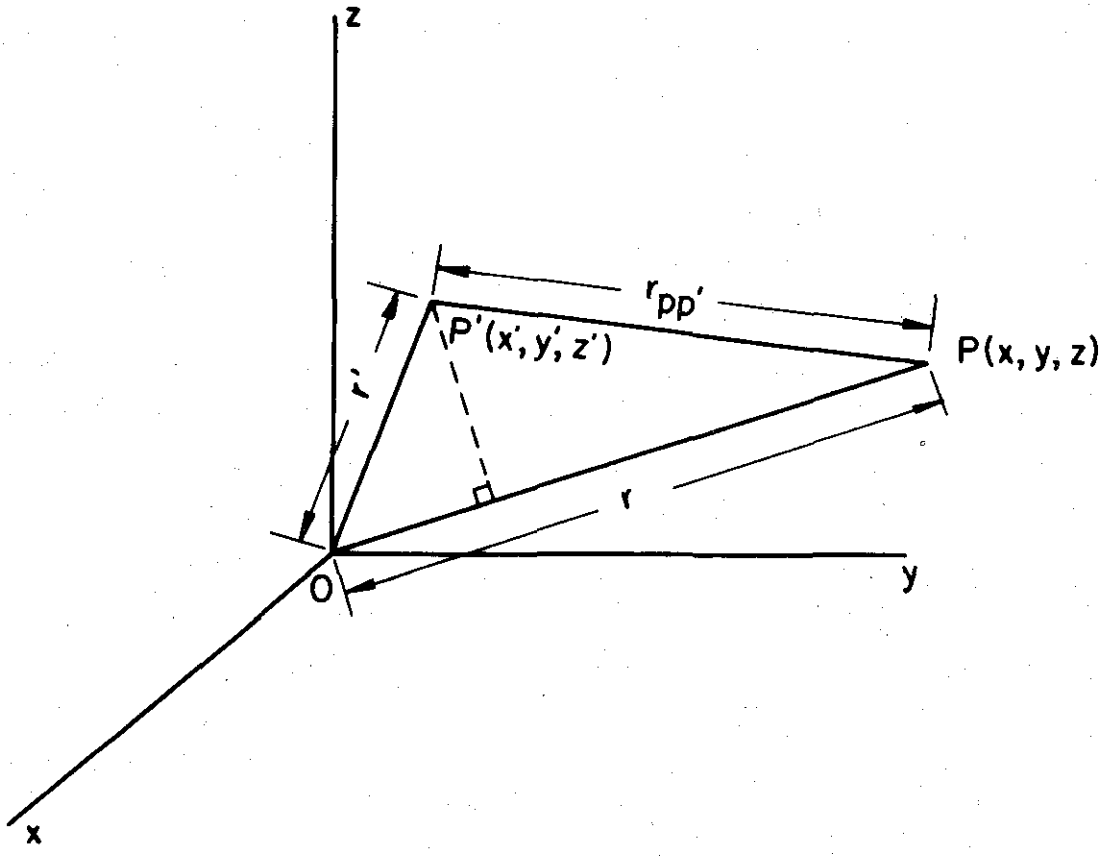

Figure 2. The distances involved in the far-zone approximations.

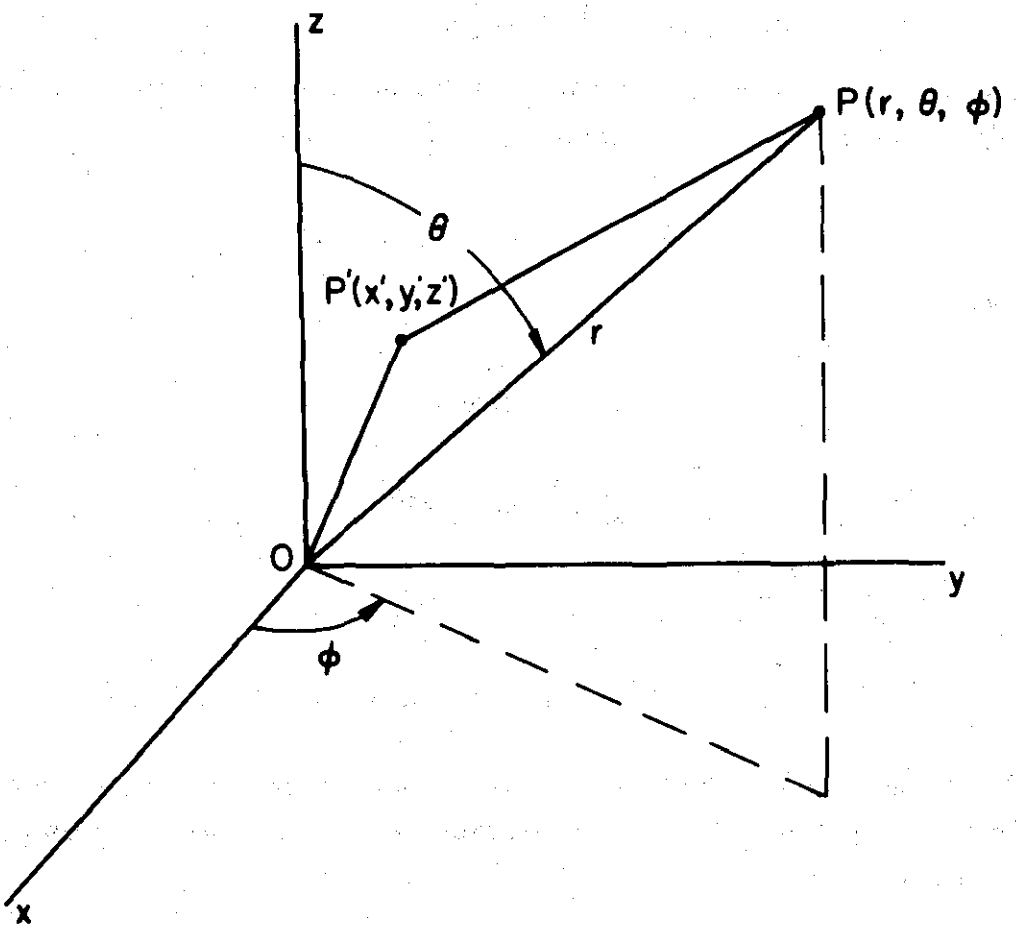

Figure 3. Spherical coordinates of the point of observation P.

is accomplished by writing

$$\hat{\underset{\sim}{r}} = \hat{\underset{\sim}{x}} \sin\theta \cos\phi + \hat{\underset{\sim}{y}} \sin\theta \sin\phi + \hat{\underset{\sim}{z}} \cos\theta \tag{14}$$

$$\hat{\underset{\sim}{r}}' = \hat{\underset{\sim}{x}}\, x' + \hat{\underset{\sim}{y}}\, y' + \hat{\underset{\sim}{z}}\, z' \tag{15}$$

Equation (13) can now be factored into two terms: one a scalar function of r only, the other a vector function of θ and ϕ only.

$$\underset{\sim}{A} \sim g(r)\, \underset{\sim}{f}(\theta,\phi) \tag{16}$$

where

$$g(r) \equiv \frac{e^{-jkr}}{4\pi r} \tag{17}$$

$$\underset{\sim}{f}(\theta,\phi) \equiv \iiint_{\text{source}} \underset{\sim}{J}(x',y',z')\, e^{jk(\hat{\underset{\sim}{r}} \cdot \underset{\sim}{r}')}\, dx'\, dy'\, dz' \tag{18}$$

and

$$\hat{\underset{\sim}{r}} \cdot \underset{\sim}{r}' = x' \sin\theta \cos\phi + y' \sin\theta \sin\phi + z' \cos\theta$$

This factorization simplifies considerably the evaluation of the distant fields. Performing the curl operation of (10) in spherical coordinates, we obtain

$$\underset{\sim}{H} \sim \frac{1}{4\pi r \sin\theta}\, g(r) \left\{ \hat{\underset{\sim}{r}} \left[\frac{\partial}{\partial\theta} (\sin\theta\, f_\phi) - \frac{\partial f_\theta}{\partial\phi} \right] + r\, \hat{\underset{\sim}{\theta}} \left[\frac{1}{r} \frac{\partial f_r}{\partial\phi} + j\beta \sin\theta\, f_\phi \right] - r \sin\theta\, \hat{\underset{\sim}{\phi}} \left[j\beta\, f_\theta + \frac{1}{r} \frac{\partial f_r}{\partial\theta} \right] \right\} \tag{19}$$

where

$$f_r = \hat{\underset{\sim}{r}} \cdot \underset{\sim}{f} \qquad f_\theta = \hat{\underset{\sim}{\theta}} \cdot \underset{\sim}{f} \qquad f_\phi = \hat{\underset{\sim}{\phi}} \cdot \underset{\sim}{f}$$

Note that the r-component varies as $1/r^2$, whereas parts of the θ- and ϕ-components vary as $1/r$. For large r, therefore,

$$\underset{\sim}{H} \sim \frac{j\beta\, g(r)}{4\pi} \left[\underset{\sim}{\theta}\, f_\phi - \underset{\sim}{\phi}\, f_\theta \right] \tag{20}$$

From the Maxwell equation curl $\underset{\sim}{H} = y\underset{\sim}{E}$, we find that

$$\underset{\sim}{E} \sim \frac{\eta\, g(r)}{4\pi r} \left\{ -\hat{\underset{\sim}{r}} \left[\frac{\partial}{\partial\theta} (\sin\theta\, f_\theta) + \frac{2f_\phi}{\partial\phi} \right] \right.$$

$$\left. -j\beta r\, \hat{\underset{\sim}{\theta}}\, f_\theta - j\beta r\, \hat{\underset{\sim}{\phi}}\, f_\phi \right. \tag{21}$$

where $\eta = \sqrt{z/y}$ is the intrinsic impedance of the medium. In the distant field, therefore, neglecting $1/r^2$ terms, we have

$$\underset{\sim}{E} \sim \frac{-j\beta\,\eta}{4\pi}\, g(r) \left[\hat{\underset{\sim}{\theta}}\, f_\theta + \hat{\underset{\sim}{\phi}}\, f_\phi \right] \tag{22}$$

It is now apparent that the distant fields are readily found once the spherical components of the vector $\underset{\sim}{f}$ have been determined by evaluating the integral given in Equation (18). The integration is likely to be done in cartesian coordinates, but it is possible to transform the cartesian components of $\underset{\sim}{f}$ to spherical components by using

$$f_\theta = f_x \cos\theta \cos\phi + f_y \cos\theta \sin\phi - f_z \sin\theta \tag{23}$$

$$f_\phi = -f_x \sin\phi + f_y \cos\phi \tag{24}$$

Several properties of the distant field are readily discovered by inspection of Equations (20) and (22). Note that there is no radial component of either electric or magnetic vector. Also, since

$$\underset{\sim}{H} = \sqrt{\underset{\sim}{H} \cdot \underset{\sim}{H}^*} = \frac{\beta\, |g(r)|}{4\pi} \sqrt{|f_\phi|^2 + |f_\theta|^2} \tag{25}$$

$$\underset{\sim}{E} = \sqrt{\underset{\sim}{E} \cdot \underset{\sim}{E}^*} = \frac{\eta\,\beta\, |g(r)|}{4\pi} \sqrt{|f_\theta|^2 + |f_\phi|^2} \tag{26}$$

the ratio of magnitudes of the electric and magnetic vectors is the intrinsic impedance of the medium.

1.4 Periodic Structures

The results of Sections 1 and 2 would yield the radiation pattern of any antenna providing the idealized current distribution for the antenna is known. Determination of the current distribution is, therefore, the basic problem of pattern calculations and is by far the most difficult

part. Only in a very few cases is it possible to solve Maxwell's equations subject to the boundary conditions suitable to describe a specific antenna configuration and excitation. When such a complete solution is possible, the current distribution can be found by evaluating the tangential magnetic vector on the conducting surfaces. For the most part, however, practical antennas do not closely conform to a shape for which Maxwell's equations can be solved rigorously. It is, therefore, customary to devise various approximations to the current distribution by extrapolating from the few known solutions. For example, the current along a linear dipole is taken to be given by a trigonometric function since this can be shown to be the case for a thin prolate spheroid.

Now it would appear, since the current distribution on such a simple shape as a dipole is so difficult to obtain, that conductors with bends and corners or other discontinuities would present a hopeless task. This would indeed be unfortunate since many very useful antennas may contain all manner of geometric designs. Fortunately, there is a class of shapes which can be geometrically complex and yet may have rather simple current distributions - the class of periodic structures.

A uniform periodic structure is composed of a number of identical cells as depicted in a general way in Figure 4. The width of each cell is W and the length "a" of each cell is called the period. Translation of an infinite periodic structure along its axis through a distance equal to the period does not change the structure.

One approach to the analysis of such periodic structures would be to solve for the fields of a single isolated cell and then superpose these to find the fields of the entire structure. Unfortunately, there is usually considerable coupling from one cell to the next so that the current distribution of a cell in the environment of its neighbors is considerably different from that of the isolated cell. For simple geometries such as dipoles it may be possible to account for this coupling and find the current distribution and input impedance of each element in the presence of a few other elements. However, when the number of elements or cells becomes large, such an approach is hopelessly complicated. In this case it may be advantageous to consider a periodic structure to be infinite in extent and look for the modes of propagation which are characteristic of the structure. It then may be possible to express the current distribution along a finite periodic structure in terms of a limited number of

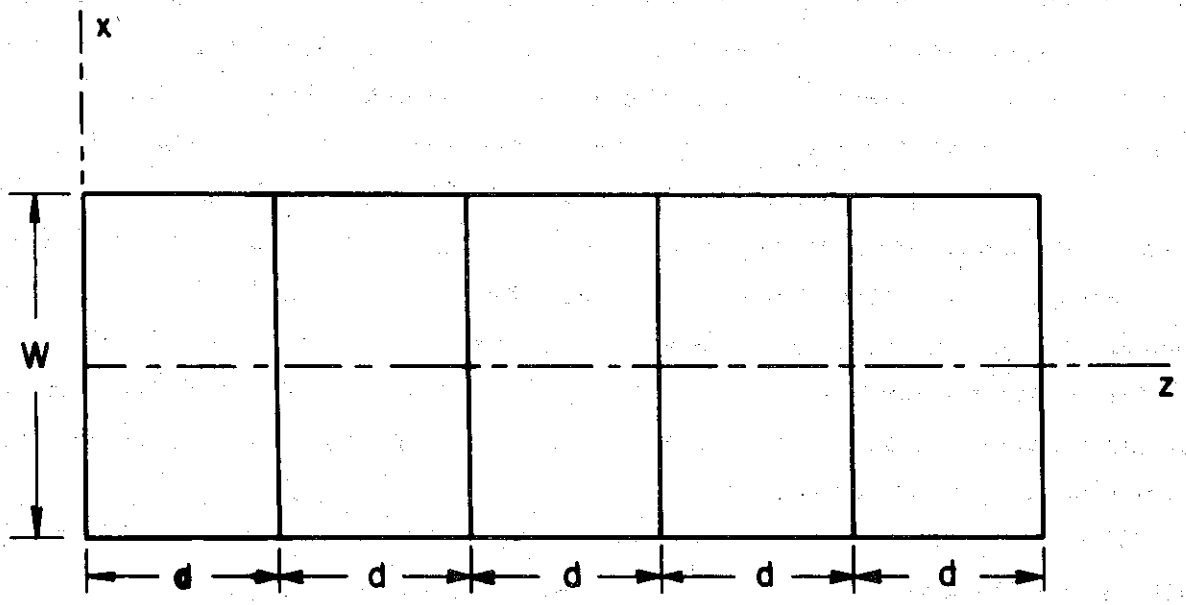

Figure 4. A periodic structure with five cells.

modes. The radiation patterns which correspond to modal distributions of current are readily calculated. In certain frequency ranges a single mode may be adequate to describe the current and the modal pattern will apply directly. In other cases, it may be necessary to use a combination of modes to represent the current. However, if the complex coefficients of the modal constituents of the current can be found, the pattern can once again be determined by superposition of the patterns of the modal currents. Although representation of the current distributions on finite, open structures completely in terms of modal components cannot be justified rigorously, the results of this approach have proved accurate enough to be very useful in a number of cases and the great simplification which this approach affords certainly justifies its use as an aid to engineering design.

One of the most important classes of practical antennas is that of frequency-independent antennas.[3] Many of these are unidirectional log-periodic antennas which can be considered to be nonuniform periodic structures.[4] If the rate of taper is low enough, the performance of a log-periodic structure can be inferred from the performance of the uniformly periodic counterpart. Thus, the analysis of periodic structures is further motivated by the need for better understanding of frequency-independent antennas.

The basis for analysis of periodic structures is a theorem of the French mathematician Floquet which may be stated as follows:[5]

> For a given mode of propagation the fields at one cross section of a periodic structure differ from those one period away only by a complex constant.

If z represents the axial coordinate and h(z) represents a component of the field, then Floquet's theorem states that

$$h(z+d) = u\, h(z) \tag{27}$$

where u is a complex constant. Now suppose we take

$$h(z) = e^{-\gamma z}\, p(z) \tag{28}$$

then Equation (27) gives

$$h(z+d) = e^{-\gamma(z+d)}\, p(z+d) = e^{-\gamma d}\, e^{-\gamma z}\, p(z+d) = u\, e^{-\gamma z}\, p(z) \tag{29}$$

which can be satisfied with

$$u = e^{-\gamma d} \tag{30}$$

and

$$p(z+d) = p(z) \tag{31}$$

Equation (31) requires that p(z) be a periodic function and so can be expanded in a Fourier series.

$$p(z) = \sum_{n=-\infty}^{\infty} C_n e^{-j2\frac{n\pi z}{d}} \tag{32}$$

and the fields can thus be written in the form

$$h(z) = e^{-\gamma z} \sum_{n=-\infty}^{\infty} C_n e^{-j2\frac{n\pi z}{d}} = \sum_{n=-\infty}^{\infty} C_n e^{-(\gamma + j2\frac{n\pi}{d})z} \tag{33}$$

The wave given by the n = 0 term in this series is called the fundamental wave; the other terms are called space harmonics. Equation (33) shows that the propagation constant of the n^{th} space harmonic is given by

$$\gamma_n = \gamma + j2\frac{n\pi}{d} \tag{34}$$

Further consideration will be given to the space harmonics and how each contributes to pattern characteristics later. Next we shall use the Floquet property of the fields in a periodic structure to obtain radiation pattern equations.

1.5 Radiation Patterns of Periodic Structures

Let us suppose for the present that the current distribution along a finite periodic structure corresponds to a single mode on an infinite structure. Further clarification of how this may be achieved will be given later. If the periodic structure is planar and aligned in the xz-plane as shown in Figure 4, the current density vector $\mathcal{J}$ can be written in terms of only two components as

$$\mathcal{J}(x',y',z') = \hat{x}\, \mathcal{J}_x(x',y',z') + \hat{z}\, \mathcal{J}_z(x',y',z') \tag{35}$$

Furthermore, since the current is confined to the xz-plane, it is completely described by the surface current density $\mathcal{J}_s$, where

$$\mathcal{J}(x',y',z') = \mathcal{J}_s(x',z')\, \delta(y') \tag{36}*$$

---

*$\delta(y')$ is the delta distribution which has the integral property

$$\int_a^b f(y')\, \delta(y')\, dy' = f(0) \text{ if } a < y' < b$$
$$= \text{otherwise}$$

According to Floquet's theorem the current in the n^{th} cell is related to that in the zeroth cell by

$$\mathcal{J}_{sn}(x',z'+na) = \mathcal{J}_{so}(x',z')\, e^{-\gamma nd} \tag{37}$$

An expression for the complete current distribution across N cells can be written by adding expressions for the current in the individual cells

$$\mathcal{J}_{s}(x',z') = \sum_{n=0}^{N-1} \mathcal{J}_{sn}(x',z') \left[U\,(z'-nd) - U(z'-(n+1)d) \right] \tag{38}$$

where $\mathcal{J}_{sn}$ represents the current density in the n^{th} cell and $U(z'-z_o)$ is the unit step function defined by

$$\begin{aligned} U\,(z'-z_o) &= 1 \qquad & z' > z_o \\ &= 0 \qquad & z' < z_o \end{aligned} \tag{39}$$

Substituting (14), (15), (36) and (38) into (18) gives

$$\underset{\sim}{f}(\theta,\phi) = \int_{-W/2}^{W/2} \int_{o}^{Na} \sum_{n=0}^{N-1} \mathcal{J}_{sn}(x',z') \left[U\,(z'-nd) - U\,(z'-(n+1)d \right] x$$

$$e^{jk(x' \sin\theta \cos\phi + z' \cos\theta)} dx'\, dz' \tag{40}$$

The properties of the unit step functions can be used to interchange the order of integration and summation.

$$\underset{\sim}{f}(\theta,\phi) = \sum_{n=0}^{N-1} \int_{-W/2}^{W/2} \int_{nd}^{(n+1)d} \mathcal{J}_{sn}(x',z')\, x$$

$$e^{jk(x' \sin\theta \cos\phi + z' \cos\theta)}\, dx'\, dz' \tag{41}$$

Consider now the n^{th} integral in this sum

$$I_n \equiv \int_{nd}^{(n+1)d} \mathcal{J}_{sn}(x',z') e^{jk(x' \sin\theta \cos\phi + z' \cos\theta)} dx'\, dz' \tag{42}$$

and apply a transformation of coordinates corresponding to a translation

along the longitudinal (z) axis. Let

$$\zeta = z' - na \tag{43}$$

$$I_n = e^{jknd \cos\theta} \int_o^a \mathcal{J}_{sn}(x', \zeta + nd)\, e^{jk(x' \sin\theta \cos\phi + \zeta \cos\theta)}\, dx' d\zeta \tag{44}$$

By virtue of (37) this can be written in terms of the current in the zeroth cell as

$$I_n = e^{(jk \cos\theta - \gamma)nd} \int_o^a \mathcal{J}_{so}(x', \zeta) e^{jk(x' \sin\theta \cos\phi + \zeta \cos\theta)}\, dx' d\zeta \tag{45}$$

which yields the result for $\underset{\sim}{f}(\theta, \phi)$.

$$\underset{\sim}{f}(\theta, \phi) = \sum_{n=0}^{N-1} e^{(jk \cos\theta - \gamma)nd} \int_{-W/2}^{W/2} \int_o^a \mathcal{J}_{so}(x', \zeta) e^{jk(x' \sin\theta \cos\phi + \zeta \cos\theta)}\, dx'\, d\zeta \tag{46}$$

The terms in (46) can be readily related to the results of linear array theory. The integral I_o gives the field due to a single cell; when combined with the directional factors in (23) and (24), this yields the "element pattern." Similarly, the summation

$$\mathcal{S} = \sum_{n=0}^{N-1} e^{(jk \cos\theta - \gamma)\, nd} \tag{47}$$

represents the directional characteristics of an array of isotropic sources[6] separated by distance a and having progressive amplitude and phase differences given by a parameter γ. It is thus apparent that the radiation patterns corresponding to each mode on the periodic structure depend upon the current distribution in a single cell and the propagation constant for that mode. It is frequently the case that the dimensions of a single cell will be small compared with the wavelength so that the element pattern can be well approximated by that of a simple dipole or other low gain antenna. The principal contributions to directivity then arise from the "array factor," $\mathcal{S}$. A knowledge of the propagation constant *versus frequency* characteristics of the periodic structure can then be used to calculate radiation patterns for a periodic antenna over a wide range of operating parameters.

Before proceeding with examples let us review the conditions under which (46) can be expected to give reasonably accurate results.

1. The current on the structure must be predominantly that due to a single mode. If more than one mode is present, then the complex modal coefficients must be known to superpose the modal patterns given by (46).
2. Only a wave traveling in one direction is present on the structure. This may be accomplished by a proper termination on one end or it may be that γ is complex so that the current decays to a negligible value before reaching the end of the finite structure. If neither is the case, (46) can be modified to account for multiple reflections which may result when waves with small attenuation encounter mismatched terminations.

1.6 Universal Array Factors

The array factor S has been shown to contribute largely to the determination of the radiation patterns of periodic antenna structures. The dependence of the distant field upon period a, wavelength λ and the propagation constant γ, as well as the directional coordinate θ, is simply displayed in the array factor, (47). However, it is possible to facilitate calculations by considering further development of this formula and producing some curves which are applicable to a wide variety of operating parameters. Let us define

$$\xi = \gamma d - jka \cos \theta \tag{48}$$

so that (47) becomes

$$S = \sum_{n=0}^{N-1} e^{-n\xi} \tag{49}$$

which can be written as the difference between two infinite series

$$S = \sum_{n=0}^{\infty} e^{-n\xi} - e^{-N\xi} \sum_{n=0}^{\infty} e^{-n\xi} = (1 - e^{-N\xi}) \sum_{n=0}^{\infty} e^{-n\xi} \tag{50}$$

This series is of the form

$$1 + w + w^2 + w^3 + \ldots = \frac{1}{1-w} \tag{51}$$

so that (50) reduces to

$$S = \frac{1-e^{-N\xi}}{1-e^{-\xi}} \tag{52}$$

If γ is complex, $\gamma = \alpha + j\beta$, with a real part α of sufficient magnitude so that $e^{-N\alpha} \ll 1$ then (52) becomes

$$S = \frac{1}{1 - e^{-\xi}} \tag{53}$$

This corresponds to the case where the current decays to negligible values before reaching the end of the structure, and it is apparent from (53) that the number of cells is irrelevant in this case.

Equation (53) has been used as the basis of calculation of a set of universal array factors.[4] Each value of attenuation gives rise to a different curve which can be used to obtain the radiation pattern. Since

$$\xi = \alpha d + jd\,(\beta - k\cos\theta) \tag{54}$$

we can represent the universal array factors for several values of $A = \alpha a$ as functions of $\Psi = (\beta - k\cos\theta)d$. Such a family of curves is shown in Figure 5 for values of A ranging from 0.05 to 0.95 (nepers). Since the curves are symmetrical with respect to ϕ, only the range for $\phi > 0$ is shown.

Now let us consider how the curves of Figure 5 may be transformed into polar radiation patterns using values of attenuation and phase progression which have been previously determined either theoretically or experimentally. We note first that (54) defines a transformation of variables between the abscissa of Figure 5 and the direction angle θ. The maximum value of $S(\Psi)$ occurs at $\Psi = 0$ which corresponds to $\cos\theta = \beta/k$. As the angle θ varies from 0 to π, the value of Ψ ranges from $(\beta-k)d$ to $(\beta+k)d$. Consider the rotating vector shown in Figure 6 which pivots about the point $\Psi = \beta d$ and has a length $\ell = kd$. If the angle which the vector makes with the horizontal Ψ-axis is identified with the direction angle θ, then the projection of the end point of the vector onto the Ψ-axis falls at the point $\Psi = \beta d - kd\cos\theta$. This construction therefore relates a value of Ψ to each direction in space as located by the polar angle θ.

As an example of how the curves of Figure 5 may be combined with Figure 6, consider the case where $A = 0.35$, $kd = 45^\circ$ and $\beta d = 35^\circ$. The universal array factor corresponding to $A = 0.35$ is plotted in Figure 7 and the vector with length $kd = 45^\circ$ is pivoted about the point $\Psi = 35^\circ$ on the auxiliary Ψ-axis

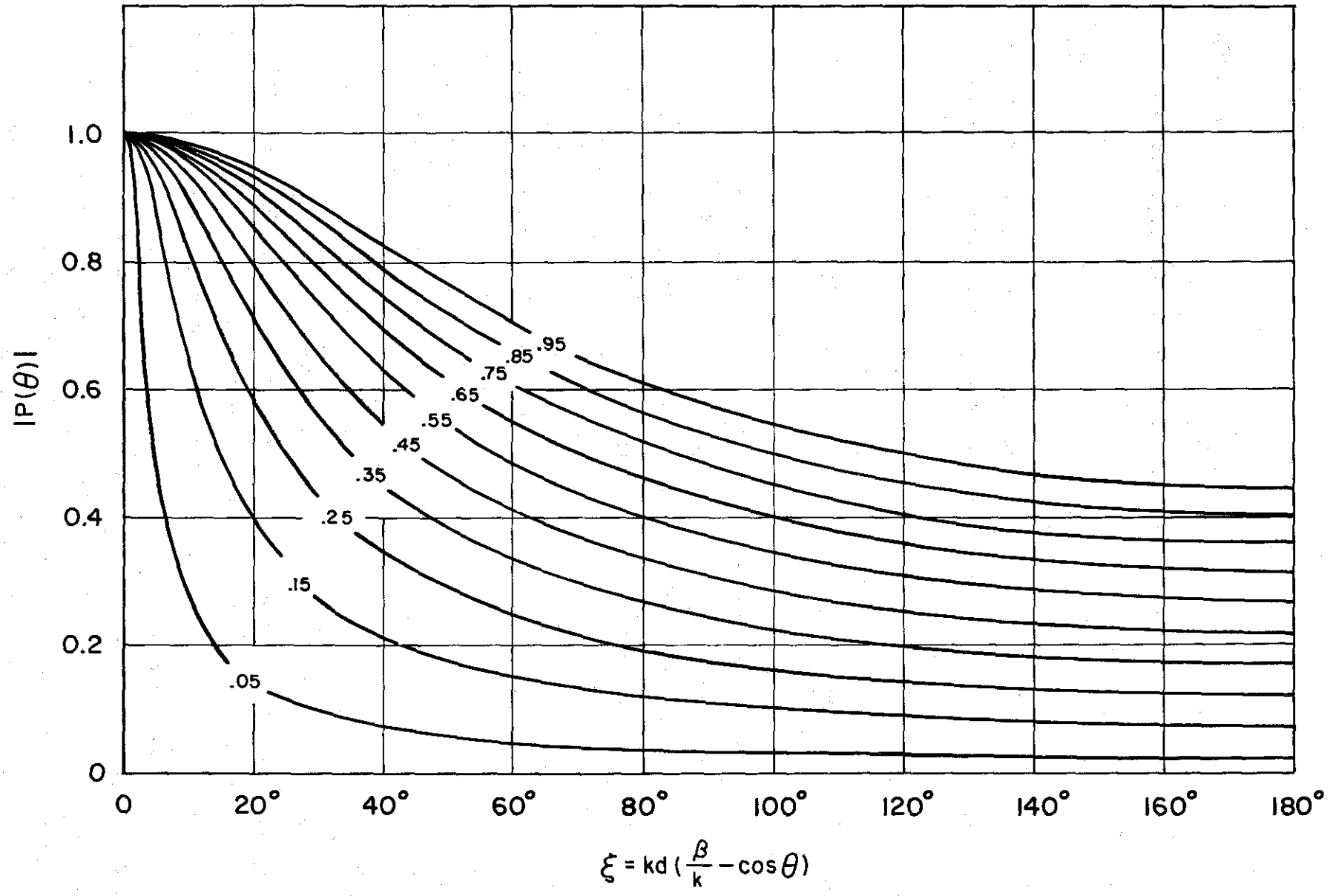

Figure 5. Universal pattern chart for exponential current distributions on discrete arrays.

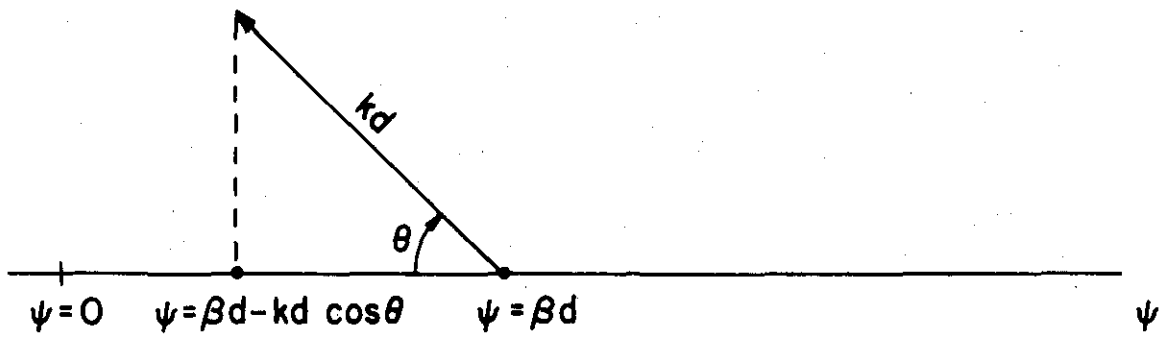

Figure 6. Rotating vector of length kd showing correspondence between θ and Ψ.

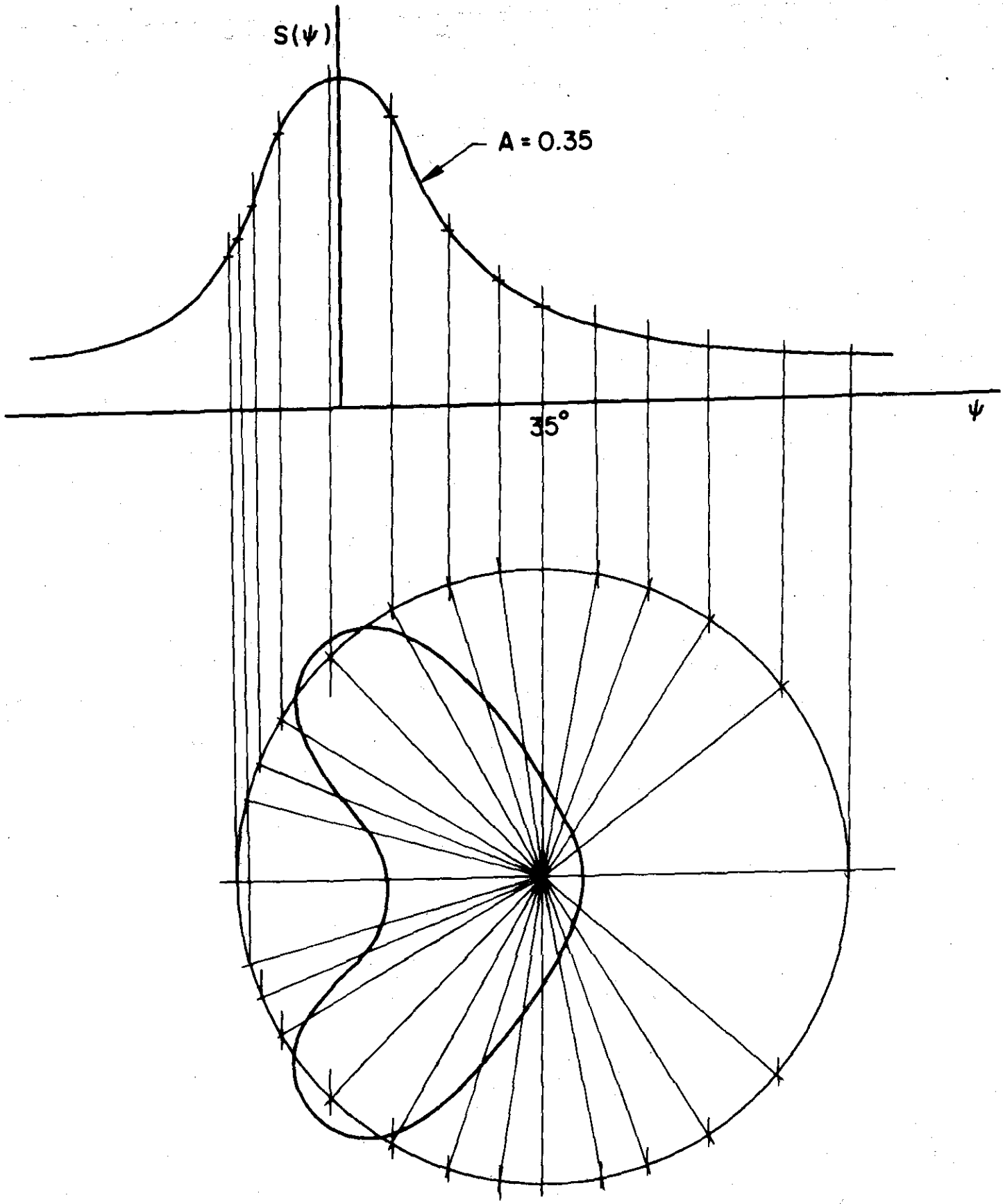

Figure 7. Graphical construction of the polar pattern of a modal current distribution with A = 0.35, ka = 45° and βa = 35°.

located parallel to but below the ψ-axis of the array factor. The locus of end points of the vector is shown in Figure 7 as a circle of radius $kd = 45^{o}$. The values of ψ corresponding to various angles θ are obtained by projecting points on the circle onto the ψ-axis. In Figure 7 the projections are shown up to to the array factor curve so that values of $S(\psi)$ corresponding to particular directions can be measured. These distances are then measured from the origin along the appropriate radial lines. The curve shown connecting the points so determined is the desired polar plot. The lower half of the plot is the mirror image of the upper half due to symmetry of the structure.

1.7 Summary

The purpose of the foregoing discussion is to demonstrate the utility and limitations of using dispersion data to calculate radiation patterns of antennas. The usefulness lies in being able to predict certain features of the pattern from knowledge of only a few geometric parameters of a periodic structure. Refinements in these calculations can be made if either theoretical or experimental dispersion data are available. It is important to know the attenuation versus frequency as well as phase constant versus frequency. When appreciable attenuation is present, particularly simple results can be derived using universal array factors. Polar patterns can be obtained from the universal array factor curves by graphical means. In all cases, however, the results are presented for traveling wave modal current distributions and adaptations must be made for end-reflections and multiple mode distributions. With this background as a motivation for further consideration of dispersion data for open periodic structures, further attention will be directed to the methods of obtaining these data.

PART II

DISPERSION CHARACTERISTICS OF SOME SMOOTH AND PERIODIC STRUCTURES

2.1 Introduction

For transverse electromagnetic waves in free space, the phase constant is directly proportional to frequency. This simple relationship may be perturbed by the presence of material media and the perturbation is referred to as dispersion. Dielectric materials exhibit dispersion because the permittivities are frequency-dependent. Of course, for some materials the variation is so slight over the frequency range of interest that they may be thought of as nondispersive.

There are various other ways by which dispersion occurs. In dielectric materials and gaseous plasmas, dispersion is due to the interaction of the electromagnetic field with the atomic or molecular constituents of the medium. Dispersion is present in waveguides because the conducting boundaries force the electromagnetic waves to propagate in various zigzag paths down the guide rather than in a straight line along the axis. The path which the wave must take is dependent upon the frequency of operation. Another viewpoint which can be taken is to consider the waveguide as a transmission line with inductance and capacitance per unit length which are functions of frequency. This concept can be carried over to open structures, such as a helix, and periodically loaded transmission lines. Tapered versions of the latter can serve as models for practical log-periodic antennas. This correspondence will be discussed in greater detail in a later section.

Graphs showing the variation in phase constant as a function of frequency are called dispersion diagrams. Dispersion diagrams for periodic structures are often referred to as Brillouin diagrams for Leon Brillouin, who first made extensive use of them.[7] Brillouin considered elastic wave propagation in crystal lattices, as well as wave propagation in periodic electrical systems and electrical-mechanical analogies. He demonstrated that in certain bands of frequency, propagation of an undamped wave is not possible. This consideration led to the separation of the frequency spectrum into passbands where propagation is allowed, and stopbands where

it is not. Many other authors have used the Brillouin diagram to illustrate the nature of wave propagation on various periodic structures. Until recently most of these structures have been of slow-wave or surface-wave type. An excellent survey and bibliographical listing up to January, 1959 has been written by Harvey.[8] He gives a list of 293 references, many of which make use of Brillouin diagrams or closely related graphs to present theoretical or experimental dispersion data.

One structure which has received a great deal of attention because of its application in traveling wave tubes and delay lines is the helix and its variants.[9,10,11,12,13,14,15,16,17] More recently, helices and tapered helices have been studied for their radiation characteristics.[18,19,20,21] This has led to the extension of the dispersion data for helices to include frequency bands where the propagation constant is complex. There are many articles in the literature on surface wave supporting structures, such as dielectric rods and slabs, stratified plasmas and corrugated metallic surfaces.[22,23,24,25,26,27] A number of different types of structures have been studied because of their ability to act as antennas or because they are related to practical antenna structures.[28,29,30,31,32,33] The references given here are representative, but do not necessarily form a complete listing of articles on the topics mentioned.

2.2 Interpretation of Dispersion Diagrams

In its original and simplest form, the Brillouin diagram is a plot of (angular) frequency ω on the ordinate and phase constant β along the abscissa. For smooth structures, the free-space propagation constant ($k = \omega/c = 2\pi/\lambda$) is often used on a vertical axis. However, for periodic structures it is common to plot kd vs. βd where d is the period of the structures.

Figure 8 illustrates a useful classification of regions on the k-β plots. The two lines $\beta = \pm k$ serve to separate the regions where the phase velocity $v_p = \omega/\beta$ along the chosen axis is greater or less than the intrinsic phase velocity in free space $c = \omega/k$. The region below the $\beta = \pm k$ lines is thus referred to as the slow-wave region, whereas the region above is called the fast-wave region. Positive values of β result in a wave with phase progression in one direction, whereas negative values of β are

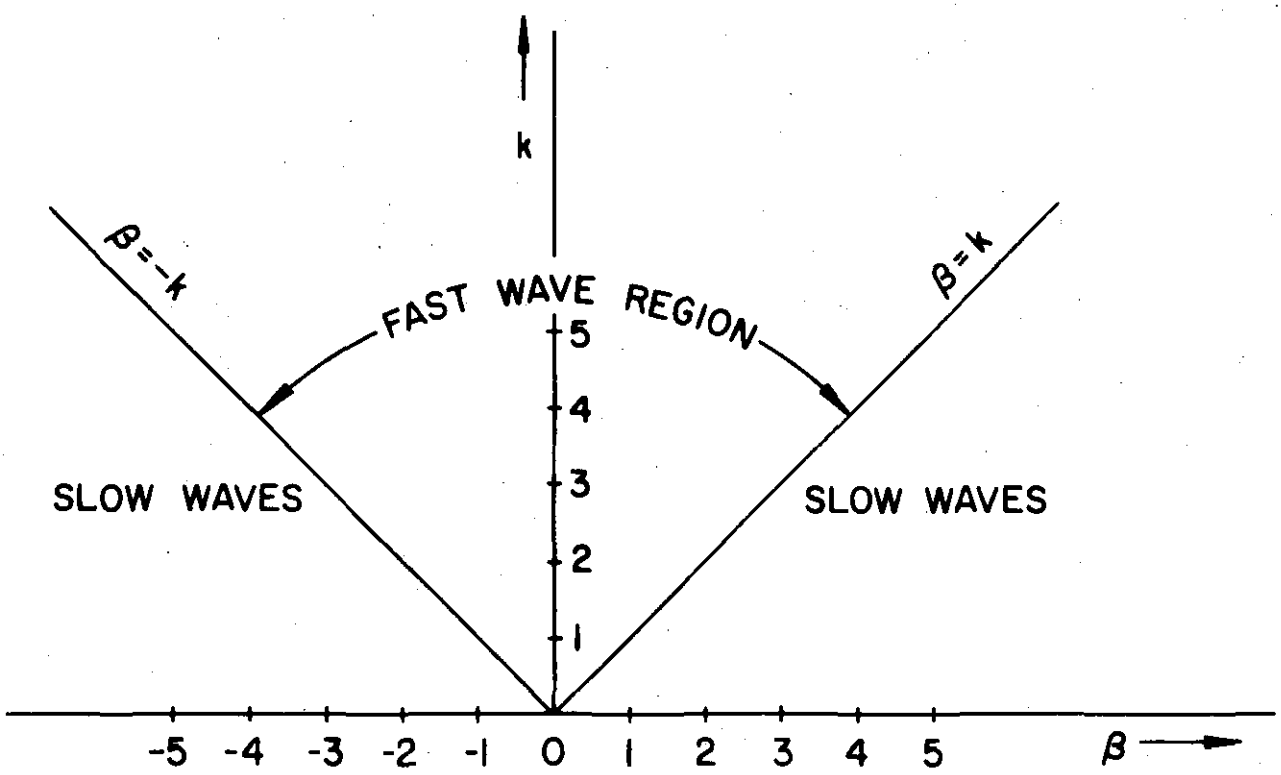

Figure 8. Interpretation of regions on the k-β plane.

associated with a wave in the opposite direction. We shall refer to the former as a "forward wave," and the latter as a "reverse wave." (The reverse wave has sometimes been called a backward wave; however, it is preferable to avoid this nomenclature since the term "backward wave" has another connotation.)

The relationship between k and β is obtained analytically by separating the electromagnetic field problem into transverse and longitudinal parts. The longitudinal axis corresponds to the direction for which β is to be determined. This technique is associated with the method of separation of variables which is commonly used to reduce partial differential equations to several ordinary equations. The partial differential equation of interest for electromagnetic problems is the time-reduced wave equation.

$$\nabla^2 \Psi + k^2 \Psi = 0 \tag{55}$$

Let us suppose that the axis along which β is to be evaluated corresponds to the z-axis of a cartesian coordinate frame. The variables of the transverse plane can be taken as general curvilinear coordinates u_1, u_2. To separate Equation (55) into transverse and longitudinal parts, we assume that $\Psi(u_1,u_2,z)$ can be written as a product of a transverse function $T(u_1,u_2)$ and a longitudinal function L(z). Substituting in Equation (55), we obtain

$$\frac{1}{T} \nabla^2 T + \frac{1}{L} \frac{d^2L}{dz^2} - k^2 = 0 \tag{56}$$

Since the first term on the left depends only upon transverse coordinates u_1,u_2 and the second term only upon the longitudinal coordinate z, and since their sum is a constant, each term must be a constant. We, therefore, obtain the equation

$$\kappa^2 - \gamma^2 = k^2 \tag{57}$$

relating the separation constants κ, γ; and Equation (55) is reduced to two differential equations

$$\nabla^2 T + \kappa^2 T = 0 \tag{58}$$

$$\frac{d^2L}{dz^2} - \gamma^2 L = 0 \tag{59}$$

The solutions of Equation (59) are of the form

$$L(z) = e^{\pm\gamma z} \tag{60}$$

showing that the factor γ gives the properties of the propagation along the z-axis as desired.

It is apparent from Equation (58) that the dispersion properties and the solution of the field problem in the transverse plane are intimately connected. For example, in the case of a hollow pipe waveguide, with perfect conducting boundaries, the permissible values of the transverse phase constant κ form a set of constants (eigenvalues) which depend upon the geometry of the boundary. To each eigenvalue there corresponds an eigenfunction which describes the transverse behavior of the field. For example, a rectangular waveguide of width a and height b has eigenvalues given by[34,35]

$$\kappa_{LM}^2 = (L\frac{\pi}{a})^2 + (\frac{M\pi}{b})^2 \tag{61}$$

where L and M are positive integers. Because of the vector nature of the electromagnetic field, there are two infinite sets of eigenfunctions which have the above eigenvalues. Transverse magnetic fields are obtained from

$$F_{LM}(x,y) = \sin L\pi x/a \sin M\pi y/b \tag{62}$$

whereas transverse electric fields are obtained from

$$F_{LM}(x,y) = \cos L\pi x/a \cos M\pi y/b \tag{63}$$

Each eigenfunction corresponds to a mode in the waveguide.

Let us suppose that κ_n is the eigenvalue of the nth waveguide when the guide is operated above the cut off frequency for the nth mode, then $\gamma_n = j\beta n$ and Equation (57) can be written in the form

$$k^2 - \beta_n^2 = \kappa_n^2 \tag{64}$$

from which a dispersion curve is readily plotted since this represents the equation of a hyperbola with a vertex at $k = \kappa_n$ as shown in Figure 9. We note that the asymptotes for the given hyperbola bisect the angle between the β and k axes, and, therefore, fall on the boundary between the fast and slow wave regions. Any mode in the closed waveguide is, therefore, a fast wave with respect to the interior medium. Note that the form of Equation (64) is dependent upon k exceeding a certain minimum value (the vertex) $k = \kappa_n$. There are no real values of β which will satisfy Equation (64) for k less than κ_n. Equation (64) yields the cutoff frequency for the nth mode. Undamped propagation for this mode is possible

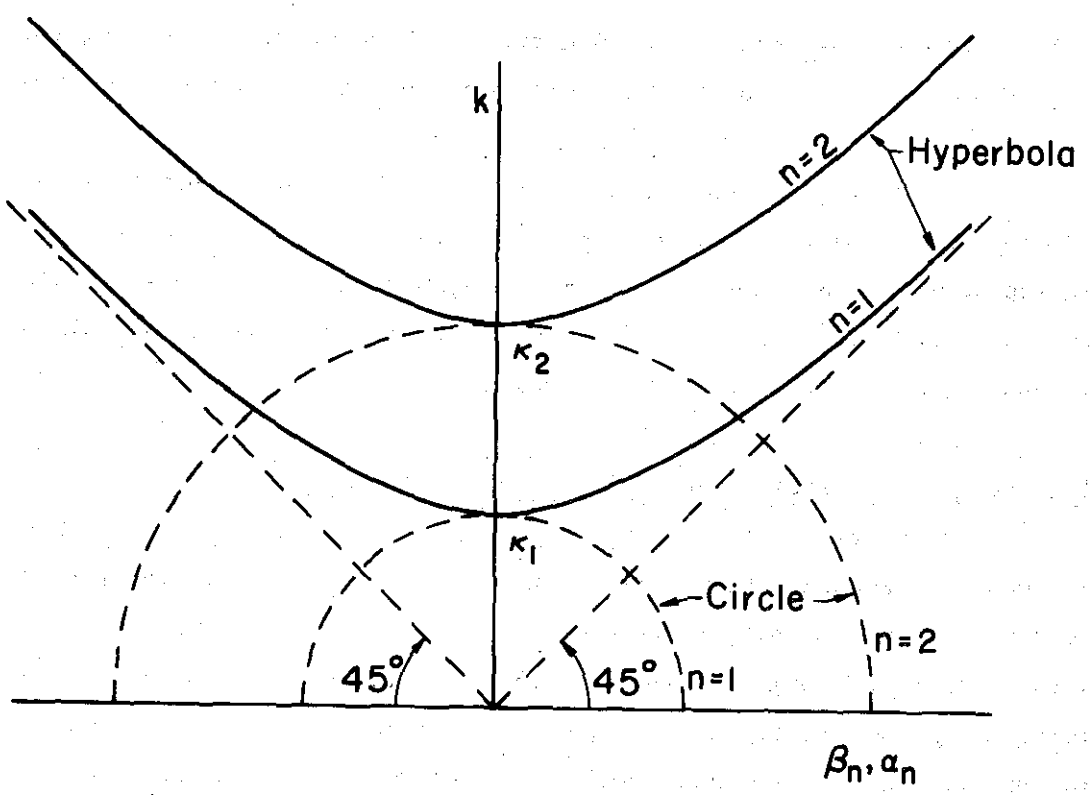

Figure 9. Dispersion diagram for hollow-pipe waveguide.

only if k is greater than κ_n. For frequency such that $k < \kappa_n$, $\beta_n = \sqrt{k^2 - \kappa_n^2}$ will be imaginary, $\beta_n = j\alpha_n$, and Equation (64) becomes

$$k^2 + \alpha_n^2 = \kappa_n^2 \tag{65}$$

Substitution of $\beta_n = j\alpha_n$ into Equation (64) shows that the longitudinal variation of the field in this case corresponds to a damped (evanescent) wave.

It is oftentimes useful to extend the dispersion plot to include the imaginary or complex values of β. The plot of Figure 9 can be so extended by labeling the horizontal axis as α (attenuation in nepers per meter) as well as β. From Equation (65) it is apparent that for $k < \kappa_n$ the plot of k versus α_n has the form of a circle.

2.3 Radiation Properties of Dispersive Structures

Since we are primarily interested in the application of dispersion data to antenna problems, let us next consider how some radiation properties can be obtained very simply from the dispersion curves. Suppose some dispersive structure is contained in the cylindrical volume shown in Figure 10. By using Huygen's principle, an equivalent current distribution can be obtained on the surface of the cylinder.[36,37] Let us assume the current is describable by a single wave with a longitudinal phase constant, β. Once again the separation into transverse and longitudinal problems is possible. However, the boundary condition on the transverse problem in this case is chosen to insure appropriate field behavior at infinity.

The transverse and longitudinal separation constants are still related by Equation (57), with $\gamma = j\beta$

$$\kappa^2 + \beta^2 = k^2$$

but discrete values of κ are not dictated by the boundary condition. We can consider, therefore, that k and β are fixed by the operating frequency and the structure boundaries, respectively, and Equation (57) can be solved for κ. We note that $\beta > k$ corresponding to values in the slow wave region on Figure 8 leads to imaginary values of κ, whereas for $\beta < k$, κ is real. Real values of κ give propagating waves in the transverse direction. Imaginary values give damped transverse behavior.

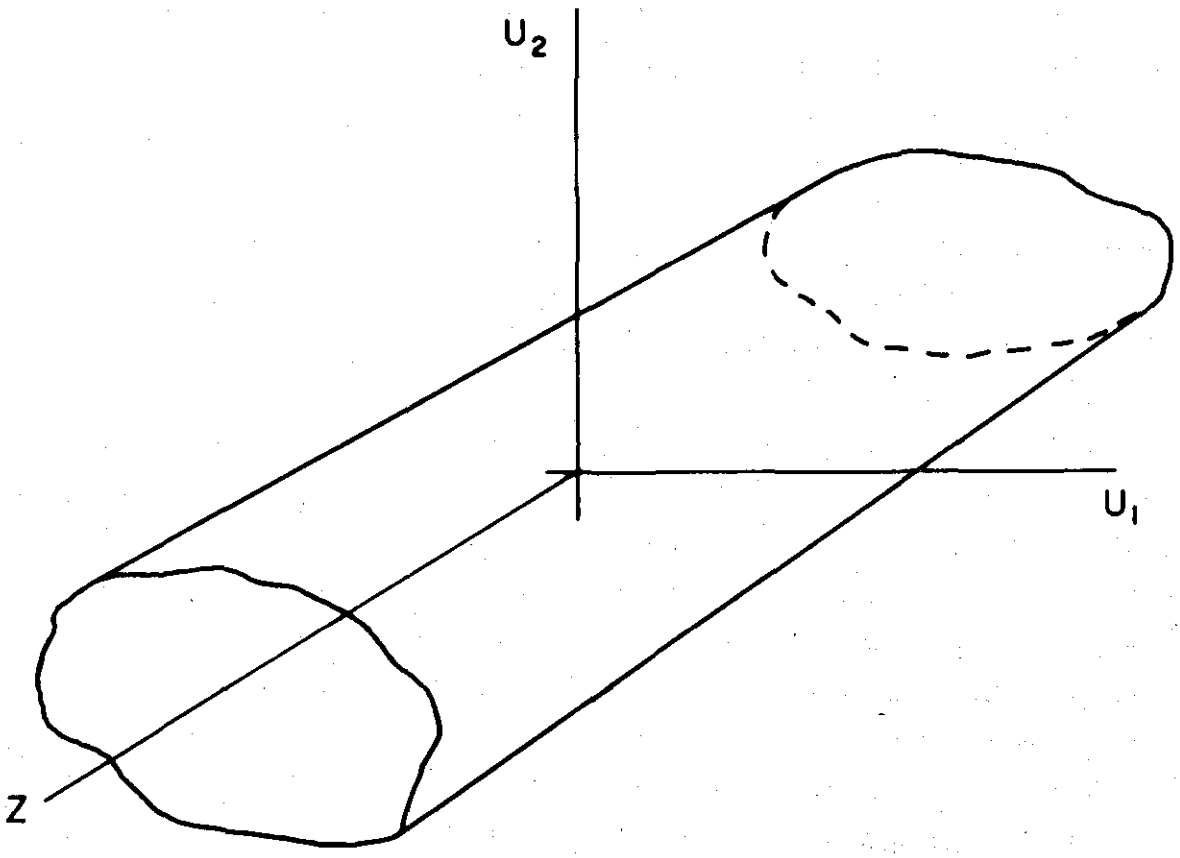

Figure 10. Hypothetical cylindrical surface used.

At large radial distances, the fields will vary as $\frac{e^{-j\kappa\rho}}{\rho}$ representing outgoing waves. It is thus apparent that the distant field is representable in terms of a propagation vector $\vec{\beta} = \hat{\rho}\,\kappa + \hat{z}\,\beta$ as $e^{-j\vec{\beta}\cdot\vec{r}}$ where $\vec{r}$ is the position vector. The angle which the propagation vector β makes with the z axis is given by

$$\cos\theta = \frac{\beta}{k} \tag{66}$$

as shown in Figure 11.

We conclude, therefore, that a fast wave ($\beta/k < 1$) along the z-axis will give rise to a wave traveling at an angle with respect to the z-axis, whereas a slow wave ($\beta/k > 1$) along z will produce only a damped transverse wave. When β is less than k the length of the propagation vector is fixed, equal to k. The locus of all possible such vectors is, therefore, a circle in the κ-β plane that is shown in Figure 11. For any given $\beta/k < 1$ the direction of propagation in the distant field is obtained by a projection upward from the given point on the β/k -axis to the point of intersection with the circle of unit radius. A line from the origin to the intersection makes an angle θ with respect to the β-axis which is identical to the angle of propagation by virtue of Equation (66).

The foregoing discussion applies to the case where the longitudinal field variation on the surface of the cylinder of Figure 10 is limited to that of a single undamped wave. A practical system which could be considered to give rise to such a distribution on a circular cylinder is composed of a narrow longitudinal slit cut in the wall of a circular waveguide operating in a dominant mode, as shown in Figure 12. However, since the slit will couple energy from the waveguide interior to the exterior region, the wave in the guide will no longer be undamped and will have an attenuation factor due to the energy loss. In this case, the propagation constant along the cylindrical surface will be complex, and a modification of the previous discussion is in order.

When considering a complex wave, the source must be restricted in extent in one direction to avoid a singularity in the source description. A semi-infinite line source is chose, therefore, as a simple model and the current along the line is assumed to vary as $e^{-\gamma z}$, where $\gamma = \alpha + j\beta$.

The far-field radiation pattern is proportional to the Fourier transform of the damped current wave. Thus, the pattern is given by

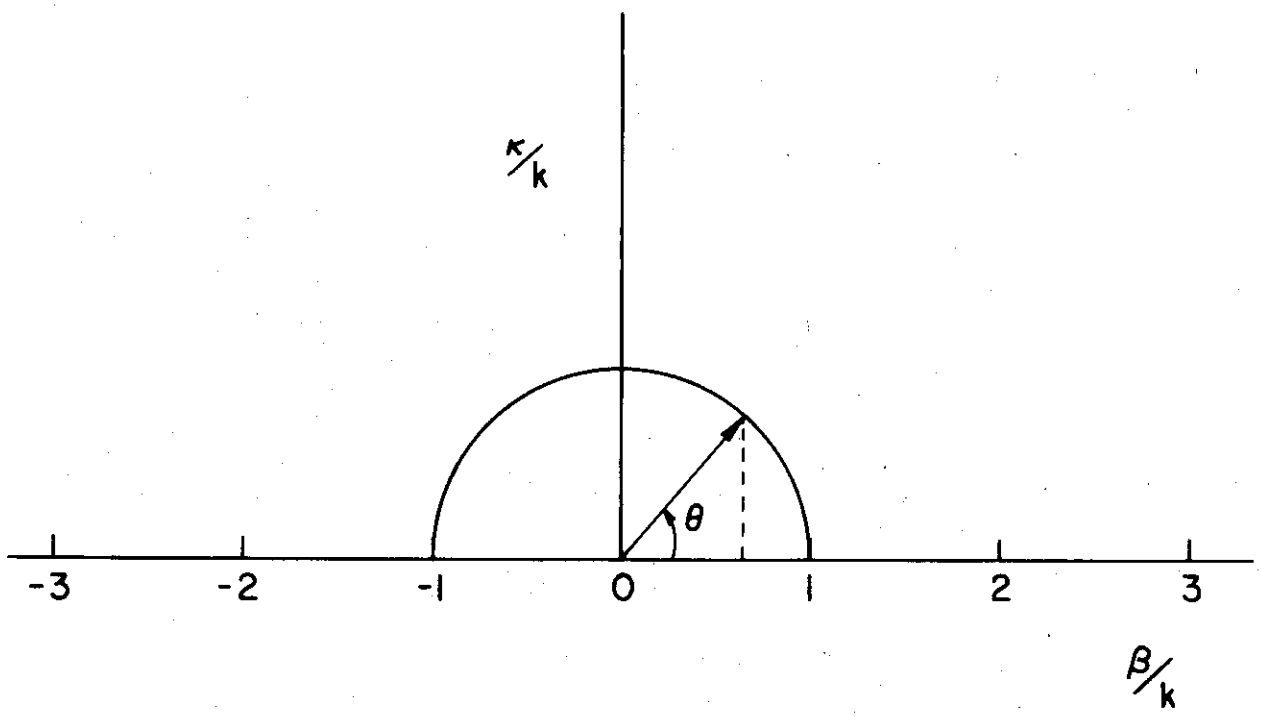

Figure 11. Normalized space spectrum diagram showing relation between longitudinal phase constant and direction of propagation.

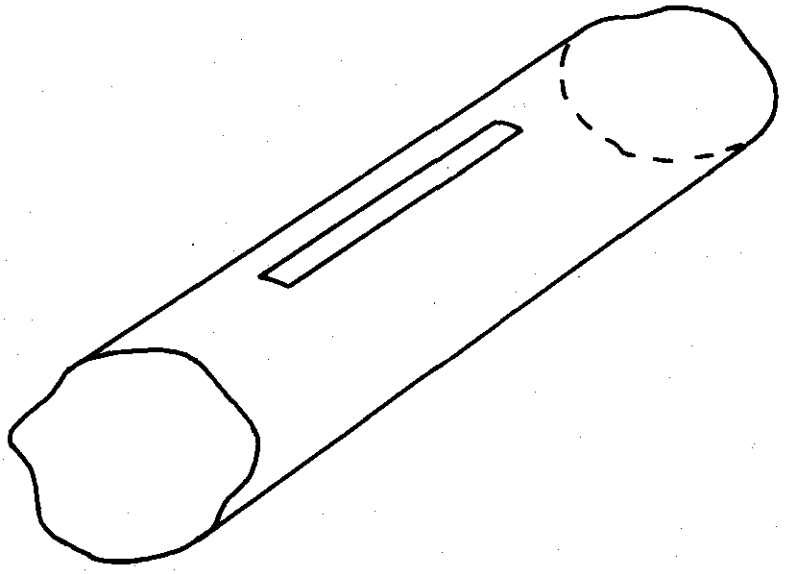

Figure 12. Cylindrical waveguide with long, narrow slit in the conducting wall.

$P(\theta) = \int_0^\infty e^{-\gamma z} e^{jkz \cos\theta} dz$, which yields $P(\theta) = \frac{+1}{\alpha+j(\beta-k\cos\theta)}$. Thus, the magnitude of the distant field is given by

$$|P(\theta)| = \frac{1}{[\alpha^2 + (\beta-k\cos\theta)^2]} \quad 1/2 \tag{67}$$

The maximum field occurs where $\frac{dP}{d\theta} = 0$, which gives $\beta = k\cos\theta$ as before. However, the patterns of Equation (67) have finite beamwidth, the angle between half-power points θ_1 and θ_2 being given by

$$\cos\theta_1 - \cos\theta_2 = \frac{2\alpha}{k} \tag{68}$$

If α is large, the term α^2 dominates the expression for the pattern for all angles of θ and the beamwidth is large. However, as α becomes smaller, the beam narrows. The limiting case, as α goes to 0, gives a delta function of the form $\delta(\beta-k\cos\theta)$. From the foregoing discussion it should be clear how β controls the direction of radiation and α controls the width of the radiated beam.

2.4 Dispersion Characteristics of Periodically Loaded Structures

In the previous sections, we have seen how the dispersion relation is obtained in closed waveguides, and how the dispersion properties can be used to predict certain radiation characteristics when the waveguide is coupled to space along the longitudinal axis. In many cases, the coupling between interior and exterior regions takes the form of discrete periodic loading rather than continuous coupling. Whereas the continuous coupling gives rise to a perturbed dispersion curve primarily because of the attenuation due to radiation, the case of discrete periodic loading may give rise to a different type of change in the dispersion curve. As an example of the latter case, let us consider a closed waveguide which is periodically loaded with obstacles, such as shown in Figure 13. If the hole in the coupling irises is almost equal in diameter to that of the waveguide itself, then we would expect the effect of the irises to be small and the dispersion curve should follow very closely that of the unloaded waveguide shown in Figure 9. However, at each obstacle there will be relection as well as transmission. At certain frequencies the reflections from the successive obstacles will add in-phase. These frequencies will be nearly equal to the frequencies for which the one-way phase shift

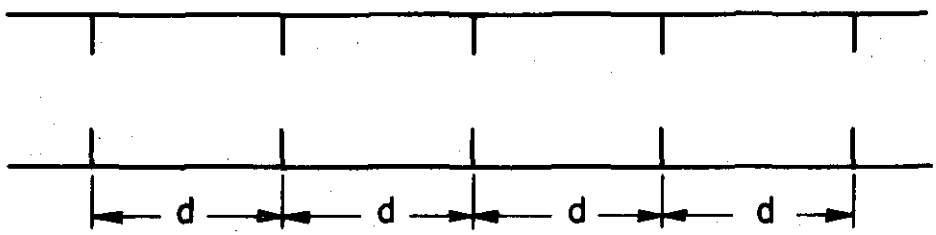

Figure 13. Longitudinal section of waveguide showing periodic placement of irises.

between obstacles in the unloaded guide is in integer multiple of π. These frequencies correspond to the centers of the stopbands in which undamped propagation is not possible.

A qualitative argument can be given for the form of the dispersion curves for the iris-loaded waveguide. From the results of Floquet's theorem given in Section 1, it is apparent that additional waves must be added to each mode in the unloaded waveguide in order to satisfy the additional boundary conditions introduced by the periodic discontinuities. As was previously shown, these new waves (space harmonics) differ in cell-to-cell phase shift by an integer multiple of 2π. Dispersion curves for each individual space harmonic could be added, therefore, to a k-β plot by simply shifting the curves the appropriate amount along the horizontal axis. Since little perturbation of the diagram is expected in the case when the iris hole is almost as large as the waveguide cross-section, the curve corresponding to minimum phase shift will be approximately the same as the dispersion curve of the unloaded waveguide. Figure 14 shows this curve for the fundamental wave along with the displaced curves representing the n=1 and n= -1 space harmonics.

The principal effect due to the irises occurs at the frequencies where the various space harmonic curves intersect. This occurs at cell-to-cell phase shifts which are equal to an integer multiple of π, as previously stated. In the vicinity of these points, the stopbands are formed. Throughout the stopband, the phase shift is maintained constant with frequency, but the attenuation increases from zero to a maximum and then back to zero. The form for the dispersion curve of the iris loaded waveguide is thus as shown in Figure 15. It can be shown that no energy propagates down the guide at any frequency which falls inside the stopband. Neglecting losses, the input impedance of a periodically loaded waveguide at any frequency in the stopband is, therefore, purely reactive, whereas the impedance in the passbands is real. A section of periodically loaded waveguide can be used, therefore, as a filter since signals at frequencies in the passband will appear unattenuated at the output, whereas signals at frequencies in the stopband will be attenuated.

In many antenna systems, particularly in the VHF band and at lower frequencies, the radiating elements are excited from a two-wire line with a small

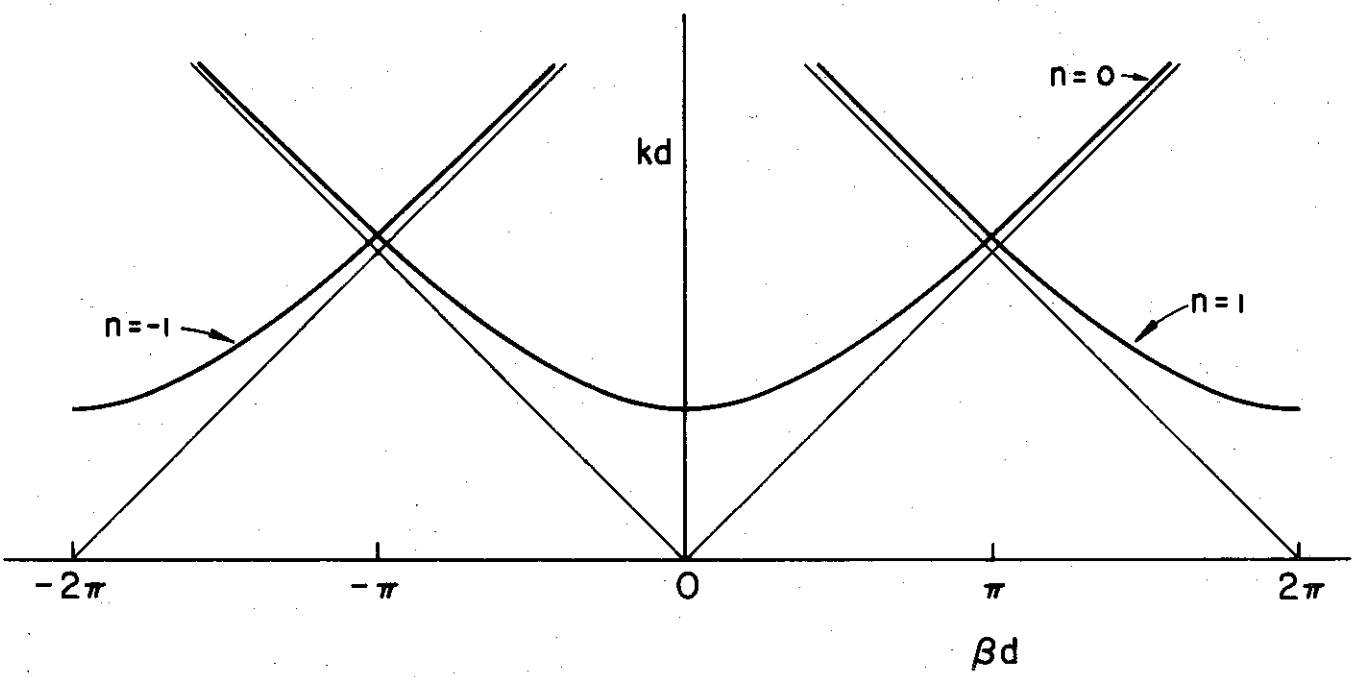

Figure 14. Dispersion curve for unloaded waveguide plus shifted curves representing approximate locations of n= ± 1 space harmonics for small loading.

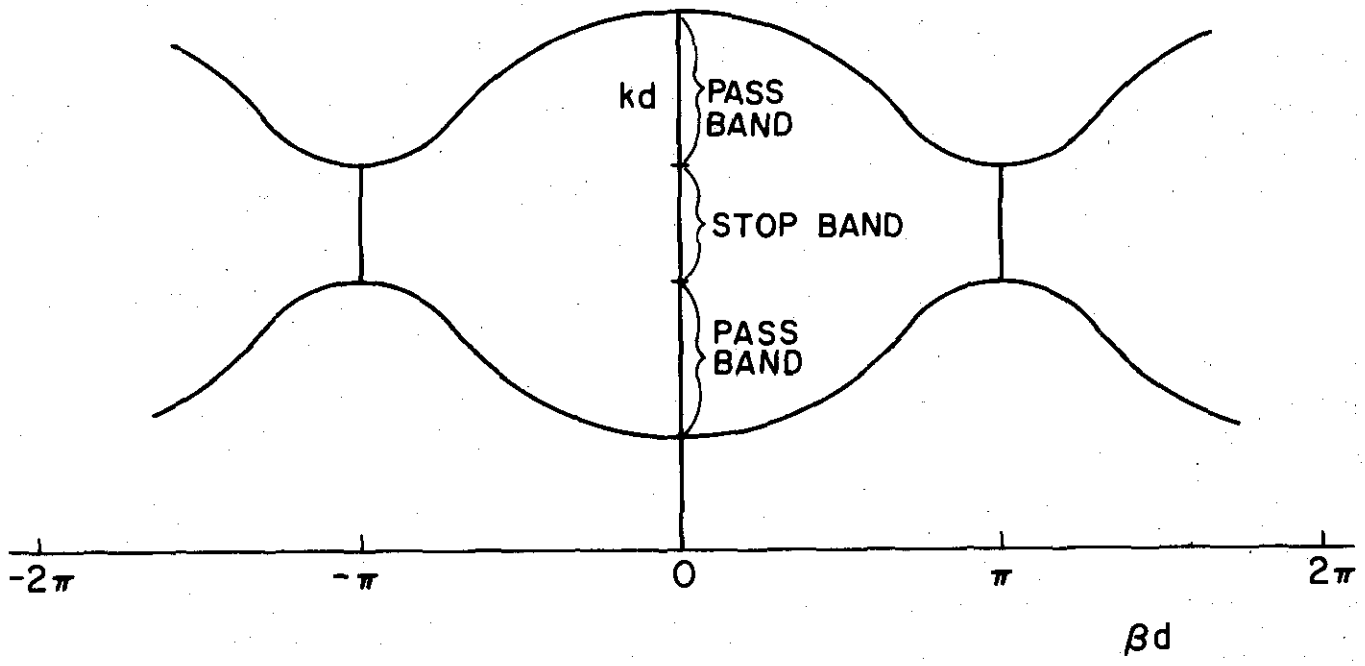

Figure 15. Dispersion diagram for waveguide with periodic iris loading showing formation of stopband due to loading.

cross section in wavelengths so that only the TEM mode need be considered. It is a relatively simple matter to study the dispersive properties of such a line when it is periodically loaded with discrete elements. As an example, consider the case of a two-wire line which is periodically shunted with identical admittances, Y_L, as shown in Figure 16. An equation for the propagation constant for a wave on such a line is easily derived by using the compensation theorem for networks. Alternate methods of derivation are discussed in the next section.

The voltage and current along the line are unchanged when each shunt element is replaced by a constant voltage generator which maintains the same voltage across the line that was originally present. The circuit then appears as shown in Figure 17. The current into the zero node is now composed of only five terms since generators corresponding to nodes $m = -1,0,+1$ are the only ones which can contribute due to the short circuit conditions which the other voltage generators apply across the line. First, there is the current through the zeroeth generator, which is given by $-\mathcal{V}_o Y_L$. The currents into node zero due to $\mathcal{V}_0$ correspond to the input currents of two short-circuited sections of line of length d, and free-space phase constant, k. Since the input admittance of such a line is given by $-j Y_c$ ctn kd, where Y_c is the characteristic admittance of the line, the total current into the node due to $\mathcal{V}_0$ is given by $\mathcal{V}_0 2j Y_c$ ctn kd. The current into the node due to the $n = -1$ generator is the short-circuit current which flows when $\mathcal{V}_{-1}$ is applied at a distance d away. This current is given by $-j \mathcal{V}_{-1} Y_c$ csc kd. Similarly, the short circuit current due to generator $\mathcal{V}_1$ is given by $-j \mathcal{V}_1 Y_c$ csc kd. Summing the currents into node zero, therefore, yields the following result.

$$j \mathcal{V}_{-1} Y_c \csc kd + \mathcal{V}_o (Y_L - 2j Y_c \operatorname{ctn} kd) + j \mathcal{V}_1 Y_c \csc kd = 0 \qquad (69)$$

Now by virtue of Floquet's theorem, we can write that $\mathcal{V}_{n+1} / \mathcal{V}_n$ is equal to $e^{-\gamma d}$. Substituting for $\mathcal{V}_{-1}$ and $\mathcal{V}_1$ in terms of $\mathcal{V}_0$ using this relation, and simplifying, leads to the following result:

$$\cosh \gamma d = \cos kd + j \frac{Y_L}{2Y_c} \sin hd \qquad (70)$$

It follows from duality that the characteristic equation for a line periodically loaded with series impedances is given by

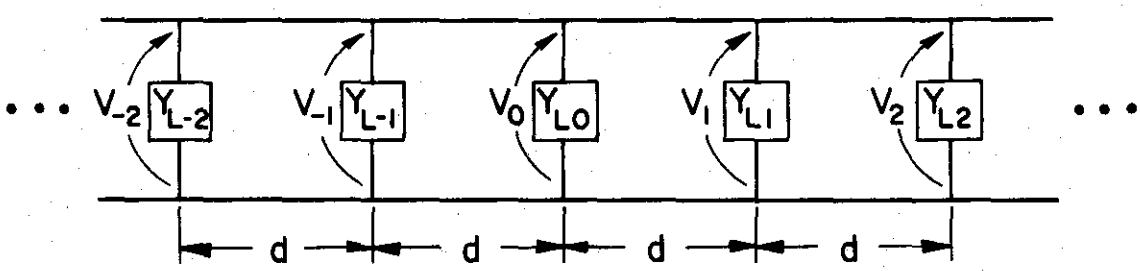

Figure 16. A transmission line periodically loaded with shunt elements.

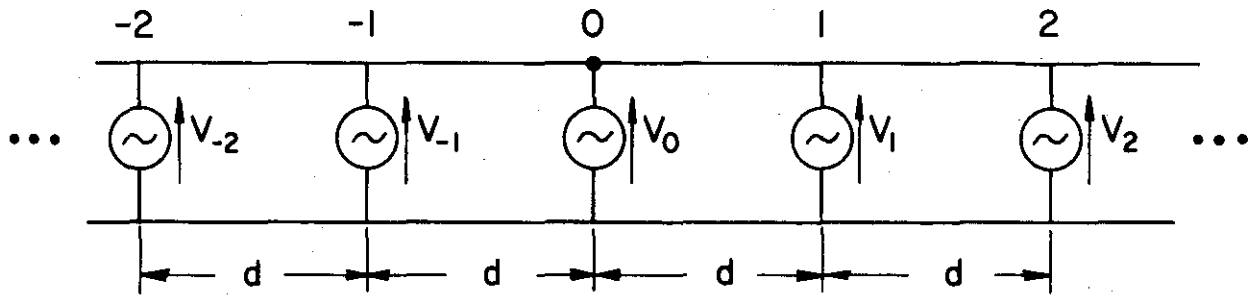

Figure 17. Periodically loaded line with loads replaced by voltage generators according to compensation theorem.

$$\cosh \gamma d = \cos kd + j \frac{Z_L}{2Z_c} \sin kd \tag{71}$$

Several characteristics of the dispersion curves of periodically loaded lines are apparent from these equations. When the loading is purely reactive, $Y_L = j B_L$ or $Z_L = j X_L$ and the right hand side of Equations (70) and (71) is real. Since

$$\cosh \gamma d = \cosh (\alpha + j\beta) d = \cosh \alpha d \cos \beta d + j \sinh \alpha d \sin \beta d \tag{72}$$

we have

$$\cosh \alpha d \cos \beta d = \cos kd - K \sin kd \tag{73}$$
$$\sin h \alpha d \sin \beta d = 0$$

where

$$K = \frac{B_L}{2Y_c} \qquad \text{or} \qquad \frac{X_L}{2Z_c}$$

The latter equation can be satisfied in either of two ways. If $\alpha d = 0$, then we obtain

$$\cos \beta d = \cos kd - K \sin kd = F(kd) \tag{74}$$

and if $\beta d = n\pi$, $n = 0, 1, 2, \ldots$, we get

$$\pm \cosh \alpha d = F(kd) \tag{75}$$

Equation (74) has solutions only if

$$|F(kd)| \quad < \quad |$$

which serves to define the frequency ranges corresponding to pass bands. When $F(kd) > 1$, Equation (75) must be used and it, therefore, defines the stopbands. Note that in the stopbands the phase shift between adjacent cells must be either zero or an integer multiple of π for the case where K is real (reactive loads on a line with real characteristic impedance).

If the reactive loading is series capacitive or shunt inductive, then K is negative. For series capacitance loading

$$K = - \frac{1}{2\omega C Z_c} = - \frac{d}{2cCZ_c} \frac{1}{kd} = - \frac{M_C}{kd} \tag{76}$$

while for shunt inductive loading

$$K = - \frac{1}{2\omega L Y_c} = - \frac{d}{2cLY_c} \frac{1}{kd} = - \frac{M_L}{kd} \tag{77}$$

($c = 3 \times 10^8$ m/sec). For small kd, F(kd) becomes

$$F(kd) \approx 1 - \frac{(kd)^2}{2} + M \tag{78}$$

Since $F(kd) > 1$ for small kd in this case, the series capacitive and shunt inductive loads produce a low frequency stopband.

The upper limit of the stopband is given by

$$F(kd) = \cos kd + M \frac{\sin kd}{kd} = 1 \tag{79}$$

where

$$M = M_c \quad \text{or} \quad M_L$$

depending upon the type of loading. The value of the upper limit is thus determined by the intersection of curves for $f_1(kd) = \cos kd$ and $f_2(kd) = 1\text{-}M \frac{\sin kd}{kd}$ as shown in Figure 18. Note that this intersection occurs at small kd for M small, near $\pi/2$ for M of the order of unity, and approaches π for large values of M.

The lower and upper limits of the next higher stopband are given by

$$F(kd) = -1$$

or the intersections of $f_1(kd) = \cos kd$ and $f_3(kd) = -1\text{-}M \frac{\sin kd}{kd}$. As is apparent from Figure 19, the first intersection always occurs at $kd = \pi$ and the width of the stopband increases with increasing M. Successive higher order stopbands begin at $kd = n\pi$ and have widths which are governed by M in the same manner as for the first stopband. However, the bandwidth of each succeeding stopband is reduced by the effect of the factor 1/kd multiplying sin kd in F (kd).

If the reactive loading is series inductance or shunt capacitance, then K is positive. For series inductance

$$K = \frac{\omega L}{2Z_c} = \frac{kc\ dL}{2dZ_c} = \frac{cL}{2dZ_c}\ kd = N_L\ kd \tag{80}$$

while for shunt capacitance

$$K = \frac{\omega C}{2Y_c} = \frac{kc\ dC}{2d\ Y_c} = \frac{cC}{2d\ Y_c}\ kd = N_C\ kd \tag{81}$$

so that $K = Nkd$ where

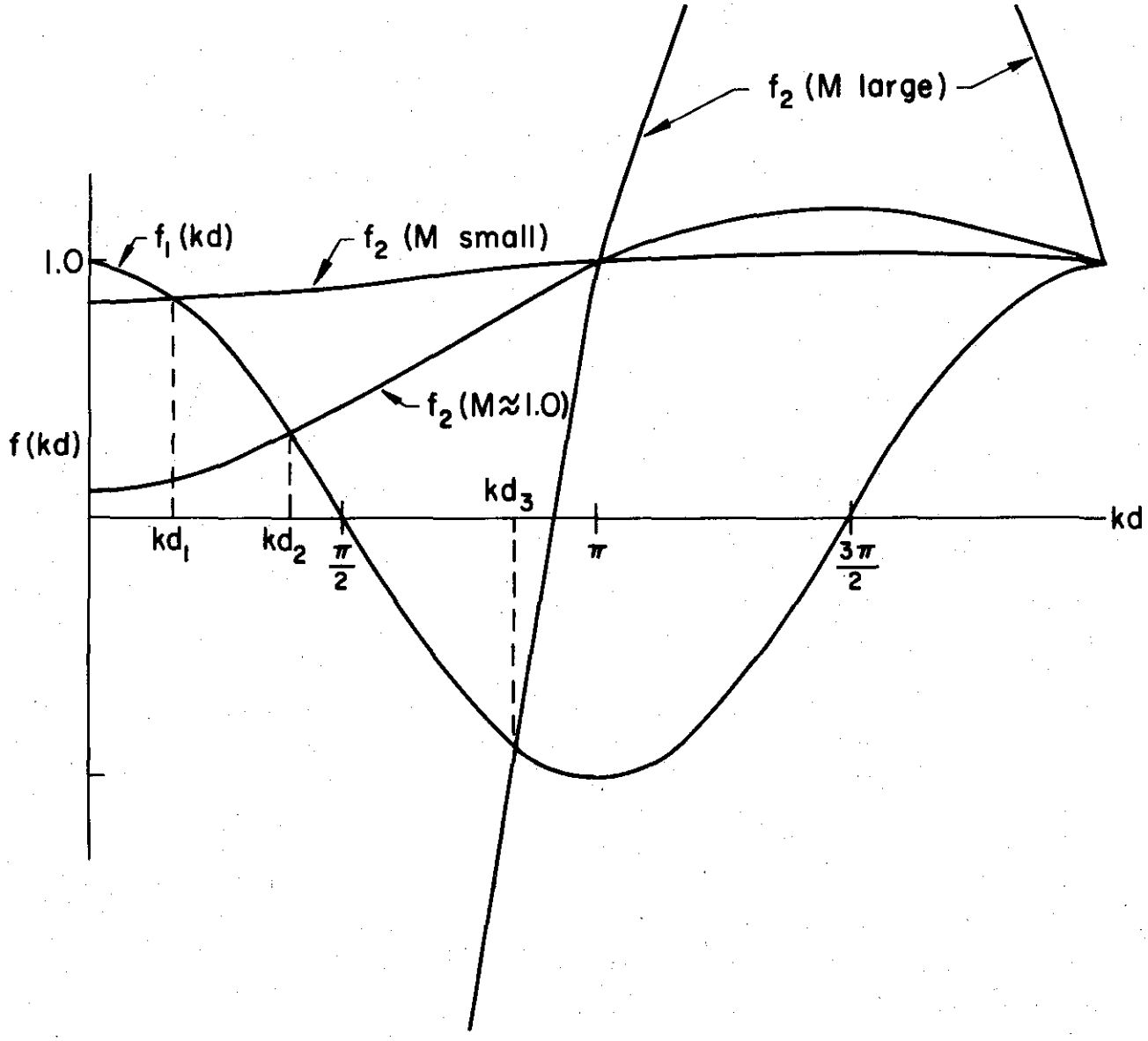

Figure 18. Location of upper limit of low frequency stopband as determined by parameter $M = \frac{d}{2cCZ_c}$ or $\frac{d}{2cLY_c}$.

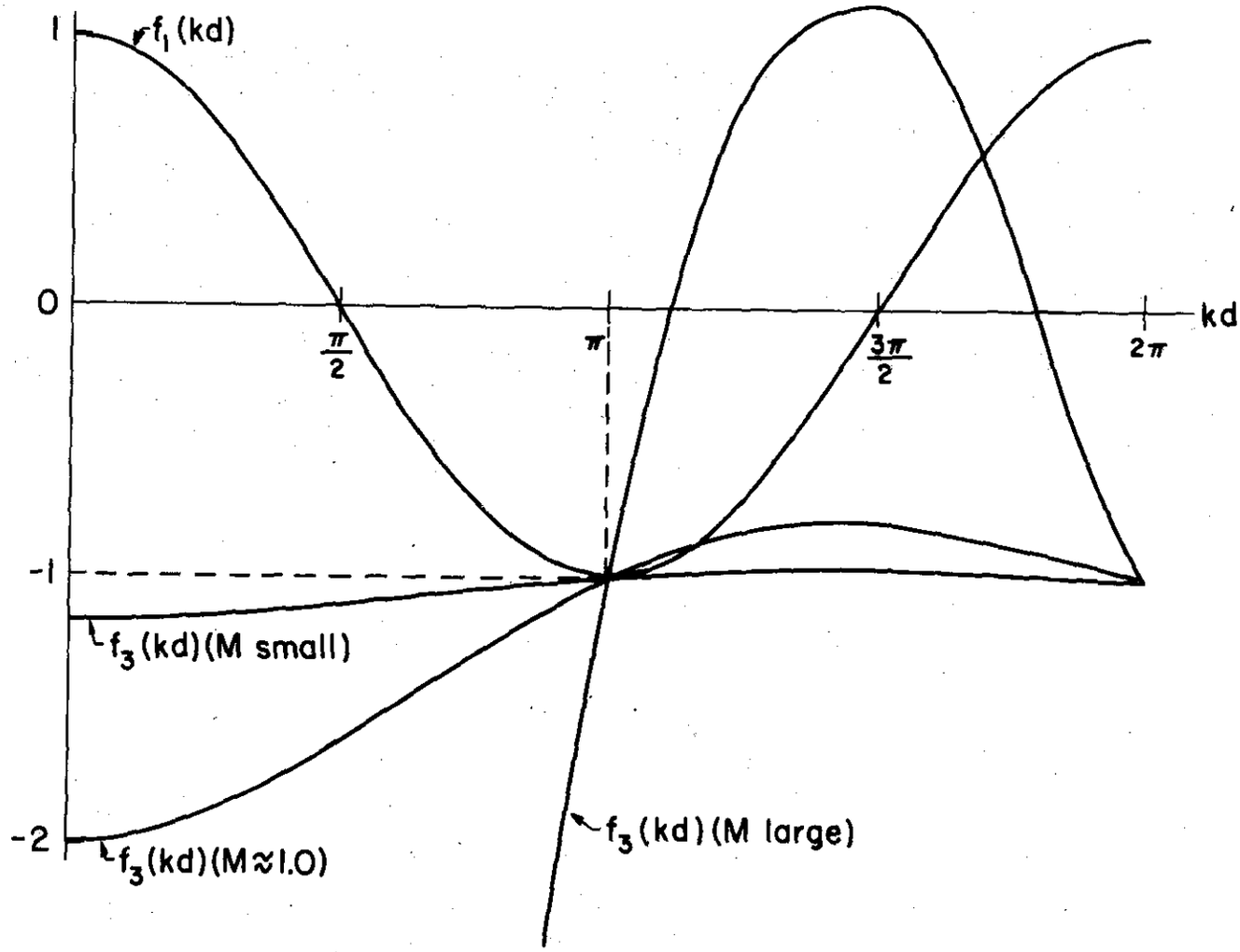

Figure 19. Plots of $f_1(kd) = \cos kd$ and $f_3(kd) = -1-M\frac{\sin kd}{kd}$ showing the intersections which determine the lower and upper limits of the second stopband for case of series capacitive or shunt inductive loading.

$$N_L = \frac{cL}{2dZ_c} \qquad N_C = \frac{cC}{2dY_c}$$

Hence, in this case,

$$\cosh \gamma d = \cos kd - N\, kd \sin kd = G(kd) \tag{82}$$

For small kd

$$G(kd) \approx 1 - (N + 1/2)\,(kd)^2 \tag{83}$$

and the low frequencies correspond to a passband in this case. The lower edge of the first stopband is given by

$$G(kd) = -1$$

Figure 20 shows the curves $f_1(kd)$ and $f_4(kd) = -1 + N\, kd \sin kd$ intersecting at the lower edge of the first stopband. For small N the stopband begins just below $kd = \pi$, for N of order unity, the lower limit of the stopband is about $kd = \pi/2$ and as N increases the lower limit approaches kd = 0. The upper limit of the stopbands are given by

$$G(kd) = \pm 1$$

occur at $kd = n\pi$. Stopband widths are governed by N and increase for higher order.

The foregoing points are illustrated in the kd-βd plots shown in Figures 21 and 22. The first shows calculated dispersion data for the case series capacitive loading for which M = 1/3, 2/3 and 4/3. This may, for example, correspond to putting 5 pfd capacitors in a 50 ohm line at spacings of 0.05, 0.1 and 0.2 meter. Figure 22 shows calculated data for series inductive loading with N = 15, 6 and 3 which corresponds to one μhy inductors in a 50 ohm line at spacings of 0.2, 0.5 and 1 meter.

Using series reactive loading of the foregoing types in log-periodic fashion has only recently been investigated and so far there is little data available. However, some success in achieving frequency stability in impedance of a high efficiency, long wire antenna using log-periodic series capacitors has been reported.[38] There are many successful log-periodic antennas that have been extensively investigated, however, which can be approximately analyzed by allowing the reactive loads of Figure 16 to become resonant circuits.[39,40]

It is well known that the impedance characteristics of linear dipole antennas are very similar to those of open transmission line sections.

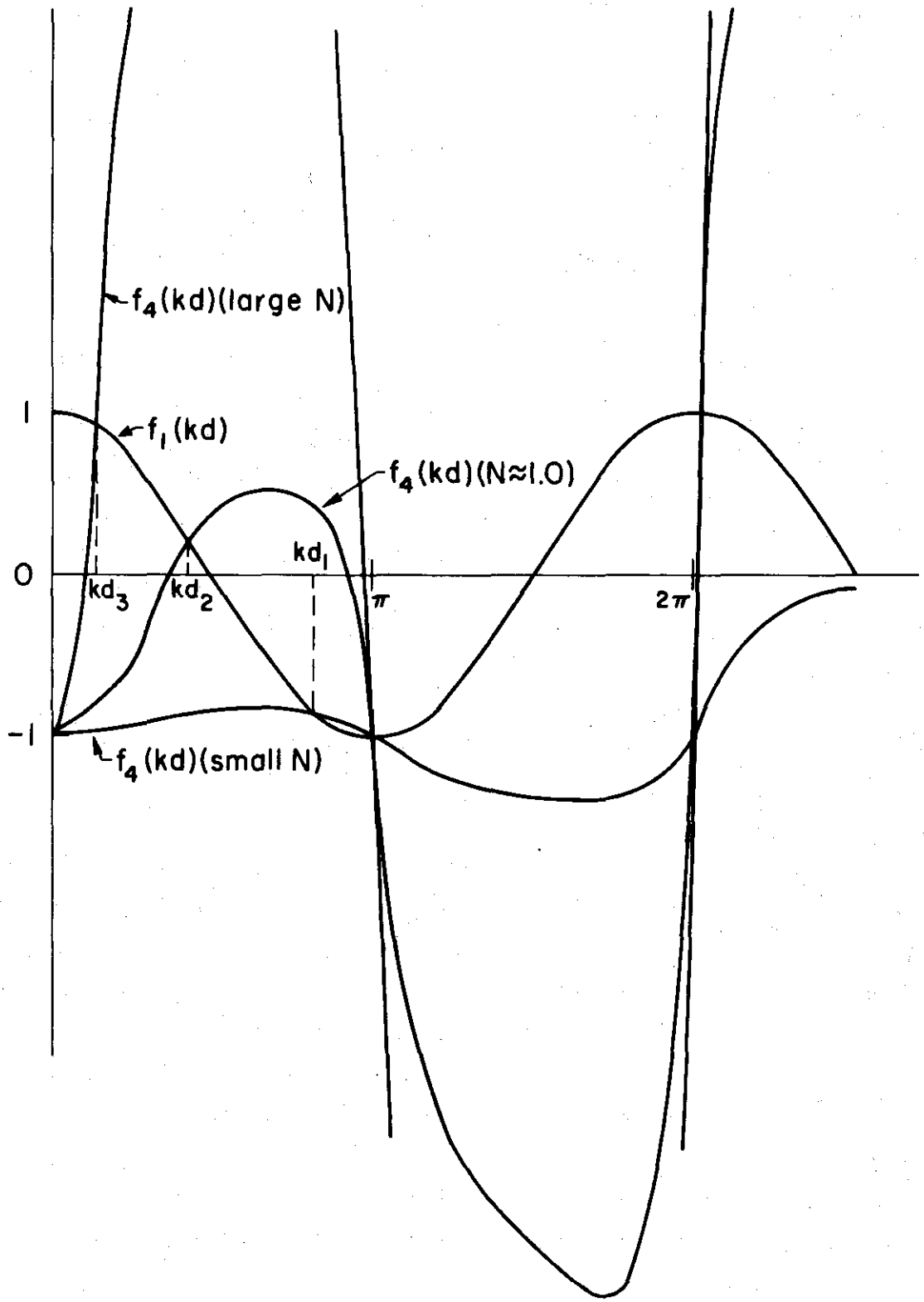

Figure 20. Plots of $f_1(kd)$ and $f_4(kd) = 1+Nkd \sin kd$ showing the intersections which determine the limits on the first stopband for series inductive or shunt capacitive loading.

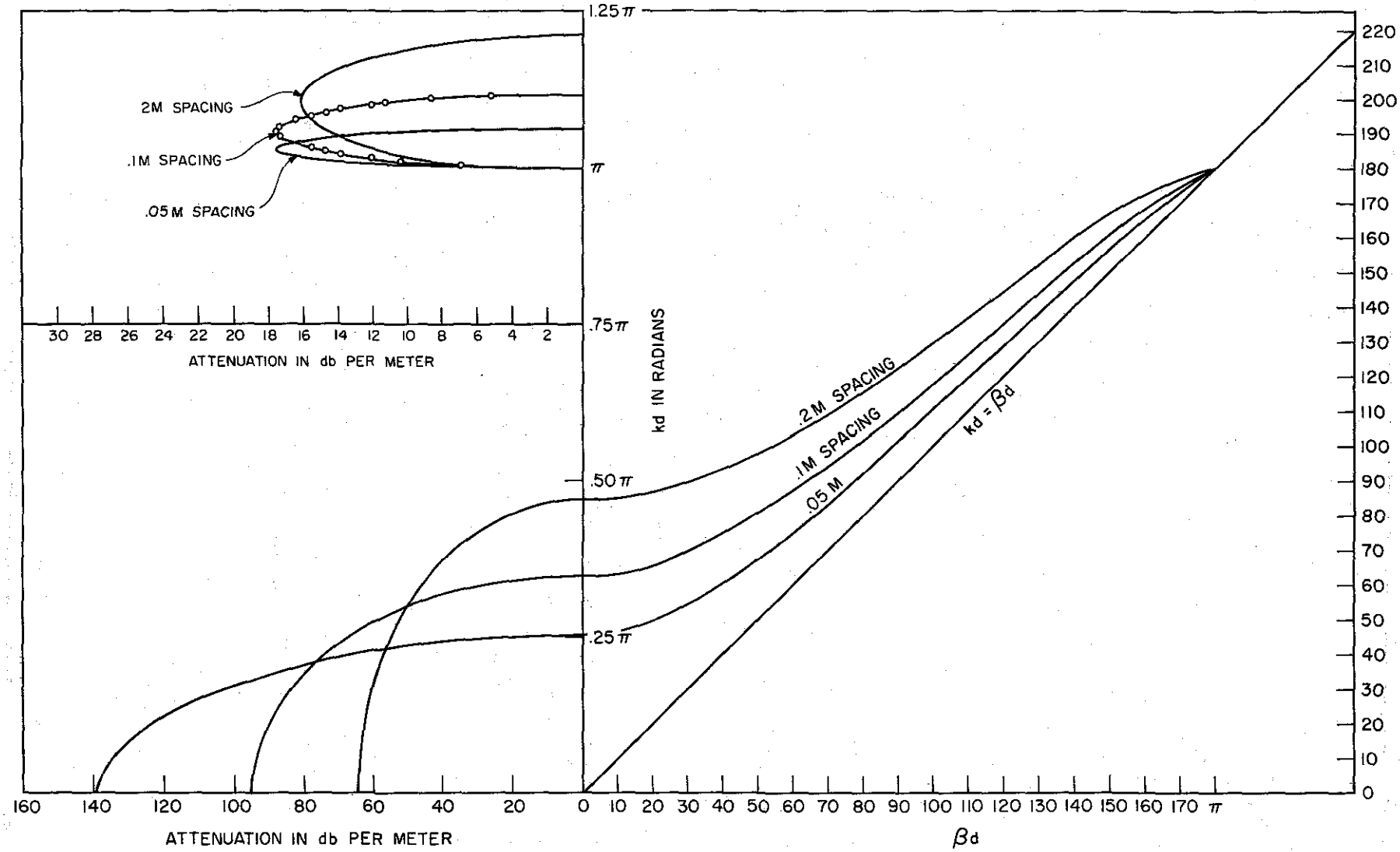

Figure 21. Calculated kd-βd plots for the series capacitive loading cases where M = 1/3, 2/3 and 4/3.

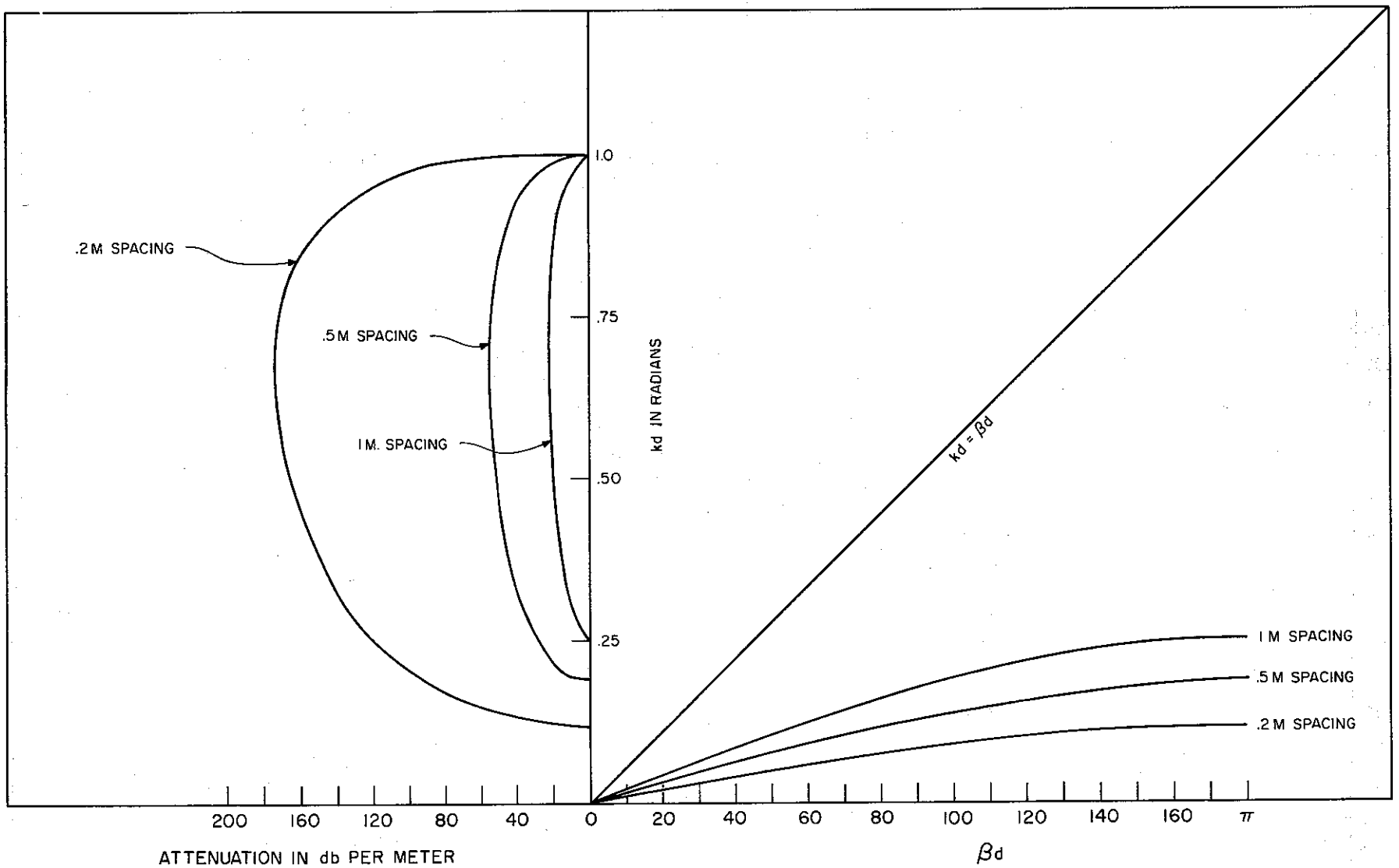

Figure 22. Calculated kd-βd plots for the series inductive loading cases where N = 15, 6 and 3.

It is instructive, therefore, to consider the k-β diagrams for transmission lines which are periodically loaded with transmission line stubs, as shown in Figure 23 and seek a correspondence between this model and periodic and log-periodic arrays of dipoles. A series resistor is introduced in the stubs to simulate the radiation loss of the dipole. The parameters of such a system are now composed of the period, d, the stub length, L, the characteristic impedance of the feeder Z_0, the characteristic impedance of the stubs, Z_s, and the series resistance, R_s. It is apparent, of course, that this simple transmission line model does not include the effects of field coupling between dipoles.

Equation 70 can be readily solved on a digital computer for the model described in Figure 23. Figure 24 shows a number of k-β plots as the value of R_s is varied from 0 to 73 ohms. The stub length was chosen so that the first resonance occurs at 275 Mc. Note that a stopband occurs near 250 Mc. When $R_s = 0$, the phase shift in the lower part of the stopband is constant with frequency at a value of π radians per cell. This value corresponds to the result which was obtained in the case of the periodically loaded waveguide and reactance-loaded lines. As R_s is increased, however, the maximum penetration of the k-β curve to the right decreases until for the case $R_s = 73$ ohms the maximum phase shift in the stopband is less than 7/10 radian per cell. Note also that the attenuation in the stopband decreases as the value of R_s increases. However, even though there is attenuation at all frequencies due to the loss in the resistors, the attenuation reaches a maximum in the stopband.

Significant difference between the k-β plots of the stub-loaded transmission line and those of the iris-loaded waveguide or reactance loaded lines is produced by the resonant nature of the loading in the former case. The sign reversal on the reactance of the loading which occurs at resonance produces a rapid change in the phase shift near that frequency. In the lossless case, the k-β plot is seen to reverse direction abruptly at 275 Mc. Whereas the phase shift in the stopband below 275 Mc is fixed at a value of π radians per cell, above the resonant frequency the phase shift corresponds to zero throughout the remainder of the stopband. Although the effect of losses is such to change the abruptness of the cutback in the curve, the effect nevertheless remains observable for all values of R_s.

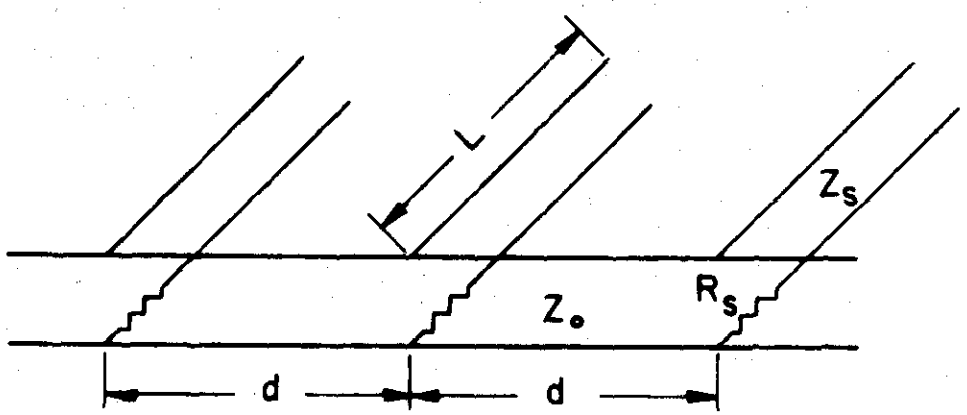

Figure 23. **Transmission line periodically loaded with resistor-stub elements.**

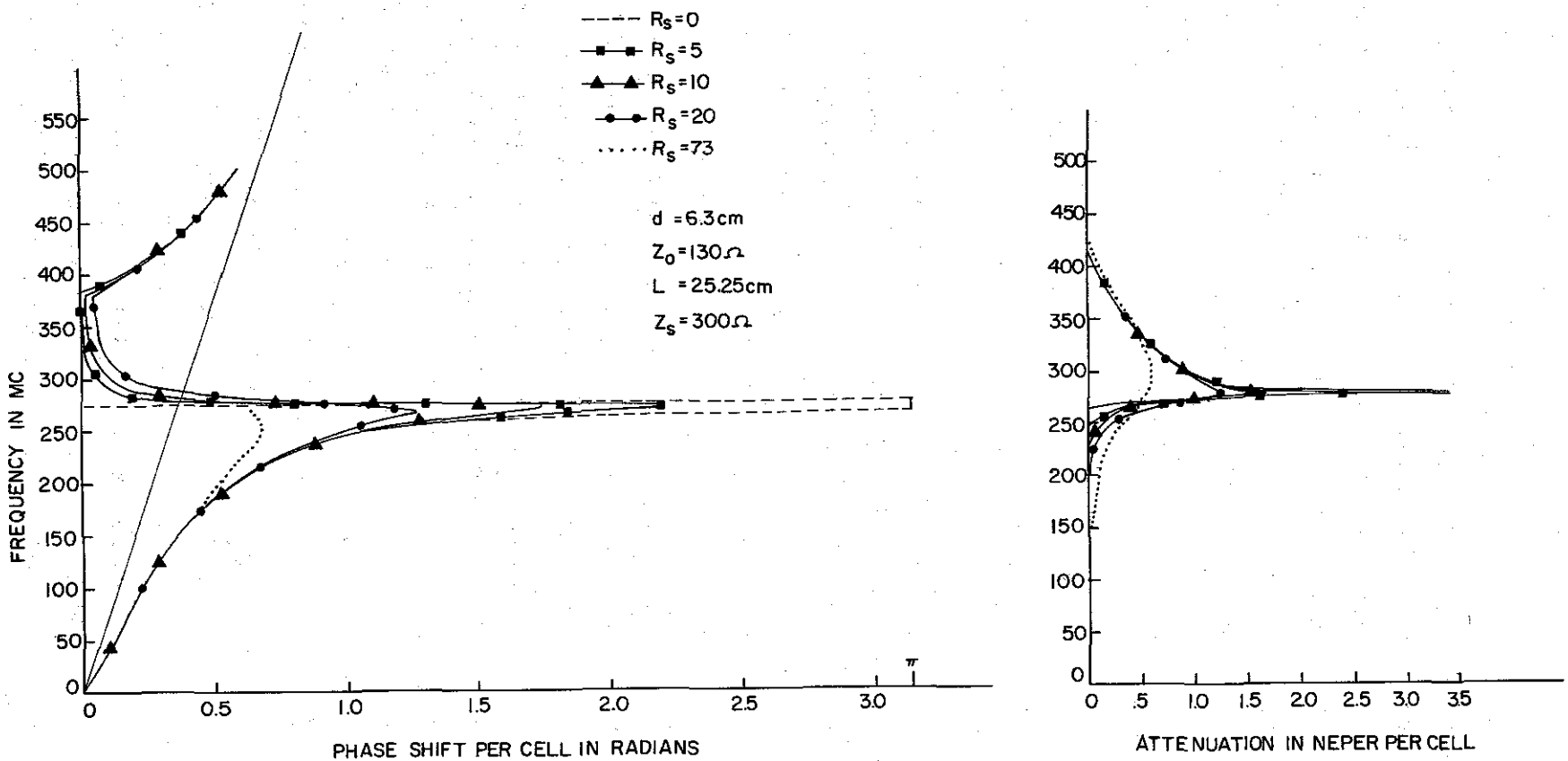

Figure 24. Dispersion diagram for transmission line which is periodically loaded with sections of lossy line showing dependence upon loss resistance.

A set of calculated k-β plots for the stub-loaded line showing the variation as the characteristic impedance of the stub is changed is given in Figure 25. In this case the resistance R_s is held fixed at a value of 10 ohms and it is to be noticed that the maximum phase shift corresponding to this value of R_s is changed very little by changes in the value of Z_s. It is also noted that the maximum attenuation is affected very little by changes in Z_s. However, the frequency span of the complex wave region where there is appreciable attenuation is dependent upon Z_s, being largest for the smallest value of Z_s.

It is apparent from the data shown in Figures 24 and 25 that the maximum phase shift in the complex wave region (which corresponds to the stopband in the lossless case) is governed by the value of R_s. This is also true of the maximum value of attenuation. Figure 25 and Equation (70) show that the frequency span of the complex wave region as before, is governed by the relative value of the stub to transmission line feeder characteristic impedance. Both of these factors have important consequences in the design of log-periodic antennas, which will be considered in greater detail later.

The k-β plots shown in Figures 24 and 25 correspond to periodic elements which are very closely spaced in terms of the wavelength, being approximately 0.06λ apart at the resonant frequency of the stubs. This close spacing was chosen to correspond to a laboratory model of a uniformly periodic dipole array which was designed to simulate the conditions of the active region of a log-periodic dipole array. Such close-spaced elements are not uncommon in log-periodic antennas. Although they may not give rise to optimum gain, they do result in a compact antenna.

Nevertheless, it is instructive to also consider how the k-β plots are affected by increased spacing between the reactive loads. Figure 26 shows computed k-β plots for $Z_s = 300$, $R_s = 10$, $Z_o = 130$, (stub length $L = 27.25$ cm) for various values of spacing between stubs. As could reasonably be expected, the maximum phase shift is greatest for the dipoles which are separated by the greatest distance. However, there is sizeable departure from the result which would be obtained by assuming the wave travels with free-space velocity along the line. The β=k line is shown for $d = 27.25$ cm for comparison. Figure 27 shows computed dispersion

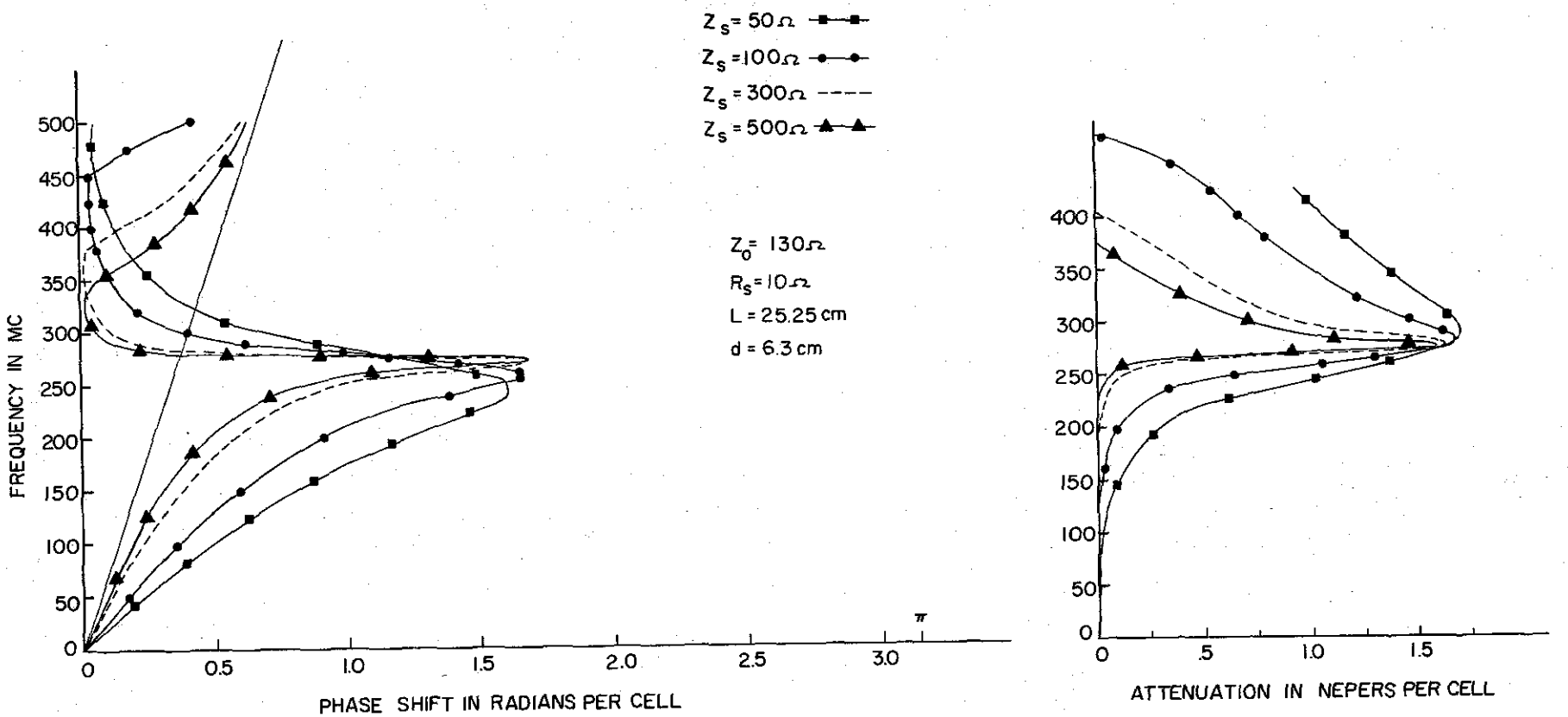

Figure 25. Dispersion diagram for transmission line which is periodically loaded with sections of lossy line showing dependence upon characteristics impedance.

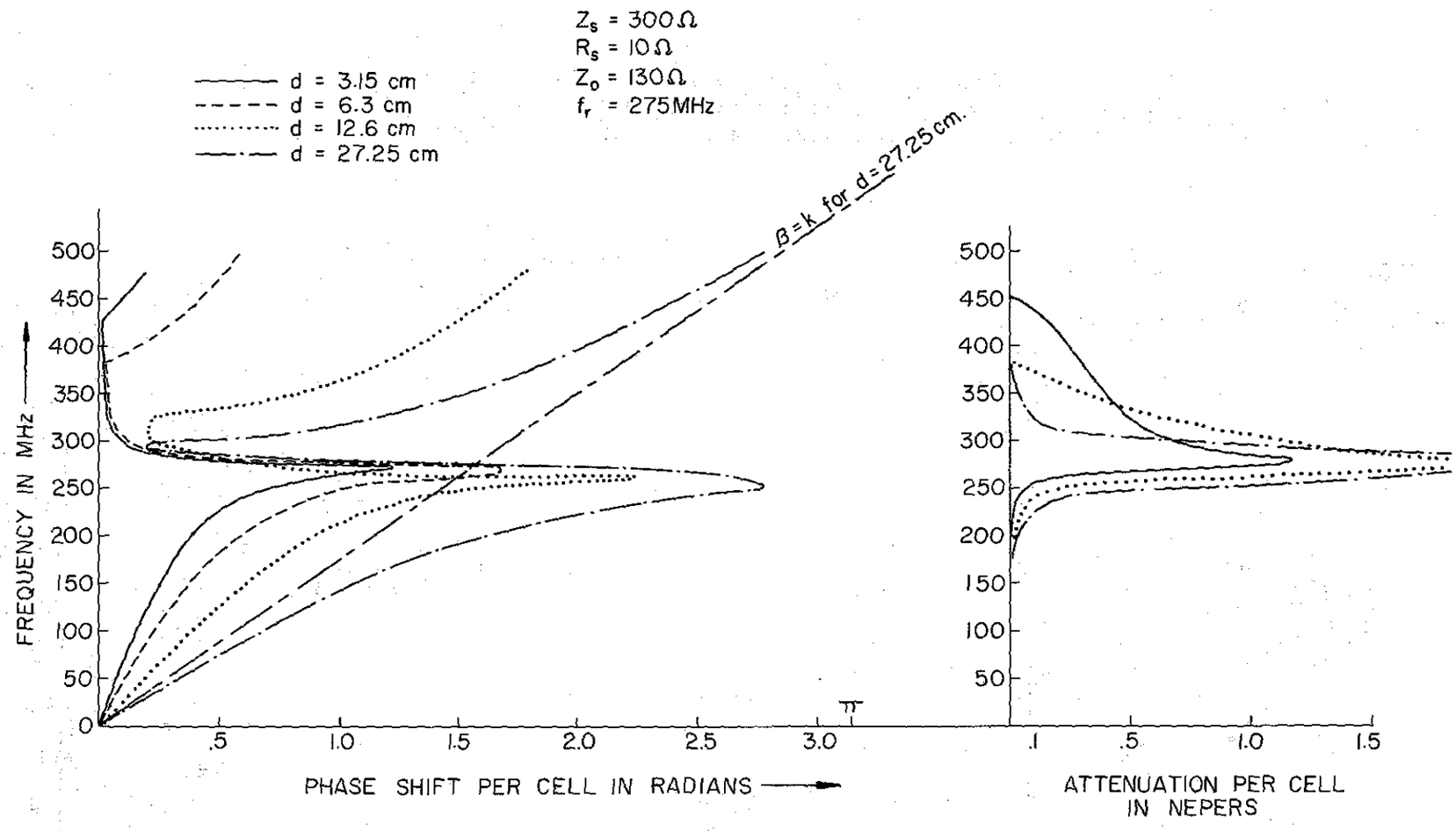

Figure 26. Dispersion data for transmission line which is periodically loaded with sections of lossless line showing dependence upon characteristic impedance of line.

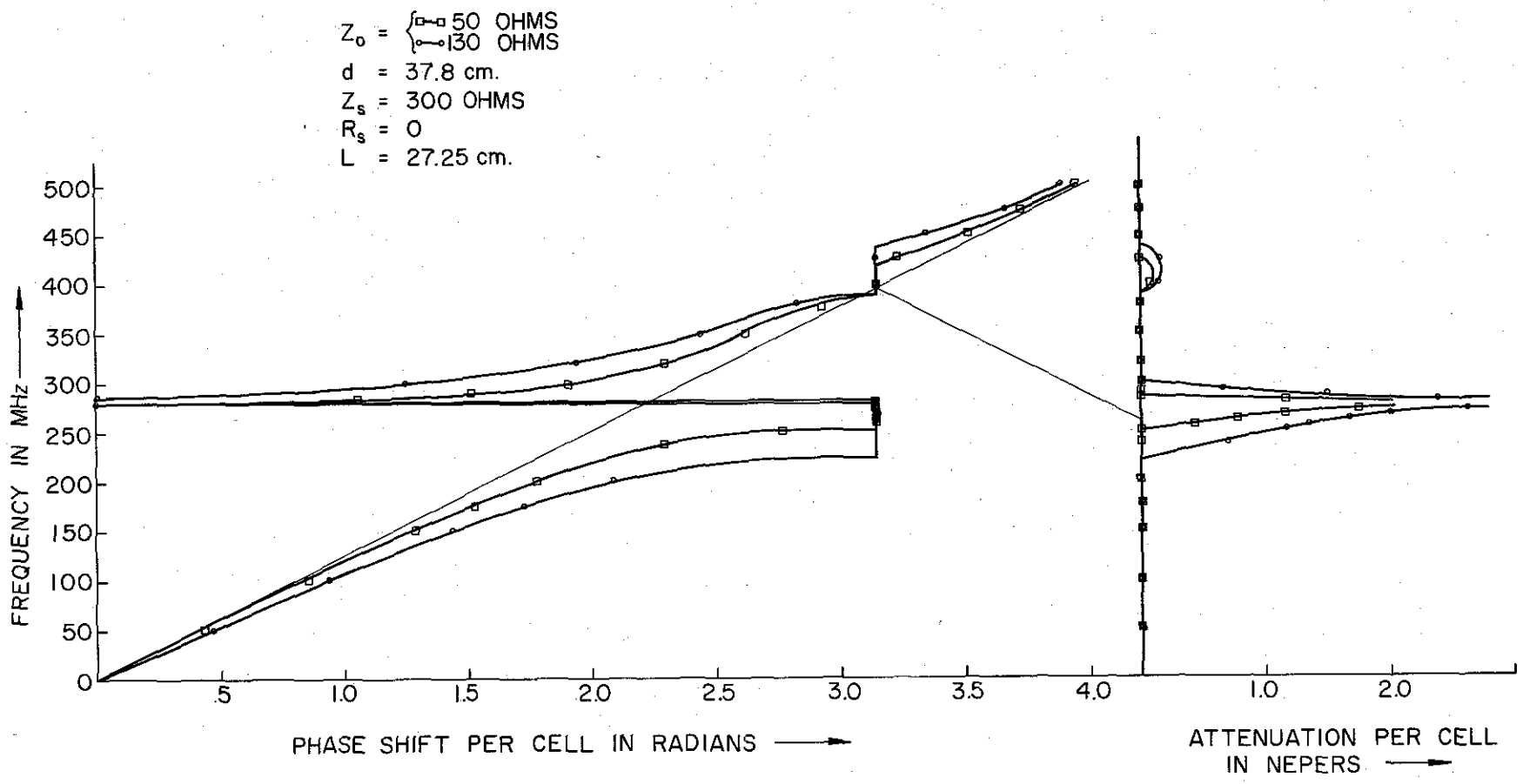

Figure 27. Dispersion data for transmission line which is periodically loaded with sections of lossless line showing dependence upon characteristic impedance of line.

data for the stub-loaded line when d has been increased to 37.8 cm. Two values of characteristic impedance are illustrated, Z_o = 50 ohms and 130 ohms. The calculations are extended in frequency through and past the second stopband. The stub resistor was omitted in both cases. Once again it is seen that the width of the stopbands is dependent upon the relative characteristic impedances of the stubs and feeder.

As noted before, the loss in the stub tends to decrease the perturbation in the dispersion curve. An extreme case is shown in Figure 28 where the value of R_s has been increased to 73 ohms for values of Z_o of 50 and 130 ohms and stub impedance Z_s of 300 ohms. In this case, the reversal in direction of the dispersion curve at resonance does not occur and shows only slight perturbations in the region near resonance where the stopband would ordinarily occur. Note also the double-humped characteristic of the attenuation curve in this case.

Of the foregoing data, Figures 24 and 25 represent most closely the type of conditions found in a typical log-periodic array of resonant dipoles. The succeeding plots indicate that a wider variation in amplitude and phase characteristics is available through variation of parameters and suggests that antennas with characteristics quite different from the early log-periodic arrays may be feasible. Further investigations directed toward employing a wider variety of parameters in log-periodic antenna design, therefore, are deemed appropriate and the utilization of both calculated and experimental dispersion data would appear to be quite useful in these efforts. However, there certainly exist limitations in the applicability of the dispersion data for uniform periodic structures of the closed type considered up to this point when considering structures which are open and also log-periodic. Further discussion of these limitations is contained in the following section.

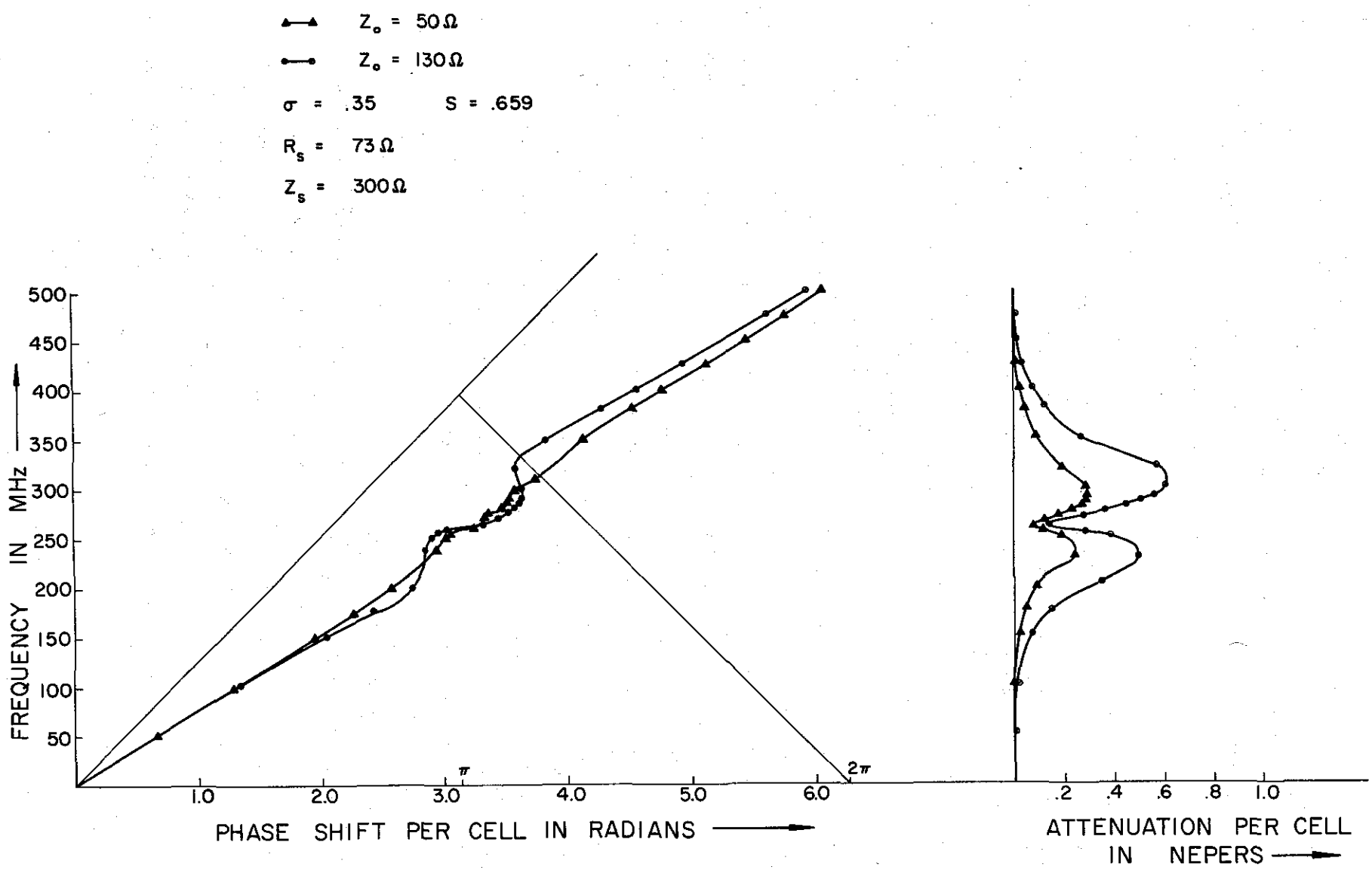

Figure 28. Dispersion data for transmission line which is periodically loaded with sections of lossy line showing reduced effect achieved with large values of loss resistance and stub impedance.

PART III

DETERMINATION OF DISPERSION CHARACTERISTICS OF OPEN PERIODIC AND LOG-PERIODIC STRUCTURES

3.1 Introduction

Many log-periodic antennas can be explained in terms of the idealized model considered in the previous section. This model consists of a transmission line with lumped series impedance Z_L, or shunt admittance Y_L, or both. In open structures the model previously considered may not be adequate due to the field coupling between cells. It is thus desirable to consider a new model which accounts for the field coupling by considering the mutual impedance between cells. In order to relate this model to the previous chapters on periodic structures and the k-β diagram, we start with the periodic version of the model and derive the equation for propagation constant, β. An approximate solution for the k-β diagram is obtained and this is related to the k-β diagram of a transmission line with distributed but nonuniform series impedance, shunt admittance, or both. An approximate solution for the nonuniform line is obtained, and an approximate solution for the space harmonics is also obtained. It is shown that at most one pseudo traveling wave and its associated reflected pseudo wave may be present on the structure and still have the voltage and current scale continuously with frequency. This condition is vital to the success of a log-periodic structure as a frequency independent antenna.

3.2 Periodically Loaded Transmission Lines

Figure 29 shows a periodically loaded line with coupling between cells. A current generator is connected to each mode. The normal modes that may exist on the structure are obtained by setting the driving functions I_n to zero and also using Floquet's theorem described in Part I. However, the matrix equation describing the open network shown in Figure 29 is complicated by the addition of mutual admittances to account for the field coupling from cell to cell. Thus, we have

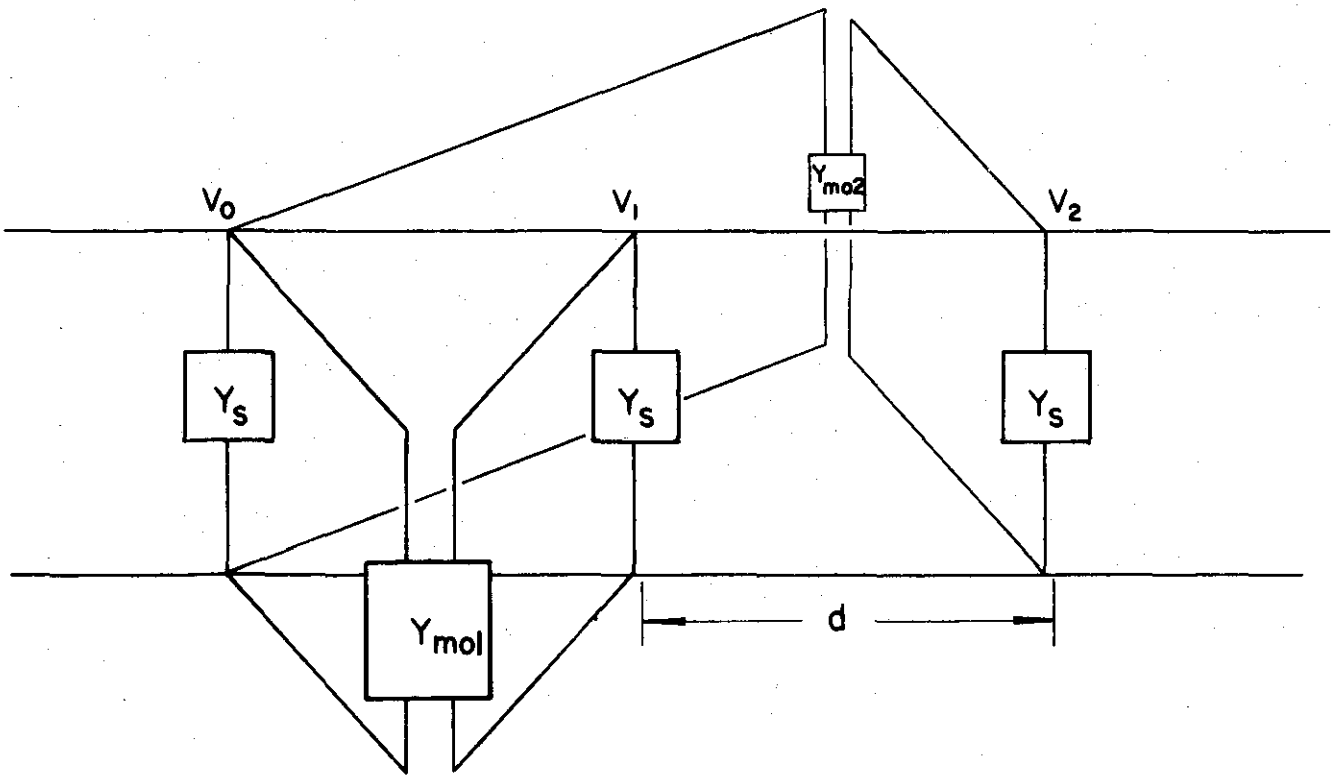

TRANSMISSION LINE LOADED PERIODICALLY WITH SHUNT ELEMENTS Y_s AND MUTUAL ADMITTANCES Y_{moi}.

Figure 29. A periodically-loaded line with coupling between cells.

$$\begin{bmatrix} \vdots \\ I_{-2} \\ I_{-1} \\ I_0 \\ I_1 \\ I_2 \\ \vdots \end{bmatrix} = \begin{bmatrix} \cdots & \vdots & \vdots & \vdots & \vdots & \vdots & \cdots \\ \cdots & Y_{-2-2} & Y_{-2-1} & Y_{-20} & Y_{-21} & Y_{-22} & \cdots \\ \cdots & Y_{-1-2} & Y_{-2-1} & Y_{-10} & Y_{-11} & Y_{-12} & \cdots \\ \cdots & Y_{0-2} & Y_{0-1} & Y_{00} & Y_{01} & Y_{02} & \cdots \\ \cdots & Y_{1-2} & Y_{1-1} & Y_{10} & Y_{11} & Y_{12} & \cdots \\ \cdots & Y_{2-2} & Y_{2-1} & Y_{20} & Y_{21} & Y_{22} & \cdots \\ & \vdots & \vdots & \vdots & \vdots & \vdots & \end{bmatrix} \begin{bmatrix} \vdots \\ V_{-2} \\ V_{-1} \\ V_0 \\ V_1 \\ V_2 \\ \vdots \end{bmatrix} \tag{84}$$

where I_n and V_n are, respectively, the current and voltage at the nth input port. The matrix elements Y_{mn} can be interpreted as the ratio of current at port m(I_m) due to a unit voltage generator at port n with all other ports short-circuited. In this case, all generators will contribute due to field coupling although many terms may be small due to large distance of separation between ports.

Consider the equation for I_o which is

$$I_0 = \cdots Y_{0-2} V_{-2} + Y_{0-1} V_{-1} + Y_{00} V_0 + Y_{01} V_1 + Y_{02} V_2 + \cdots \tag{85}$$

Y_{00} is the input admittance at the zeroth port with the other ports shorted so that $V_n = 0$, $n \neq 0$. Hence, Y_{00} is given by

$$Y_{00} = Y_s + \sum_{i=-\infty}^{\infty} Y_{moi} - 2j\, Y_o \cot kd \tag{86}$$

Y_s is the admittance of each shunt element, $Y_{st} = -j\, Y_0 \cot kd$ is the admittance of each of the shorted lines of length d extending away from the zeroth port and Y_{moi} is the mutual admittance between ports zero and i. The characteristic admittance of uniform transmission lines is Y_0, and it is assumed that the propagation constant on the uniform line is the free-space wave number, k. The term Y_{01} can be obtained in a similar manner since

$$Y_{01} = \frac{I_0}{V_1} \quad \text{with } V_n = 0 \qquad n \neq 1 \tag{87}$$

where I_0 is the short circuit current at port zero of the transmission line with voltage V_1 applied at port one, plus the short circuit current at

port zero due to the mutual coupling with voltage V_1 applied to port one. The transmission line portion of Y_{01} is given by

$$Y_\ell = j\, Y_0 \csc kd \tag{88}$$

The mutual part depends on the type of open cell loading the transmission line. However, for small kd, $j\, Y_0 \csc kd$ is very large and the mutual term may be negligible in comparison, so that

$$Y_{01} \approx j\, Y_o \csc kd \tag{89}$$

The above approximation cannot be made for the remaining Y_{oi} terms as the transmission line portion is no longer present.

From Floquet's theorem we have that $\frac{V_{n+1}}{V_n} = e^{-j\beta d}$. Since the normal modes of the system correspond to source-free conditions, we set I_o to zero, and Equation (85) reduces to

$$0 = \cdots Y_{0-2}\, e^{j^2\beta d} + Y_{0-1}\, e^{j\beta d} + Y_{00} + Y_{01}\, e^{-j\beta d} + Y_{02}\, e^{-j^2\beta d} + \cdots \tag{90}$$

Since by symmetry $Y_{o-n} = Y_{on}$, Equation (90) can be put in the following form:

$$j2Y_0 \cos \beta d \csc kd \approx j2Y_0 \cot kd - \left[Y_s + 2 \sum_{n=2}^{\infty} Y_{on} \cos n\beta d + \sum_{i=-\infty}^{\infty} Y_{moi} \right] \tag{91}$$

Comparing with the standard form of a transmission line loaded periodically with lumped loading circuits, as determined in Part II,

$$\cos \beta d \approx \cos kd + \frac{jY_L}{2\, Y_0} \sin kd \tag{92}$$

we see that Equation (91) is of the same form where

$$Y_L = Y_s + 2 \sum_{n=2}^{\infty} Y_{on} \cos n\beta d + \sum_{i=-\infty}^{\infty} Y_{moi} \tag{93}$$

The equation for the k-β curve for the transmission line periodically loaded with lumped series elements with coupling between cells may be derived in a similar manner and the solution is given by

$$\cos \beta d \approx \cos kd + j \frac{Z_L}{2 Z_o} \sin kd$$

where

$$Z_L = \frac{1}{\frac{1}{Z_s} + \sum_{i=-\infty}^{\infty} \frac{1}{Z_{moi}}} + 2 \sum_{n=2}^{\infty} Z_{on} \cos n\beta d \qquad (94)$$

where Z_s is the impedance of each series element and Z_{moi} is the mutual impedance between ports 0 and i.

The procedure for obtaining the equation for the k-β curves for lines with both series and shunt elements periodically placed as shown in Figure 30 is identical. However, the assumption can be made that Y_L already includes the coupling effects. The only difficulty introduced is then the determination of Y_{00} and Y_{01}. The equation for Y_{00} is given by

$$Y_{00} = Y_L + Y_{inL} + Y_{inR} \qquad (95)$$

where Y_{inL} is the input admittance looking to the left with the n=-1 port shorted, and Y_{inR} is the input admittance looking to the right with the n=+1 port shorted. The equation for Y_{00} is, therefore,

$$Y_{00} = \frac{Y_0 \cos kd \,(2 + Z_L Y_L) + j \sin kd \,(Y_L + Y_0^2 Z_L)}{Y_0 Z_L \cos kd + j \sin kd} \qquad (96)$$

and Y_{01} is given by

$$Y_{01} = - \left[Z_L \cos kd + j Y_0 \sin kd \right]^{-1} \qquad (97)$$

After a few algebraic manipulations the dispersion relation can be put in the following form

$$\cos \beta d \approx \left(1 + \frac{Z_L Y_L}{2} \right) \cos kd + j \left(\frac{Y_L}{2Y_0} + \frac{Z_L}{2Z_0} \right) \sin kd \qquad (98)$$

It can easily be seen that Equations (92) and (94) are special cases of (98).

For the periodic structures the k-β diagram represents the variation of β as frequency is changed on a structure with fixed d. In the log-periodic

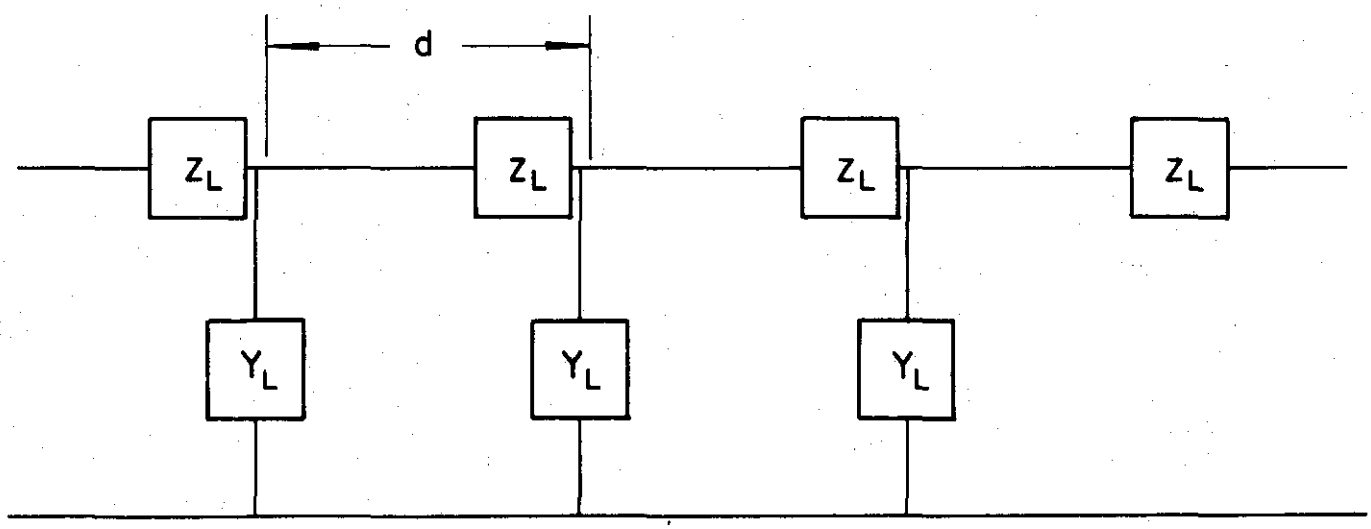

TRANSMISSION LINE LOADED PERIODICALLY WITH SERIES ELEMENTS Z_L AND SHUNT ELEMENTS Y_L.

Figure 30. A line periodically loaded with both series and shunt elements.

case, d becomes variable. For the information contained in the k-β plot for a periodic structure to be applicable to the corresponding log-periodic structure at a single frequency a change in d must be equivalent to a change in k. In order to investigate this requirement further, consider once again the shunt-loaded case.

If a change in d is equivalent to a change in k then Y_L must be a function of the product kd, and the effect of mutual coupling upon Y_L must be independent of the taper angle. If Y_L is such a function, then the kd-βd diagram obtained from the periodic structure may be applied exactly to the LP structure. This restriction is not as severe as it first appears since all geometrical shapes whose dimensions are proportional to d will have this property provided mutuals are not important. However, the dispersion curves yield no information about the relative amplitudes of the various space harmonics. From this, one can see that the equivalence is not exact for arbitrary periodic structures. The kd vs βd curves for the periodic and log-periodic structures will not be the same in the region where distant mutuals are important on the periodic structure. For example, the mutual impedance terms in a periodic array of linear dipoles are insignificant when the frequency is considerably below the half-wave resonant frequency of the elements. Therefore, the kd-βd diagrams of the periodic and log-periodic structures will be almost identical in this region. However, in the frequency region near the half-wave resonance of the dipoles on the periodic array the mutual terms from elements several periods away are significant. In the tapered version these mutual terms are considerably influenced by the change in the distant element length; consequently, one should not expect an exact correspondence of the kd vs. βd curves in this region. This is most unfortunate as it is the region near dipole resonance that is of most interest on the log-periodic dipole array.

From the above one can conclude that there is an exact correspondence of the kd-βd diagram of the periodic structure and the kd-βd diagram of the LP structure only if the propagation constant is determined by the local behavior of the structure. However, if the angle of taper is small enough and $\tau \approx 1$ for the LP case, then the dispersion curves for the uniform periodic and log-periodic are approximately the same in all regions.

Next we will obtain an approximate solution for the propagation constant of (92) and derive the relationships between the propagation constants on periodic, log-periodic and continuously scaled structures.

If the spacing d is $\leq \lambda_g/10$, where λ_g is the wavelength on the transmission line, Equation (92) can be approximated by keeping the first two terms of the cosine series and the first term of the sine series. Then the approximate equation is

$$1 - 1/2\ (\beta d)^2 = 1-1/2\ (kd)^2 + j\ \frac{Y_L}{2Y_o}\ kd$$

and

$$\left(\frac{\beta}{k}\right)^2 \approx 1 - j\ \frac{Y_L}{Y_0\ kd} \tag{100}$$

If Y_L is a smooth function of frequency one can make the further approximation that Y_L/d is a continuous and distributed function. This allows the interpretation that a continuous change in frequency is equivalent to a continuous change in d or the position on the structure. Before proceeding further with this result, a nonuniform but continuously scaled transmission line will be investigated.

It has been established by Mittra and Jones[39] that the voltage and current on a nonuniform transmission line will scale as a continuous function of frequency if the admittance per unit length is of the form f(kx)/x or k f(kx). If one chooses the admittance per unit length on the nonuniform line as $j\omega C + \frac{Y_L(kx)}{(1-\tau)X}$, then the differential equation for the voltage along the transmission is given by

$$V'' + (k^2 - j\ \frac{\omega L\ Y_L}{(1-\tau)X})\ V = -\ j\omega L\ \ \delta(x-x_o) \tag{101}$$

$$V'' + (k^2 - j\ \ \frac{k\ \ Y_L}{(1-\tau)Y_o X}\ )\ V = -j\omega L\ \ \delta(x-x_o) \tag{102}$$

Notice that the transmission line must be infinite and $x_o = 0$ if the voltage is to scale in a continuous manner. However, if there is a region of large attenuation on the transmission line, the continuous scaling property will not be greatly perturbed by truncation past the attenuation.

Next define a new variable $z = kx$. Now (102) can be rewritten as

$$\frac{d^2V}{dz^2} + (1-j\ \frac{Y_L}{(1-\tau)Y_o z})\ \ V = -j\ Z_0 L\ \ \delta(z-z_o) \tag{103}$$

where it has been recognized that $\frac{-j\omega L}{k^2}\ \delta(\frac{z}{k} - \frac{z_o}{k}) = -jZ_0\ \delta(z-z_o)$ and Z_0 is the characteristic impedance of the unloaded line. From (103) it can be seen that the position of excitation, x_o, must be scaled if the voltage is to be a function of the product kx. For an arbitrary input signal the frequency components must be restricted such that $kx_o \ll 1$ for all frequencies of interest. This implies that x_o must be small in comparison to the shortest wavelength of interest.

It can be seen from (103) that $(\beta/k)^2$ on the nonuniform line is identical to the approximate $(\beta/k)^2$ given by (100). The properties of (103) were studied by Mittra and Jones[39] for a Y_L of the form

$$[R + j(\omega L_1 x - 1/\omega C_1 x)]^{-1}$$

and

$$[R\,\omega^2 x^2 + j\,(\omega L_1 x - 1/\omega C_1 x)]^{-1} \tag{104}$$

The forms given by (104) were chosen because they are a reasonable representation of the dipole loads on the log-periodic dipole array. It was found that the WKB[2,3] approximate solution of (103) is fairly accurate if the Q of the series resonant circuit given by (104) is on the order of 10 or less. For the series circuits Q is defined as $\omega L_0/R_0$, where

$$x_\phi = \left[\omega^2 L_1 C_1\right]^{-1/2}$$

$$L_o = L_1 x_1$$

$$R_o = R \text{ or } R\,\omega^2 x_1^2$$

The approximate solution of (103) is given by

$$V(k,x) = V(z_0) \left[\frac{\gamma(z_0)}{\gamma(z)}\right]^{1/2} e^{-j \int_x^z \gamma(y)\, dy} \tag{105}$$

where γ is defined as β/k. Notice that it is β/k which is a function of z only.

If x_o is small in comparison to the wavelength, there is little error introduced by assuming that $x_o = 0$. If x_o is small enough to make this

assumption accurate, then V(k,x) is a function of the product kx = z, and V(kx) is given by

$$V(z) = V(0)\left[\frac{\gamma(0)}{\gamma(z)}\right]^{1/2} e^{-j\int_0^z \gamma(y)\,dy} \tag{106}$$

The solution expressed in Equation (106) is valid when the local reflections are small. A general second-order equation of the form given by

$$\frac{d^2V}{dz^2} + \gamma^2(z)V = 0 \tag{107}$$

may be separated into two coupled first-order equations[40,41] given by

$$dV_1/dz + (j\gamma(z) + \gamma'(z)/2\gamma(z))\ V_1 = \gamma'(z)\ V_2/2\gamma(z) \tag{108a}$$

$$dV_2/dz + (-j\gamma(z) + \gamma'(z)/2\gamma(z))\ V_2 = \gamma'(z)\ V_1/2\gamma(z) \tag{108b}$$

and the total solution is $V_1(z) + V_2(z)$.

Equation (104) is the solution of (108a) under the assumption that $|\gamma'(z)/2\gamma(z)| \ll 1$. The solution of (108b) may be obtained by using (104) for V_1 and then integrating the first-order differential equation. The V_2 solution represents the reflected pseudo wave and is always present even though it may be very small. If it is small (108b) can be solved by multiplying both sides by the integrating factor

$$\exp \int_{z_o}^{z} [-j\gamma(\mu) + \gamma'(\mu)/2\gamma(\mu)]\ d\mu \tag{109}$$

and integrating both sides of the equation to obtain

$$V_2(z) = [\gamma(z_o)/\gamma(z)]^{1/2} \exp\left[j\int_{z_o}^{z} \gamma(y)\ dy\right] \left\{V_2(z_o) + V_1(x_o)\int_{z_o}^{z} [\gamma'(y)/2\ \gamma(y)] \exp\left[-j2\int_{z_o}^{y} \gamma(\mu)\ d\mu\right] dy\right\} \tag{110}$$

The constants $V_1(z_o)$ and $V_2(z_o)$ must be determined by the boundary conditions at the termination points x_o and x_T. One possible condition is to insist that the wave be outgoing at x_T as x_T approaches infinity. With the above restriction, plus the restriction that the total V at $x = x_o$ be V_o, the total V is given by

$$V(z) = V_1(z_o)\ [\gamma(z_o)/\gamma(z)]^{1/2} \left\{ \exp\ [-j \int_{z_o}^{z} \gamma(y)\ dy] \right.$$

$$\left. - [\exp\ (j \int_{z_o}^{z} \gamma\ dy)][\int_{z}^{\infty} (\gamma'/2\gamma)\ [\exp(-j \int_{z_o}^{y} \gamma\ d\mu)]dy] \right\} \qquad (111)$$

where

$$V_1(z_o) = V_o/[1 - \int_{z_o}^{\infty} (\gamma'/2\gamma)\ \exp\ (-j2 \int_{z_o}^{y} \gamma\ d\mu)\ dy]$$

The input impedance of a transmission line which satisfies (111) is given by

$$Z_{in} = \frac{V(z_o)}{I(z_o)} = \frac{-zV(z_o)}{k\ V'\ (z_o)} =$$

$$\frac{-j\ Z_o[1 - \int_{z_o}^{\infty} (\gamma'/2\gamma)\ \exp\ (-j2 \int_{z_o}^{y} \gamma\ du)\ dy]}{-j\gamma(z_o) + (\gamma'(z_o)/2\gamma(z_o) - j\gamma(z_o)) \int_{z_o}^{\infty} (\gamma'/2\gamma)\ \exp\ (-j2 \int_{z_o}^{y} \gamma\ d\mu)\ dy} \qquad (112)$$

In general, the input impedance has a reactive component and is frequency independent provided $z_o = kx_o \ll 1$. This phenomena has been observed by Ingerson* and Mayes[43] on experimental antennas.

Next we will consider the case of series loading only. For this case,

$$(\beta/k)^2 \approx 1 - j\ \frac{Z_L}{Z_0 kd} \qquad (113)$$

This type of loading has been studied in some detail by R. DuHamel.* The differential equation for this case is the same as that of (103); however, in this case, the equation is for the current instead of the voltage. This type of loading may be used to explain the log-periodic folded dipole array[42] and the conical spiral antenna.[43] Mittra and Klock[44] recently derived the

*Unpublished results.

approximate current distribution on the conical spiral by using the k-β diagram of the uniform bifilar helix. Part of their solution for the current density

$$J(z) = J(0) \left[\frac{\gamma(z_o)}{\gamma(z)}\right]^{1/2} e^{-j \int_{z_o}^{z} \gamma(y)\, dy} \tag{114}$$

Equation (114) is for the current along the tape arm and includes rotating as one progresses down the structure. However, if the fields are probed with a loop or small dipole which is not rotated as the probe is moved down the structure, the phase progression will not be given by (114) which may be considered as the fundamental, but rather by a harmonic. Equation (114) is the approximate solution for the zero order harmonic, and the bifilar backfire helix and the log-spiral have the n = -1 harmonic as the dominant term in the near fields. This is a natural consequence of the twisted pair transmission line. The n= -1 harmonic is also characteristic of the LP folded monopole array and the LP dipole array because of the reversal of alternate radiating elements or the twisted pair feeder transmission line

We will investigate the modifications necessary to take into account the nth harmonic before investigating the more complicated structure with both series and shunt loading.

As it was previously pointed out, Equation (114) is the approximate solution for the zero-order harmonic. For the LP dipole array every other element is fed in alternate phase and, since the total current through an element is $V(-Y_L)$, it is immaterial whether the phase change is attributed to Y_L or the voltage V. The latter case corresponds to a twisted pair transmission line feeder. Since mathematically it makes no difference, we will attribute the change to the voltage on the transmission line, and the currents to alternate dipoles will not be reversed. For the periodic case β_n is given by $\beta_o + n\pi/d$ and for the log-periodic case it is given by

$$\frac{\beta_n}{k} = \frac{\beta_o}{k} - \frac{n\pi}{z(\ln \tau)} \tag{115}$$

Equation (115) is derived by mapping the periodic solution with the transformation

$$y = A \ln x \tag{116}$$

with the restrictions

$$y_o = x_o, \quad y_o + d = x_o + d/\tau = \tau^{-1} x_o \tag{117}$$

From Equations (116) and (117) the transformation is given by

$$y = - \ln x/\ln \tau \tag{118}$$

$$dy = - dx/x \ln \tau \tag{119}$$

Consequently, a differential phase shift in the periodic case given by βdy may be obtained from Equation (119).

The continuous version of the nth harmonic of the voltage or current is then given by

$$\begin{pmatrix} V_n \\ I_n \end{pmatrix} = \begin{pmatrix} V_n(0) \\ I_n(0) \end{pmatrix} \left[\frac{\gamma(z_o) - \frac{n\pi}{z_o(\ln\tau)}}{\gamma(z) - \frac{n\pi}{z(\ln\tau)}} \right] \exp(-jn\pi \ln(z/z_o)/\ln\tau) \cdot e^{-j\int_{z_o}^{z} \gamma(y)\,dy} \tag{120}$$

If x_o is small, the truncation error for the zero harmonic may be negligible; however, for the other harmonics this is not true. If x_o is fixed, as it is on any practical antenna, the phase term is very sensitive to a change in frequency since $z_o = kx_o$ and $\ln(z/z_o) = \ln(x/x_o)$. With this, it is easy to see that the individual harmonics of the voltage or current approximately scale continuously with frequency except for the phase.

It was shown earlier that n= -1 is the term on the periodic structure which gives the backfire radiation, and with n= -1 (120) gives the 2π phase rotation principle observed by DuHamel[47] and others. Notice that for each n the terms are approximately scaling continuously with frequency except for the phase terms that involve $\ln(x/x_o)$. The solution that is obtained by adding more than one term is frequency sensitive because the phase angle of the individual terms are frequency sensitive. If β_o is a solution, then $-\beta_o$ is also a solution. With this additional type of solution there exists the possibility of having two terms present and still have the voltage scale continuously. The $\pm\beta_o$ terms may exist as a pair. The -1 harmonic of $+\beta_o$ and +1 of $-\beta_o$ may exist as a pair, and in general the -nth harmonic of $+\beta_o$ and the nth harmonic of the $-\beta_o$ solution may exist as a pair. However, the sum of these pairs does not scale continuously with frequency but does scale at LP frequencies. It was pointed out earlier that if both $\pm\beta_o$ terms are present, the input impedance is constant

with frequency even though it has a reactive component. The same is also true for a general pair $\pm\beta_n$. If the -1 harmonic is the dominant term, the other terms will be present and these terms represent LP perturbations over a log-period. Notice, however, that if the source is scaled the phase term disappears because x_o is changed by the same factor as the point of observation x. This approximate solution predicts that all LP devices which can be analyzed in terms of the -1 harmonic will have a phase rotation which is linear with ln (x) if the source truncation point is not scaled with frequency. There is yet another assumption that is made when Equation (120) is written. In general, the wave equation for a tapered structure may be formulated as an infinite set of coupled first-order equations. In order to write the solution as (120) it must be assumed that the coupling is negligible, which may not be true for an arbitrary set of LP elements loading the transmission line.

The near fields of the dipole array[40] and the conical spiral[46] may be explained in terms of the -1 harmonic from the feedpoint through the radiation region. However, the stub-loaded LP monopole array[47] cannot be explained entirely in terms of the -1 harmonic. The measurements made by Hudock and Mayes[49] on the periodic version of this antenna indicate that the zero-order harmonic is predominant at the launch region and shifts to the -1 harmonic in the radiation region. The previous theory does not apply to this antenna for at least two reasons. The first reason is that the structure has a distinct double periodicity, i.e., two different loads per period. Such doubly periodic structures with distinct periods are beyond the scope of this present work. The second reason is that one of the approximations made was that Y_L has a smooth behavior as a function of frequency. The stubs on the monopole array do not exhibit a smooth behavior near quarter wave resonance; consequently, the approximation that Y_L/d is a distributed load is not valid.

Next we will treat the more complicated case with both Z_L and Y_L. The approximate solution of (98) for small kd is given by

$$(\beta d/kd)^2 \approx 1 + \frac{Z_L Y_L}{2} - \frac{Z_L Y_L}{(kd)^2} - j\left(\frac{Y_L}{Y_0 kd} + \frac{Z_L}{Z_0 kd}\right) \qquad (121)$$

The corresponding differential equation for this type of loading does not reduce in a simple way as in the two previous special cases. The differential equations are given by

$$\frac{dV}{dx} = - \left(j\omega L + \frac{Z_L}{(1-\tau)x}\right) \quad I \tag{122}$$

$$\frac{dI}{dx} = - \left(j\omega C + \frac{Y_L}{(1-\tau)x}\right) \quad V \tag{123}$$

Next take the derivatives of (122) and (123) and by letting kx = z the equations may be put in the following form:

$$\frac{d^2V}{d^2} - \frac{d}{dz}\left[\ell n\left(jZ_o + \frac{Z_L}{(1-\tau)z}\right)\right] \frac{dV}{dz} + \left[1 \frac{Y_L Z_L}{(1-\tau)^2 z^2} + j\left(\frac{Y_L}{(1-\tau)Y_o z} + \frac{Z_L}{(1-\tau)z_o z}\right)\right] V = 0 \tag{124}$$

$$\frac{d^2I}{d^2} - \frac{d}{dz}\left[\ell n\left(jY_0 + \frac{Y_L}{z}\right)\right] \frac{dI}{dz} + \left[1 - \frac{Y_L Z_L}{2} + j\left(\frac{Y_L}{Y_0} + \frac{Z_L}{Z_0 z}\right)\right] I = 0 \tag{125}$$

The solution of a general second-order differential equation of the form

$$\frac{d^2V}{dz^2} + P(z) \frac{dV}{dz} + Q(z)\ V = 0 \tag{126}$$

may be solved by assuming a product solution of the form

$$V = Y \cdot W \tag{127}$$

By putting (127) into (126) and putting the restriction

$$2Y' + P(z)\ Y = 0 \tag{128}$$

on Y, the solution of V is given by

$$V = e^{-1/2 \int_o^z P(x)dx}\ W \tag{129}$$

where W is the solution of the equation

$$\frac{d^2W}{dz^2} + R^2(z)\ W = 0 \tag{130}$$

and

$$R^2(z) = Q(z) - 1/2\ P'(z) + 1/4\ P^2(z)$$

$$= 1 - \frac{Y_L Z_L}{(1-\tau)^2 z^2} + j\left(\frac{Y_L}{(1-\tau)Y_o z} + \frac{Z_L}{(1-\tau)z_o z}\right) - 1/2 \frac{d^2}{dz^2}\left[\ln\left(jZ_0 + \frac{Z_L}{(1-\tau)z}\right.\right.$$

$$\left.\left. + 1/4 \left\{\frac{d}{dz}\left[\ln\left(jZ_0 + \frac{Z_L}{(1-\tau)z}\right.\right.\right.\right.\right] \tag{131}$$

Since P(z) in this case is an exact differential, the Y part of the solution is simple; however, the W part does not appear to have a propagation constant which is simply related to (122). The WKB approximate solution of (124) is given by

$$V = \frac{A\left(jZ_0 + \frac{Z_L}{(1-\tau)z}\right)^{1/2} e^{-j\int_0^z R(y)dy}}{R(\,)^{1/2}} \tag{132}$$

It is clear from (131) that in order for the solution to exist, then in the limit as $z \longrightarrow 0$ the ratio Z_L/z must be finite. Because of our inability to relate the solution given by (131) to the approximate $(\beta d/kd)^2$ in (121), no attempt is made to find the other harmonic solutions.

3.3 Conclusions

In this chapter we have shown the connection between the k-β diagrams of periodic and log-periodic continuously scaled structures. Several problems related to numerical correspondence between these cases still remain. Nevertheless, the dispersion data for the periodic case has proved very useful as an aid to qualitative analysis of log-periodic structures. Examples of the applications will be given in the next chapter.

It was demonstrated that the approximate β_o or fundamental harmonic scales continuously with frequency and the other harmonics approximately scale except for the $2n\pi$ phase rotation. It was also shown that the 2π phase rotation observed by DuHamel[47] is associated with -1 harmonic which is the harmonic that is associated with the backfire radiation.

PART IV

APPLICATIONS OF DISPERSION DATA TO THE DESIGN OF FREQUENCY INDEPENDENT ANTENNAS

4.1 Early Work in Frequency Independent Antennas

An antenna is said to be frequency independent if the principal characteristics (radiation pattern and input impedance) change negligibly with frequency over a band which is limited only by the construction of the antenna and if the band can be readily extended by adding to the structure in a manner which is apparent from the structure geometry. This definition is designed to distinguish the frequency independent antenna from that which is loosely termed broadband. The above definition serves to separate the log-spiral and log-periodic antennas from the so-called broadband antennas of the past, such as the biconical and its flat counterpart, the bow-tie. However, it was from these early broadband types, which followed the angle concept as outlined by V. H. Rumsey, that the development of log-periodic antennas has proceeded.[50,51]

The troublesome thing about the bow-tie could be termed "end effect." For, although this shape of triangular fins would have frequency independent properties when extended to infinity, the truncation which is necessary in the practical antenna produces a length in the defining parameters and this length produces variations in the radiation pattern. DuHamel theorized that the end effect in a bow-tie might be eliminated if the energy could be removed by radiation in the region between feed point and truncation.[51] This reasoning led to the first successful log-periodic antennas, with a shape which is shown in Figure 31. The serrations were designed to produce the desired radiation. They were also designed to improve the chances that the resulting structure would be frequency independent. First, the shape is self-complementary; that is, if we consider the outlined region to be a flat sheet of conductor, the open region between the elements has a shape which is identical to the shape of the conducting region. When such a self-complementary structure is infinite, Babinet's principle tells us that the input impedance is constant at 189 ohms regardless of the frequency. If the end effect is truly eliminated by the serrations, the antenna will appear infinite at the input terminals, and the impedance

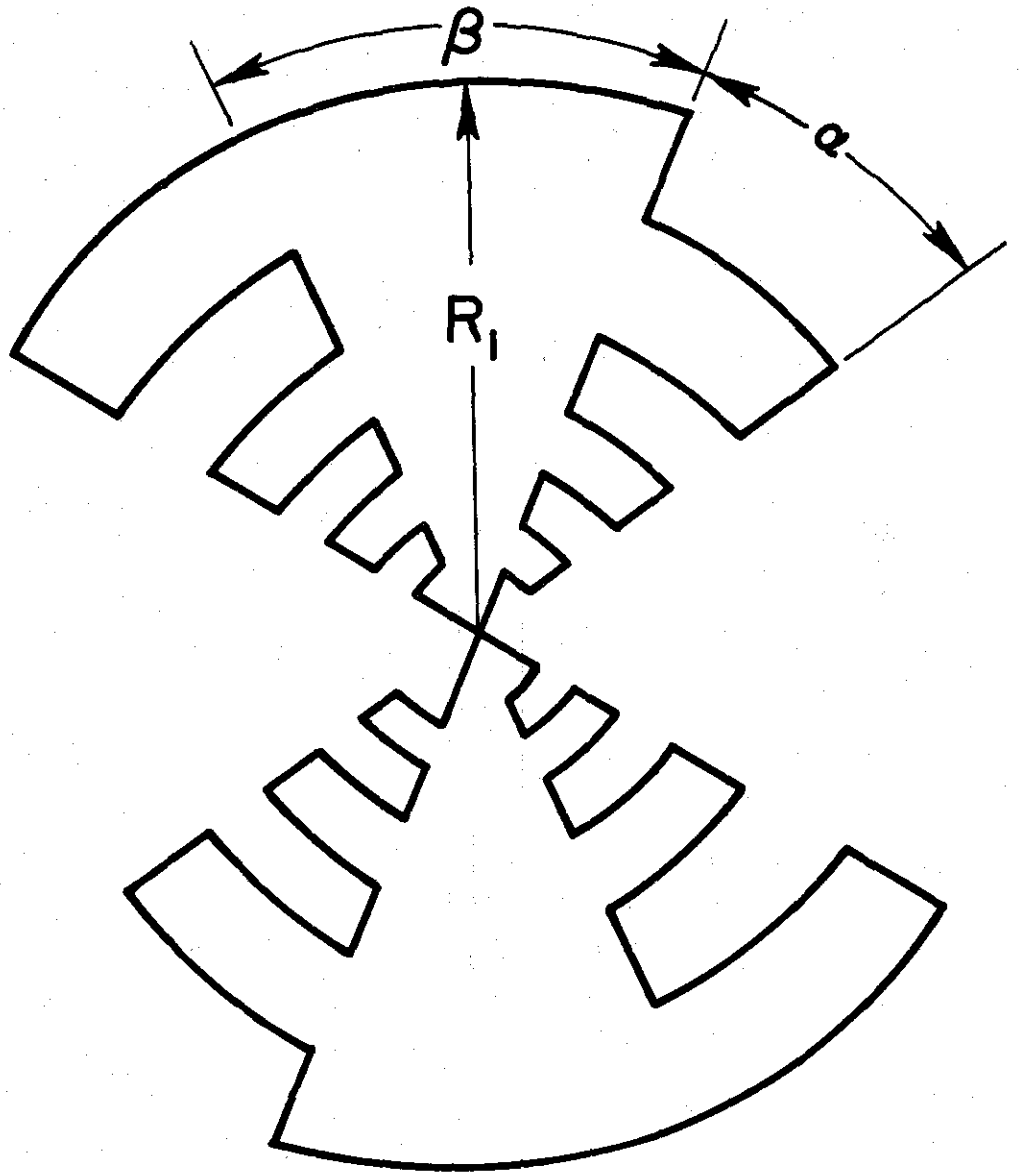

Figure 31. An early planar log-periodic structure.

will be frequency independent. Although it was later found that this was not a necessary condition for frequency independent input impedance, it no doubt played an important part in the success of the first models.

The second general principle follows from similitude, which has been used for many years as a basis for testing antennas by using a scale model. The shape shown in Figure 31 is such that the application of a certain scale factor to this figure would result in the same figure except in the area near the truncation of the large and small ends of the structure. Hence, insofar as the truncations are unimportant to the antenna performance, the electrical characteristics of the antenna must be repeated at frequencies which are related by the scale factor, which is usually called τ. Since the same results could be obtained by many successive applications of the same scale factor (when the truncation effects are negligible), the performance should repeat at frequencies related by any integral power of the scale factor τ. This property of the geometry, that the electrical performance should repeat periodically with the logarithm of the frequency, was the motivation for for the name "logarithmically periodic" or "log-periodic" structures.

The flat sheet metal antenna shown in Figure 31 produced a bidirectional beam which was linearly polarized with the electric vector parallel to the teeth. This latter observation confirmed that it was the currents flowing on the serrations which produced the radiation and the triangular fin merely acted as a transmission line to feed the radiating elements.

Important as they were, these first log-periodic antennas were not of great practical usefulness. The principal drawback was the bidirectional characteristic of the radiation which would naturally result from the symmetry of a planar structure. For most applications, a unidirectional radiation pattern is preferable. The obvious thing to try, then, is to spoil the symmetry of the structure in order to change the radiation pattern from a bidirectional one to a unidirectional one. Figure 32 shows a log-periodic antenna with elements tilted toward each other that was first investigated by Isbell.[52] It indicates that the desired unidirectional radiation was achieved, but, instead of radiating in the direction of phase progression of the current along the fin, the beam was produced in the opposite direction--that is, toward the feed point. That such a "backfire" characteristic should be inherent in the operation of most

successful unidirectional frequency independent antennas follows directly from the shape of the dispersion curve for the uniform periodic structures.

The first development of wire outline versions of log-periodic antennas was done primarily by DuHamel and his co-workers at Collins Radio.[53,54] Figure 33 shows some of the modifications which were made to convert the first unidirectional log-periodic antennas into structures which would be practical for applications in the high frequency communications band--6 to 30 megahertz. Most of the conductor has been eliminated from the elements, leaving only a central boom and the edges of the elements. The element shape has been changed from circular arc to straight line. The essential properties are retained, however, due to the common scale factor associated with the dimensions of any two adjacent elements.

Another very practical form of the antenna was developed by Isbell.[55] Although he proceeded along a different line of reasoning, the same result is achieved if we apply several perturbations to the antenna in Figure 33. If we let the element widths become small and then allow the angle between the planes of elements to go to zero, the result is the familiar log-periodic array of dipole elements shown in Figure 34. The perturbation just described leads naturally to the transposed feeder line shown in Figure 34.

Rumsey has pointed out the common symmetry properties in a self-complementary structure and the dipole array with transposed feeder.[50] It is interesting to note that the shape of the first log-periodic antennas was governed by a desire to obtain a self-complementary structure, and this dictated the staggered location of the "teeth" on the antenna shown in Figure 31. Although the perturbations in the structure of Figure 31 which lead to the dipole array of Figure 34 are rather severe, the symmetry is maintained through the use of the transposed feeder.

4.2 Dipole Array Analysis

Using the known properties of dipole antennas in a computer program which solved an equivalent circuit for the antenna, Carrel was able to compute many of the operating characteristics of the log-periodic dipole which agree well with experimental observations.[56] For example, Figure 35 shows some radiation patterns presented by the computer in both the E- and H-planes of the antenna for frequencies which correspond to the resonant

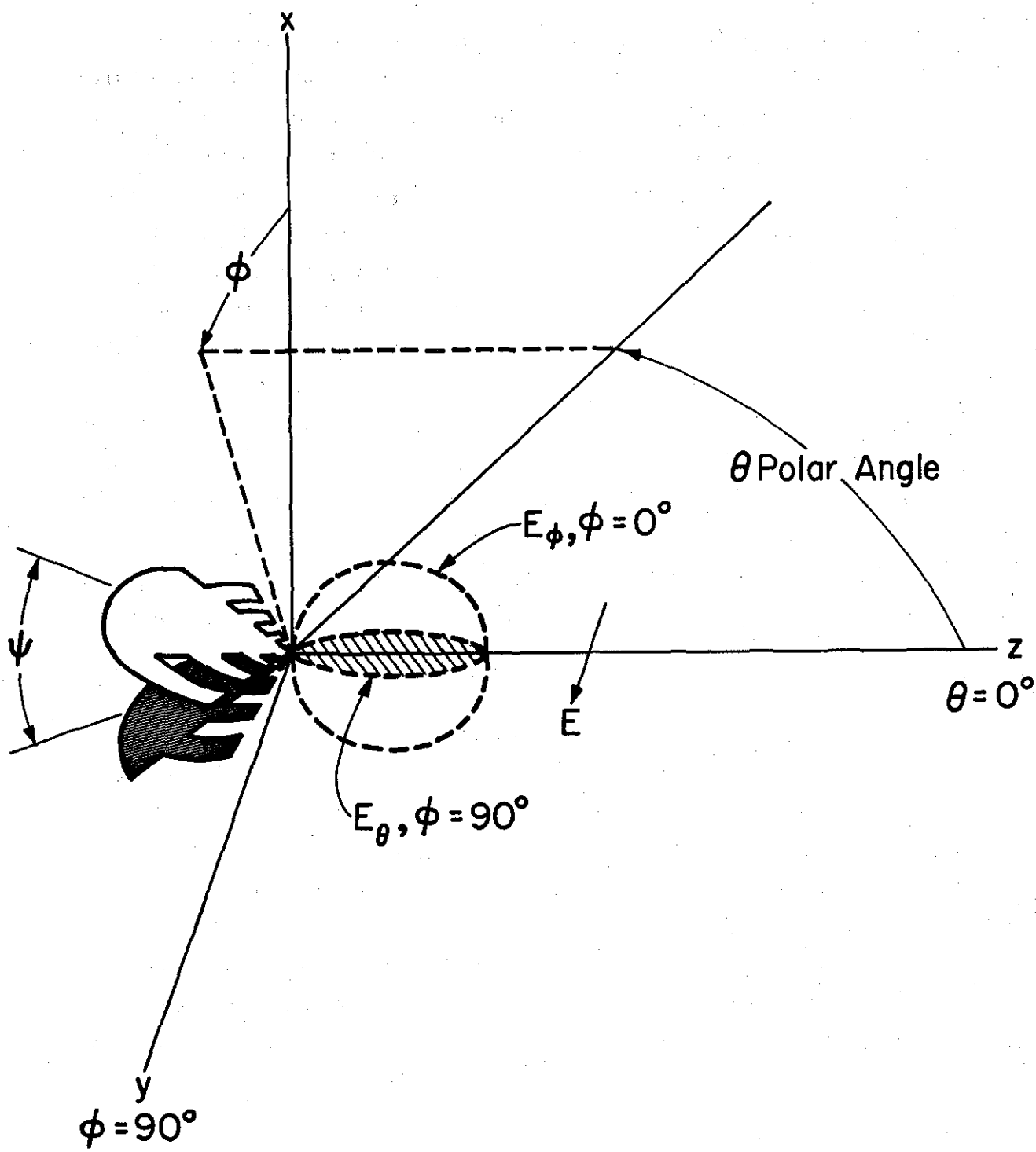

Figure 32. The first unidirectional log-periodic antenna showing the backfire beam.

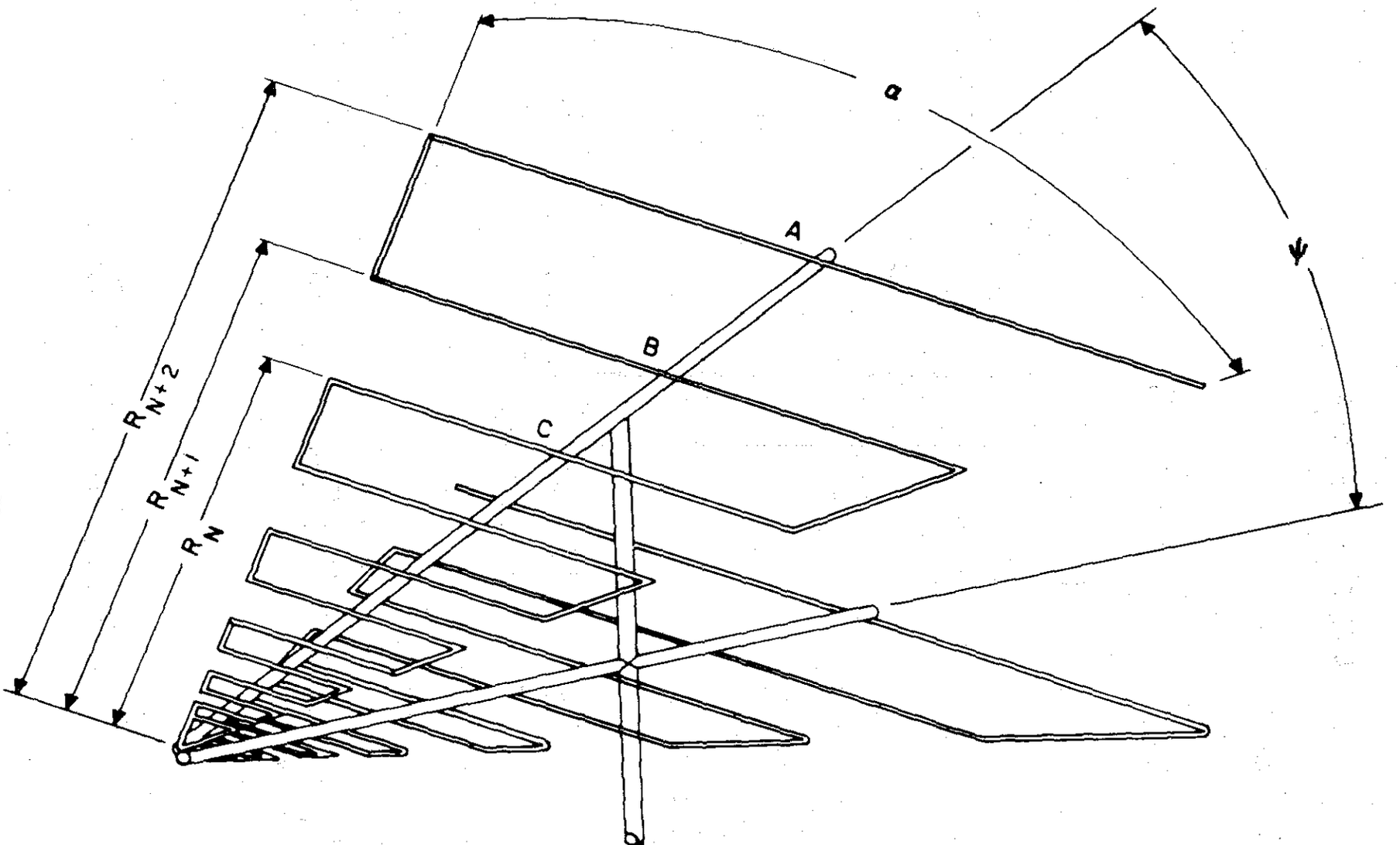

Figure 33. A wire-outline log-periodic antenna (Collins Radio Company).

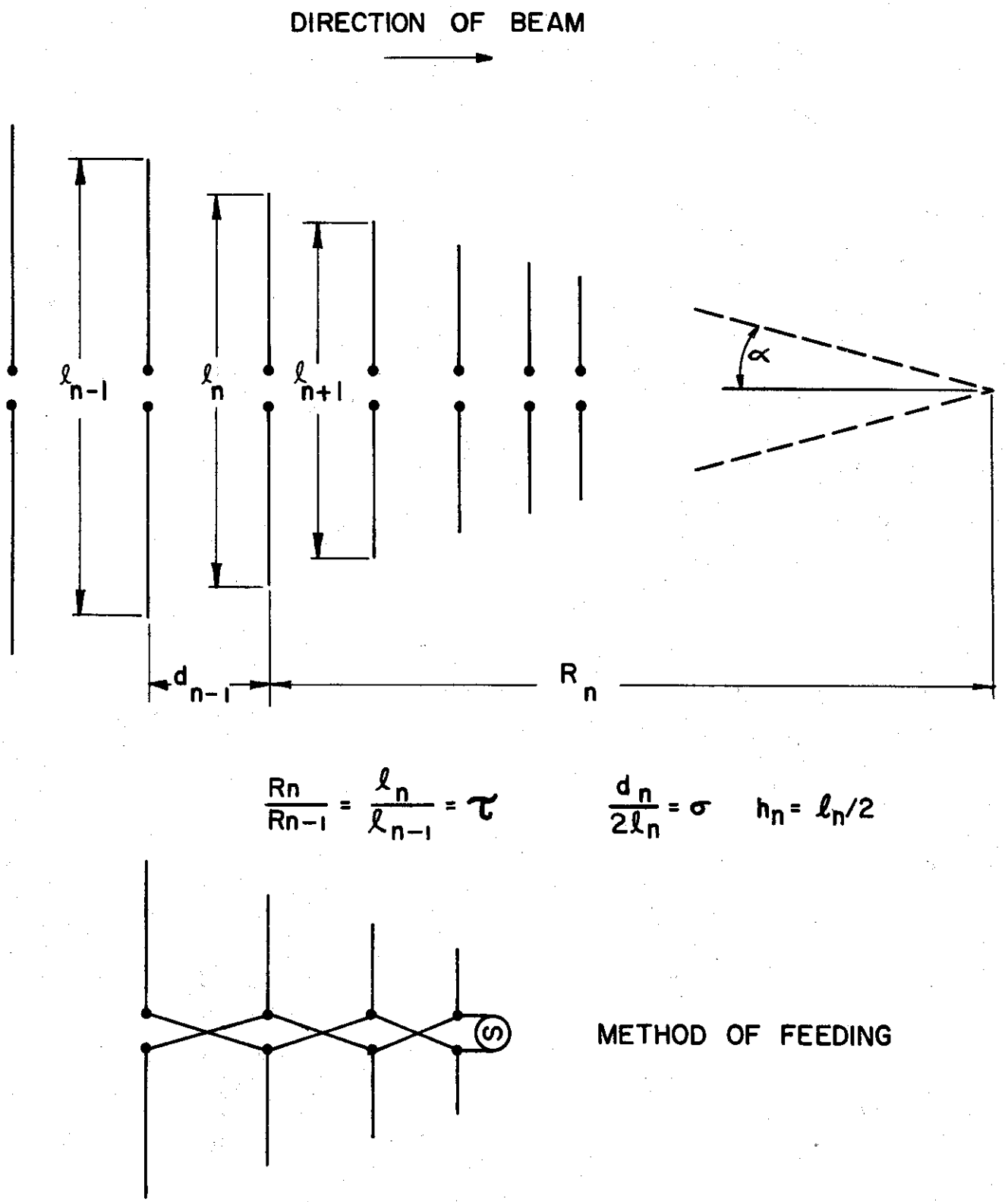

Figure 34. Schematic diagram of the log-periodic dipole array.

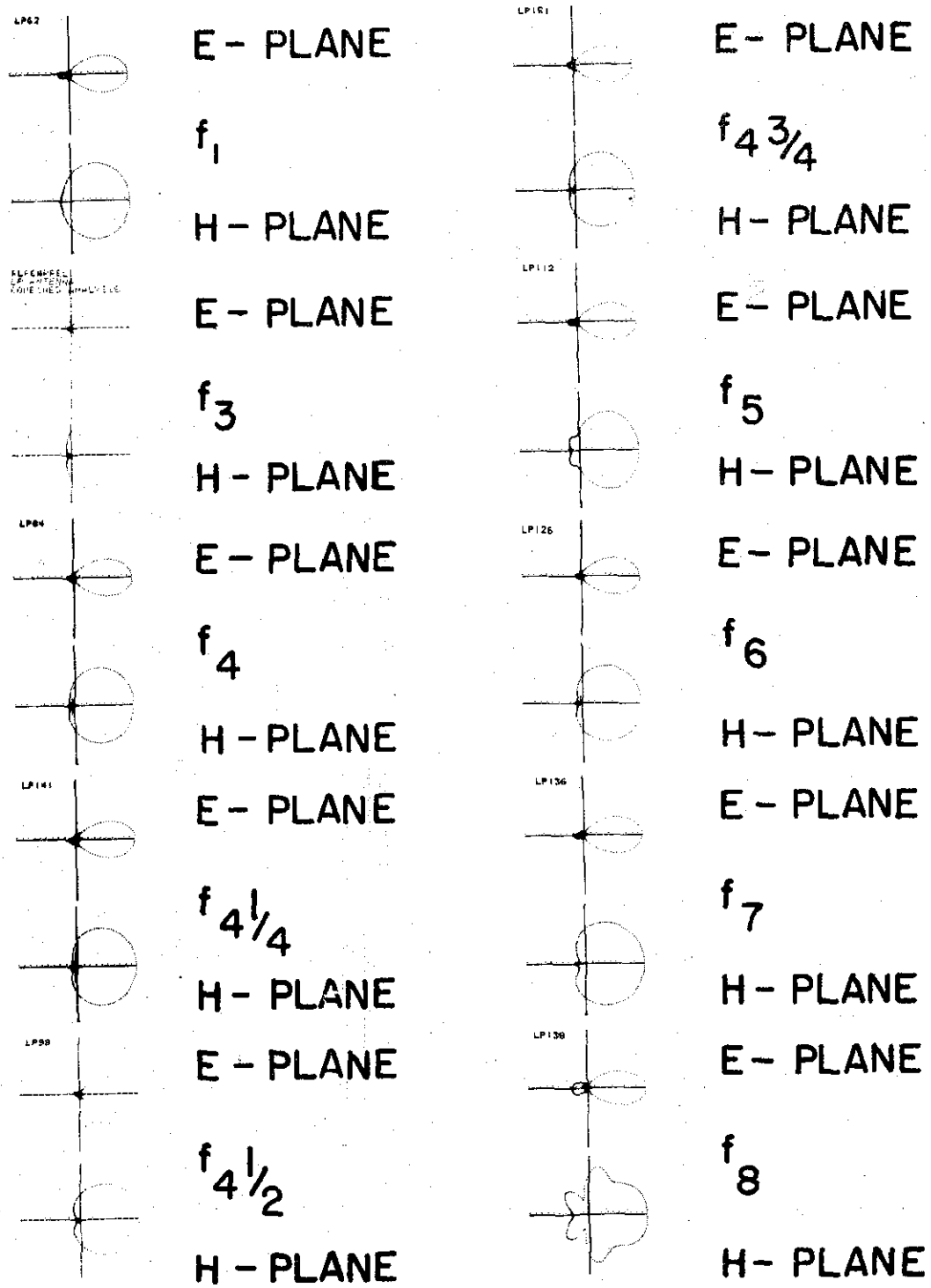

Figure 35. Calculated radiation patterns of a log-periodic dipole array (f_n = resonant frequency of nth dipole).

frequencies of a number of elements on the antenna. This was an eight-element log-periodic dipole array. We can observe that over a frequency range which extends from the resonant frequency of the longest dipole, f_1, down to about the resonant frequency of the next to the last dipole, f_7, these radiation patterns are very much the same. Evidence of front end truncation appears first in the H-plane pattern calculated at f_8, the resonant frequency of the shortest dipole.

The computer program could also be used to calculate the input impedance. Figure 36 shows a Smith chart which displays the computed input impedance for a particular log-periodic dipole which had eight dipoles, $\tau = 0.888$, $\alpha = 17.5$ degrees, $Z_0 = 100$ ohms, and terminal impedance = 100 ohms. In many cases the actual value of the terminal impedance is unimportant because the energy is gone from the feeder line before it reaches the termination.

Figure 35 shows a typical characteristic of a frequency independent impedance where most of the points are grouped in a very compact locus on the Smith chart. It is only at frequencies f_7 and f_8, corresponding to resonant frequencies of the two shortest dipoles on the antenna, that the impedance departs from this locus appreciably.

Figure 37 shows the measured and calculated phase and amplitude of the feeder voltage along a log-periodic dipole antenna. The abscissa is the distance along the axis of the antenna normalized with respect to wavelength. On the left ordinate, phase is plotted in degrees, and on the right hand ordinate the amplitude is plotted in decibels. The calculated values are shown by triangles for the phase and by small squares for the amplitude, and the measured values are shown by continuous curves. Of principal importance in Figure 37 are the slow wave nature of the feeder wave near the feed point on the left-hand side of the figure and the rapid decay of voltage near the half-wavelength element. Calculations were also performed for the amplitude and phase of the currents in the dipole elements themselves. These currents are more directly related to the directional characteristic of the antenna. The amplitude curve of Figure 38 shows that only a few dipoles carry the important currents, and that these dipoles are in the vicinity of the half-wavelength element. From these results the concept of an "active region" on the antenna

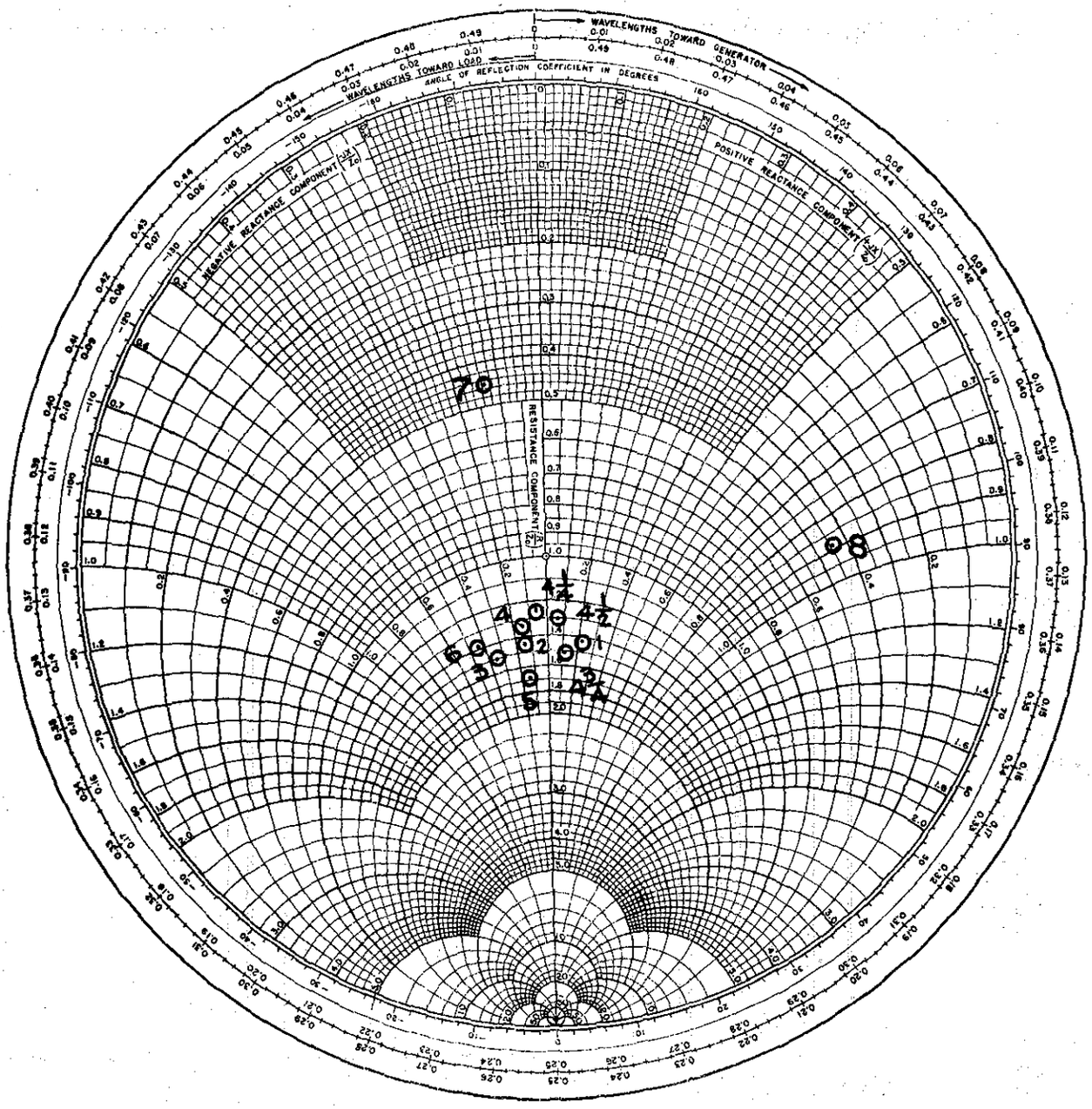

Figure 36. Calculated input impedance of a log-periodic dipole array (nth point is at resonant frequency of nth dipole).

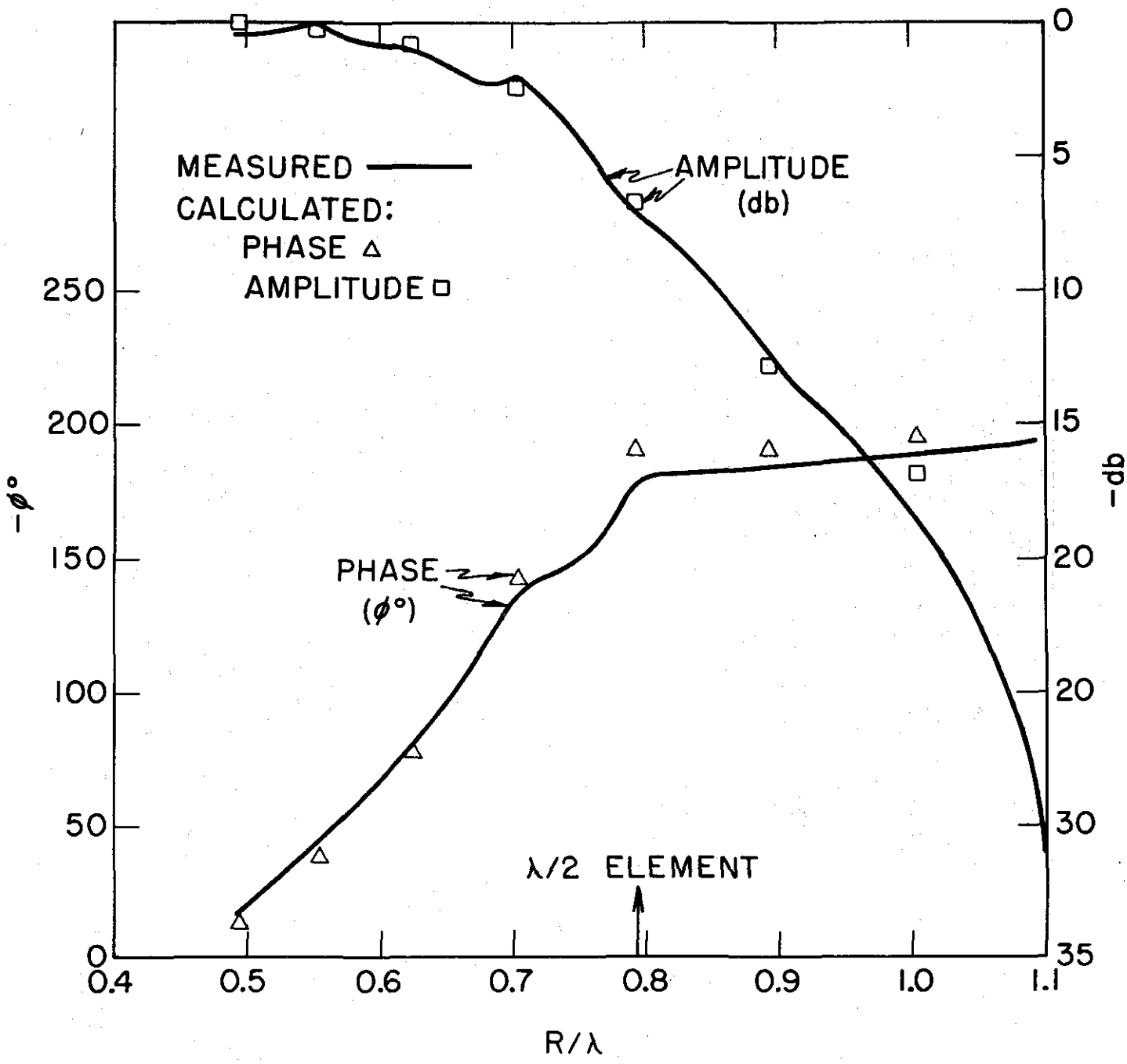

Figure 37. Calculated and measured feeder voltage on log-periodic dipole array.

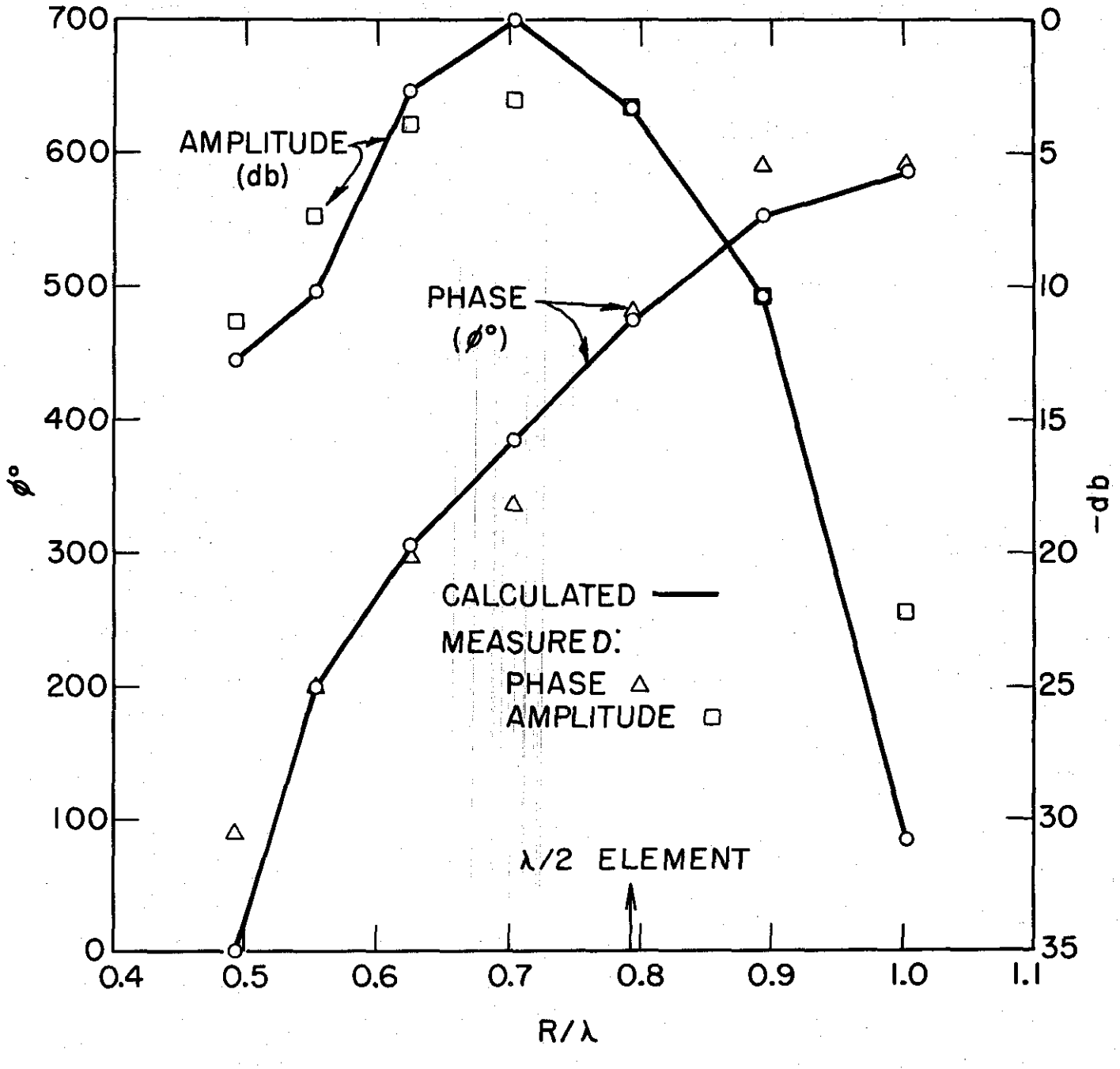

Figure 38. Calculated and measured amplitude and phase of dipole input currents on a log-periodic dipole array.

was developed. The "active region" varies with frequency in a way which tends to keep the properties of the radiation pattern constant as frequency is varied. The results of Carrel's analysis produced valuable design information for the log-periodic dipole.[56]

4.3 Backfire Zigzag Analysis

If we return to a serrated bow-tie similar to the one shown in Figure 31 but with triangular serrations, and eliminate the conductor in a different way by allowing one edge of the structure to approach the other edge, we get a result which is depicted by an experimental model shown in Figure 39. This is a balanced log-periodic zigzag antenna:[57] half of it is visible and the other half is hidden by the polyfoam support.

The log-periodic zigzag is a simple geometric shape for which a very simple approximate analysis for the dispersion data has proved useful. Similar results have been applied in greater detail to the conical logarithmic spirals.[15,16] A uniform zigzag is shown in Figure 40. The structure is divided into cells by dotted lines. The period of the structure with respect to translation is a; the width of the structure is W; the variable running along the direction of the wire is s; the pitch angle of the zigzag is γ; and I indicates a current in the zigzag wire. Let us assume that the current is a traveling wave with a free-space propagation constant k. As illustrated in Part I, the important factor in calculating the radiation pattern is the cell-to-cell phasing. The length of wire in one cell is $s_c = 2\ W \sec \gamma$. The wave of current traveling with free-space phase velocity along the wire produces a phase at the right-hand side of cell 1 with respect to the phase at the left-hand side which is determined by multiplying the length of wire in one cell by the free-space phase constant. This can also be determined from a phase constant β_o which describes the progression of a wave from cell 1 to cell 2 along the axis, where the distance between adjacent cells is d. It is then apparent that $\beta_o d = \beta s_c$. Substituting from the formula $s_c = 2W \sec \gamma$, the phase constant β_o is found to be $\beta_o = \beta \csc \gamma$. Since the cosecant is always greater than unity, this equation describes a slow wave. In fact, the slowness factor is the ratio of the wire length in one cell to the cell length d. Slow waves are ordinarily tightly bound to a guiding surface

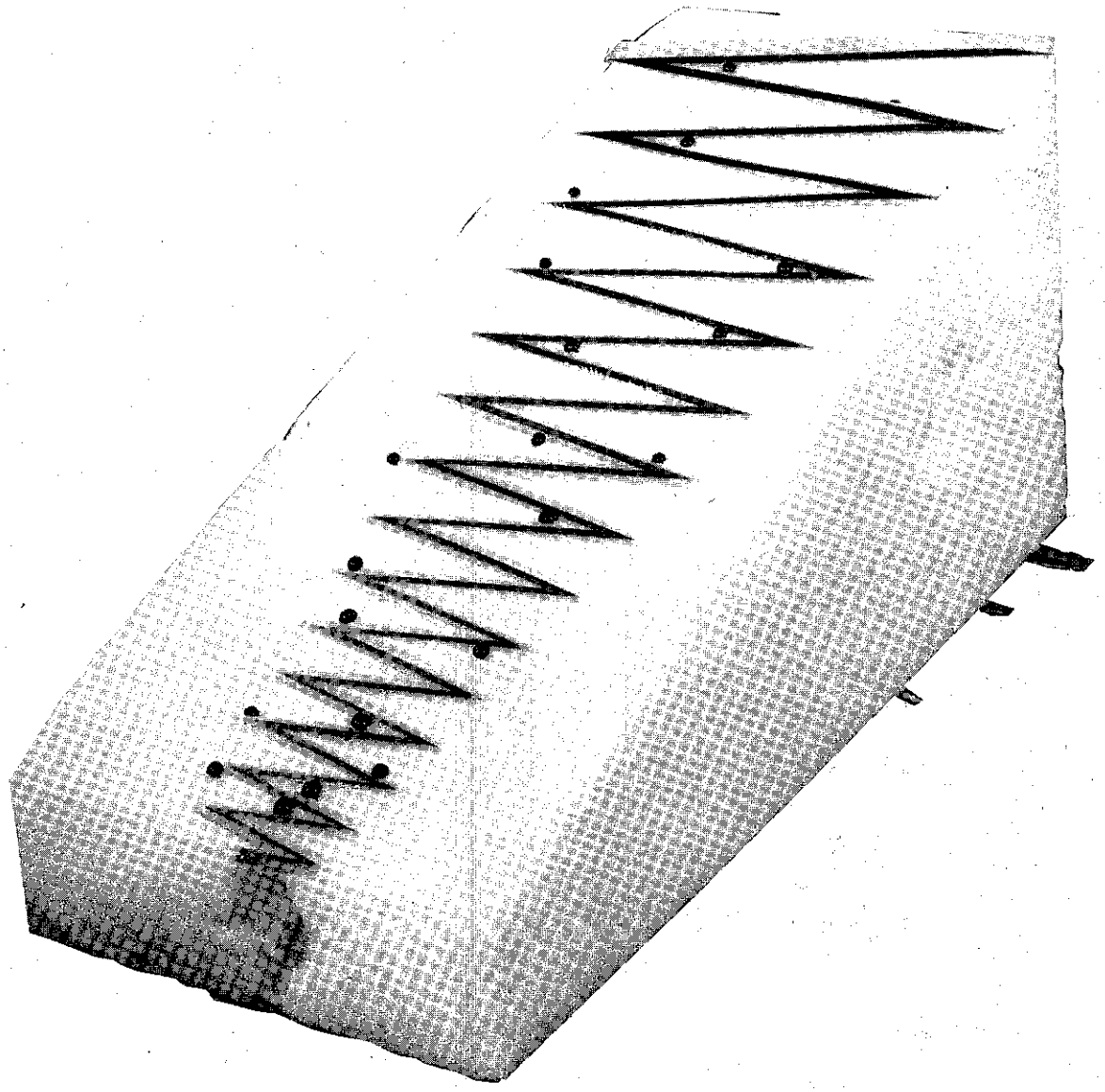

Figure 39. A balanced log-periodic zigzag antenna.

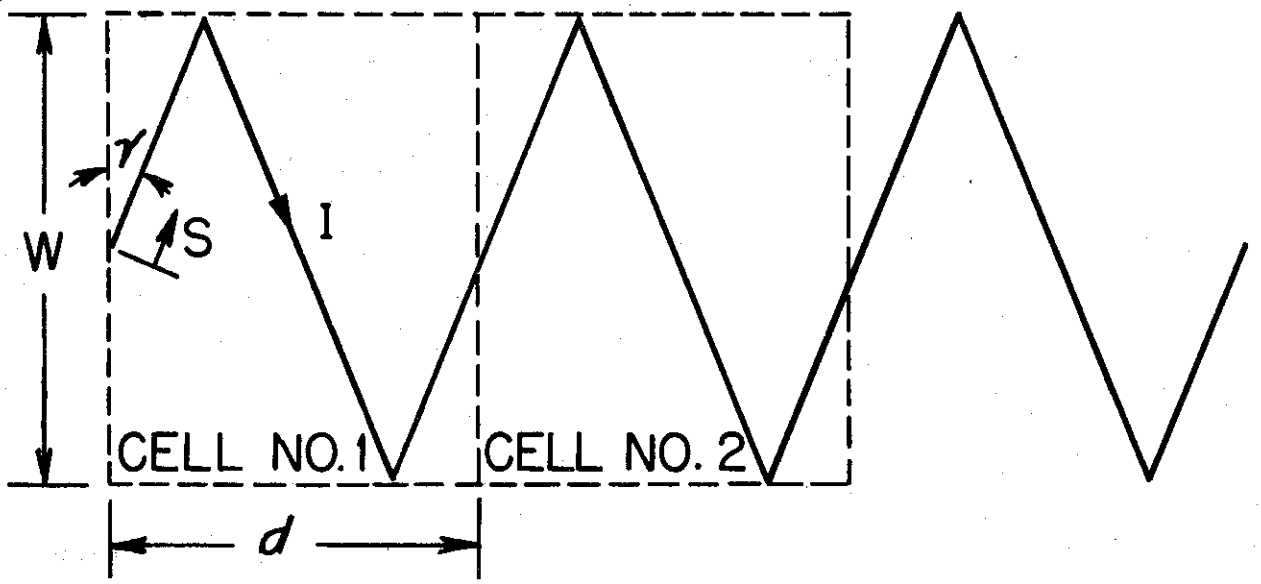

ASSUME $I = e^{-j\beta S}$

$S_c = 2W \sec\gamma$

$\beta_0 d = \beta S_c$

$\beta_0 = \beta \csc\gamma$

Figure 40. A uniform periodic zigzag conductor showing approximate phase constant formulas.

structures, the fundamental slow wave may be accompanied by other waves which are not slow and may, therefore, radiate considerable energy as they propagate.

Consider, for example, the case when each cell contains one wavelength of wire. Then, because of the multiple-valued nature of phasors, each cell of the structure is in phase with every other cell. Array theory tells us that the linear array of elements of the same phase radiates broadside. If each cell contains slightly less than one wavelength of wire, the resulting phase progression from cell to cell is toward the feed point and produces a beam tilted toward the back-fire direction; if each cell contains slightly more than a wavelength, the phase progression is away from the feed point, and the beam is tilted toward endfire. The backfire condition is one of primary interest for log-periodic antennas. It is described by a cell-to-cell phase difference which is the negative of the intrinsic free-space value. Phase progression slightly greater than this value gives somewhat higher directivity than obtained by using the backfire condition exactly. This corresponds roughly to the Hansen-Woodyard condition, which is sometimes employed in linear arrays by adding excess phase shift to the array to get the narrowest possible beam.

The fields in and around each cell of a periodic structure are composed of many space harmonics which differ only in phase constant and are related by

$$\beta_n = \beta_o - \frac{2n\pi}{d}$$

Let us apply to the periodic zigzag antenna the theory according to the normalized space spectrum shown in Figure 11 of Part II. We assume the slowness factor of two, which could be adjusted by selecting the proper pitch angle of the wire. When $\lambda/a = 4$ and the fundamental wave is at the point $\beta_o/k = 2$, the various other space harmonics are found at $\beta/k = -6$, -2 and $+6$ as shown in Figure 41. All of the waves near the structure at this frequency are in the slow region; there is only one, β_{-1}/k, which has even begun to approach the visible range of the diagram.

Now, we change the frequency so that $\lambda/a = 3$ rather than 4, and assume that the normalized fundamental wave phase constant is not a function of frequency, but stays fixed at two. By the formula for calculation of the phase constants, we observe that the n= -1 space harmonic, β_{-1}/k, has moved up to the edge of the visible range. It is moving in such a direction as to enter

$$\beta_n/k = \beta_0/k - n(\lambda/a)$$

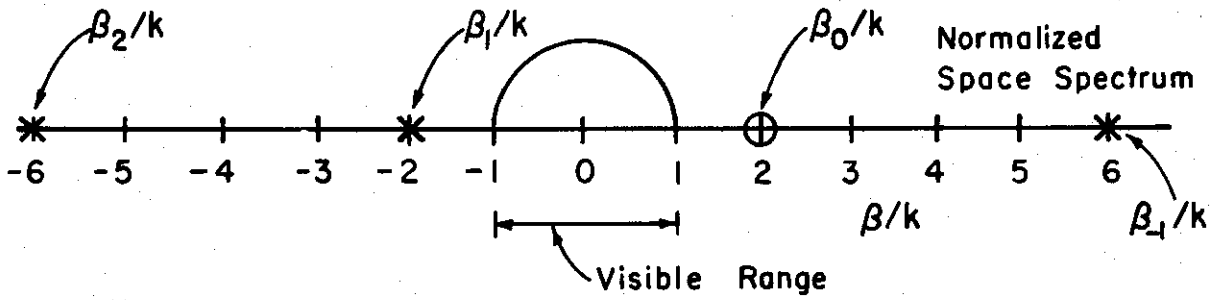

(a) $\lambda/a = 4$

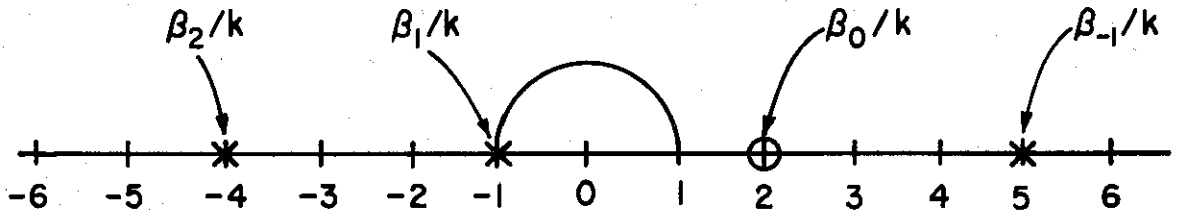

(b) $\lambda/a = 3$

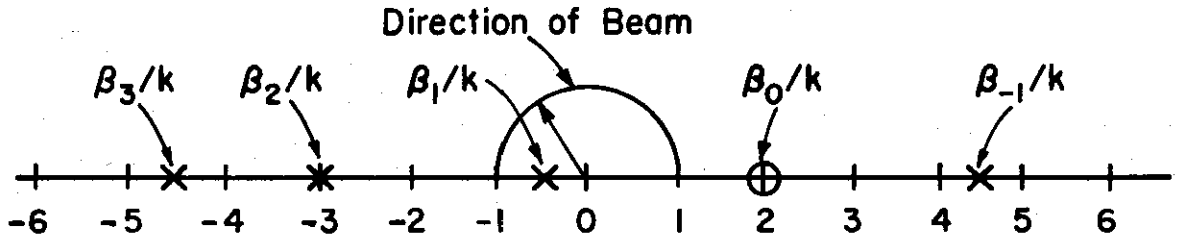

(c) $\lambda/a = 2.5$

Figure 41. Variation of space harmonics with frequency.

the visible range at the backfire side to first produce radiation in that direction. The other space harmonic phase constants also moved, but they are still a long way from the visible range. We now go on up in frequency, until $\lambda/a = 2.5$. The n= -1 space harmonic phase constant has moved inside the visible range; and, by the above-described construction in the unit circle, we can obtain the direction of the beam.

If this simple theory has any validity, we should be able to observe it experimentally with a uniformly periodic zigzag antenna.

The H-plane radiation patterns of a monofilar zigzag antenna are shown in Figure 42. At a frequency of 1.3 GHz the n= -1 harmonic is actually slightly out of the visible range according to the approximate theory. However, we find that there is a well-formed backfire radiation pattern from the monofilar zigzag at this frequency. As frequency is increased the pattern broadens so that we might, for example, at 1.4 GHz be in the free-spacing phasing condition. As frequency is further increased the pattern takes on a maximum at some angle other than backfire, and that maximum value of radiation tends to scan around toward broadside. The beams here are not formed to the extent that we can trace the scan across the entire visible range. Hence, the range of validity of our original simple, assumed current distribution is limited. However, for uniform zigzags with narrow-width conductors and pitch angles greater than about 30 degrees, the perturbation in the simple theory is small and a well-formed beam can be observed to scan across the visible range.

Figure 43 shows the actual dispersion data as determined from measurements made on several uniform periodic zigzag antennas with various pitch angles. The dashed lines show the phase constants that would result on the basis of geometric slowing factor of the antenna, assuming that a free-space wave travels along a wire. The solid lines are the experimental results. These experimental results were obtained by two methods. First of all, in the case where the points are below the two 45-degree lines, we can produce a reflected guided wave on the structure by placing an improper termination on it. For example, we could put an open circuit or a short circuit at one end which would produce a standing wave in the near field. From the distance between the nulls in the standing wave the guide wavelength is determined, and from that, the phase constant. However, when the points lie in the fast-wave region corresponding to the visible range on the space spectrum, the wave

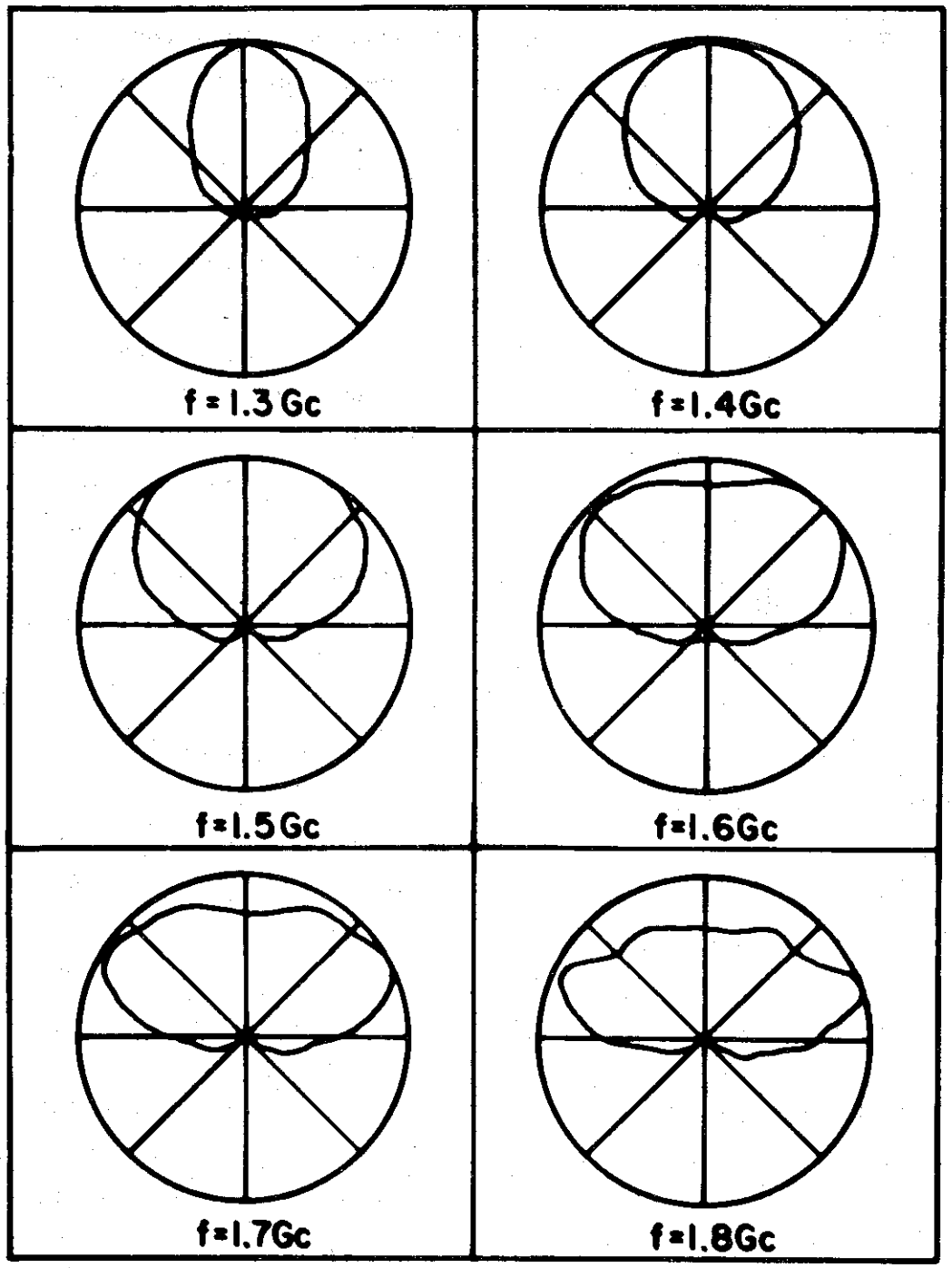

Figure 42. H-plane radiation patterns of a monofilar zigzag antenna.

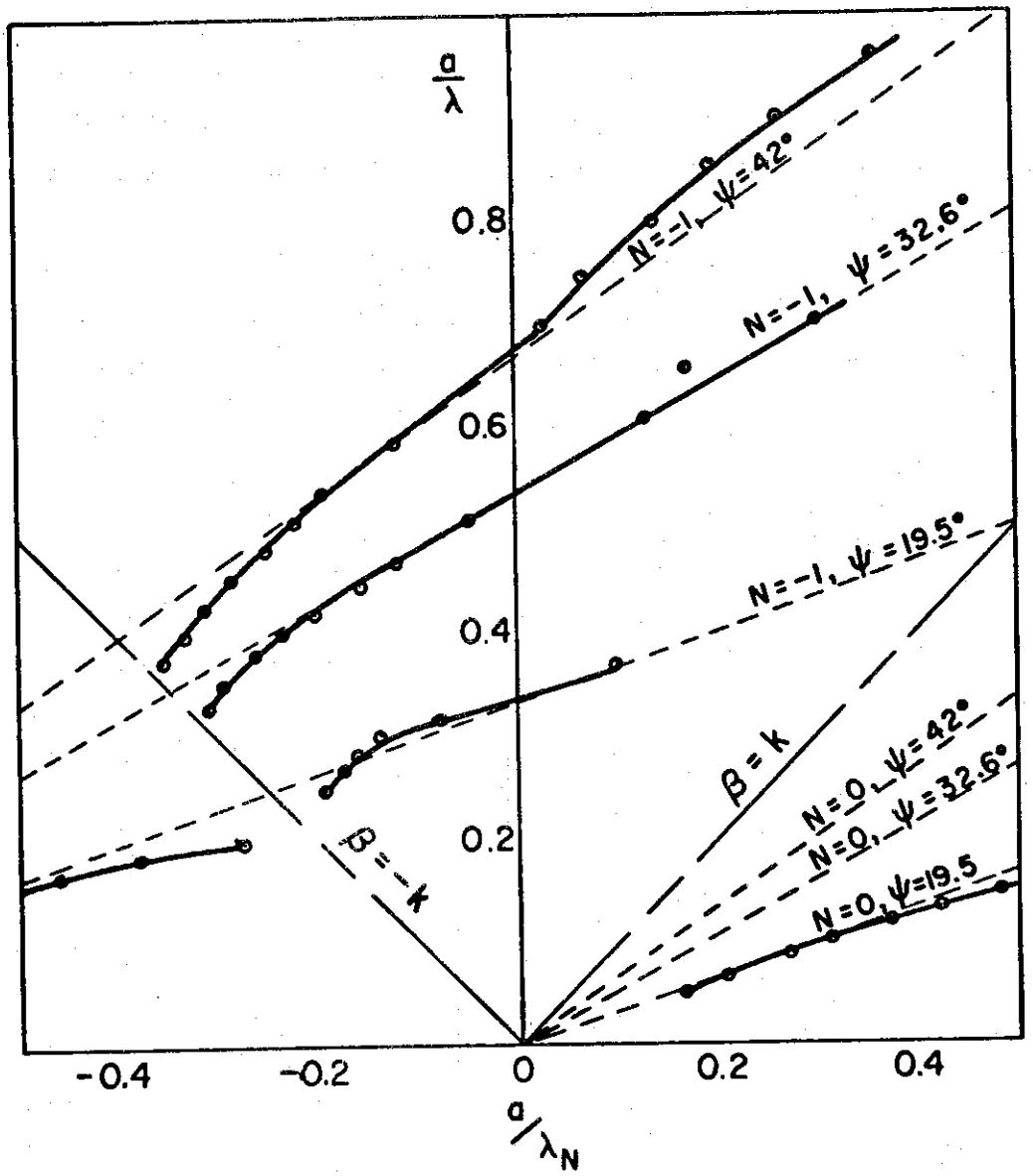

k-β DIAGRAM SHOWING VARIATION WITH PITCH ANGLE

Figure 43. k-β diagram for uniform balanced zigzag antennas showing variation of dispersion curve with pitch angle.

has a complex propagation constant and decays rapidly enough that reflections from the end would be negligible. In this region of the diagram, radiation pattern measurements have been used to determine the fundamental wave constant. From the direction of the observed beam the space harmonic phase constant was calculated.

It has already been discussed how the results for the uniform periodic antennas can be carried over, at least approximately, to log-periodic. The variations with frequency observed on the uniform periodic structure correspond to variations of the cell dimensions on the log-periodic structure. The region of small cells near the front of a log-periodic zigzag would correspond to the low-frequency condition on the uniform structure. The fundamental wave and all space harmonics are slow and, therefore, small radiation results. However, the region where the first reverse space harmonic approaches the backfire condition produces appreciable radiation and corresponds to the active region on the structure. If radiation is sufficiently large, the larger cells will be unexcited, and this is generally desirable to avoid appreciable radiation in directions other than backfire.

4.4 Design of Log-Periodic Antennas

Let us now consider how the knowledge of even approximate dispersion data can aid in the design of some log-periodic antennas. Considerable effort has been expended on the design of vertically polarized log-periodic antennas for use over ground. A number of designs have been proposed and used with varying degrees of success. The excellent results obtained with both balanced zigzag in free space and with one horizontally polarized zigzag element over ground make this geometry a likely candidate for vertical polarization as well. So, it was proposed to mount a zigzag element vertically over ground;[65] this works as expected. However, a major drawback to the utilization of this antenna in the high frequency (3-30 MHz) range (probably where the principal applications are found), is the fact that it has a rather large height——exceeding one-half the maximum wavelength of the band to be covered. One solution to this problem developed by Greiser[66] is diagramed in Figure 44.

The vertical zigzag element has been bent along its axis. Figure 44a shows the vertical radiating elements and the end-on view of the horizontal elements. The bend may be somewhere other than on the axis of symmetry

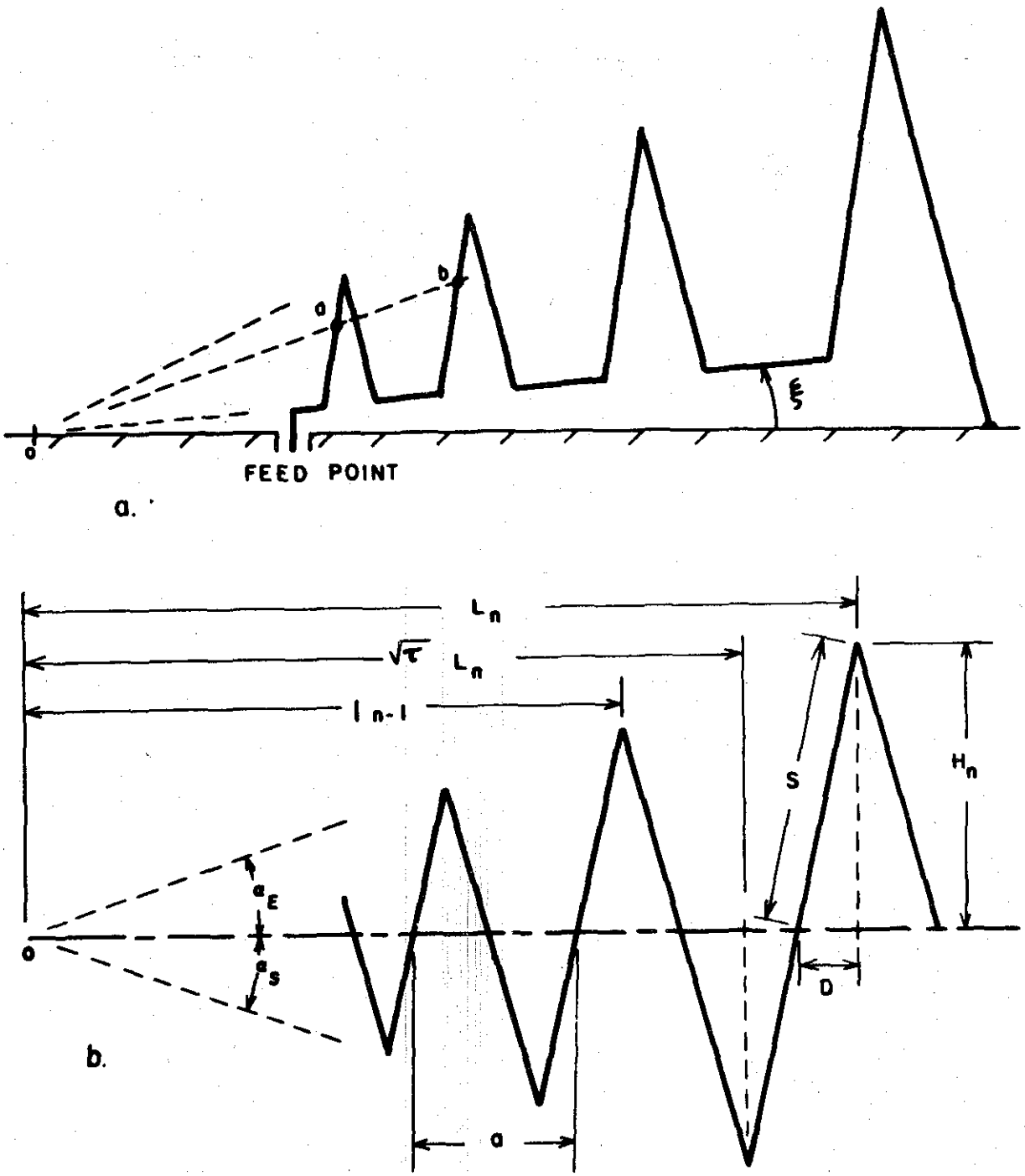

Figure 44. The bent log-periodic zigzag antenna for vertical polarization.

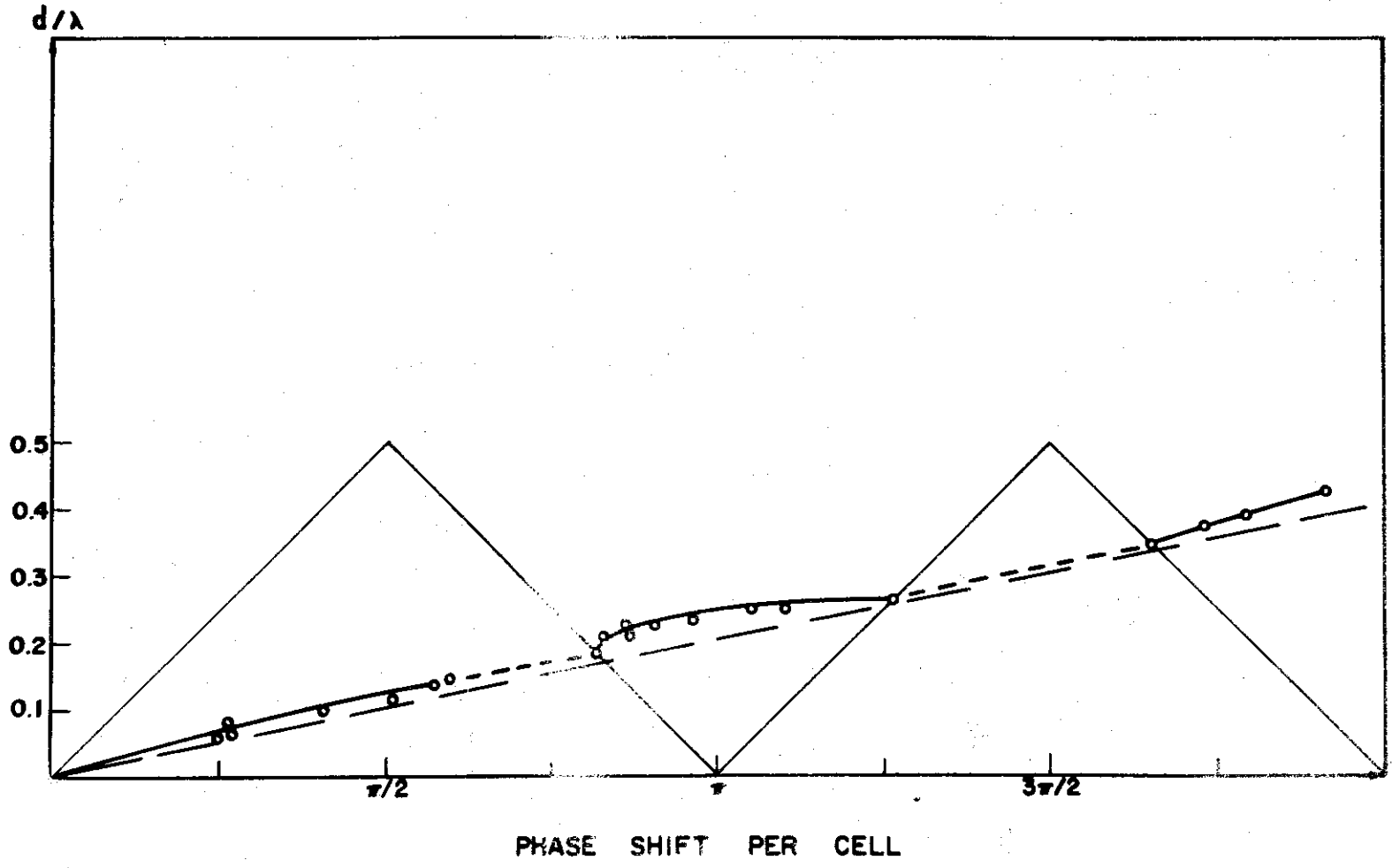

Figure 45. k-β diagram for a periodic bent zigzag antenna.

of the structure. This is indicated in Figure 44b by having two angles alpha, α_E for the vertical elements and α_S for the horizontal elements. The operation according to the preceding approximate theory was verified by measuring the Brillouin diagram on a uniform structure. The results of this measurement are shown in Figure 45. In this case the Brillouin diagram is plotted for only the fundamental wave, whereas previous diagrams were confined to the first Brillouin zone from minus π to plus π and showed several space harmonics. Notice in Figure 45 the possibility of going through another transmission region inside the second triangle. Then, the second reverse space harmonic enters the visible region at the right-hand side of the second triangle. Scanning of the beam is also observed in this region and, from the beam direction it is possible to determine the phase shift per cell in the structure. The dashed line in Figure 45 is the prediction for the propagation constant from cell to cell, based on the assumption of a free-space current wave propagating along the wire.

A unique feature of the bent zigzag which proved very useful in the design was the adjustment of the cell-to-cell phasing made possible by the horizontal conductors. The horizontal elements can be replaced with zigzag delay lines or other equivalent phasing elements so that appropriate phasing from output of one element to input of the other can be adjusted by changing the length of wire in each of the delay lines. Either of these methods can be made to work with appropriate design to produce frequency independent backfire radiation.

Figure 46 shows how the analysis can be related to the performance, and how appropriate phasing can be determined. The cell-to-cell phase constant at the quarter wavelength element is labeled n on the normalized space spectrum diagrams at the bottom of the figure. For the first antenna, this nth cell falls in the visible range. In fact, the phase constant at the nth cell occurs near the center of the unit circle, and the accompanying H-plane radiation pattern (shown to the left in the figure) shows considerable broadside radiation, resulting in a very wide H-plane pattern. The second antenna, however, has a different slowness factor which can be obtained through a proper adjustment of the cell-to-cell phasing. This phasing was chosen so that nth cell falls outside the visible region. The nth cell here has a slowness somewhere between 2 and 3. The resulting H-plane pattern for this antenna is considerably improved. Variations in H-plane beam width are usually attributable to energy

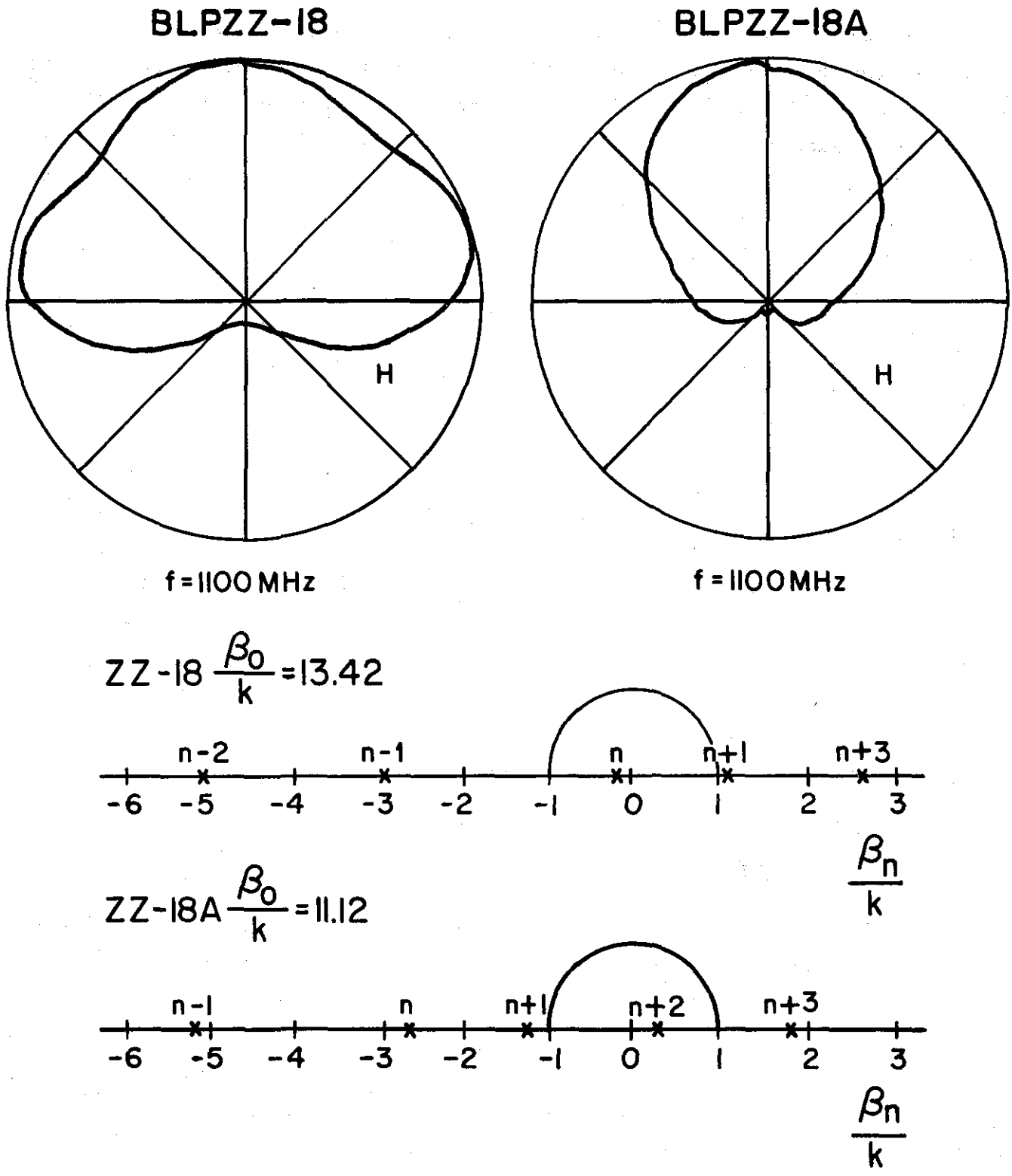

Figure 46. Variation in H-plane patterns of log-periodic zigzag antenna as function of cell-to-cell phasing.

which penetrates to cells having phasing corresponding to waves in the visible region. If this is a problem in design which cannot be corrected through phasing, the rate of attenuation of the currents can be increased by increasing the size of conductors used in the zigzag, thus reducing the beam variations.

The zigzag is an example of the type of structure for which the dispersion effect is rather small and mainly due to radiation. The dispersion properties of the helix are very similar as are those for the sinusoidal tape. The relatively simple geometry of the helix and sinusoidal tape has made it possible to calculate the dispersion data even in the complex wave region. Generally speaking, however, the dispersion data are more readily obtained by measurements than by calculation and the results obtained from measurements on periodic structures may give important clues to the design of log-periodic antennas.

As an example of the application of experimental dispersion data, consider the design of a frequency-independent flush-mounted, cavity-backed, slot array such as might be employed on high-speed aircraft or rockets. Working on the basic premise of duality applied to the familiar log-periodic dipole array, the geometry shown in Figure 47 was originally suggested as a proposed design. The antenna consists of a number of waveguide-fed slots which are arranged in log-periodic fashion and mounted in a common ground plane. The feed system which was proposed consisted of a series of loops. Every other loop was transposed to correspond to the transposed feeder of the dipole array. After considerable experimentation it was determined that the antenna could be made to work fairly well over a relatively narrow band near the upper end of the predicted bandwidth providing the coupling holes between adjacent cavities were enlarged so that only a vestigial side wall remained.

Near-field measurements indicated that the feeder wave was being attenuated near the feed point even at low frequencies and thus was not penetrating as far as the most efficient slot for that frequency. At higher frequencies, this attenuation disappeared and the antenna performance was satisfactory. This behavior suggested that a low frequency stop-band might be preventing the energy from penetrating the structure until a frequency had been reached where the stopband condition no longer existed between the feedpoint and the active region. Near-field measurements on the uniform periodic counterpart of the log-periodic slot antenna substantiated this viewpoint.

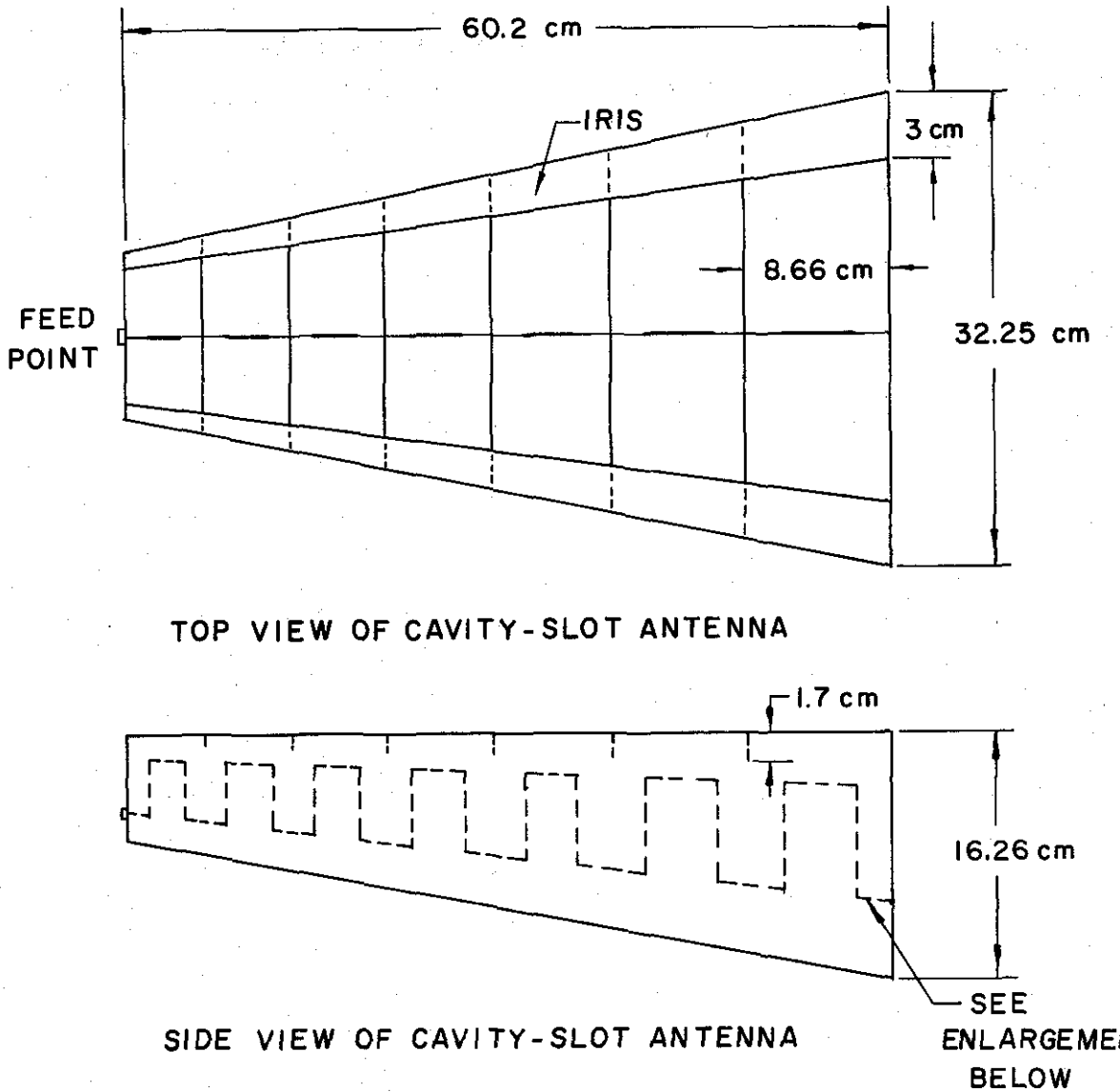

Figure 47. Log-periodic cavity-backed slot antenna construction and dimensions.

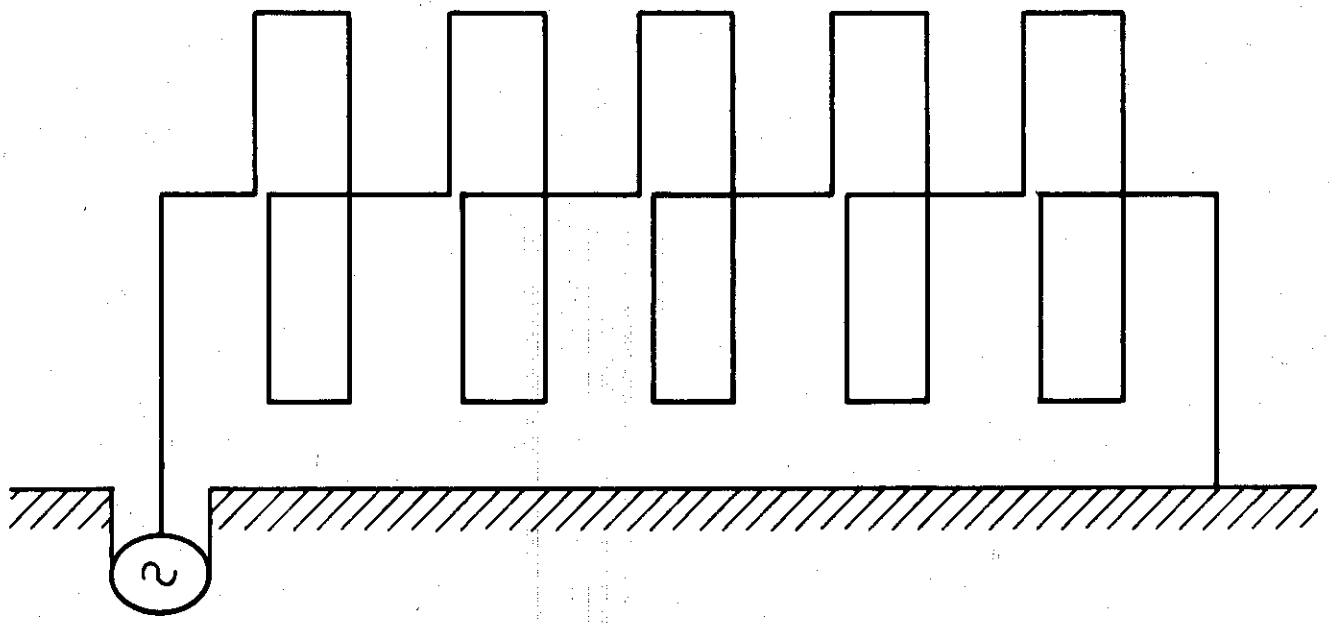

Figure 48. Series loop feed system used in cavity-backed slot array.

Since the behavior had persisted through numerous modifications of the cavity, suspicions began to center on the loop feed. The feed system was removed from the slot array and placed over a ground plane as shown in Figure 48.

The Brillouin diagram for this structure was determined by observing the near field amplitude of the loop system over a range of frequencies. The values of β were calculated from the distance between the nulls of the near-field amplitude observations. The Brillouin diagram for the loop system shown in Figure 48 is shown in the graph of Figure 49. The line OA represents the relative "slowing" of the wave due to total length of conductor in one period and would represent the locus of βd if the energy traveled along the conductor at the speed of light. It is noticed that at $kd = 0.8$ an appreciable amount of attenuation is observed. However, we also note that at this particular value of ka, βa is such that its locus falls inside the slow wave triangle and also falls below the line OA which makes the slope of the kd-βd locus approach the value of zero for this frequency. This is characteristic of periodic structures possessing stop bands; hence, we conclude that a stopband is present on the structure. Therefore, it is evident that such a structure when scaled log-periodically would not operate in a frequency-independent manner. This conclusion arises from the fact that in the corresponding log-periodic structure, it would not be possible to propagate energy past the location of the stop band which, in this case, occurs in front of the active region.

This phenomenon correlated very well with the previous observations on the log-periodic, cavity-backed slot array. It was found that for those frequencies where the stop band occurred in front of the active region, the impedance locus of the log-periodic structure appeared on the periphery of the Smith Chart indicating that essentially no net energy was being radiated by the antenna. However, as the frequency of operation was raised to the point where the stop band went beyond the front end (i.e., the small end) of the log-periodic slot array, the impedance locus on the Smith Chart appeared well inside the chart.

In order to eliminate the stop band the loop-feed system was altered to correspond more closely to the zigzag configuration for which no low frequency stop band has been found. The feed system for the uniform cavity-slot array was then of the form shown in Figure 50. However, it is shown here again placed over an infinite ground screen for near-field amplitude observations to determine the Brillouin diagram for this structure. The results are plotted

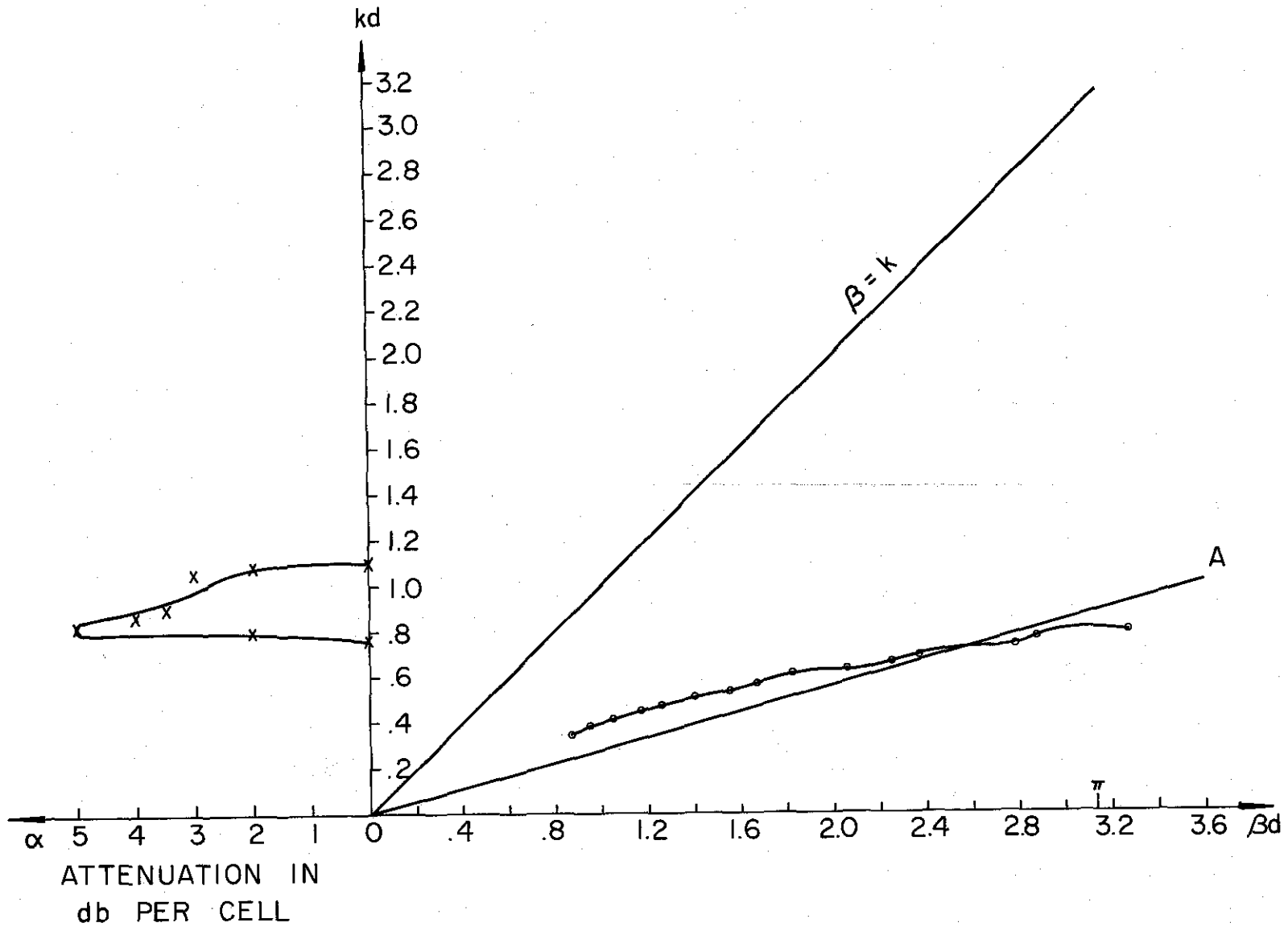

Figure 49. Experimental dispersion data for feed system shown in Figure 48.

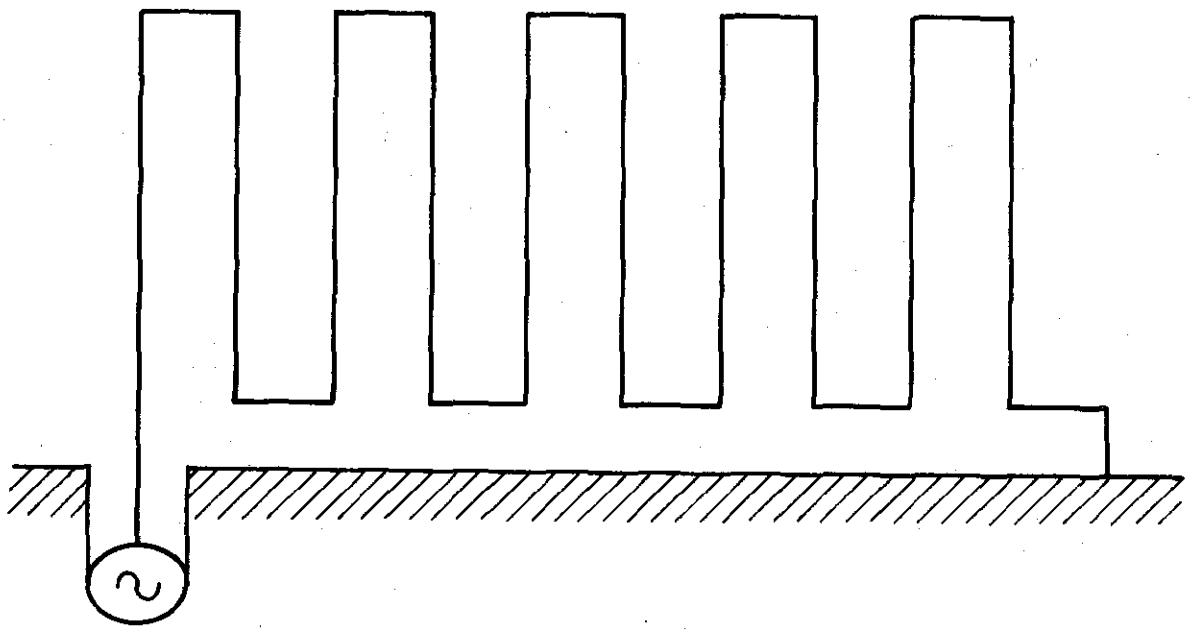

Figure 50. Modified feed system for cavity-backed slot array.

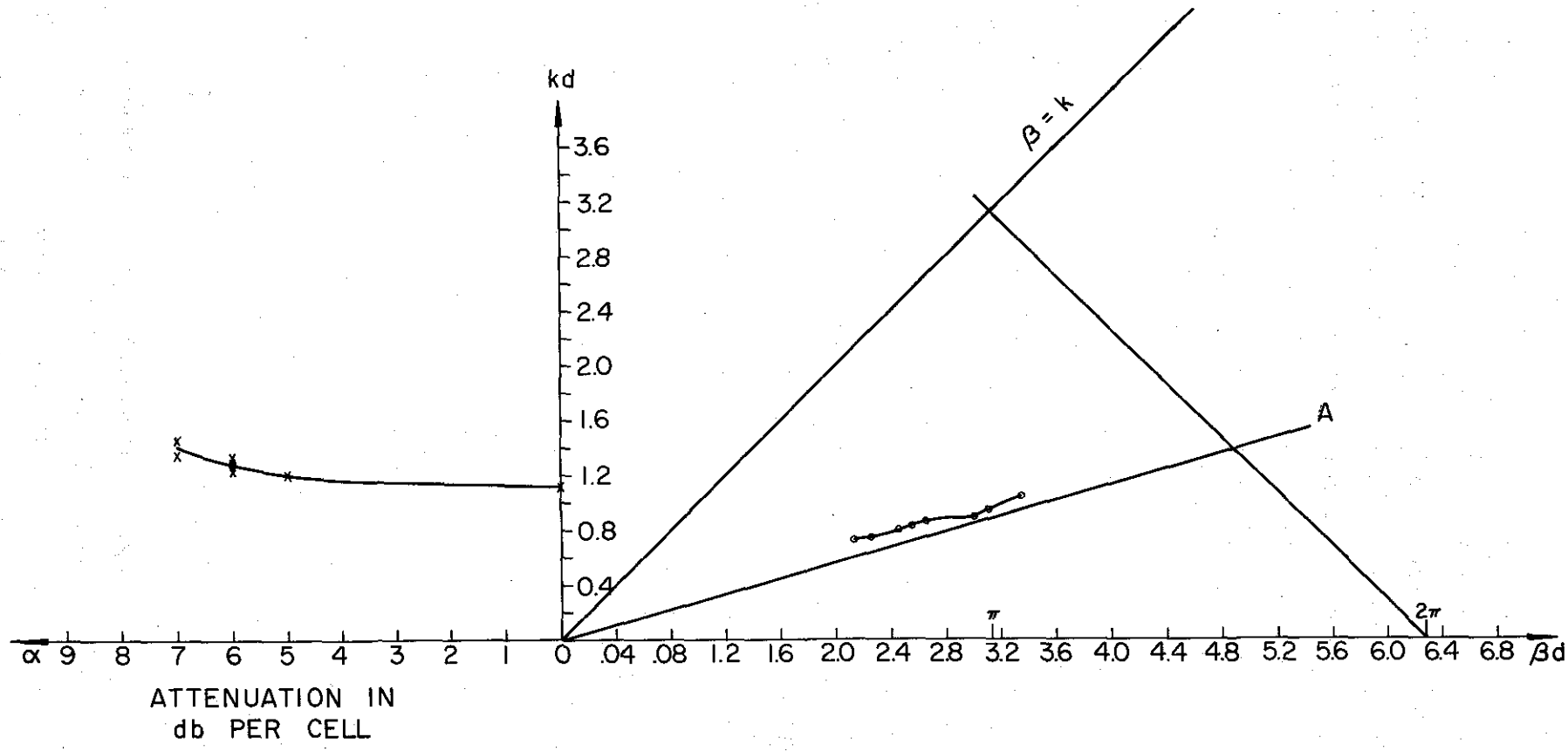

Figure 51. Experimental dispersion data for feed system shown in Figure 50.

in Figure 51. It is first of all noted that an attenuation of the near-field is observed at a higher frequency than in the previous case (kd = 1.2). Secondly, we note that the locus of kd vs. βd does not cross the line 0A before the radiation region so that the slope does not approach zero in the region. This indicates that a "directional coupling" phenomenon is occurring rather than a stop-band phenomena as was noted in the previous case.

A log-periodic version of the feed system of Figure 49 was also used as a feed system in a log-periodic, cavity-backed slot array. The results confirmed that there was no stop band present on the structure over the entire operating bandwidth. For all frequencies, the Smith Chart impedance locus appeared well inside the chart, indicating considerable radiation by the slot array. A typical impedance plot for an antenna designed to have 2.7:1 bandwidth is shown in Figure 52. Note that the measured dispersion data indicates the approximate frequency at which backfire phasing is obtained from the feed system over a ground plane. This is helpful in achieving a properly located active region on the slot array although some shift is caused by interaction between the cavity structure and the feeder. Nevertheless, with proper adjustments, well-formed backfire patterns are obtained over the operating bandwidth as shown in Figure 53.

4.5 Summary of General Principles

In Part II the existence of stop bands on any periodically loaded line was demonstrated. Since the log-periodic dipole array consists of line which is shunted log-periodically with resonant elements, stop bands can be expected to also exist on such a structure.

The discussion of Part III, which relates the continuous scaled and log-periodic antennas, emphasized the point that successful operation of such a structure is dependent upon the loss. Hence, not only the dipole elements, but the array configuration must be simultaneously efficient radiators. It seems good at this point to relate the results of Parts II and III as applied to the dipole array to serve as another example of how dispersion data can be related to antenna design.

Using the lossy stub analogy for the dipole array, the results of Part II show that the resistance of each element determines the maximum phase shift in the region where the attenuation of the complex wave becomes appreciable. Hence, this parameter will be predominant in controlling the phase shift in the

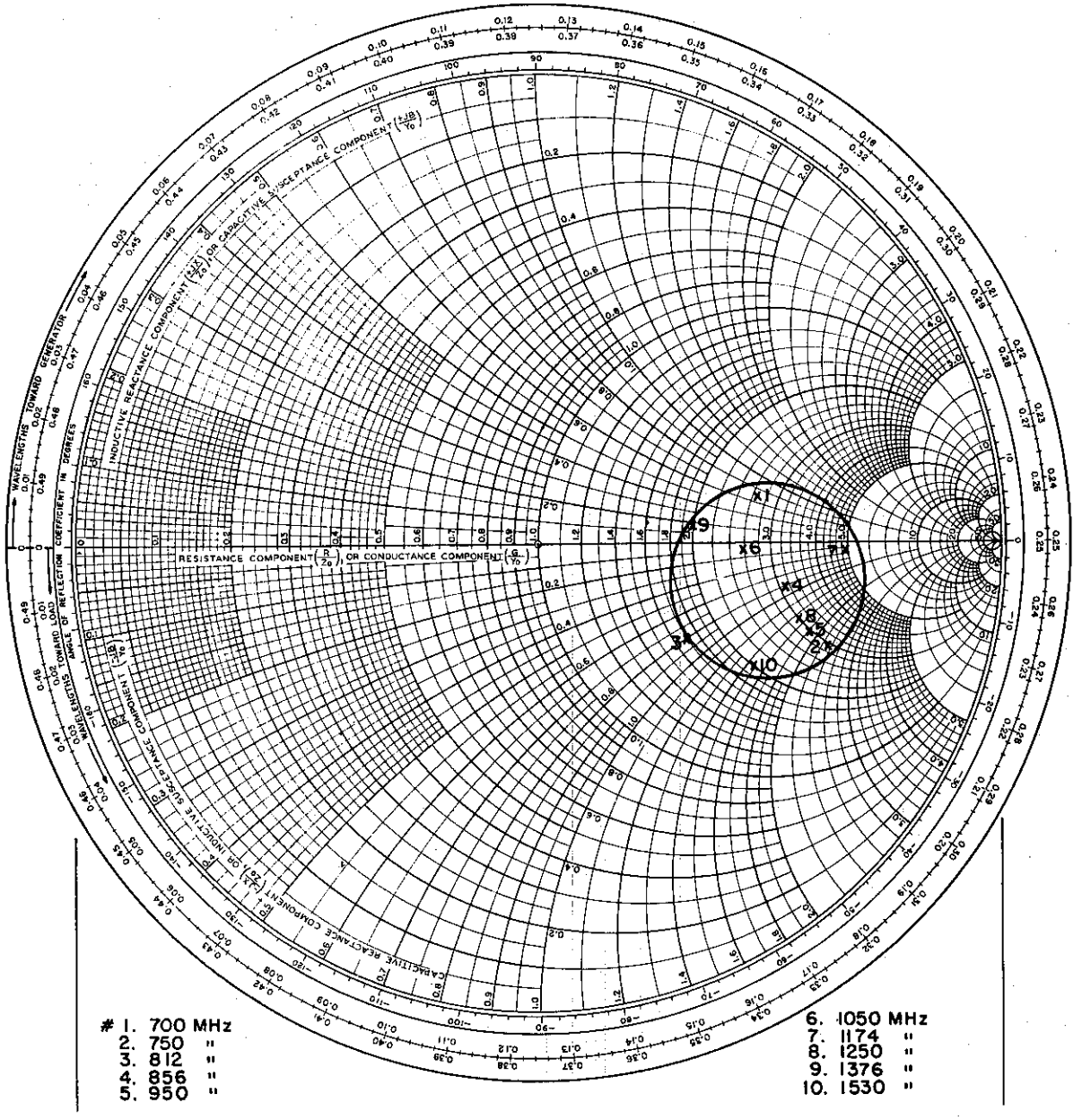

Figure 52. Measured impedance data for log-periodic cavity-backed slot antenna.

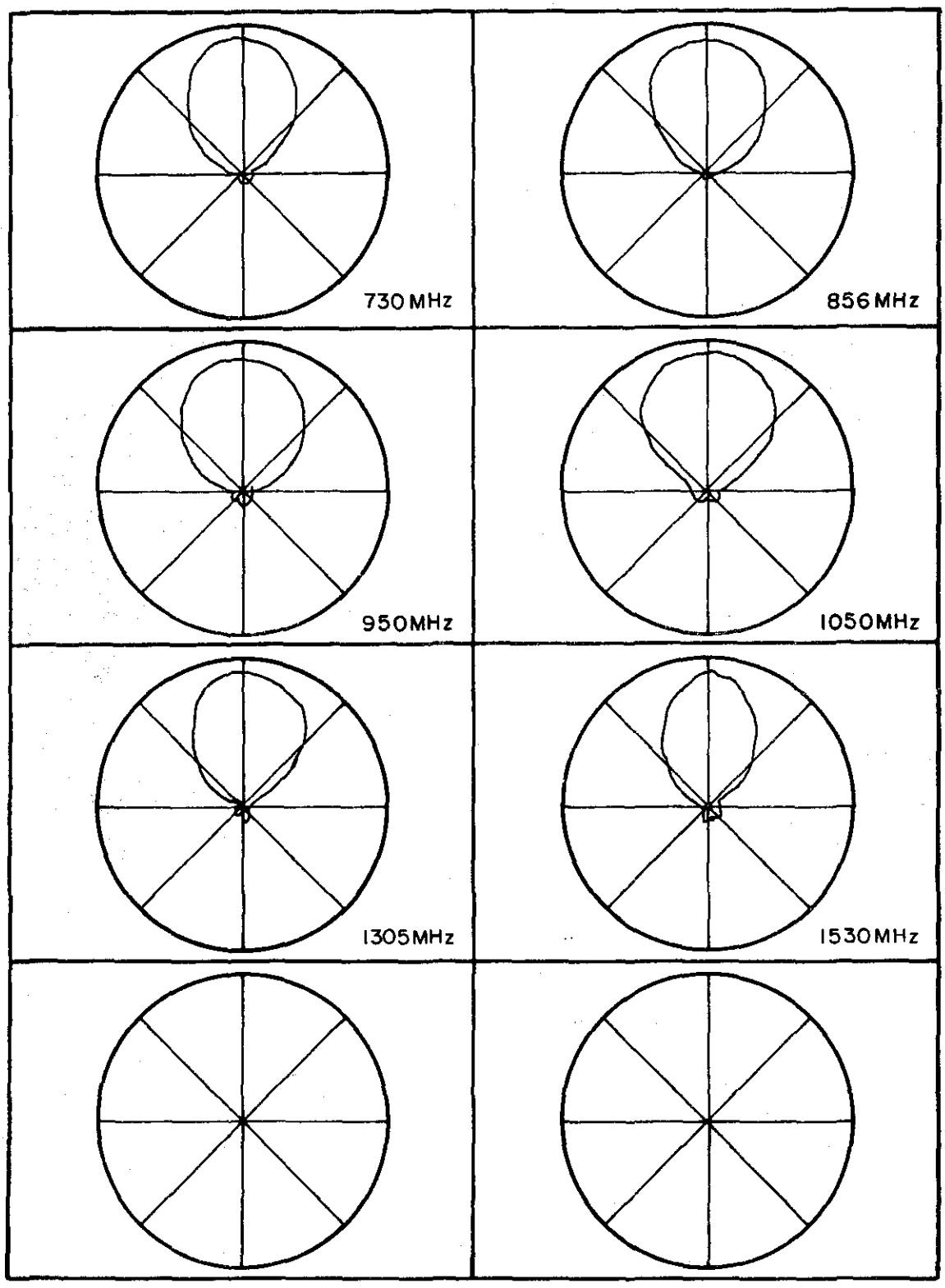

Figure 53. Radiation patterns of log-periodic cavity-backed slot array.

active region. Of course, in the dipole array the real part of the base impedance of each element depends upon the coupling to other elements. The frequency band over which appreciable attenuation exists is governed primarily by the stub impedance. This parameter also controls the Q of the loading element.

The following points now arise for consideration in log-periodic arrays of dipoles or monopoles.

(a) The cell-to-cell phasing of element currents should be such that appreciable radiation can be expected to occur from the array, i.e., the element current progressive phase shift should be in the vicinity of that of a free-space wave (or possibly a fast wave) along the array. This is accomplished in the conventional dipole array by means of the transposed feeder. The phase shift between adjacent dipoles is thereby altered from the phase shift between the loading elements of Part II by a difference of 180 degrees or π radians. As a result, the dispersion data plotted for dipole currents is related to the dispersion data for load currents as shown in Figure 54. Note the approach of the dipole currents dispersion curve to the backfire free-space line is dependent upon the real part of the load impedance.

(b) The attenuation in the complex wave region on the structure should be large enough so that very little energy penetrates to the rear termination or truncation point. The magnitude of the attenuation is also dependent upon the real part of the load impedance. However, the maximum attenuation occurs for zero load resistance which is not desirable for frequency independence. Hence, the optimum load resistance must be chosen on the basis of assuring negligible end effect as well as suitable cell-to-cell phasing.

(c) The number of elements needed in the complex wave region depends upon the width of the region as well as the attenuation. Consideration of the load resistance level plus the bandwidth of each element thus enters into choice of an appropriate scaling factor τ.

The above guidelines are offered as helpful aids to log-periodic antenna design based upon dispersion data. Additional work is in progress in making these design procedures more precise. Hopefully, future work will extend the methods to many additional types of antenna elements as well as active and passive log-periodic networks.

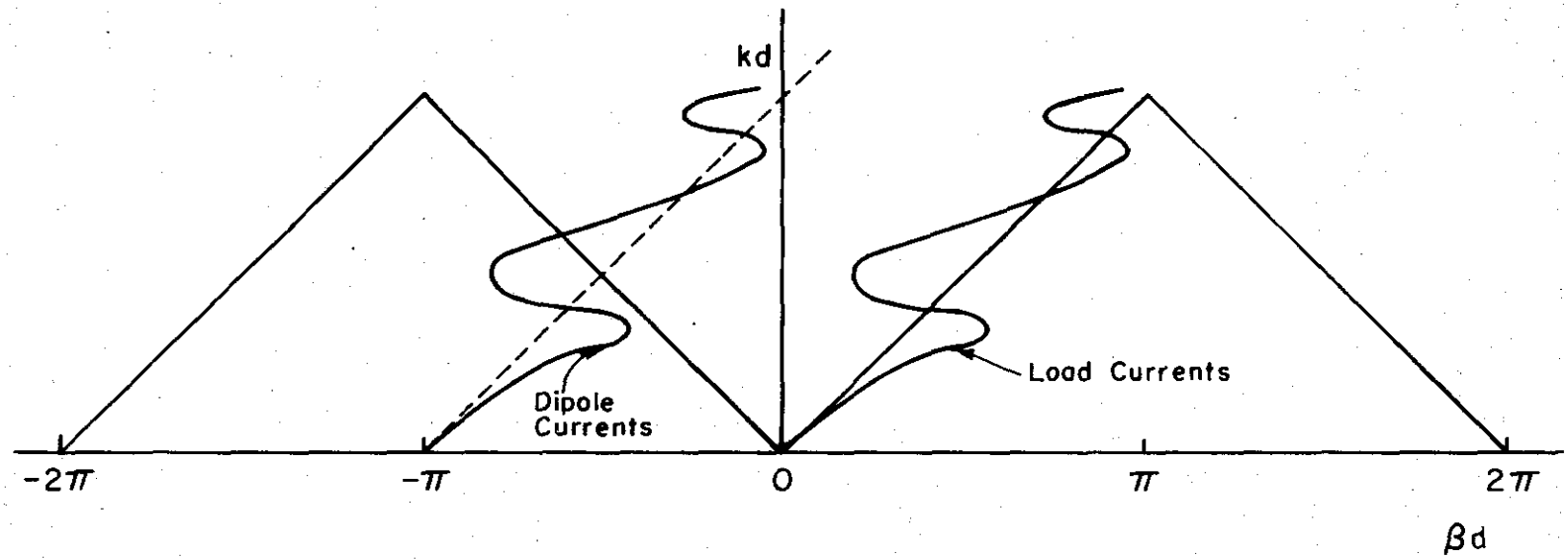

Figure 54. Relation between dipole currents and load currents on a periodic dipole array with transposed feeder.

4.6 Variations for Special Applications

The measured Brillouin diagram of a periodic dipole array indicates that when the period is small enough, conditions in the vicinity of the three-halves wavelength resonance are similar to those in the vicinity of the half-wavelength resonance. It thus seems reasonable to expect a region of backfire radiation near other odd integer multiples of a half-wavelength. The element patterns of dipoles at higher order resonances are not very useful, however. The side lobes are comparable in size; in fact, they may even be larger than the principal lobe. These side lobes can be reduced to small values by forming the dipoles in the shape of a V. Hence, by tilting all the elements of a log-periodic dipole array forward to make a log-periodic array of resonant-V dipoles, the antenna range can be extended to higher frequency bands by operating in these higher modes.[60] The directivity increases in the higher modes because one can make use of a wider effective aperture (measured in terms of the wavelength). Figure 55 shows radiation patterns in the E- and H-planes which are typical of several modes of operation in a particular log-periodic resonant-V antenna. Not only is the beamwidth in the E-plane narrower, but also the beamwidth in the H-plane is reduced as operation is stepped up into the higher modes. The input impedance of the log-periodic-V array has also been measured over several modes which encompass a bandwidth considerably greater than 20 to one. Each mode has a characteristic impedance locus on the Smith Chart which can be described in terms of a mean impedance R_o and a maximum VSWR with respect to that impedance. For feeder impedances between 75 and 150 ohms, elements tilted 50 degrees from perpendicular to feeder, typical ranges of R_o and VSWR are as shown in Table 1.

TABLE I

Mode	R_o (ohms)	VSWR
$\lambda/2$	40- 60	1.5-1.6
$3\lambda/2$	110-170	1.5-1.8
$5\lambda/2$	120-230	1.5-1.8
$7\lambda/2$	90-150	1.4-1.7

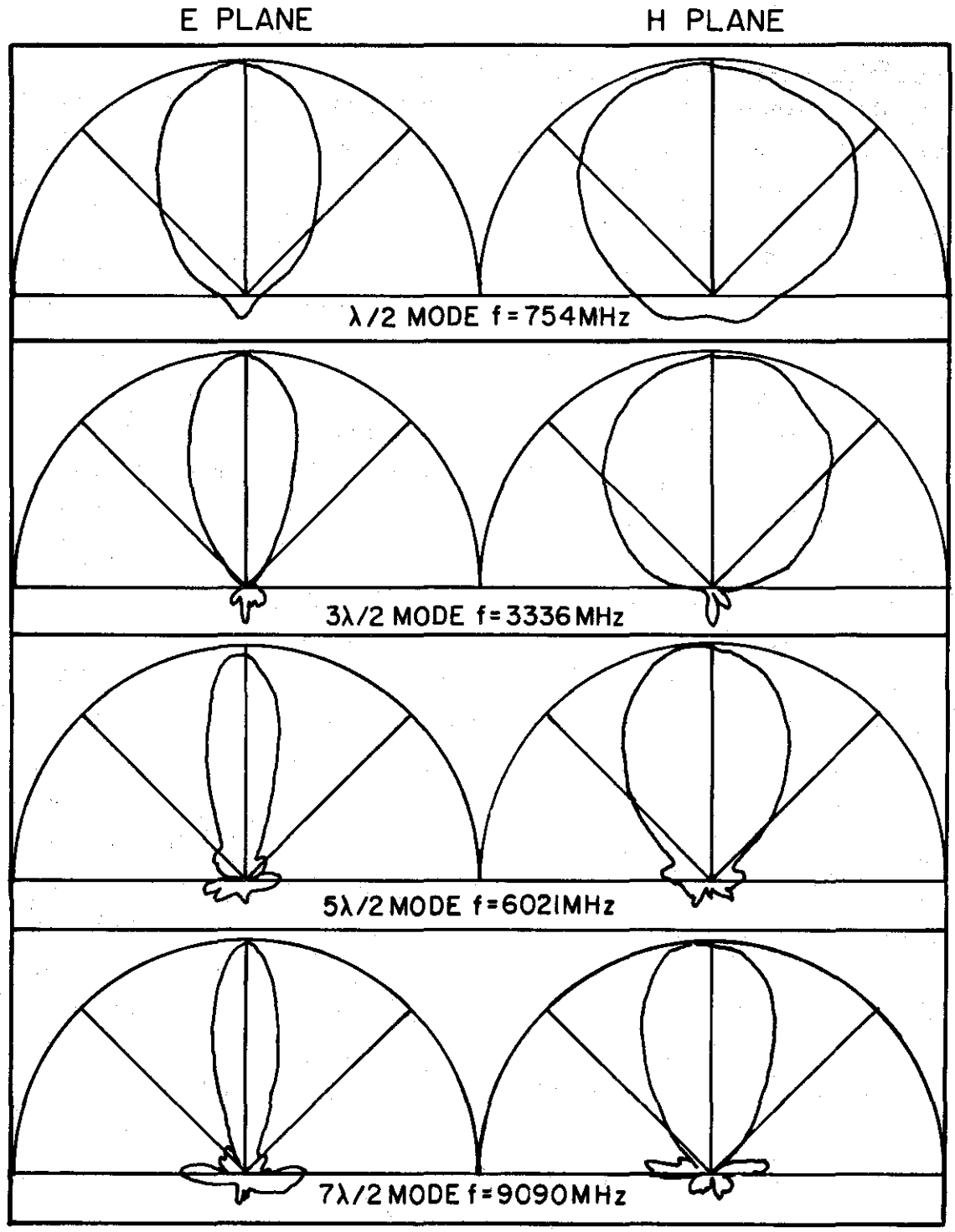

Figure 55. Radiation patterns of log-periodic resonant-V array operating in several modes.

There is a transition band between the various modes wherein the patterns break up and the VSWR increases. This deterioration in performance is most severe in the transition between the $\lambda/2$ and $3\lambda/2$ modes and, in fact, may be reduced to almost negligible effects in the transitions between the higher modes. The foregoing principles can be used in the design of all-channel (VHF-UHF) television receiving antennas and of antennas for use in communications services with frequency allocations in discrete bands such as radio amateurs, etc. Modifications have recently been made which shift the frequencies of the higher order resonances of the dipoles so that a multiband backfire array can be designed to cover bands which are not exactly harmonically related.[70]

It still remains that many applications of frequency independent antennas are in the HF communications band where even a half-wave dipole can become impracticably large. Hence, another interesting line of study involves methods of reducing the length of the dipoles of a log-periodic array. Several methods of loading the dipoles have been suggested and tried with varying degrees of success.[69,70] We shall confine our consideration to the method of continuous inductive loading, which involves replacing the linear dipoles with normal mode helices.[61] Since we know that the performance of an individual dipole is impaired by going to a shorter helical dipole, we expect that the performance of the log-periodic array will also be adversely affected. However, the properties of the log-periodic dipole are generally good enough that some deterioration of performance can be tolerated.

The original method of design was to adjust the helical dipoles so that their resonant frequencies fall in the log-periodic sequence, rather than necessarily having their lengths correspond to the log-periodic formula. The method of feed is the familiar one using twin booms and transposed connection to the feed line. However, when covering a large bandwidth, the structure bandwidth (i.e., the ratio of the largest to the smallest element on the structure) will be large. Hence, it is probable that only some of the dipoles will have impractical lengths, and this suggests the use of mixed arrays. In this case, the front of the antenna is an ordinary log-periodic array of linear dipoles. But it is possible to fix the length for the last few dipoles and adjust the resonant frequencies

of these elements to correspond to the resonant frequencies of the original linear dipole elements that would have occupied these same positions on the antenna.

This design can be further improved by tapering the spacing from that which is employed on the linear dipoles to a value more nearly optimum for the helical dipoles. It is also beneficial to ascertain the bandwidth of each helical dipole and choose the lengths of the elements so that the responses of adjacent dipoles overlap. In this manner a dipole array of restricted width can be made which has impedance versus frequency characteristics comparable to a log-periodic array of full-size half-wave dipoles.[68] However, due to the reduced bandwidth of the shorter dipoles, more elements are required and the overall length of the array is thereby increased.

4.7 Conclusions

Many useful new antenna designs have been produced through frequency-independent antenna research. These include a number not discussed here for a lack of time and data. However, there are still some notable examples of desirable performance which have not yet been achieved. A vertically polarized omnidirectional pattern and a broadside directional beam* are two such examples. A fruitful area for further work lies in the joining of research in pattern synthesis with that in frequency-independence. It is expected that dispersion data for uniform periodic structures will continue to play a major role in this effort.

*Since this manuscript was originally prepared results of workers at University of California[72] and University of Illinois[73] indicate that beams very close to broadside can be obtained by altering the design parameters of a log-periodic dipole array and adding parasitic elements. Consideration of dispersion data played an important role in achieving these results.

REFERENCES

1. Jordan, E. C., Electromagnetic Waves and Radiating Systems, Chapter 10, Prentice-Hall, New York, 1950.

2. Ramo, S., Whinnery, J. R., and Van Duzer, T., Fields and Waves in Communication Electronics, John Wiley & Sons, Inc., New York, 1965.

3. Jasik, H. (ed.), Antenna Engineering Handbook, Chapter 18, McGraw-Hill, 1961.

4. Mayes, P. E., Deschamps, G. A., Patton, W. T., "Backward-Wave Radiation from Periodic Structures and Applications to the Design of Frequency-Independent Antennas," Proc. IRE, (correspondence), Vol. 49, No. 5, May 1961, pp. 962-963. Also Antenna Laboratory Technical Report No. 60, Contract AF33(616)-8460, University of Illinois, Urbana, Illinois, December 1962.

5. Watkins, D. A., Topics in Electromagnetic Theory, John Wiley, New York, 1958, p. 2.

6. Jordan, E. C., Electromagnetic Waves and Radiating Systems, Chapter 12, Prentice-Hall, New York, 1950.

7. Brillouin, Leon, Wave Propagation in Periodic Structures, Dover Publications, Inc., 1953.

8. Harvey, A. F., "Periodic and Guiding Structures at Microwave Frequencies," Proc. IRE, PGMTT, January 1960, pp. 30-61.

9. Pierce, J. R., and Tien, P. K., "Coupling of Modes in Helices," Proc. IRE, Vol. 42, Sept. 1954, pp. 1389-1396.

10. Sensiper, S., "Electromagnetic Wave Propagation on Helical Structures," (a review and survey of recent progress), Proc. IRE, Vol. 43, February 1955, pp. 149-161.

11. Marsh, J. A., "Current Distributions on Helical Antennas," Proc. IRE, Vol. 39, Part 1, June 1951.

12. Watkins, D. A. and Dow, D. G., "Strapped Bifilar Helices for High Peak-Power Traveling-Wave Tubes," IRE Trans. on Electron Devices, January 1959, p. 106.

13. Johnson, H. R., Everhard, T. E., and Siegman, A. E., "Wave Propagation on Multifilar Helices," IRE Trans., ED-3, January 1956, pp. 85-202.

14. Nevins, J. E., Jr., "An Investigation and Application of the Contrawound Helix," IRE Trans. on Electron Devices, April 1959, pp. 195-202.

15. Johnson, C. C., "Impedance and Dispersion Characteristics of the Flattened Helix," IRE Trans. on Electron Devices, April 1959, pp. 195-194.

16. Berezin, A. K. et al, "Determination of the Dispersion Relation for Waveguide with Helices," Soviet Phys.-Tech. Phys., Vol. 4, No. 7, January 1960, pp. 730-739.

17. Brykov, V. S., "The Double-Screen Helical Delay Line," Radio Engineering and Electronic Physics, March 1963, pp. 381-385.

18. Kraus, J. D., Antennas, McGraw-Hill, New York, 1951.

19. Patton, W. T., "The Backfire Bifilar Helical Antenna," University of Illinois Antenna Laboratory, Technical Report No. 61, Contract AF33(657)-8460, September 1962.

20. Klock, P. W., "A Study of Wave Propagation on Helices," University of Illinois Antenna Laboratory, Technical Report No. 68, Contract AF33(657)-10474, March 1963.

21. Dyson, J. D., "The Characteristics and Design of Conical Log-Spiral Antennas, IEEE Trans., PTGAP, Vol. AP-13, July 1965.

22. Clarricoats, P. J. B., "Propagation Along Unbounded and Bounded Dielectric Rods," Parts 1 and 2, Proc. IEE, Monograph 409E, October 1960, pp. 170-186.

23. Longaker, P. R., "Propagation Constants for TE and TM Surface Waves on an Anisotropic Dielectric Cylinder," IEEE Trans. on MTT, Vol. MTT-11, November 1963, pp. 543-546.

24. Zucker, F. J., "Surface and Leaky Wave Antennas," Antenna Engineers Handbook, H. Jasik (ed.), 1961, Chapter 16.

25. Cassedy, E. S., and Oliner, A. A., "Dispersion Relations in Time-Space Periodic Media," P.I.B. Report PIBMRI 22-63, Polytechnic Institute of Brooklyn, February 1963.

26. Hurd, R. A., "The Propagation of an Electromagnetic Wave Along An Infinite Corrugated Surface," Canadian Journal of Physics, Vol. 32, No. 12, December 1954, pp. 727-734.

27. Oliner, A. A. and Hessel, A., "Guided Waves on Sinusoidally Modulated Reactance Surfaces," IEEE Trans. PTGAP, Vol. AP-17, December 1959.

28. Serracchioli, F. and Levis, C. A., "The Calculated Phase Velocity of Long Endfire Uniform Dipole Arrays," IRE Trans., P-GAP, Vol. AP-7, Special Supplement, December 1959.

29. Cheo, R. S., Rumsey, V. H., and Welch, W. J., "A Solution to the Frequency-Independent Antenna Problem," IRE Trans. PGAP, Vol. AP-9, November 1961, pp. 527-534.

30. Rumsey, V. H., "Propagation Over a Sheet of Sinusoidal Wires and Its Application to Frequency Independent Antennas," Electromagnetic Theory and Antennas, E. C. Jordan (ed.), Vol. 2, MacMillan Co., New York, 1963, p. 1011.

31. Morshed, H., "Dispersive Property of Periodic Slot Arrays at the Interface Between Two Dielectric Media," University of Illinois Antenna Laboratory, Technical Report 10, Contract Nobsr 89229, October 1964.

32. Greiser, J. W., "The Propagation of Current Along Infinite Sinusoidal Tapes," University of Illinois Antenna Laboratory, Technical Report No. 11, Contract Nobsr 89229, July 1965.

33. Mittra, R., and Jones, K. E., "Theoretical Brillouin (k-β) Diagrams for Monopole and Dipole Arrays," IEEE International Convention Record, Part 1, 1963, pp. 98-108.

34. Jordan, E. C., Electromagnetic Waves and Radiating Systems, Chapter 9, Prentice-Hall, New York, 1950.

35. Ramo, S. et al., Fields and Waves in Communication Electronics, John Wiley & Sons, Inc., New York, 1965, Chapter 8.

36. Jordan, E. C., Electromagnetic Waves and Radiating Systems, Chapter 15, Prentice-Hall, New York, 1950.

37. Ramo, S. et al., Fields and Waves in Communication Electronics, John Wiley & Sons, Inc., New York, 1965, Chapter 12.

38. Ore, F. R. and Mayes P. E., "A Study of Periodic and Log-Periodic Series Reactance Loading with Application to a High Efficiency Long-Wire Antenna," Technical Report No. 11, Contract No. N123(964)-51806A, February 1966.

39. Mittra, R. and Jones, K. E., "On Continuously Scaled and Log-Periodic Structures," Technical Report No. 73, Contract No. AF33(657)-10474, University of Illinois Antenna Laboratory, September 1963.

40. Ingerson, P. G. and Mayes, P. E., "Dispersion Characteristics of Periodic Dipole Arrays," Technical Report No. AFAL-TR-66-120, Contract No. AF33 (615)-3216, University of Illinois Antenna Laboratory, June 1966.

41. Morse, P. M. and Feshbach, H., Methods of Theoretical Physics, McGraw-Hill Book Company, New York, 1953, p. 1092.

42. Rydbeck, O. E. H., "Lecture Notes on a Course on Wave Propagation in Inhomogeneous Media," Ionospheric Research Scientific Report No. 215, The Pennsylvania State University, AD 608 102, August 1, 1965.

43. Mayes, P. E., "Log-Periodic Zigzag Antennas," Quarterly Report No. 3, Contract AF33(657)-10474, pp. 14-22, June 25, 1963.

44. Balmain, K. G., and Dyson, J. D., "The Series-Fed, Log-Periodic Folded Dipole Array," 1963 PTGAP International Symposium on Space Telecommunications, pp. 143-148. Also, Technical Report No. 5, NEL 30508A, January 1964.

45. Dyson, J. D., "The Characteristics and Design of Conical Log-Spiral Spiral Antennas," Trans. IEEE, Vol. AP-13, July 1965.

46. Mittra, R. and Block, P. W., "A Theoretical Study of the Conical Spiral Antenna," presented at the U.R.S.I. Symposium on Electromagnetic Wave Theory, Delft, Netherlands, September 1965.

47. Deschamps, G. A. and DuHamel, R. H., "Frequency-Independent Antennas," Antenna Engineering Handbook, H. Jasik (ed.), McGraw-Hill Book Company, Inc., New York, 1961, pp. 18-22.

48. Berry, D. G. and Ore, F. R., "Log-Periodic Monopole Array," CRR No. 222, Collins Radio Company, Cedar Rapids, Iowa, October 1960.

49. Hudock, E. and Mayes, P. E., "Near-Field Investigation of Uniform Periodic Arrays," IEEE Trans., Vol. AP-13, No. 6, November 1965, pp. 840-855.

50. Rumsey, V. H., "Frequency-Independent Antennas," IRE National Convention Record 5 (1957), Part 1, pp. 114-118.

51. DuHamel, R. H., and Isbell, D. E., "Broadband Logarithmically Periodic Antenna Structures," IRE National Convention Record 5 (1957), Part I, pp. 119-128.

52. Isbell, D. E., "Non-Planar Logarithmically Periodic Antenna Structures," Proceedings Seventh USAF Antenna Research and Development Program Symposium, Electrical Engineering Department, University of Illinois, October, 1957, also, Antenna Laboratory Technical Report No. 30, Contract AF 33(616)3220, Electrical Engineering Department, University of Illinois, February 1958.

53. DuHamel, R. H., and Berry, D. G., "A New Concept in High Frequency Antenna Designs," IRE National Convention Record 7, 1957, Part 1, pp. 119-128.

54. DuHamel, R. H., and Ore, F. R., "Logarithmically Periodic Designs," IRE National Convention Record 6, Part 2, pp. 139-152, 1958.

55. Isbell, D. E., "Log-Periodic Dipole Arrays," IRE Trans. AP-8, May 1960, pp. 260-267; also Antenna Laboratory Technical Report No. 39, Contract AF33(616)-3220, Department of Electrical Engineering, University of Illinois, June 1959.

56. Carrel, R. L., "The Design of Log-Periodic Dipole Antennas," IRE International Convention Record 9, 1961.

57. Mayes, P. E., "Balanced Backfire Zigzag Antennas," IRE International Convention Record 12, 1964, Part I.

58. Mayes, P. E., Deschamps, G. A. and Patton, W. T., "Backward-Wave Radiation from Periodic Structures and Applications to the Design of Frequency-Independent Antennas," Proceedings of the IRE 49, No. 5, May 1961; pp. 962-963; also Antenna Laboratory Technical Report No. 60, Contract AF33(616)-8460, Department of Electrical Engineering, University of Illinois, December 1962.

59. Mittra, R. and Jones, K. E., "Theoretical Brillouin (k-β) Diagram for Monopole and Dipole Arrays and Their Application to Log-Periodic Antennas," Technical Report No. 70, Contract No. AF33(657)-10474, University of Illinois Antenna Laboratory, April 1963.

60. Mayes, P. E., "Broadband Backward Wave Antennas," Microwave Journal, Vol. 6, No. 1, January 1963, pp. 61-71.

61. Stephenson, D. T. and Mayes, P. E., "Log-Periodic Helical Dipole Arrays," WESCON, San Francisco, California, 1963. Also, "Broadband Arrays of Helical Dipoles," Technical Report No. 2, Contract No. NEL 30508A, Antenna Laboratory, University of Illinois, January 1964.

62. Greiser, John, "Research on Log-Periodic Arrays of Slots," Technical Report No. 3, Contract No. NOBSR 85243, University of Illinois, Antenna Laboratory, February 1964.

63. Klock, P. W. and Mittra, R., "On the Solution of the (k-β) Diagram of the Helix and its Application to Helical Antennas," 1963 IEEEE-PTGAP International Symposium Digest, pp. 99-103.

64. Dyson, J. D., "The Design of Conical Log-Spiral Antennas," IEEE International Convention Record, March 1964, Part 6 (Radio Communications).

65. Carr, J. W., "Some Variations in Log-Periodic Antenna Structures," Trans. IRE, Vol. AP-9, March 1961, p. 229.

66. Greiser, J. W. and Mayes, P. E., "Bent Backfire Zigzag," IEEE Trans., Vol. AP-12, No. 3, May 1964, pp. 381-290.

67. Mikenas, V. A., "A Log-Periodic Cavity-Backed Slot Antenna," Technical Report No. 78, Contract No. AF33(657)-10474, University of Illinois Antenna Laboratory, June 1964.

68. Stephenson, D. T. and Mayes, P. E., "Variations of Broadband Helical Dipole Arrays," Antenna Laboratory Report No. 65-3, Contract N123(964)-51806A, University of Illinois, April 1966.

69. DiFonzo, D. F., "Reduced Size Log-Periodic Antennas," Microwave Journal, Vol. 7, No. 12, December 1964, pp. 37-42.

70. Elfving, C. T., "Foreshortened Log-Periodic Dipole Array," 1963 WESCON, San Francisco, California, August 1963. Also, Technical Memo. EDL-M401, Contract No. DA 36-039-AMC-00088(E), Electronic Defense Laboratories Sylvania Electric Products, Inc., September 12, 1963.

71. Mayes, P. E., "Designing an All-Channel TV Antenna," Electronics World, February 1966.

72. Mei, K. K. and Johnstone, D., "A Broadside Log-Periodic Antenna," Proc. IEEE, (correspondence), Vol. 54, No. 6, June, 1966, pp. 889-890.

73. Ingerson, P. and Mayes, P. E., "Design of Log-Periodic Structures Using Complex Dispersion Data for Periodic Lines," Tech. Rep. No. 66-10, Antenna Laboratory, University of Illinois, August, 1966.

00264

NOTICE
THIS PRINT
SUPERSEDED BY
ISSUED TO DATE
JFD SOUTHERN

UNITED STATES DISTRICT COURT
NORTHERN DISTRICT OF ILLINOIS
BEFORE JUDGE HOFFMAN
DEFENDANT EX. NO.
DOROTHY L. BRACKENBURY
OFFICIAL COURT REPORTER

REV.	DESCRIPTION	DATE	APP.
A	ADDED $\frac{1}{4}$ R.	10-3-63	
B	ADDED SLOT. SEE VIEW "B-B"	1-20-65	
C	ADDED TABLE	5-12-65	
D	ABS TYPE WAS FORTIFLEX "A" A60-250 "UV" STABILIZED	10-8-65	
E	MATERIAL WAS ABS TYPE	12-22-65	

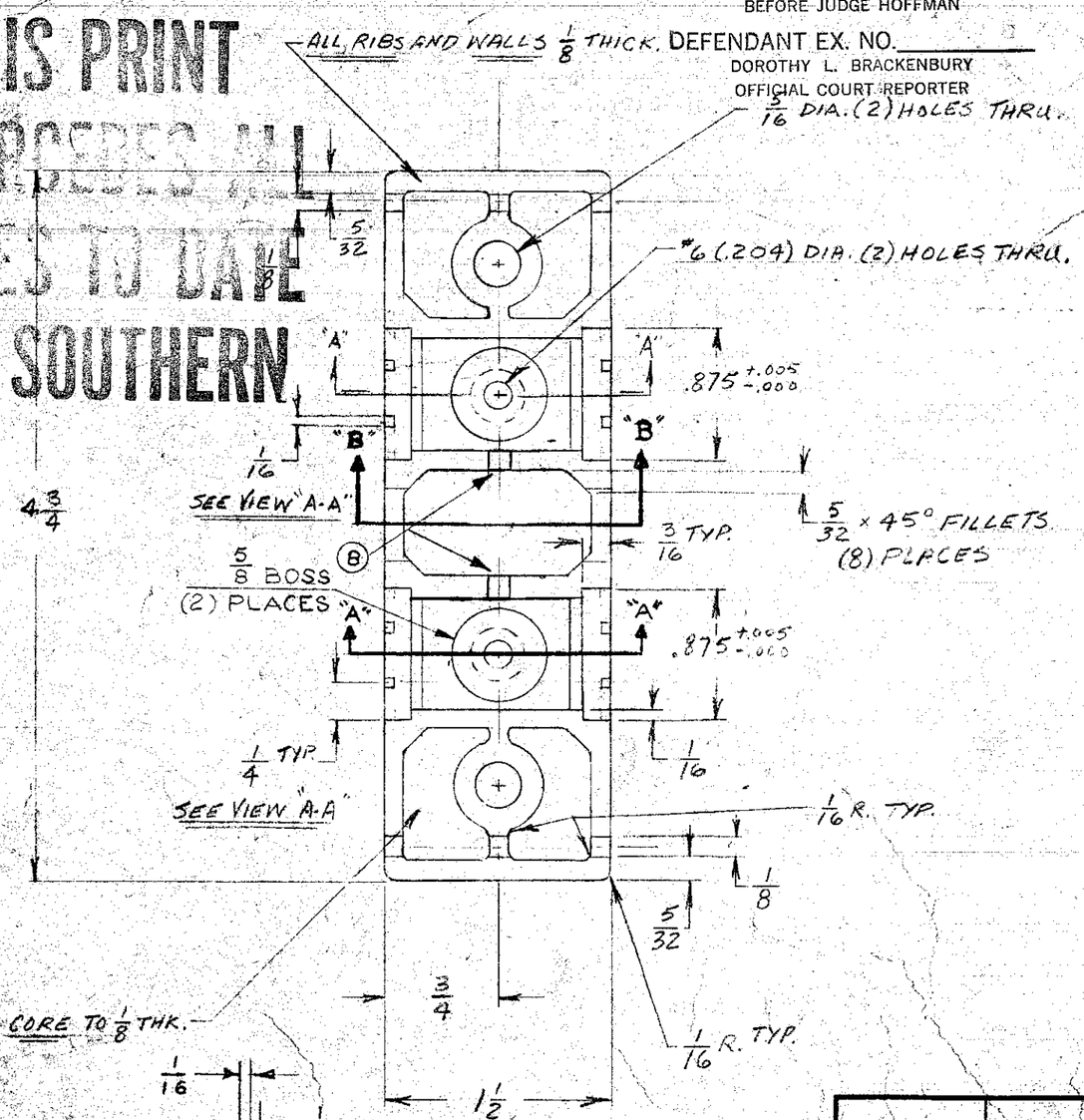

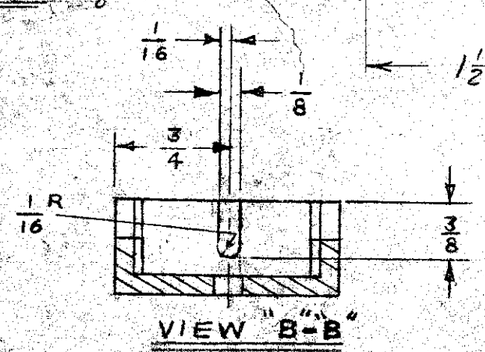

VIEW "B-B"

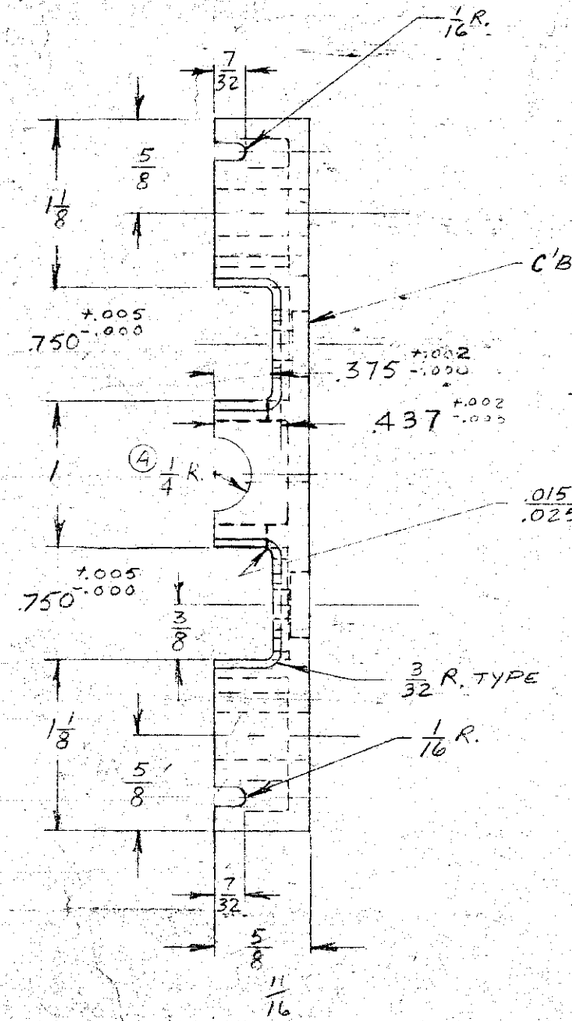

PART NO.	COLOR
12395-0001	BLACK
12395-0101	
12395-0201	YELLOW
12395-0301	

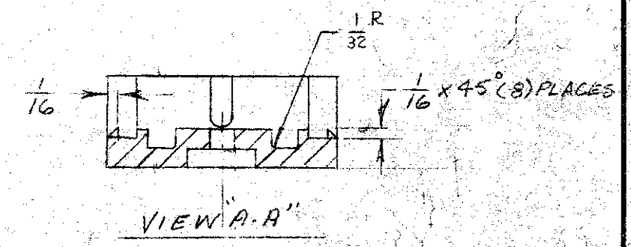

VIEW "A-A"

NOTE: PART TO BE FREE OF ALL SINKS FLASHING & DISTORTIONS. ALL EDGES & FILLETS TO BE $\frac{1}{32}$ R. UNLESS OTHERWISE NOTED

ITEM NO.	NO. REQ'D	PART NO.	DESCRIPTION	MATERIAL	SPECIFICATION	NOTE

SCALE: FULL
NO. REQ'D PER ASSEMBLY: 2
TOLERANCES UNLESS OTHERWISE SPECIFIED
FRACTIONAL ± 1/64
DECIMAL ± .005
ANGULAR ± 1/2°
DOUBLE PLUM INSULATED FOR U'BOLT & BOOM MOUNTING
MATERIAL: CYCOLAC GR IMPLEX "A"
HEAT TREAT:
FINISH: SEE TABLE

DRAWN	CHECKED	ENG. APP.	PROD. APP.
EV and 6-23-65			

JFD ELECTRONICS CORP.
BROOKLYN 19, N.Y.

DATE OF PRINTING: NOV 8 1965
NEXT ASSEMBLY:
DRAWING NO. 12395-0001